Vol. 289, No. 3, May 10, 1994
Completing Volume 289

ISSN 0003-2670

ANALYTICA CHIMICA ACTA

An international journal devoted to all branches of analytical chemistry

ELSEVIER

ANALYTICA CHIMICA ACTA

Scope. *Analytica Chimica Acta* publishes original papers, rapid publication letters and reviews dealing with every aspect of modern analytical chemistry. Reviews are normally written by invitation of the editors, who welcome suggestions for subjects. Letters can be published within **four months** of submission. For information on the Letters section, see inside back cover.

Submission of Papers

Americas

Prof. Harry L. Pardue
Department of Chemistry
1393 BRWN Bldg, Purdue University
West Lafayette, IN 47907-1393
USA

Tel:(+1-317) 494 5320
Fax:(+1-317) 496 1200

Computer Techniques

Prof. J.T. Clerc
Universität Bern
Pharmazeutisches Institut
Baltzerstrasse 5, CH-3012 Bern
Switzerland

Tel:(+41-31) 6314191
Fax:(+41-31) 6314198

Prof. Sarah C. Rutan
Department of Chemistry
Virginia Commonwealth University
P.O. Box 2006
Richmond, VA 23284-2006
USA
Tel:(+1-804) 367 1298
Fax:(+1-804) 367 7517

Other Papers

Prof. Alan Townshend
Department of Chemistry
The University
Hull HU6 7RX
Great Britain

Tel:(+44-482) 465027
Fax:(+44-482) 466410

Prof. Willem E. van der Linden
Laboratory for Chemical Analysis
Department of Chemical Technology
Twente University of Technology
P.O. Box 217, 7500 AE Enschede
The Netherlands
Tel:(+31-53) 892629
Fax:(+31-53) 356024

Prof. Paul Worsfold
Dept. of Environmental Sciences
University of Plymouth
Plymouth PL4 8AA
Great Britain

Tel:(+44-752) 233006
Fax:(+44-752) 233009

Submission of an article is understood to imply that the article is original and unpublished and is not being considered for publication elsewhere. *Anal. Chim. Acta* accepts papers in English only. There are no page charges. Manuscripts should conform in layout and style to the papers published in this issue. See inside back cover for "Information for Authors".

Publication. *Analytica Chimica Acta* appears in 16 volumes in 1994 (Vols. 281-296). *Vibrational Spectroscopy* appears in 2 volumes in 1994 (Vols. 6 and 7). Subscriptions are accepted on a prepaid basis only, unless different terms have been previously agreed upon. It is possible to order a combined subscription (*Anal. Chim. Acta* **and** *Vib. Spectrosc.*).
Our p.p.h. (postage, packing and handling) charge includes surface delivery of all issues, except to subscribers in the U.S.A., Canada, Australia, New Zealand, China, India, Israel, South Africa, Malaysia, Thailand, Singapore, South Korea, Taiwan, Pakistan, Hong Kong, Brazil, Argentina and Mexico, who receive all issues by air delivery (S.A.L.-Surface Air Lifted) at no extra cost. For Japan, air delivery requires 25% additional charge of the normal postage and handling charge; for all other countries airmail and S.A.L. charges are available upon request.

Subscription orders. Subscription prices are available upon request from the publisher. Subscription orders can be entered only by calendar year and should be sent to: Elsevier Science B.V., Journals Department, P.O. Box 211, 1000 AE Amsterdam, The Netherlands. Tel: (+31-20) 5803 642, Telex: 18582, Telefax: (+31-20) 5803598, to which requests for sample copies can also be sent. Claims for issues not received should be made within six months of publication of the issues. If not they cannot be honoured free of charge. Readers in the U.S.A. and Canada can contact the following address: Elsevier Science Inc., Journal Information Center, 655 Avenue of the Americas, New York, NY 10010, U.S.A. Tel: (+1-212) 6333750, Telefax: (+1-212) 6333990, for further information, or a free sample copy of this or any other Elsevier Science journal.
Advertisements. Advertisement rates are available from the publisher on request.

US mailing notice - Analytica Chimica Acta (ISSN 0003-2670) is published 3 times a month (total 48 issues) by Elsevier Science B.V. (Molenwerf 1, Postbus 211, 1000 AE Amsterdam). Annual subscription price in the USA US$ 3035.75 (valid in North, Central and South America), including air speed delivery. Second class postage paid at Jamaica, NY 11431. *USA Postmasters*: Send address changes to Anal. Chim. Acta, Publications Expediting, Inc., 200 Meacham Av., Elmont, NY 11003. Airfreight and mailing in the USA by Publication Expediting.

ANALYTICA CHIMICA ACTA

An international journal devoted to all branches of analytical chemistry

(Full texts are incorporated in CJELSEVIER, a file in the Chemical Journals Online database available on STN International; Abstracted, indexed in: Aluminum Abstracts; Anal. Abstr.; Biol. Abstr.; BIOSIS; Chem. Abstr.; Curr. Contents Phys. Chem. Earth Sci.; Engineered Materials Abstracts; Excerpta Medica; Index Med.; Life Sci.; Mass Spectrom. Bull.; Material Business Alerts; Metals Abstracts; Sci. Citation Index)

VOL. 289 NO. 3 CONTENTS MAY 10, 1994

Letter

TCDD equivalents of mono-*ortho* substituted chlorobiphenyls. Influence of analytical error and uncertainty of toxic equivalency factors
J. De Boer (IJmuiden, Netherlands) and U.A.Th. Brinkman (Amsterdam, Netherlands) 261

Ion Mobility / Mass Spectrometry

Analysis of ion mobility spectra for mixed vapors using Gaussian deconvolution
D.M. Davis, C.S. Harden, D.B. Shoff (Aberdeen, MD, USA), S.E. Bell, G.A. Eiceman and R.G. Ewing (Las Cruces, NM, USA) 263

Fluorimetry

Fluorimetric studies of some quinones and quinonoid compounds after reduction reaction
S.K. De Barros Alcanfôr, S.V. Cardoso and C.G. De Lima (Brasilia, Brazil) 273

Electroanalytical Chemistry and Sensors

Determination of arsenic in sea water by cathodic stripping voltammetry in the presence of pyrrolidine dithiocarbamate
J. Zima and C.M.G. Van den Berg (Liverpool, UK) 291

Influence of perchlorates and halides on the electrochemical properties of indium(III)
M. Zelić, M. Mlakar and M. Branica (Zagreb, Croatia) 299

Detection of actomyosin depolymerization with a piezoelectric quartz crystal
S. Kurosawa (Sapporo, Japan), E. Nemoto (Katsuta, Japan), M. Muratsugu (Asahikawa, Japan), M. Yoshimoto, Y. Mori and N. Kamo (Sapporo, Japan) 307

Rapid detection of *Escherichia coli* using a separated electrode piezoelectric crystal sensor
F. He, Q. Geng, W. Zhu, L. Nie, S. Yao and C. Meifeng (Changsha, China) 313

Electrochemical deposition of avidin on the surface of a platinum electrode for enzyme sensor applications
T. Hoshi, J.-i. Anzai and T. Osa (Sendai, Japan) 321

Adsorption and association of 6-thiopurine and 6-thiopurine riboside at charged interfaces
Z.A. Ahmed, M.E. Ahmed, M.S. Ibrahim, M.M. Kamal and Y.M. Temerk (Assiut, Egypt) 329

Flow Injection

Flow-injection biamperometry of phenothiazine derivatives
J. Michałowski, A. Kojło, B. Magnuszewska (Białystok, Poland) and M. Trojanowicz (Warsaw, Poland) 339

Dual-wavelength photometry with light emitting diodes. Compensation of refractive index and turbidity effects in flow-injection analysis
H. Liu and P.K. Dasgupta (Lubbock, TX, USA) 347

Zone circulating flow-injection analysis: theory
Y. Li and Y. Narusawa (Tokyo, Japan) 355

(Continued overleaf)

Contents (continued)

Flow-injection method for the determination of tin in fruit juices using solid-phase spectrophotometry
L.F. Capitán-Vallvey, M.C. Valencia and G. Mirón (Granada, Spain) 365

Chromatography
Orthogonal array designs for the optimization of liquid chromatographic analysis of pesticides
H.B. Wan, W.G. Lan, M.K. Wong and C.Y. Mok (Singapore) 371

Instructions to Authors 381

Author Index 385

ELSEVIER

Analytica Chimica Acta 289 (1994) 261–262

ANALYTICA CHIMICA ACTA

Letter

TCDD equivalents of mono-*ortho* substituted chlorobiphenyls. Influence of analytical error and uncertainty of toxic equivalency factors

Jacob de Boer [a,*], Udo A.Th. Brinkman [b]

[a] *DLO-Netherlands Institute for Fisheries Research, P.O. Box 68, 1970 AB IJmuiden, Netherlands*
[b] *Department of Analytical Chemistry, Free University, De Boelelaan 1083, 1081 HV Amsterdam, Netherlands*

(Received 15th February 1994; revised manuscript received 4th March 1994)

Abstract

The influence of the analytical error in the multidimensional gas chromatographic determination of mono-*ortho* substituted chlorobiphenyls in biota on the calculation of their TCDD equivalents is negligible compared with the influence of the high uncertainty of toxic equivalency factors reported in the literature.

Key words: Gas chromatography; Chlorobiphenyls; TCDD equivalents; Toxic equivalency factors

1. Determination of mono-*ortho* CBs

Since the introduction of capillary gas chromatography (GC), individual chlorobiphenyl congeners (CBs) have been determined extensively in various matrices. Information from toxicological research identified non- and mono-*ortho* substituted CBs as the major contributors to the total toxic effect (expressed as TCDD equivalents or TEQs) of CBs in organisms [1,2]. Because of their extremely low concentrations, special pre-separation techniques had to be developed in which non-*ortho* CBs were separated from the other CBs by liquid chromatography (LC), using pyrene or graphitized carbon columns, prior to GC analysis [3,4]. Although mono-*ortho* CBs can be determined after similar pre-separation, it is less time-consuming to determine these CBs without pre-separation by single-column GC, which is possible for the major mono-*ortho* CBs 105, 118 and 156, or by multidimensional GC (MDGC) for the CBs 60, 74, 114, 123, 157, 167 and 189. Experiences from interlaboratory studies have shown that reliable determination of the minor peaks of the latter group of CBs cannot be carried out by single-column GC because co-elution will easily occur [5].

We have developed a method for the determination of mono-*ortho* CBs by MDGC with electron capture detection (ECD). Pre-treatment of the samples was similar to that of a normal PCB analysis: Soxhlet extraction, clean-up over alumina and fractionation over silica columns [6]. A Sichromat 2-8 gas chromatograph with two ovens was used in which an HP-Ultra 2 and an HP-

* Corresponding author.

SSDI 0003-2670(94)00123-4

Table 1
CB-TEQ values (ng kg^{-1}) of CBs 60, 74, 114, 123, 157, 167 and 189 in fish calculated using different TEFs

Sample	Kannan, 1988		Dutch WG, 1991		Safe, 1992		Safe, 1993	
	TEQ [a]	% of total [b]	TEQ [a]	% of total [b]	TEQ [a]	% of total [b]	TEQ [a]	% of total [b]
Eel Meuse	0.07	0.2	2.4	6	23	6	0.78	1
Eel Ketelmeer	0.07	0.07	1.6	5	15	10	0.42	0.7
Eel Rhine	0.08	0.1	3.8	12	44	22	0.78	1.5
Pike-perch Rhine	0.04	0.05	0.16	4	2.0	15	0.06	< 1
Cod liver North Sea	0.1	0.02	3.0	1	40	9	0.45	< 0.1

[a] TEQ of CBs 60, 74, 114, 123, 157, 167 and 189. [b] Total CB-TEQ based on CBs 77, 126, 169, 105, 118, 156, 60, 74, 114, 123, 157, 167 and 189.

FFAP column, both 25 m × 0.20 mm, were installed. Using a pressure switch, heart-cuts from the Ultra 2 column, which can be made with a precision of seconds, were sent to the FFAP column for a second chromatographic analysis. It was possible to combine heart-cuts of CBs 74, 114, 157 and 167 in one run without creating new co-elutions. The total analysis time is 130 min. Standard deviations for the repeatability of the method ($n = 5$), tested for an eel sample from the river Rhine delta, varied between 8% (CB 74) and 23% (CB 114) at a concentration level of 2–25 $\mu g\ kg^{-1}$ wet weight. Recoveries of CBs from spiked samples ranged from 83 to 98% ($n = 2$) and detection limits from 0.05 to 0.4 $\mu g\ kg^{-1}$.

2. TCDD equivalents (TEQs)

CB concentrations can be expressed as TEQs by multiplying them with a toxic equivalency factor (TEF). Various authors have reported a wide range of TEFs for CBs [7–10]. We have calculated CB-TEQs in five fish samples using four different sets of published TEFs (Table 1). The contribution of TEQs of the mono-*ortho* CBs 74, 157 and 167 – the contribution of CBs 60, 114, 123 and 189 is negligible – to the total CB-TEQ ranges from 0.02 to 22%. More importantly, the broad range of TEF values presently in use makes the TEQ values of the mono-*ortho* CBs studied cover an approximately 1000-fold wide range for all samples analysed (0.04–44 ng kg^{-1}); the total CB-TEQ also varies dramatically (from 4 to 500 ng kg^{-1}; data not shown). Obviously, compared with this huge uncertainty in TEQ values, the analytical error of 8–23% is negligible. Even when the MDGC method would be applied by several laboratories, which could lead to standard deviations for the reproducibility of around 100%, as has been shown for other CBs [5], this error would still be much smaller than the uncertainty in the TEFs. In other words, sound interpretation of analytical data on CBs requires a stronger toxicological basis which would enable the use of much more precise TEF values.

References

[1] S. Tanabe, N. Kannan, A. Subramanian, S. Watanabe and R. Tatsukawa, Environ. Pollut., 47 (1987) 147.
[2] S.D.P. Safe, Crit. Rev. Toxicol., 21 (1990) 51.
[3] P. Haglund, L. Asplund, U. Järnberg and B. Jansson, Chemosphere, 20 (1990) 887.
[4] J. de Boer, C.J.N. Stronck, F. van der Valk, P.G. Wester and M.J.M. Daudt, Chemosphere, 25 (1992) 1277.
[5] J. de Boer, J. van der Meer, L. Reutergårdh and J.A. Calder, J. Assoc. Off. Anal. Chem., (1994) in press.
[6] J. de Boer, Chemosphere, 17 (1988) 1811.
[7] N. Kannan, S. Tanabe and R. Tatsukawa, Bull. Environ. Contam. Toxicol., 41 (1988) 267.
[8] A.K.D. Liem, R.M.C. Theelen, W. Slob and J.H. van Wijnen, Report 730501.034 (1991), National Institute of Public Health and Environmental Protection, Bilthoven, Netherlands.
[9] S. Safe, Chemosphere, 25 (1992) 61.
[10] S. Safe, in H. Fiedler, H. Frank, O. Hutzinger, W. Parzefall, A. Riss and S. Safe (Eds.), Proc. 13th Int. Symp. Dioxin '93, Vienna, Organohalogen Compounds, 14 (1993) 53.

ELSEVIER

Analytica Chimica Acta 289 (1994) 263–272

ANALYTICA CHIMICA ACTA

Analysis of ion mobility spectra for mixed vapors using Gaussian deconvolution

Dennis M. Davis *[,a], Charles S. Harden [a], Donald B. Shoff [a], Suzanne E. Bell [b], Gary A. Eiceman [b], Robert G. Ewing [b]

[a] *U.S. Army Edgewood Research, Development and Engineering Center, Aberdeen Proving Ground, MD 21010-5423, USA*
[b] *Department of Chemistry and Biochemistry, New Mexico State University, Las Cruces, NM 88003-0001, USA*

(Received 2nd August 1993; revised manuscript received 10th November 1993)

Abstract

A central issue in the utilization of ion mobility spectrometry for chemical analysis is the proper interpretation of ion mobility spectra and the assignment of peak identities. Ion mobility spectra for contemporary drift tubes generally produce broad peaks and simple patterns without obvious details associated with structures. These features can hinder the analyses of spectra derived from mixed vapors. However, additional information from such spectra can be extracted through Gaussian deconvolutions. A deconvolution algorithm was examined for sensitivity toward parameters and for boundaries of operation using ion mobility spectra from binary mixtures. An ion–molecule cluster ion, not obvious in traditional spectra analysis, was disclosed by deconvolution analysis and confirmed by independent ion mobility spectrometry–mass spectrometry.

Key words: Mass spectrometry; Ion mobility spectrometry; Gaussian deconvolution

1. Introduction

Modern analytical ion mobility spectrometry (IMS) [1,2] is based on the drift of gas phase ions in the presence of a weak electric field through air or nitrogen at constant temperature and pressure. When an electric field is applied uniformly, ions move along the field lines, with an average drift velocity, v_d (cm/s), which is proportional to the electric field strength, E (V/cm), and the constant of proportionality is defined as the ion mobility, K ($cm^2/V \times s$) per Eq. 1.

$$v_d = K \times E \quad (1)$$

Ion mobility is dependent upon both the size and structure of the ions and the neutral gas through which the ions pass. Collisional interactions between the sample and drift gas molecules are the crucial factors determining the ion mobility in an IMS. Since IMS is performed at, or near, atmospheric pressure, comparisons between spectra require using normalization through a "re-

* Corresponding author.

SSDI 0003-2670(93)E0691-Y

duced mobility" K_0, which is the ion mobility at 760 Torr and 273 K per Eq. 2,

$$K_0 = K \times 273/T \times P/760 \quad (2)$$

where T and P are the temperature and pressure at which the ion mobility spectrum was recorded.

The drift tube of an IMS instrument is continually swept with air or nitrogen, to clear neutral sample molecules from the drift tube, and to serve as the drift gas of the instrument. The most common form of primary ionization is by β-particle radiation from a ^{63}Ni foil in the reaction region of the IMS cell. A series of cascading reactions progresses [1] and results in the formation of a set of reactant ions. Sample vapors are introduced into the reaction region via a carrier gas where reactant ions collide with sample vapor molecules and product ions are formed. The predominant mechanism of formation for positive ions is proton transfer from $(H_2O)_nH^+$ reactant ions to the sample molecule. This is followed by a number of possible complex reactions which include reactions with additional sample molecules present, reactions with water vapor molecules, and reaction with other neutral molecules present in the reaction region of the mobility spectrometer. Product ions containing one analyte molecule are refefred to as "monomers", two analyte molecules, "dimers", etc.

Ions are injected into the drift region of the instrument using an electric shutter. Characteristic constant velocities are attained for particular ions which form a near-Gaussian distribution during drift tube traversal [3]. At the end of the drift region, ions strike a collector electrode (Faraday cup) and a weak source signal (typically 10–100 pA) at a frequency of 30–40 Hz results. The structure and function of a typical ion mobility spectrometer and features of a typical spectrum are illustrated in Fig. 1.

The chemical environment of IMS is complex and the ion–molecule reactions are competitive. Neutral sample molecules compete with reactant ions and product ions for protons. In mixtures, relative concentrations and relative proton affinities will determine which species survive to detec-

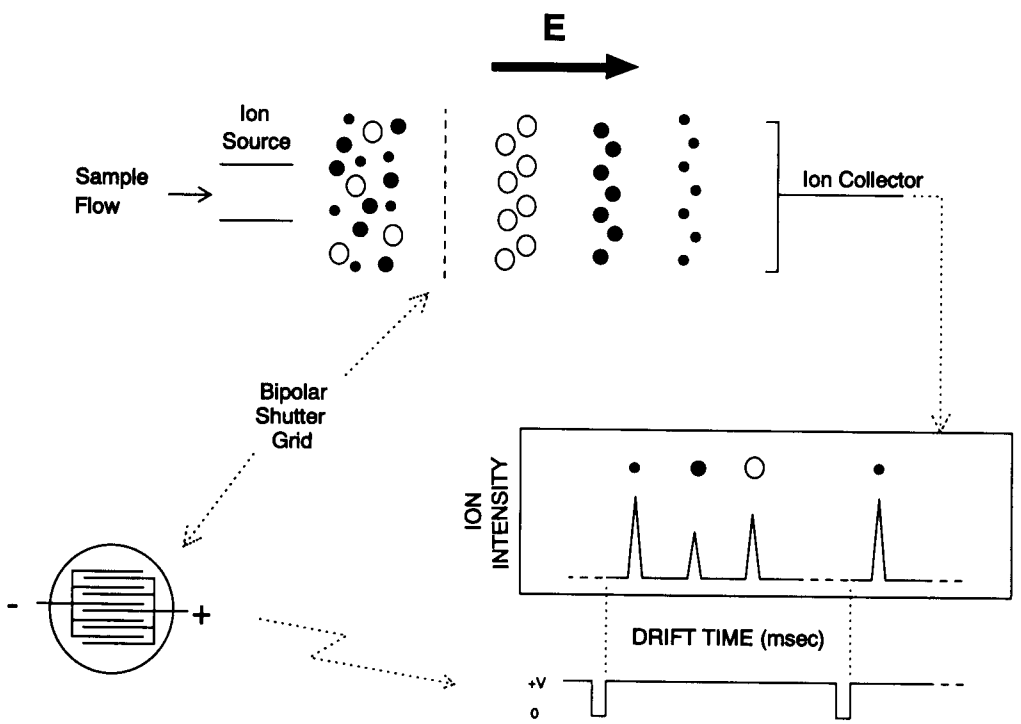

Fig. 1. Schematic diagram of an ion mobility spectrometer showing the typical shape of the sample gating pulse.

tion. IMS spectra of mixtures thus usually represent a non-linear combination of individual spectra depending on experimental variables. The formation of heterogeneous species, primarily mixed dimers, is a concern to the analyst and complicates the interpretation of spectra. Unlike infrared spectroscopy, near-infrared spectroscopy, ultraviolet spectroscopy, and gas chromatography (GC), all areas in which deconvolution has been useful and chemical interactions within the gas mixtures are generally assumed to be absent, it is the potential for significant chemical interaction among the mixture components which makes deconvolution of IMS spectra an attractive technique. Thus, development of a deconvolution program capable of detecting possible heterogeneous ion/molecule clusters in an ion mobility spectrum would be particularly valuable.

Essential parameters which define IMS spectral features are the peak intensity, peak drift time, peak width defined as full-width at half maximum (FWHM), and peak shape distortions. Factors that distort normal velocity distributions or peak profiles include the initial event of ion injection, ion–ion repulsions [4,5], and ion-molecule reactions [6] in the drift region. The latter two effects can be minimized through control of the ion injection process, however, peak width is mainly dependent on diffusion processes [7].

The gating pulse, which produces the ion injection into the drift region, has traditionally provided an electrical trigger for synchronization of signal processing via digital signal averaging. The gating pulse duration is also critical in determining both peak shape and the sensitivity of the IMS. For example a narrow gating pulse which introduces small ion packets into the drift region, limits ion–ion repulsions and minimizes band broadening in the spectra. The drawback to shorter gating pulses is that the intensity of the response is also curtailed. Longer gating pulses, on the other hand, improve the intensity of the response, but sacrifice resolution because of the increase in band broadening. The practical significance is that most modern ion mobility spectrometers provide low resolution [8], i.e. large FWHM values, with specialized high resolution IMS systems only recently being introduced [9]. The larger values for FWHM have not precluded useful applications [1,2] of ion mobility spectrometry when individual vapors are characterized, but even simple mixtures yielding multiple ion peaks [10] present challenges in spectral interpretation.

One solution for improving IMS resolution is pre-separation of mixtures using a gas chromatograph as the sample inlet to the IMS [11,12]. In many in situ applications, this is neither desirable nor feasible. GC is not a guarantee of complete isolation of individual mixtures as is the case with co-eluting chromatographic peaks. A second alternative is to manipulate the selectivity of the spectrometer itself using alternate reactant ions [13]. Judicious selection of reagent ions based on proton affinity is an effective method of controlling the chemistry in the reaction region of the instrument [14]. This approach is most practical when specific target compounds are known and the sample matrix is well characterized. Yet another alternative, the subject of this paper, is to devise an algorithm for spectral interpretation which is applicable to both single component and mixtures. Such an algorithm would allow more independence from instrumental and sample matrix conditions.

Contribution to the FWHM of a mobility peak from the shutter pulse arises from the duration and shape of the gating pulse, and is easily calculated from existing theoretical constructs. However, FWHM is complicated by variables including drift tube temperature, pressure, drift gas purity (e.g., humidity), ion mass and structure, and ion-molecule reactions in the IMS cell. Such contributions must be determined empirically for every ion in a spectrum, a condition that is unacceptable to prospective users of IMS. Alternatively, effective resolution might be improved through the application of algorithms based upon Gaussian deconvolution to minimize the effects of both controlled and uncontrolled variables.

In this study, composite spectra arising from binary mixtures were analyzed. The system selected for these studies, pentanal and propyl acetate, is typical of co-eluting peaks from a gas chromatograph–ion mobility spectrometer designed to monitor volatile organic compounds in

recycled atmospheres. These two compounds, pentanal and propyl acetate, were selected because proton affinities (10.04 and 9.74 eV, respectively [15]) are such that protonated species, monomers and dimers, are readily formed from both compounds thus creating conditions where the formation of heterogeneous cluster ions is likely. The ion mobilities of product ions are similar thus providing a good test set for the deconvolution algorithms that were developed for these studies. Moreover, pentanal and propyl acetate polarities favor drift tube reactions [6] which could serve to further complicate the spectral peak shapes. For field applications, this binary system would represent a challenging scenario for GC–IMS data reduction, i.e. compounds with similar GC retention times, similar ion–molecule reactivity based on proton affinity considerations, and similar ion mobility spectra.

The primary objective for this study was to determine the ease and reliability with which IMS spectra can be resolved for simple mixtures using spectral deconvolution software. Another interest was to evaluate the sensitivity of a Gaussian deconvolution algorithm toward parameters such as deconvolution peak width, number of deconvolution iterations and interpolation factors using the methods developed by Van Cittert [16], Jansson and co-workers [17-19], Willson and Edwards [20], and Blass and Halsey [21].

2. Experimental

2.1. Instrumentation

The ion mobility spectrometer used to obtain spectra was a prototype high speed gas chromatograph–ion mobility spectrometer called the Volatile Organic Analyzer (VOA, Graseby Ionics, Watford). The drift tube was heated to 150°C and was interfaced with the gas chromatograph through an on-axial design [22] with a 10 m nonpolar capillary column. The gas chromatograph was a Model 2000 (Microsensor Technology, Fremont, CA) modified with an automated air sampling trap, thermal desorption trap, temperature program elements, and software/hardware interface to a MacIntosh portable computer. The hardware and software interfaces, not commercially available, were custom built at Louisiana State University at the Environmental Studies Program and allowed microprocessor control of all GC parameters. Spectra from the ion mobility spectrometer were collected on a IBM-compatible 80386 25 MHz personal computer using digital signal averaging boards and Advanced Signal Processor software (ASP, Graseby Ionics). Conditions for analysis are summarized in Table 1.

Table 1
GC–IMS parameters

Gas chromatograph	
Carrier gas	Helium
Flow rate	Set by pressure
Temperature program	40–140°C, 0.7°C/min
VOA operation	
Drift gas	Air
Sheath flow rate	60 ml/min
Cell flow rate	300 ml/min
VOA data acquisition	
Number of waveforms averaged	4
Number of samples	640
Frequency	40 kHz
VOA shutter pulse	
Frequency	40 Hz
Delay	0 μS
Width	200 μS
Source	Internal

Data acquisition was initiated at the midpoint of the gating pulse. A spectrum of n, user defined, number of data points was collected at a specified sampling frequency. In practice, an analog signal is converted with a flash analog-to-digital converter (ADC) which has twelve bit resolution. The spectra are stored in binary format and can be converted to ASCII format as required. All chromatograms and ion mobility spectra in this study were collected in positive polarity.

Confirmation of dimer and mixed dimer identity was performed on a PCP Model MMS-290 (PCP, West Palm Beach, FL) ion mobility spectrometry–mass spectrometry system (IMS–MS) in which the IMS cell was operated at 150°C. Mass

Table 2
Deconvolution parameters

Parameter	Default setting
Number of iterations	200
Interpolation factor	1
Threshold for peak ID	0.02%
Gaussian FWHM	12
Number of smoothes	1

spectra and ion mobility spectra for pure components and mixtures were obtained in the positive polarity mode only.

The deconvolution program, written in Microsoft Fortran, Version 4.0 (Microsoft Corporation, Redmond, WA), allowed for the variation of the deconvolution parameters. Typical parameters are shown in Table 2. When variation of a parameter was performed, all other parameters were fixed to the remaining values shown in Table 2.

2.2. Chemicals

Reagent grade pentanal and propyl acetate (Polyscience Kits, Niles, IL) were used as obtained from the manufacturer and without further purification. Samples were prepared by injecting varying amounts of sample into one-liter Tedlar bags from which vapors were drawn into the sampling loop of the GC–IMS system. Several mixtures of different ratios of the two compounds were studied, with all concentrations being in the low parts-per-million (ppm, volume) in air concentration range. Concentration ratios ranged from 1:0.2 to 1:30 (pentanal–propyl acetate). Pure pentanal and propyl acetate in the same concentration range were examined as well. Relevant chemical and chromatographic characteristics of the two compounds are given in Table 3.

2.3. Pre-processing of the IMS spectra

Ion mobility spectra are generally normalized with respect to variations in temperature and pressure per Eq. 2. This normalization to the reduced mobility can only be performed when all experimental parameters are known, and field evaluation does not always easily lend itself to full knowledge of these parameters. Preprocessing is an important step, because it is generally not feasible to provide strict control over temperature, pressure, and drift gas purity. Compensation for this lack of control may be achieved by utilizing the drift time of the reactant ion peak and referencing all other data points to its location [23]. At 150°C, the protonated water species $(H_2O)_nH^+$ where n is 2, 3, or 4 is the reactant ion species [24]. Since the velocity of the ions is defined as the length of the IMS drift tube divided by the time required to traverse that distance, it can be shown that the ratio of drift times is equivalent to the inverse ratio of the reduced mobilities [21]. This ratio of drift times, and reduced mobilities, will only hold true if there is no change in reactant ion species. Thus, some care must be given to preserve the identity of the reactant ion species, by insuring that temperature, pressure and relative humidity of the IMS does not drastically change over the course of the experiment. Obtaining a ratios of drift times of the product ions to those of the reactant ions results in a normalized, dimensionless x-axis (drift time ratio) from which the spectral information may the be obtained.

In addition to the normalization of the spectra with respect to the location of the reactant ion, some type of smoothing of the data must be performed. The smoothing of the spectra attenuates the high frequency components of spectra normally associated with noise resulting in a reduction in the number of sharp features in the spectra. The deconvolution process, on the other hand, enhances the high frequency components of the spectrum. If the smoothing step is not performed, false features which are caused by noise may be noted in the deconvoluted spectra.

Table 3
Chemical and chromatographic characteristics

Compound	GC retention time (Ms)	Proton affinity [26] (eV)
Propyl acetate	129.28	10.04
Pentanal	129.68	9.74

A more detailed description of the effect of noise on the deconvolution process is discussed elsewhere [19]. In this study, a nine point Savitsky-Golay algorithm was employed [23] to achieve the necessary smoothing.

3. Results and discussion

3.1. Evaluation of deconvolution parameters

A practical issue in Gaussian deconvolution is the selection of the parameters used to perform the deconvolution. These parameters affect the accuracy and reliability of the deconvolution as well as the amount of time needed for the deconvolution. The parameters which affect the deconvolution are the FWHM data of the Gaussian used in the deconvolution, the degree of interpolation used, and the number of successive iterations used in the deconvolution.

In an iteration, a spectrum is convoluted by a Gaussian function. The spectrum to be convoluted is the original spectrum for only the first iteration. The new spectrum is subtracted from the original spectrum which entered the convolution iteration and a third spectrum, a difference spectrum, is created. The difference spectrum is then added to the original spectrum and a deconvoluted spectrum is obtained, completing the iteration. This deconvoluted spectrum is then used as the input to the next iteration, as necessary. Each iteration creates an improved deconvoluted spectrum at the expense of time or CPU access.

Full-width half maximum

The quality of spectra attained from a Gaussian deconvolution depends upon the widths of individual ion profiles and the widths of the shutter pulse, i.e. the sum of widths of all the ion profiles. Selection of the anticipated width, or FWHM here, for use in the Gaussian function should alter the deconvoluted spectra and values from 7–15 at. unit intervals were evaluated. Results from the deconvoluted spectrum of a mixture of pentanal and propyl acetate are shown in Fig. 2. The spectra were scaled with respect to the intensity of the reactant ion for each spectrum.

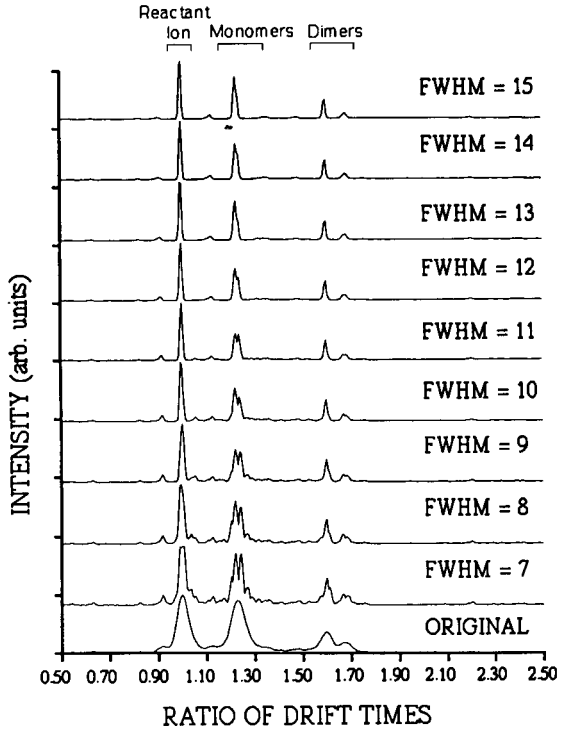

Fig. 2. Ion mobility spectrum of 1 ppm propyl acetate and 5 ppm pentanal in the volatile organic analyzer showing the effect that the full width at half maximum of the deconvoluting Gaussian has on the results.

The measured effect with ion mobility spectra from FWHM was consistent with theoretical expectations and a narrow function resulted in the creation of a large number of peaks in deconvoluted spectra (Fig. 2). These results must be carefully balanced with known or anticipated chemical reality. For example, the reactant ion or product ion may contain multiple ion species [24], such as $H^+(H_2O)_m$ or $H^+(A)_2(H_2O)_n$ where A is the analyte, but these species are in rapid localized equilibrium [6] and appear as only a single reactant ion or product ion peak, respectively, in a spectrum. Consequently, the appearance of multiple deconvoluted peaks may be suggestive of an artificial situation or of a function too sensitive for practical use.

Examination of the deconvoluted spectra for the reactant ion, Fig. 2, shows a definite splitting of the most intense peak for a FWHM of 7, and a deformation of that peak for a FWHM of 8. At larger values for FWHM, the secondary information is diminished and the deconvoluted spectra were qualitatively acceptable for FWHM values of 10–15. The product ion spectra shown in Fig. 2 suggest that FWHM values of 7–12 produce deconvoluted spectra that mirror trends with the reactant ion peak. When individual peaks in the pure components were examined (spectra not shown), it was noted that the FWHM of the peaks was not constant over the spectrum, as had been previously reported [25]. The reactant ion peak, and the monomer peaks of both pentanal and propyl acetate have a FWHM of 10 data points, while the dimers of the pentanal and propyl acetate have a FWHM of 12 data points. The implication is that FWHM of choice for the deconvolution must be greater than, or equal to, the widest pure component peak being examined; with an understood caveat of not compromising real spectral information. Precise criteria for acceptance or rejection have not been formulated; peak acceptability and selection is still somewhat subjective. Examination of the original and deconvoluted spectra resulting from a mixture of pentanal and propyl acetate (Fig. 2) provided no additional benefit in formulating selection criteria.

Comparison of the spectra in Fig. 2 revealed that as the FWHM value increased from 8 to 12 a slight decrease occurred in the peak height of the monomer ion for pentanal, the monomer ion with the greater ratio of drift times. At FWHM values of 13 to 15 this peak underwent a marked decrease, and the peak was non-existent at FWHM values of 14 and 15.

In summary, FWHM values of the widest pure component peak should be considered as a compromise for the selection of the FWHM of the Gaussian functions pending the verification of the multiple peaks with high resolution mobility spectrometers which are not yet readily available. It may even be necessary to vary the FWHM as a function of drift time ratio to ensure that peaks are not under-resolved.

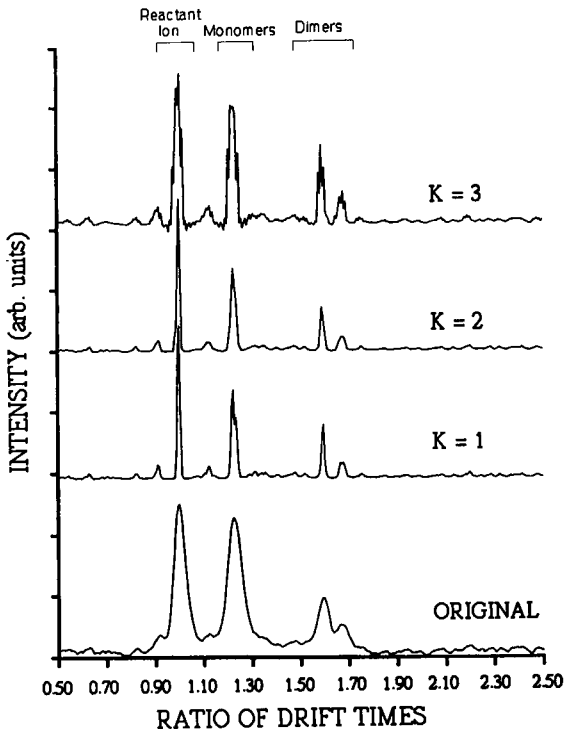

Fig. 3. Ion mobility spectrum of 1 ppm propyl acetate and 5 ppm pentanal showing the effect that changing the interpolation factor has on the deconvolution. The spectrum is deconvoluted using a Gaussian with FWHM = 12 data points.

Interpolation factors

The second parameter affecting the deconvolution is the use interpolation during the iterations. For each iterative step, the correction to the spectrum is calculated for every K^{th} data point, and interpolation is used to calculate the correction for each of the intervening data points. Interpolation would be used in the deconvolution to decrease the amount of time taken to perform the deconvolution. This decrease in deconvolution time is achieved by reducing the number of multiplications and additions performed in the analysis.

The results for using interpolating factors of J from 1 to 3 are shown in Fig. 3; the FWHM of the Gaussian used in the deconvolution was 12 data points. It is obvious from examining Fig. 3 that increasing the interpolation factor increased the inaccuracy of the deconvolution. This may

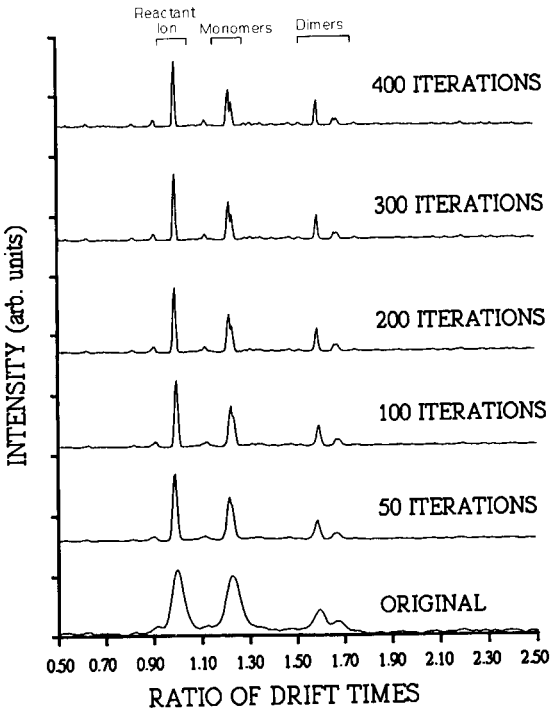

Fig. 4. Ion mobility spectrum of the reactant ion in the volatile organic analyzer showing the effect that the number of deconvolution iterations has on the results.

result in increased splitting of the peaks as shown for interpolation using every third data point, or a reduction of the splitting as shown for interpolation using every second data point on smaller peaks. Because the accuracy of the deconvolution is of prime importance, an interpolation factor of 1 is preferable, but a value of 2 may be used if computation time is also considered to be of great importance.

Number of iterations

The third parameter affecting the deconvolution is the number of iterations performed. The effects of changing the number of iterations on the resultant spectra are illustrated in Fig. 4. For this part of the study, a FWHM for the deconvoluting Gaussian of 12 data points and an interpolation factor of 1 were used. For the spectral peaks associated with the analyses of single components there was relatively little difference noted as the number of iterations was increased. For brevity, individual component spectra are not shown but the reactant ion peak in Fig. 4 is indicative of these observations. For peaks where mixtures are likely to occur, or where heterogeneous dimers are likely to be observed, or where ion–molecule clustering reactions may occur, there is a definite increase in the amount of information that can be seen in the spectrum as the number of deconvolution iterations is increased, as shown in Fig. 4. Close examination of the spectra in Fig. 4 results in the determination of the point where increasing the number of iterations no longer allows any new information to be realized for the system under study. The point of diminishing returns for the pentanal–propyl acetate system was realized at about 200 iterations.

3.2. Analysis of pentanal–propyl acetate system

Optimum, albeit somewhat subjective, values of interpolation factor, number of iterations, and FWHM of the Gaussian for the individual analyses of pentanal and propyl acetate were applied to the analysis of mixtures of these compounds; these were the values listed in Table 2. The ratios of drift times for peaks which were present in the spectra of a binary mixture consisting of 5 ppm pentanal and 1 ppm propyl acetate are given in Table 4. The raw and deconvoluted spectra of this mixture are shown in Fig. 5. From the data in

Table 4
Peaks in the spectrum after deconvolution

	Ratio of drift times		Peak identity
	for the original spectra	for the deconvoluted spectra	
From the spectra of individual compounds	1.00	1.00	Reactant ion $H^+(H_2O)_n$
	1.21	1.21	Propyl acetate monomer
	1.24	1.24	Pentanal monomer
	1.60	1.61	Pentanal dimer
	1.68	1.67	Propyl acetate dimer
From the mixture spectrum	1.00	1.00	Reactant ion
	–	1.21	Propyl acetate monomer
	1.23	1.24	Pentanal monomer
	1.60	1.61	Pentanal dimer
	–	1.66	Mixed dimer
	1.67	1.68	Propyl acetate dimer

Table 4, and the deconvoluted spectra it can be seen that deconvolution separated the spectral features associated with the pure components, and also revealed the possible presence of interactions between the various components of the system, i.e., the mixed dimer denoted by the asterisk in Fig. 5. In addition, the monomer peak at a drift time ratio of 1.23 in the original mixture spectrum was identified as a pentanal monomer but, in reality, was both monomer species as indicated in the deconvoluted spectrum.

Deconvoluted spectra of mixtures of 7 ppm pentanal and 1 ppm propyl acetate (spectrum a) and of 2 ppm propanal and 3 ppm propyl acetate (spectrum b) showed no spectral features that could be indicative of a mixed dimer. This observation leads to one of two conclusions: either the pentanal–propyl acetate mixed dimer exists only over a narrow range of concentrations and concentration ratios, or the appearance of the "mixed dimer" peak in Fig. 4 is an artifact of the deconvolution routine.

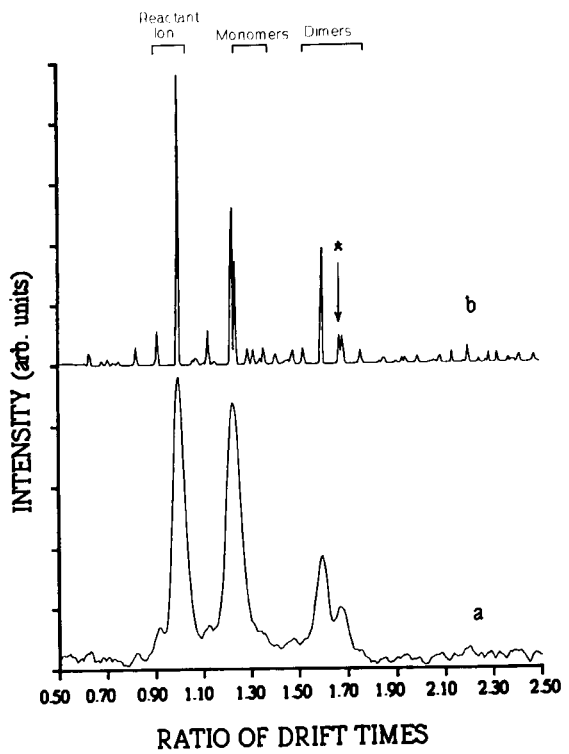

Fig. 5. IMS spectrum of 5 ppm pentanal and 1 ppm propyl acetate. Spectrum (a) is the raw spectrum, and spectrum (b) is the deconvoluted spectrum. The asterisk in spectrum (b) indicates the mixed dimer peak.

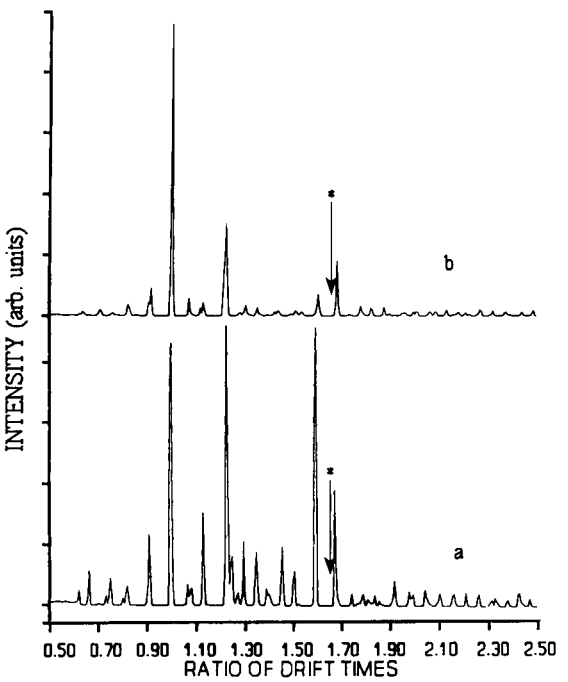

Fig. 6. Deconvoluted IMS spectrum of mixtures of pentanal and propyl acetate. Spectrum (a) is of 7 ppm pentanal–1 ppm propyl acetate and spectrum (b) is of 2 ppm pentanal–3 ppm propyl acetate. The asterisk marks the expected location of a mixed dimer peak.

To determine if the new peak is real, or an artifact of the deconvolution, the ionic species contributing to the ion mobility spectra of the propyl acetate/pentanal system were subjected to analyses by IMS and mass spectrometry (IMS–MS) in a manner which has been previously described [24]. Concentrations and concentration ratios used in the IMS experiment were duplicated. Ion mobility spectra and mass spectra were obtained for mixtures that were created by injecting varying amounts of pentanal and propyl acetate into the IMS–MS ionization chamber. Mass-to-charge ratios of ionic species that were observed pentanal, propyl acetate, and pentanal–propyl acetate mixtures are given in Table 5. IMS–MS shows the presence of a heterogenous dimer, or a mixed dimer, at $m/z = 189$. This

Table 5
Ions found using IMS–MS

Compound	m/z	Drift time ratio	Identity
Pentanal	87	1.24	$(C_5H_{10}O)H^+$
	173	1.61	$(C_5H_{10}O)_2H^+$
Propyl acetate	103	1.21	$(C_5H_{10}O_2)H^+$
	205	1.68	$(C_5H_{10}O_2)_2H^+$
5 ppm Pentanal–	87	1.24	$(C_5H_{10}O_2)_2H^+$
1 ppm propyl	103	1.21	$(C_5H_{10}O)H^+$
acetate	173	1.61	$(C_5H_{10}O_2)H^+$
mixture	189	1.66	$(C_5H_{10}O)_2H^+$
	205	1.68	$(C_5H_{10}O)(C_5H_{10}O_2)H^+$ $(C_5H_{10}O_2)_2H^+$

mixed dimer was found only for a mixture of pentanal and propyl acetate where the concentration of pentanal was 5 ppm and the concentration of the propyl acetate was 1 ppm. Under conditions where either of the concentrations was increased, or decreased, the mixed dimer was not observed. Thus, the mixed dimer does exist, but only over a narrow range of concentrations and ratios. The presence of this mixed dimer, which was revealed through the use of Gaussian deconvolution was shown to be real, not an artifact of the deconvolution.

4. Conclusions

Gaussian deconvolution is a powerful tool for enhancing the amount of information which can be obtained from an IMS spectrum. The technique can be used to separate IMS peaks where ion drift times differ by as little as 100 μs, resulting in spectra which are more easily identified. In addition to increasing resolution of peaks in relatively pure samples, Gaussian deconvolution may be used to more accurately describe the ion molecule reactions which occur in a chemical system by isolating mixed dimer peaks from those dimers found in pure samples. Gaussian deconvolution allows the ion mobility spectrometrist to use the high sensitivity advantages offered by wide sample gating pulses without sacrifice of the information content of the IMS spectrum.

References

[1] H.H. Hill, Jr. and R.H. St. Louis, Crit. Rev. Anal. Chem., 21 (1990) 321.
[2] G.A. Eiceman, Crit. Rev. Anal. Chem., 22 (1991) 17.
[3] A.H. Lawrence and R.A. Goubran, Int. J. Mass Spectrom. Ion Processes, 104 (1991) 163.
[4] G.E. Spangler and C.I. Collins, Anal. Chem., 47 (1975) 403.
[5] M.L. Glasser, J. Appl. Phys., 63 (1988) 4823.
[6] J.M. Preston and L. Rajadhyax, Anal. Chem., 60 (1988) 31.
[7] H.E. Revercomb and E.A. Mason, Anal. Chem., 47 (1975) 970.
[8] P. Watts and A. Wilder, Int. J. Mass Spectrom. Ion Processes, 112 (1992) 179.
[9] J.L. Brokenshire, 1991 Joint Meeting FACSS/Pacific Conference 27th Western Regional ACS Meeting, Anaheim, CA, Oct. 1991.
[10] G.A. Eiceman, D.A. Blyth, D.B. Shoff and A.P. Snyder, Anal. Chem., 62 (1990) 1374.
[11] A.P. Snyder, C.S. Harden, A.H. Brittain, M.-G. Kim, N.S. Arnold and H.L.C. Meuzelaar, Am. Lab., 24 (1992) 32B.
[12] A.P. Snyder, C.S. Harden, A.H. Brittain, M.-G. Kim, N.S. Arnold and H.L.C. Meuzelaar, Anal. Chem., 65 (1993) 299.
[13] G.A. Eiceman, M.R. Salazar, M.R. Rodriguez, T.F. Limero, S.W. Beck, J.H. Cross, R. Young and J.T. James, Anal. Chem., 65 (1993) 1696.
[14] G.A. Eiceman, Y.-F. Wang, L. Garcia-Gonzalez and C.S. Harden, Anal. Chem., in press.
[15] S.G. Lias, J.E. Bartmess, J.F. Liebman, J.L. Holmes, R.D. Levin and W.G. Mallard, J. Phys. Chem. Ref. Data, 13 (1984) 695.14.
[16] P.H. Van Cittert, Z. Phys., 69 (1931) 298.
[17] P.A. Jansson, R.H. Hunt and Plyler, J. Opt. Soc. Am., 58 (1968) 1665.
[18] P.A. Jansson, R.H. Hunt and Plyler, J. Opt. Soc. Am., 60 (1970) 596.
[19] P.A. Jansson, J. Opt. Soc. Am., 60 (1970) 184.
[20] P.D. Willson, Ph.D. Thesis, Michigan State University, East Lansing, 1973.
[21] W.E. Blass and G.W. Halsey, Deconvolution of Absorption Spectra, Academic Press, New York, 1981.
[22] H.H. Hill, R.H. St. Louis and W.F. Siems, J. Chromatogr., 479 (1989) 221.
[23] D.M. Davis and R.T. Kroutil, in P.C. Jurs (Ed.), Computer-Enhanced Analytical Spectroscopy, Vol. 3, Plenum Press, New York, 1992, p. 261.
[24] G.A. Eiceman, D.B. Shoff, C.S. Harden and A.P. Snyder, Int. J. Mass Spectrom. Ion Processes, 85 (1988) 265.
[25] A. Savitsky amd M.J.E. Golay, Anal. Chem., 36 (1964) 1627.
[26] G.E. Spangler and J.P. Carrico, Int. J. Mass Spectrom. Ion Processes, 52 (1983) 267.
[27] J.E. Roehl, Appl. Spectrosc. Rev., 26 (1991) 1.

ELSEVIER

Analytica Chimica Acta 289 (1994) 273–290

ANALYTICA CHIMICA ACTA

Fluorimetric studies of some quinones and quinonoid compounds after reduction reaction

Silvia K. de Barros Alcanfôr [1], Stilson V. Cardoso, Clausius G. de Lima *

Departamento de Química, Universidade de Brasília, 70910-Brasília, DF, Brazil

(Received 18th June 1993; revised manuscript received 10th November 1993)

Abstract

In the present work methods for the fluorimetric determination of some quinonic and quinonoid compounds are proposed. These compounds seldom have natural fluorescence or have a very weak fluorescent signal. Primin (2-methoxy-6-*n*-pentyl-1,4-benzoquinone), plumbagin (2-methyl-5-hydroxy-1,4-naphthoquinone), lapachol (2-hydroxy-3-(3-methyl-2-butenyl)-1,4-naphthoquinone), tingenone and pristimerin (the last two triterpenoid quinone methides), compounds with recognized pharmacological activity, were studied from the analytical point of view after reduction with sodium dithionite or sodium borohydride in aqueous ethanolic or in ethanolic medium. Parameters such as effect of solvent, fluorophore stability, acid or base addition, excess reagent, effect of irradiation and in some cases the effect of temperature were evaluated. After optimization the calibration curves and the analytical figures of merit were determined. The limits of detection ranged from 0.16 to 210 ng ml^{-1}.

Key words: Fluorimetry; Quinone, Quinonoid compounds; Reduction reaction

1. Introduction

Several quinonic or quinonoid compounds with interesting chemotherapeutic activity have been isolated from native higher plants [1,2]. The fluorimetric determination of quinones – which frequently are nonfluorescent compounds – is of interest as, according to Poulsen and Birks [3], some of these compounds not only present chemotherapeutic action, but are found in the environment as oxidation products of polycyclic aromatic hydrocarbons, are important in photosynthetic processes in plants and bacteria, act as blood coagulants and are also used in the paper industry [3].

Of the quinonic compounds, those of the vitamin K family (1,4-naphthoquinone derivatives) and in some cases ubiquinones (1,4-benzoquinone derivatives) are certainly the most studied from a fluorimetric point of view. Although most of the published work is devoted to the fluorimetric detection of these vitamins after separation using liquid chromatography (LC) with post-column reaction, some studies have been done in relation to their 'batch' determination [4–7]. One of the earliest methods proposed for the determination

* Corresponding author (at the following address: SQS 106, Bl. C, Apto 604, Brasília, DF 70345-030, Brazil).

[1] Present address: Departamento de Física e Química, Faculdades Integradas da Católica de Brasília, Qs. 07, Lt. 01, EPTC, Taguatinga, 72020, Brasília, Brazil.

SSDI 0003-2670(93)E0687-3

of menadione (vitamin K_3; 2-methyl-1,4-naphthoquinone) is that of Kofler [4] based on the reaction of menadione with *o*-phenylenediamine. Duggan et al. [5] found that menadione, after a reduction reaction, changed into a highly fluorescent product. Another 'batch' method quoted in the literature is that proposed by Veronese et al. [6], when a fluorimetric determination of vitamin K_3 precursors based on their natural fluorescence was proposed. However, as the K vitamins are nonfluorescent, the compounds studied were the water soluble derivatives of 2-methyl-1,4-naphthalenediol, as the corresponding sodium salts of the disulfuric or diphosphoric esters. Based on earlier work, Aaron et al [7] later proposed a photochemical–fluorimetric method for the determination of vitamin K_1 (phylloquinone; 2-methyl-3-phytyl-1,4-naphthoquinone). After examining several solvents, dioxane was found as the most appropriate one. Analog and digital integration methods of data collecting were also compared. Although with both methods a limit of detection of 5 ppb was found, the integration method was more precise.

Phosphorescence analytical properties of vitamin K_1, K_3 and K_5 (2-methyl-4-amino-1-naphthol) at 77 K, were also studied by Aaron and Winefordner [8]; limits of detection ranged from 70 ng ml^{-1} (with vitamin K_3 in methanol–water, 30:70, v/v) to 1500 ng ml^{-1} (with vitamin K_1 in *n*-hexane).

Using LC, K vitamins and some derivatives have been fluorimetrically detected after reduction, using either post-column chemical [9–19], photochemical [3,11] or electrochemical reactions [20–23]. Through chemical reaction, $NaHSO_3 \cdot HCl$ [10], sodium cyanoborohydride [10], sodium borohydride [9,11,15], tetramethylammonium octahydridotriborate [12,13], metalic zinc (in the presence of zinc ions) [16,17], platinum oxide (in the presence of hydrogen) [18] and platinum black catalyst [19] have been used.

In an excellent work, Lefevere et al. [11] examined the photochemical reduction of vitamin K_1 and homologues in conjunction with LC and compared it to the chemical method which uses sodium borohydride. This method was further examined by Poulsen and Birks [3] when many quinones (derivatives of 1,4-naphthoquinone and anthraquinone, etc.) and even some nitroderivatives of polycyclic aromatic hydrocarbons were determined with success. Detection limits in the sub-picogram level were found in many cases.

Quinones derived from the oxidation of benzo[*a*]pyrene were also determined using LC and post-column detection after photochemical reaction. The signals observed after photoreduction were one order of magnitude higher than the original signals from the quinone [24]; in this case, the observed existing signal from the quinone is probably due to the number of condensed aromatic rings still present in the molecule.

Kuo et al. [25] recently described a fluorimetric method for the determination of two derivatives of 1,4-naphthoquinone (2-methyl-3-acetyl-4*H*,9*H*-naphtho[2,3-*b*]furan-4,9-dione and 4*H*, 9*H*-naphtho[2,3-*b*]thiophene-4,9-dione), which are compounds of biological interest, using sodium dithionite, zinc or sodium borohydride. With the latter reagent a much stronger fluorescent signal was found. The method was successfully applied to the determination of these compounds in blood serum.

In the present work we examined the effect of some parameters which in some cases of the preliminary experiments showed to affect the fluorescent signal intensity of some quinonic or quinonoid compounds (Fig. 1) such as primin (2-methoxy-6-*n*-pentyl-1,4-benzoquinone, (I)), lapachol (2-hydroxy-3-(3-methyl-2-butenyl)-1,4-naphthoquinone (III)), plumbagin (2-methyl-5-hydroxy-1,4-naphthoquinone (II)), tingenone (IV) and pristimerin (V), (the latter compounds being triterpenoid quinone methides), using either sodium dithionite or sodium borohydride as reduction reagents.

These compounds have been studied from the chemotherapeutic action point of view and demonstrated antimicrobial and antineoplastic properties [26–38]. Lapachol also showed antiulcerogenic [39] activity. Previous and recent comprehensive reviews and new results [40,41] report other biological properties of lapachol (and several other compounds) after in vitro experiments and clinical trials.

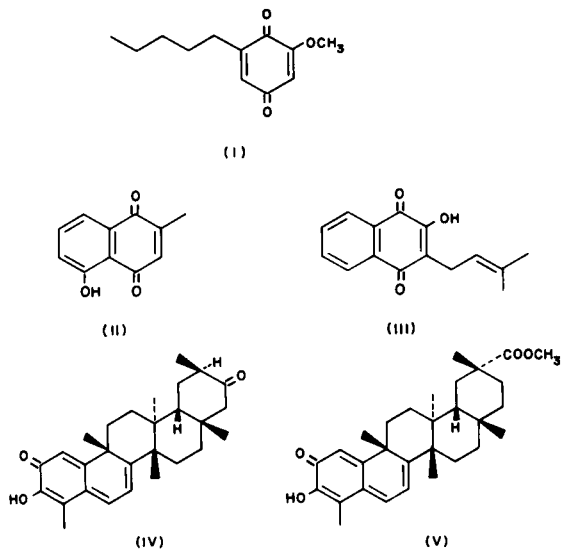

Fig. 1. Structural diagrams of the compounds studied. (I) Primin; (II) plumbagin; (III) lapachol; (IV) tingenone and (V) pristimerin.

Immunostimulatory activity was found with plumbagin [42]. Recently, it was found that the same compound showed an inhibitory action in the development of some parasitic nematodes [43]. Procedures for the fluorimetric determination of lapachol through its reduction, using sodium dithionite, have been previously examined by Finkel and Harrison [44] and Van Damme and De Nève [45]. In these cases the reduction product was extracted (either with benzene [44] or with butyl acetate [45]) and the fluorescent signal was examined from the organic layer. In [44] a linear range between 0.03 μg ml^{-1} (the limit of the detection) and 0.9 μg ml^{-1} was found. A λ_{max} of excitation and emission at 340 and 410 nm were also found. This procedure was applied to the determination of lapachol added to serum. In 'real samples' a fluorimetric technique was used for the determination of lapachol in blood plasma in the range of 5.4–35 μg ml^{-1} during early clinical trials [46,47].

In [45] a study was carried out in relation to the fluorescent assay of lapachol and several other hydroxynaphthoquinones, including plumbagin. Three methods were examined (reduction with sodium dithionite, reduction with stannous chloride, followed by extraction with chloroform, and the reaction of the quinones with cyanide, based on a previous work by Guilbault and Kramer [48]. With the first method both lapachol and plumbagin gave a limit of detection of *ca.* 0.019 μg ml^{-1}. The λ_{max} values were at 345 and 430 nm (for lapachol) and 350 and 375 nm (for plumbagin), excitation and emission respectively. The second method showed to be specific for 5-hydroxy-1,4-naphthoquinones (juglone and plumbagin). In this case the limit of detection for plumbagin was 0.016 μg ml^{-1} and the λ_{max} of excitation and emission was at 397 and 474 nm, respectively. The third method was useful for the 5,8-dihydroxynaphthoquinones.

Recently, Awang et al. [49] proposed a liquid chromatographic method with ultraviolet absorption detection for the determination of lapachol and related naphthoquinones such as α-lapachone, β-lapachone, dehydro-α-lapachone, dehydro-β-lapachone, etc., in plant extracts. Likewise, Marston and Hostettmann [50] proposed a method for the detection of plumbagin and other similar hydroxy-1,4-naphthoquinones (and some dimers) in root bark material of an African medicinal plant.

In the literature examined no fluorimetric methods for the determination of primin, tingenone or pristimerin could be found.

2. Experimental

2.1. Apparatus and reagents

The fluorescent excitation and emission spectra and intensity data were collected using an Aminco-Bowman double monochromator spectrophotofluorometer (SLM Instruments, Urbana, IL) and fused quartz cells. The characteristics of this instrument have already been described in a previous communication from this laboratory [51]. The spectra were not corrected. The instrument was routinely calibrated and the signal intensities corrected using a fluorescent standard from Carl Zeiss (fluorescent standard, F 53, No. 8831, Carl Zeiss, Oberkochen/Wuertt) with λ_{max} of excita-

tion at 425 and emission at 518 nm. The statistical treatment of the data followed a methodology described by Miller and Miller [52] and was made using a hand-calculator (Sharp Instrumentos do Brasil, Manaus). The regression curves were plotted using an Apple-type microcomputer (Spectrum Equipamentos Eletrônicos, São Paulo). Either laboratory-made software [53] (for classical linear or weighed regression) or the Curve Fitter (Interactive Microwave, State College, PA) was used in the regression analysis.

The limits of detection were calculated using the formula $3s_b/m$, where s_b is the standard deviation of the blank ($n = 16$) and m the regression coefficient of the calibration curves [54].

The samples of the pure compounds examined (Fig. 1) were kindly donated by Prof. J.S. de Barros Coelho and Prof. J.F. de Mello (Instituto de Antibióticos, Universidade de Recife) and were used without further purification. Melting points found (uncorrected) were (I) 62.5–64°C (lit. 62–63°C [1]), (II) 73–75°C (lit. 75°C [45]), (III) 139–140°C (lit. 139.5–140.2°C [29]), (IV) 153–155°C (lit. [1] 155–158°C [34,55]) and (V) 212–213°C (lit. 213–214°C [56]). The stock solutions were prepared in absolute ethanol (200 μg ml^{-1}) and serial diluted according to necessity. Analytical grade absolute ethanol (Merck, Brazil) was further purified as previously described [49]. Distilled water was further distilled in a quartz distiller (ultrapure water).

Sodium dithionite ($Na_2S_2O_4$, Aldrich, Milwaukee, WI) was used as received and its content ($86.8 \pm 0.9\%$ found) was determined using an iodimetric method, kindly sent to us by Dr. G.F. Lewis (BDH, Poole). Metabisulfite ($10.4 \pm 0.3\%$ found) and sulfite ($0.45 \pm 0.07\%$ found) were also determined using this method. Most of the solutions of dithionite were prepared in an aqueous ethanolic solvent (ethanol–water, 40 : 60, v/v), but in the case of plumbagin the solvent was water. Previous deoxygenation of the water with nitrogen was beneficial, as dithionite reacts with oxygen. The actual and initial concentration of dithionite in the solutions was 1.5% (w/v) for use in the procedures of primin and lapachol; 0.76% (w/v) for tingenone and pristimerin and 0.4% (w/v) for plumbagin. Small volumes of the dithionite solution were freshly prepared and used immediately due to the dithionite decomposition.

Sodium borohydride, $NaBH_4$ (Merck, Darmstadt) was utilized without further purification. The content of active borohydride ($86.5 \pm 1.4\%$) was determined according to the method of Lyttle et al. [57]. Also, the decomposition with ageing of this reagent in absolute ethanol was followed using this method. After a decrease of 35.5%, the content almost stabilized in the interval examined of 2.5–6 h. Fresh solutions of borohydride were prepared in absolute ethanol with an initial concentration of 1.4% (w/v). As a small amount of reagent is insoluble, the solution was centrifuged (15 min, 1500 rpm, 682 g) and the centrifugate was used. Analytical grade hydrochloric acid and sodium hydroxide (Merck, Brazil) solutions were prepared in absolute ethanol and the titres (ca. 0.1 and ca. 0.01 N, respectively) were determined using classical methods. Other analytical grade reagents were used without further purification.

The volumetric flasks, pipettes and a microsyringe (100 μl, Hamilton, Reno, NV) were previously checked by the common volumetric calibration method. All glassware was washed before use using an HNO_3 (1 : 1, v/v) solution followed by water and purified ethanol.

2.2. Procedures

Primin

Reaction with sodium dithionite. Add to a 10-ml volumetric flask an aliquot of the ethanolic analyte solution (the volume of which should be under 8 ml which results in a final concentration ≤ 20 μg ml^{-1}). A total volume of 8 ml is then obtained by the addition of absolute ethanol [2].

[1] According to Brown et al. [55] and Delle Monache et al. [34] the melting points of tingenone varied from 140 to 240°C depending on the crystallization solvent or the drying procedure.

[2] To obtain the final ethanol–water ratios suggested, the ethanol volume added during the addition of dithionite (and acid) must be taken into consideration, which is a function of the real dithionite concentration (and the acid concentration).

Next, add 0.14 ml of a freshly prepared, aqueous ethanolic dithionite solution (1.5%, w/v), which is equivalent to ca. 12 micromoles addition. Stir the reacting solution gently, and complete the volume with nitrogen deaerated ultrapure water. The final ethanol–water ratio should be 8:2 (v/v). The procedure must be carried out in low luminosity. The reading must be carried out after 5 min.

Reaction with sodium borohydride. Add to a 10-ml volumetric flask an aliquot of the analyte solution (final concentration: ≤ 8 μg ml^{-1}). Then add 30 μl of a sodium borohydride ethanolic solution (1.38%, w/v), which must be used within 90 min after preparation. After that, add 0.80 ml of an ethanolic HCl solution (0.1 N), equivalent to 80 μmol. Complete the volume with absolute ethanol. The reading should be taken in less than 10 min to avoid decrease in the signal due to irradiation.

Plumbagin

Reaction with sodium dithionite. Add to a 10-ml volumetric flask an aliquot (less than 8.26 ml, and also resulting in a final concentration ≤ 5 μg ml^{-1}) of the ethanolic analyte solution. Next add absolute ethanol to a total of 8.26 ml. Then add 87 μl of a freshly prepared solution of sodium dithionite (0.4% in aqueous medium), equivalent to the addition of ca. 2 μmol. Follow this by the addition of 0.65 ml of a 0.1 N ethanolic HCl solution, equivalent to 65 μmol of acid. Complete the volume with nitrogen deaerated ultrapure water. The final ethanol–water ratio must be of 8.9:1.1 (v/v). Carry out the whole procedure under low luminosity. Take the reading after 5 min.

Reaction with sodium borohydride. Transfer to a 10-ml volumetric flask an aliquot of less than 8 ml of an ethanolic analyte solution resulting in a final concentration ≤ 1 μg ml^{-1}. Add 2.0 ml of a borohydride solution, with a maximum ageing time of 60 min and with an initial active concentration of 1.38% (w/v).

After completing the volume with absolute ethanol, the reading should be taken after a stand by time of 5 min.

Lapachol

Reaction with sodium dithionite. Take an aliquot of less than 7.12 ml of an ethanolic analyte solution also resulting in a final concentration ≤ 50 μg ml^{-1}, and transfer it to a 10-ml volumetric flask. Add absolute ethanol to a total volume of 7.12 ml. Then add 0.48 ml of a 1.5% (w/v) freshly prepared aqueous ethanolic dithionite solution, equivalent to ca. 41.4 μmol of dithionite, stir and add 1.2 ml of 0.1 N ethanolic HCl solution (equivalent to 120 μmol). Complete the volume with nitrogen deaerated ultrapure water so that the final ethanol–water ratio is 8.6:1.4. Low luminosity should be provided during the procedure and the reading must be taken after 5 min of reaction.

The transfer of the solution to the quartz cell must be done under a flow of nitrogen, to avoid oxidation of the reduced product.

Reaction with sodium borohydride. Add to a 10-ml volumetric flask an aliquot of less than 5.3 ml of an ethanolic analyte solution also resulting in a final concentration ≤ 1 μg ml^{-1}. Next, add 4.0 ml of an aged (2.5–6 h) sodium borohydride solution (average concentration ca. 0.88 g/100 ml, equivalent to ca. 23.3 mmol/100 ml).

Then add 0.7 ml of an ethanolic HCl solution (0.1 N), which is equivalent to an addition of 70 μmol. Complete the volume with absolute ethanol and take the reading. The whole procedure must be carried out in low luminosity.

Tingenone

Reaction with sodium dithionite. Transfer by pipette to a test tube with a conic end an aliquot of less than 7.0 ml of an ethanolic analyte solution in such a way that a final concentration ≤ 50 μg ml^{-1} should result. Add absolute ethanol to a volume of 7.0 ml. Cover the test tube with a glass stopper and introduce it in a controlled water

bath (80°C) for 5 min. After that add 0.37 ml of a freshly prepared aqueous ethanolic solution of dithionite (0.76%, w/v) equivalent to ca. 16 μmol. After 15 min of heating, cool the tube in an ice bath. After having cooled the mixture to room temperature, transfer it to a 10-ml volumetric flask, immediately complete the volume with deaerated water and take the reading. The final

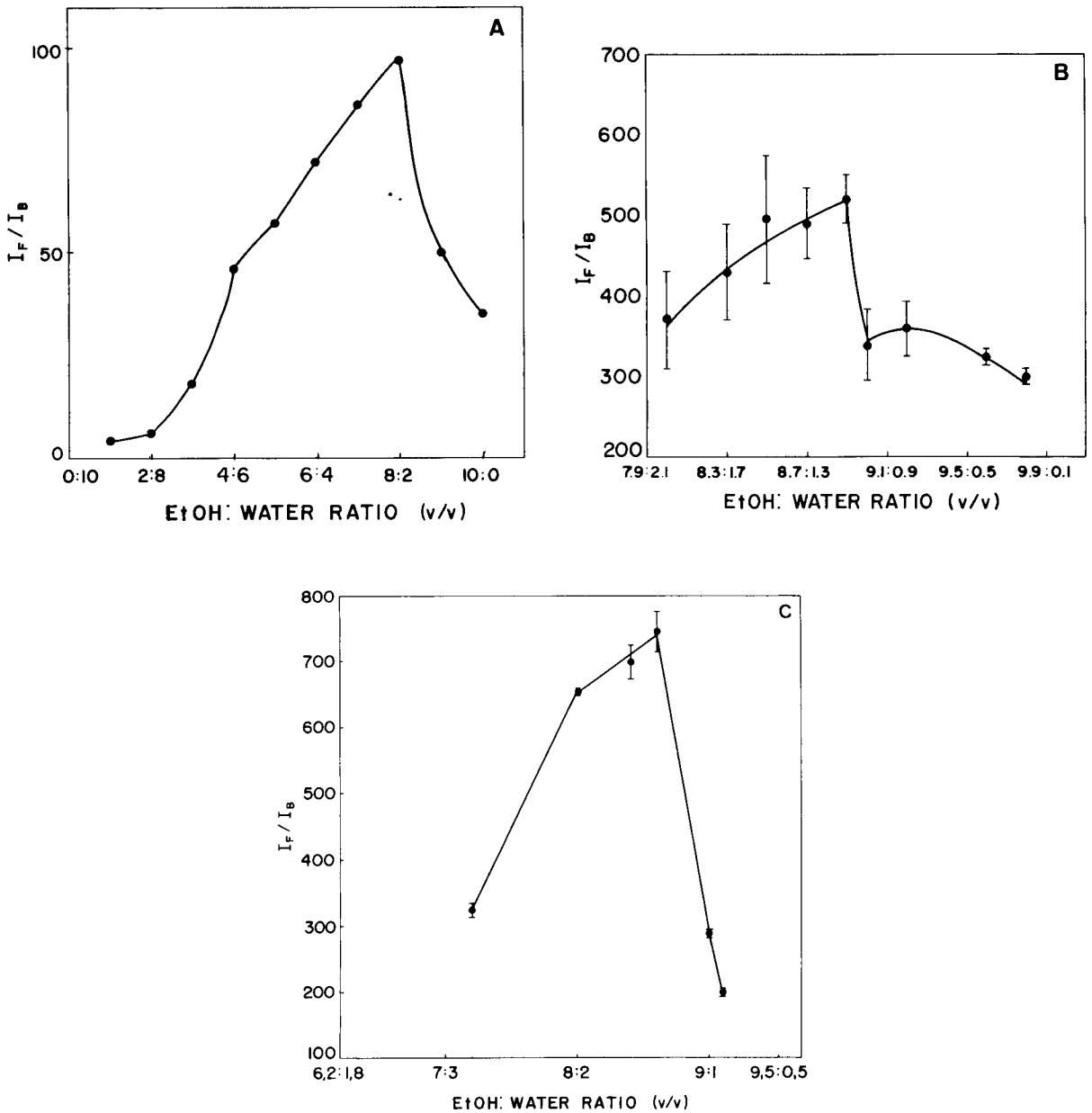

Fig. 2. Effect of the ethanol–water ratio on the I_F/I_B ratio. Fluorescent net signal intensity/background signal intensity of (A) primin; (B) plumbagin and (C) lapachol after reaction with dithionite. The final concentrations of the analytes were ca. 2.4 μg ml^{-1} with plumbagin and ca. 20 μg ml^{-1} with the other compounds.

ethanol–water ratio should be 7:3 (v/v). The whole procedure must be carried out in low luminosity.

Reaction with sodium borohydride. Transfer an aliquot of less than 6.0 ml of the analyte solution of which the final concentration should be ≤ 20 $\mu g\ ml^{-1}$, to a 10-ml volumetric flask. Then add 4.0 ml of an aged sodium borohydride solution (2.5–6 h), with an average concentration of 23 mmol/100 ml. Complete the volume with absolute ethanol, and take the reading.

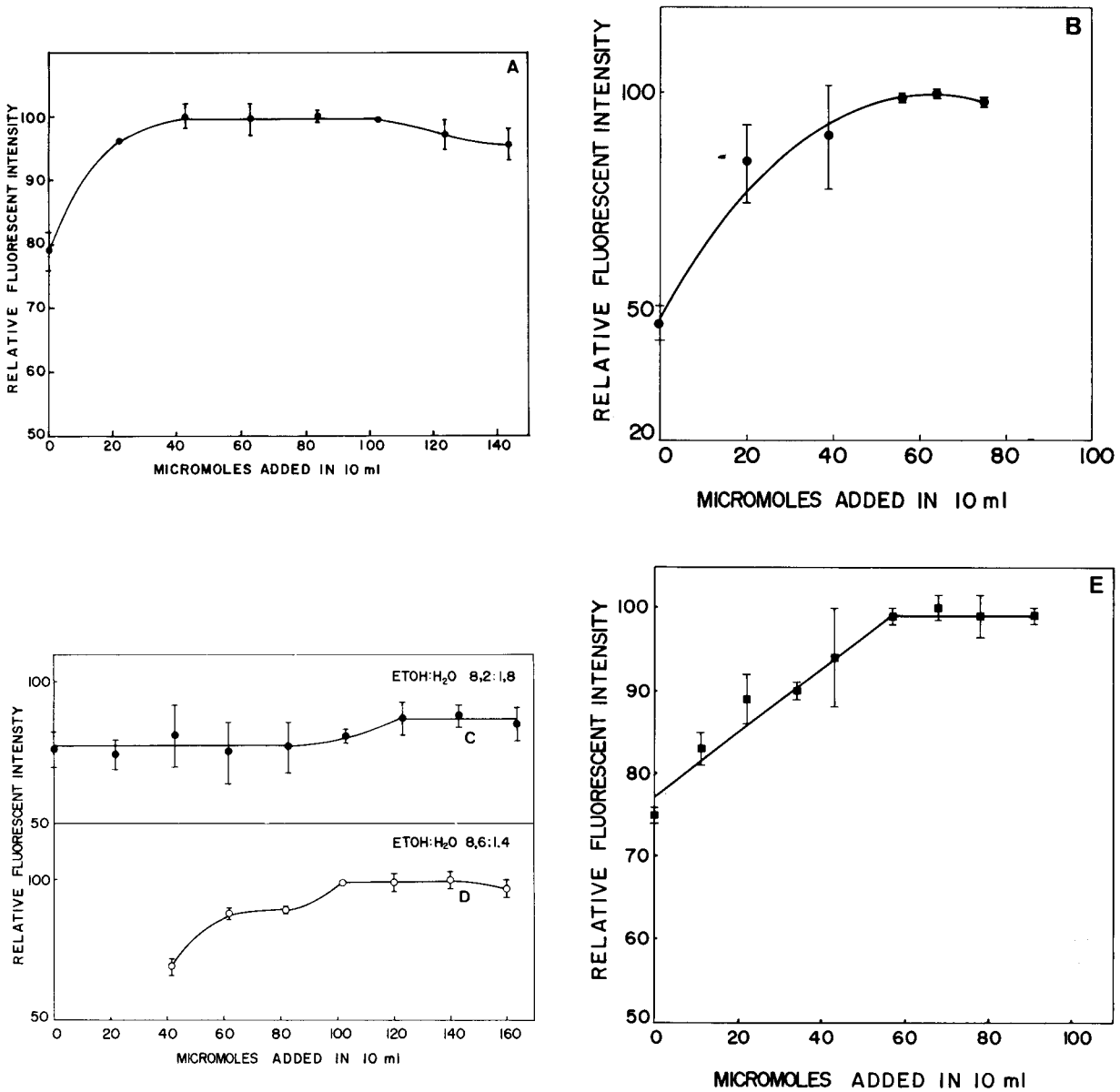

Fig. 3. Effect of acid addition in the systems. (A) Primin/borohydride; (B) plumbagin/dithionite; (C) lapachol with 32.6 μmol of dithionite; (D) lapachol with 41.4 μmol of dithionite and nitrogen blanket during transfer and (E) lapachol/borohydride. Concentrations used: primin, 2.2 $\mu g\ ml^{-1}$; plumbagin, 2.1 $\mu g\ ml^{-1}$; lapachol, ca. 21 $\mu g\ ml^{-1}$.

Pristimerin

Due to the structural similarity between this compound and tingenone the procedure used for tingenone was employed here, except that in the case of the dithionite procedure the aliquot taken should result in a final analyte concentration of less then 30 μg ml^{-1}.

3. Results and discussion

3.1. Reagent solvent and effect of solvent

Ethanol–water (40 : 60, v/v) was used as reagent solvent in most of the cases when dithionite was used, except in the case of plumbagin reduction when dithionite was dissolved in water. In the case of borohydride, absolute ethanol was used to dissolve the reagent, in the reaction and in the final dilution steps.

With dithionite, critical ethanol–water ratios in the final dilution were observed, when it was found that more ethanol than water was necessary.

Fig. 2 shows a group of curves in which the effect of solvent was observed when dithionite was used as reagent. In this study the ratio between the net signal intensity and the background signal intensity (I_F/I_B ratio) was examined. In some cases the background was due to a visible turbidity present in some ratios, which led to the appearance of Tyndall scatter. This scatter appeared either at high ethanol concentration, probably due to dithionite insolubility, or at low ethanol concentration, which is possibly due to analyte (and to the reduced product) insolubility. Most of the curves showed a sharp aspect.

In the case of primin the ethanol–water ratio of 8:2 gave the best result (Fig. 2A). With plumbagin (Fig. 2B) the curve shows a greater fluctuation in the results; nevertheless, an optimum ratio at 8.9:1.1 can be seen. At this ratio the coefficient of variation (C.V.) was ca. 10% when the reading was taken immediately after mixing. If the reading, however, is taken 5 min after mixing, the C.V. decreases to ca. 5%. As the irradiation (at the λ_{ex}), or the diffusion of oxygen, has an adverse effect, the solutions must be exposed in the spectrofluorimeter compartment for a minimum of time. As a result, the readings should be done as quickly as possible, after 5 min standby, in low luminosity.

Fig. 2C shows the effect of the solvent in the signal intensity after the reaction of lapachol with dithionite. In the experiments, a 8.6 : 1.4 ratio was found.

With tingenone, an estimated ratio of ca. 7:3 was found from the experiments. This ratio is estimated, as the reaction is carried out at 80°C and although the test tubes were capped, evaporation of the solvent is still possible, resulting in modification of the solvent composition.

3.2. Effect of acid or base

The addition of small amounts of acid was beneficial with the primin/borohydride, plumbagin/dithionite, lapachol/dithionite and lapachol/borohydride systems. In contrast, the effect of the base was either negative or had no effect in the cases studied.

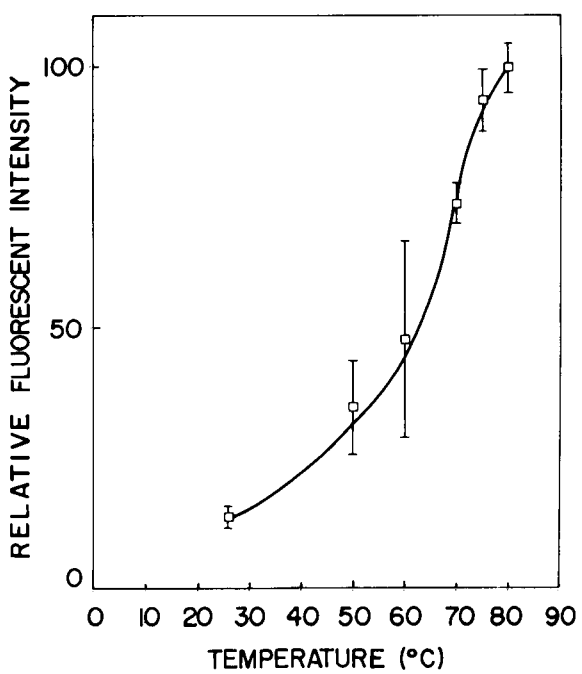

Fig. 4. Effect of temperature on the reaction of tingenone with dithionite. A heating time of 15 min was used, as found in an independent experiment.

Fig. 3 shows the effect of acid, when advantageous. In the reaction of primin with borohydride, the study demonstrated that a plateau was present between ca. 40 and ca. 100 μmol of acid (added in 10 ml) (Fig. 3A), as a result, 80 μmol was recommended in the procedure. With plumbagin/dithionite 65 μmol in 10 ml was deduced from the curve (Fig. 3B), as the results found between 56 and 76 μmol were statistically ($P = 0.95$) equivalent. In the case of lapachol/dithionite, 120 μmol/10 ml was suggested by the experiments (Fig. 3C and D) and 70 μmol/10 ml in the case of lapachol/borohydride (Fig. 3E).

In the first case (lapachol/dithionite), the effect of acid addition was also examined using two ethanol–water ratios (8.2:1.8 and 8.6:1.4, the last one being the optimum) and two different quantities of dithionite (32.6 and 41.4 μmol/10 ml) (Fig. 3C and D). In both cases, 120 μmol of acid provided both a better signal and C.V. This

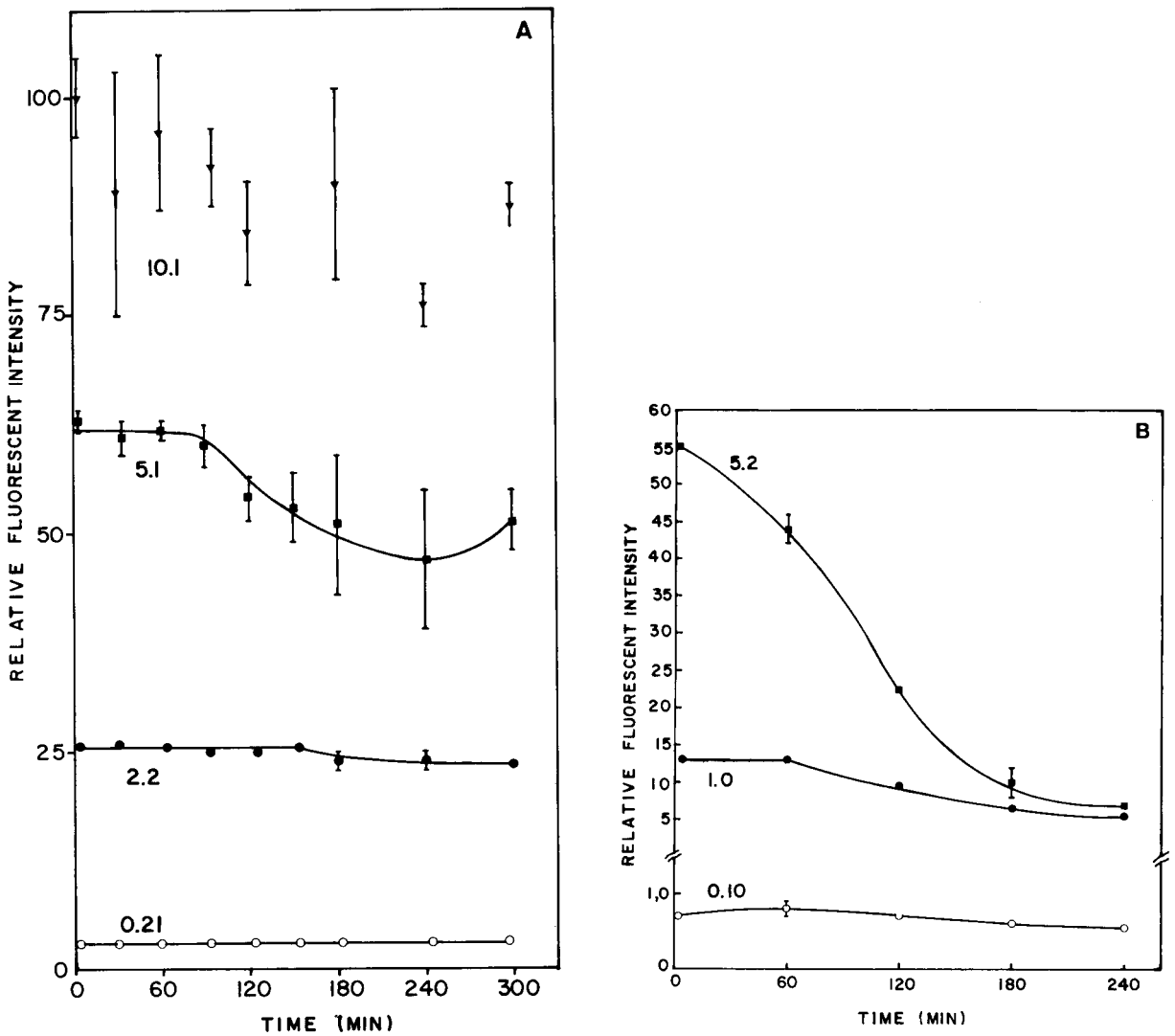

Fig. 5. Effect of sodium borohydride ageing on the fluorescent signal of (A) primin; (B) plumbagin. Numbers near the curves refer to the final analyte concentrations (in μg ml^{-1}).

addition also solved the problem of the appearance of two different fluorescent excitation spectra. Before that addition, one spectrum with a λ_{ex} at 340 and another with a λ_{ex} at 348 nm, both with the λ_{em} at 444 nm, had been observed. By increasing the acid content, only the first spectrum was present and the C.V. decreased from the original 14–25% to 2.5%.

The fluorophore produced after the reaction of lapachol with borohydride was also affected by acid: an increase of ca. 24% in the signal was observed from 0 to 57 μmol, after which a plateau was present up to 91 μmol (Fig. 3E). At this point, turbidity appeared, although the net signal did not decrease. In most cases, the effect of base addition was negative or had no effect, as in a few cases such as with the lapachol/dithionite and tingenone/dithionite systems.

3.3. Effect of temperature

Temperature was only examined with the lapachol/borohydride and tingenone/dithionite systems. In the first case an apparent increase in the signal was observed with temperature. However, a very large fluctuation of the signal intensities was present and the method was not analytically viable. Also, in the case of tingenone/dithionite, an increase of ca. 88% in the signal was found (Fig. 4A). In this experiment, the readings were taken after 15 min of heating, at 80°C, which was the optimum condition found experimentally. In this case, a reading with a low C.V. was obtained at the optimum conditions. The optimum time was found from an independent experiment (Fig. 4B). The maximum temperature was adjusted by establishing a compromise between the boiling point of the mixture and a condition of minimum evaporation.

3.4. Effect of ambient light or irradiation

Laboratory illumination (fluorescent lamps) affected the signal intensities of the primin/dithionite, plumbagin/dithionite, plumbagin/borohydride (after 30 min), lapachol/dithionite (after 15 min), lapachol/borohydride and tingenone/dithionite, the last one during the reaction step. In these cases both the reaction step and stand-by time were carried out in low luminosity (indirect illumination, with tungsten lamp, 60 W).

Irradiation of the solution in the spectrofluorimeter compartment at the λ_{ex} apparently affected the plumbagin/dithionite and lapachol/dithionite systems. Further experiments with lapachol demonstrated that when nitrogen protected the transfer of the mixture to the cell the

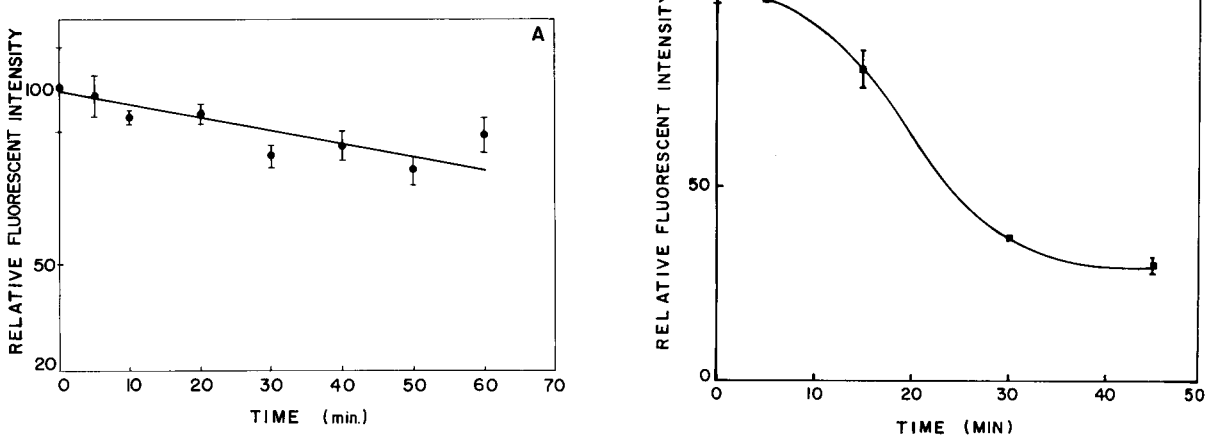

Fig. 6. Effect of time on the reaction of fluorophore stability: (A) plumbagin/dithionite; (B) plumbagin/borohydride. Concentrations of plumbagin: (A) 2.1 μg ml^{-1}; (B) 1.0 μg ml^{-1}.

effect disappeared. It is possible that a similar effect occurs with plumbagin. With primin/dithionite and primin/borohydride, exposure times higher than 30 and 10 min, respectively, also affected the signals. Lapachol reduced with borohydride showed to be beneficially affected by irradiation at the high concentration tested (20 μg ml^{-1}); this led to further experiments using a photoreactor. However, at lower concentration (2 μg ml^{-1}) the signal intensity was not proportional when compared to the signal determined at high concentration. As a result, no other attempts were carried out.

3.5. The effect of sodium borohydride ageing

Due to the fact that the reducing power of sodium borohydride decreases with time (see Experimental), the effect of reagent ageing in the signal was investigated with primin, in the presence of an optimum quantity of acid (ca. 80 μmol), the effect of reagent ageing can be seen in Fig. 5A. With a final concentration of 10.1 μg ml^{-1} of primin, a large fluctuation of the signal was observed; however, with 5.1 and smaller concentrations and with an ageing time between 20 and 90 min preparation time, the C.V.s were

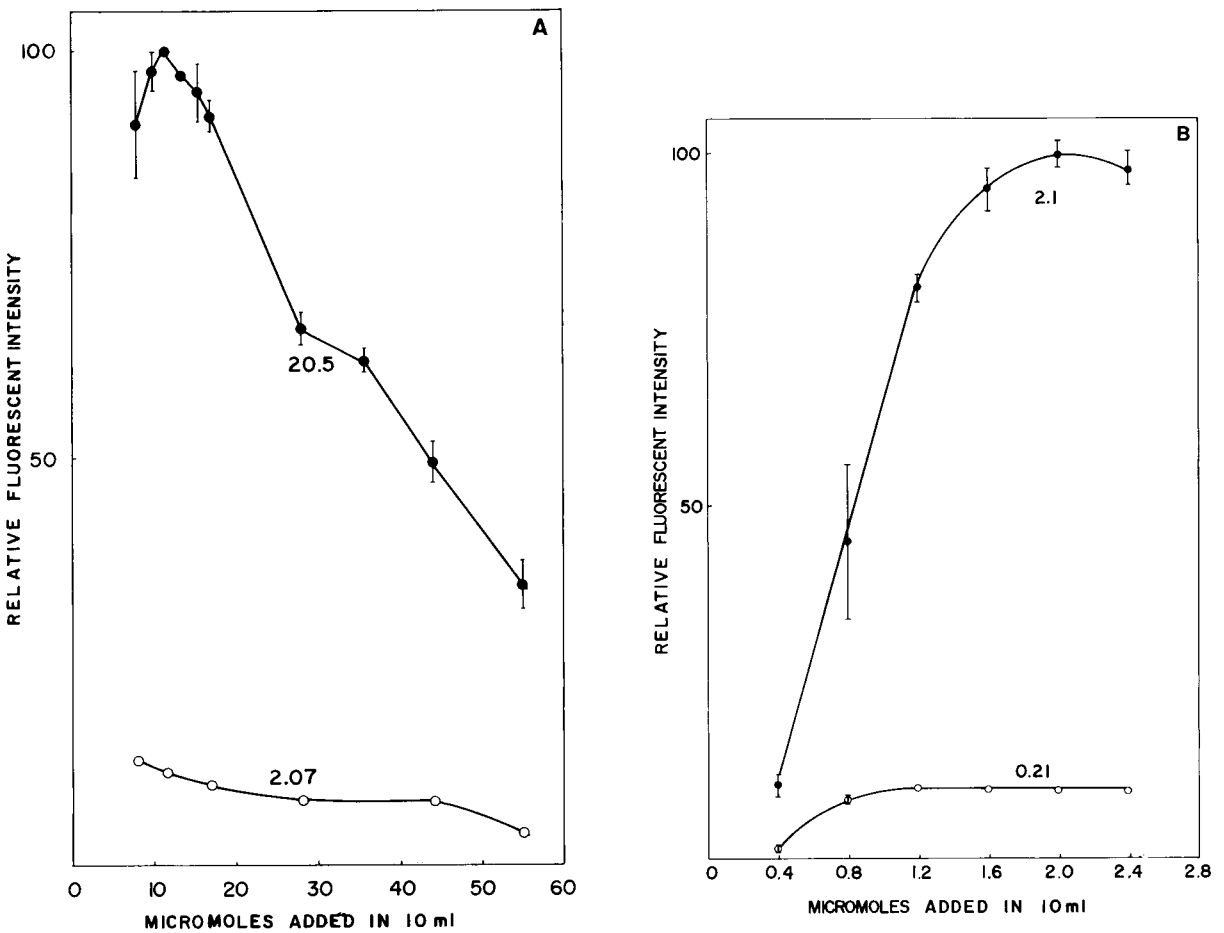

Fig. 7. Effect of excess sodium dithionite on the fluorescent signal of (A) primin; (B) plumbagin; (C) lapachol and (D) tingenone. Numbers near the curves as in Fig. 6.

acceptable. Consequently, the borohydride solution can be used during this interval. With plumbagin (Fig. 5B), the curves obtained, using an analyte concentration ranging from 5.2 to 0.1 $\mu g\ ml^{-1}$, showed that from 1.05 to 0.10 $\mu g\ ml^{-1}$ a proportional net signal was observed during an ageing time interval of 20–60 min.

In the case of lapachol a plateau is present in the time interval of 2–6 h, suggesting that the reagent can be used in this interval. However, with tingenone no effect was observed in the signal intensity up to 6 h.

3.6. Effect of time after mixture

An examination of the reaction behaviour and/or the fluorophore stability with time (up to 30–80 min) was also carried out. The effect of time was shown to be critical with plumbagin/dithionite, plumbagin/borohydride, and lapachol/borohydride. In the other cases there were no drastic effects of time on the signal. Again, in some of the negative cases oxidation process could be responsible for the instability of the fluorophore.

In the first two cases the signal decreased with time (Fig. 6A and B). With lapachol/dithionite, the signal was constant for up to 20 min decreasing afterwards in contrast with lapachol/borohydride when the signal increases continuously with time, although between 20–30 min an almost constant signal was observed. At 80 min a large C.V. on the signal was obtained; at 100 min larger fluctuation and decrease during the read-

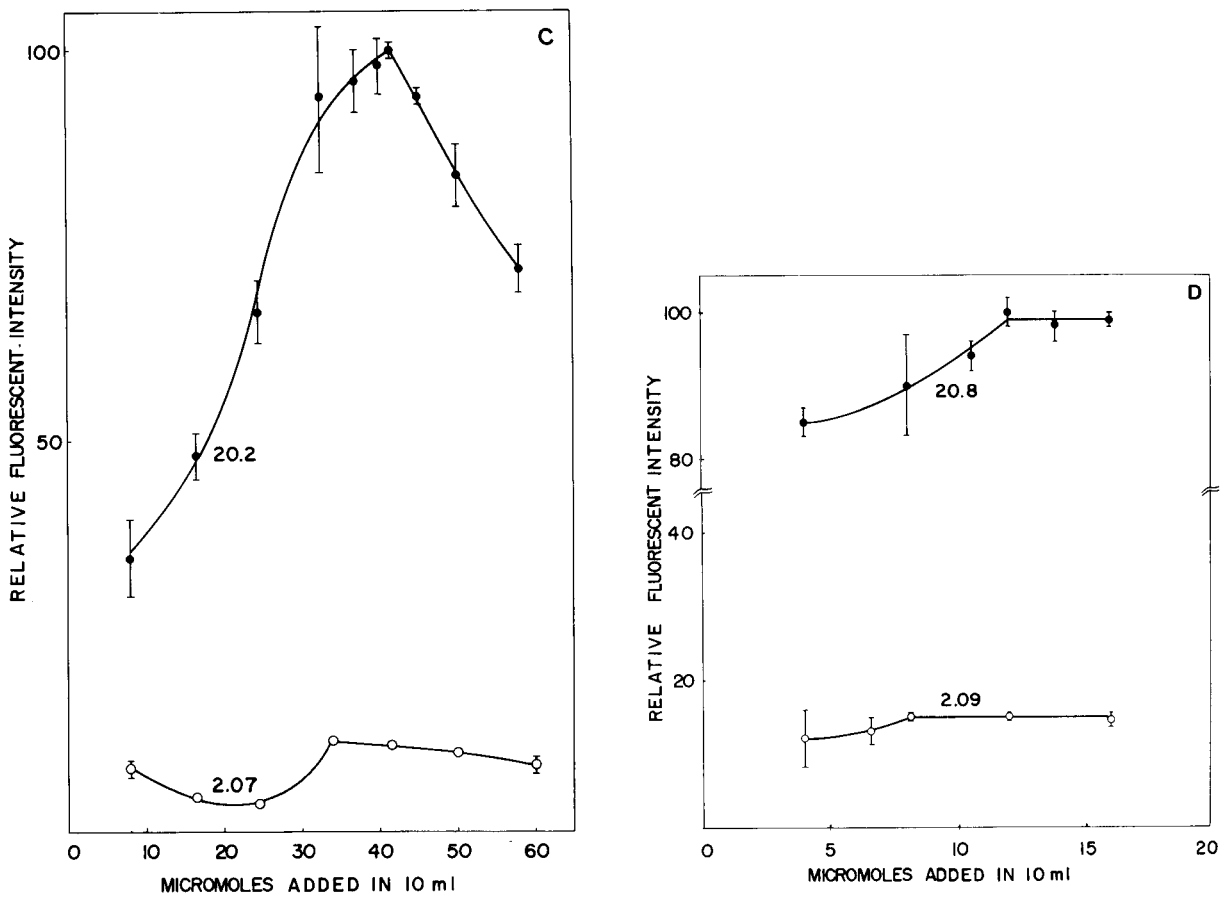

Fig. 7. (continued).

ings were found. This created a problem to the reading, which was solved later when acid was added.

3.7. Effect of excess reagent

Fig. (7A and D) shows the group of curves where the effect of excess dithionite can be observed. The primin/dithionite and lapachol/dithionite systems showed sharp peaks when a high concentration of analyte was examined (*ca.* 20 μg ml^{-1}). With low analyte concentration (2.07 μg ml^{-1}), the curves have a different aspect. Optimum amounts found were 12 and ca. 41 μmol of dithionite, respectively.

Examining the plumbagin/dithionite system at an analyte concentration of 2.1 μg ml^{-1}, a maximum was observed; with tingenone/dithionite a plateau was found. 16 μmol of reagent were needed in the case of tingenone/dithionite. (Fig. 7D).

Using borohydride, both with lapachol and tingenone, an amount of approximately 0.9 μmol/10 ml were suggested from the plotted data. Fig. 8A shows the curves obtained with tingenone.

With primin and plumbagin 30 μl and 2 ml, respectively, are recommended (Fig. 8B and C). The borohydride solutions used in these cases can be used only between ca. 20 (time of solution preparation and centrifugation) to 90 min, with primin; and between ca. 20 and 60 min of ageing time in the case of plumbagin. Starting with an active concentration of ca. 1.4% (w/v), the masses of borohydride introduced with each μl (in a final volume of 10 ml) were in the range of 10.3–9.3 μg and 1.03–0.96 mg, respectively.

3.8. Analytical figures of merit and spectral data

Table 1 and Figs. 9 and 10 show the analytical data and spectral characteristics of the fluorophore obtained after reduction of the analytes either with sodium dithionite or sodium borohydride.

The linear dynamic ranges found with the dithionite method (in some cases with the addition of acid) were better when compared to the borohydride method. Also, most of the limits of detection found with the dithionite method were lower, with the exception of the primin/borohydride system, when a smaller (although a very similar result) limit of detection was found.

In the case of primin and tingenone, the comparison of methods using the *F*-test ($\alpha = 0.95$), showed that the variances (at 3 and 5 μg ml^{-1}) were statistically identical. In the case of pristimerin/borohydride the signals obtained have a smaller variance in comparison to the pristimerin/dithionite system.

Besides the large difference in the linear dynamic range between the systems plumbagin/dithionite and plumbagin/borohydride, the first

Table 1
Analytical data and spectral characteristics

Compound	Reagent [a]	λ_{ex} [b] (nm)	λ_{em} [c] (nm)	Limit of detection [d] (ng ml^{-1})	Linear dynamic range (μg ml^{-1})	Correlation coefficient
Primin	D	236, *293*	*338*	20	0.02 –20.0	0.9982
	B	230, *293*	*338*	16	0.016 – 8.0	0.9985
Plumbagin	D	230, 245, 315, 332, *346*	*376*	0.16	0.00016– 5.0	0.9989
	B	232, *343*	*396*	4.4	0.0044 – 1.0	0.9979
Lapachol	D	238, 256, 318, *340*	*444*	10	0.01 –50.0	0.9990
	B	268, 330, *386* [e]	*486* [e]	150	0.15 – 1.0	0.9974
Tingenone	D	246, *290*, 313	*358*	34	0.034 –50.0	0.9960
	B	228, 243, *292*	*340*	190	0.19 –20.0	0.9977
Pristimerin	D	246, *290*, 313	*358*	27	0.027 –30.0	0.9988
	B	228, 243, *292*	*340*	210	0.21 –20.0	0.9997

[a] D = Sodium dithionite; B = sodium borohydride. [b] λ_{ex} = Excitation peaks; maxima in *italics*. [c] λ_{em} = Emission peaks; maxima in italics. The uncertainty in assignment of wavelengths is estimated to be ± 4 nm. [d] The limit of detection was calculated using the expression $3s_b/m$. [e] λ_{ex} and λ_{em} change with increase of concentration, up to these values.

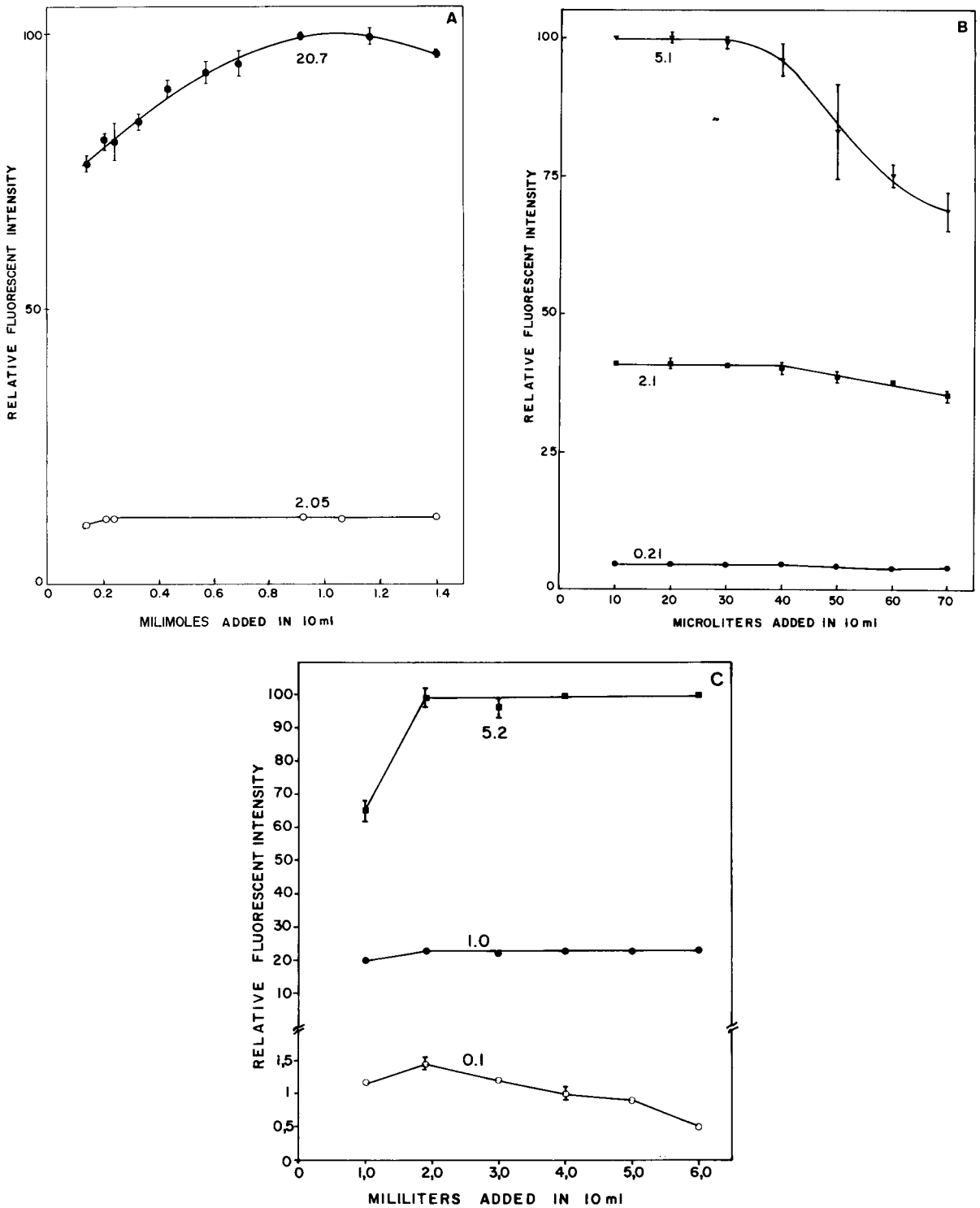

Fig. 8. Effect of excess sodium borohydride on the fluorescent signal of (A) tingenone; (B) primin and (C) plumbagin. Numbers near the curves as in Fig. 6.

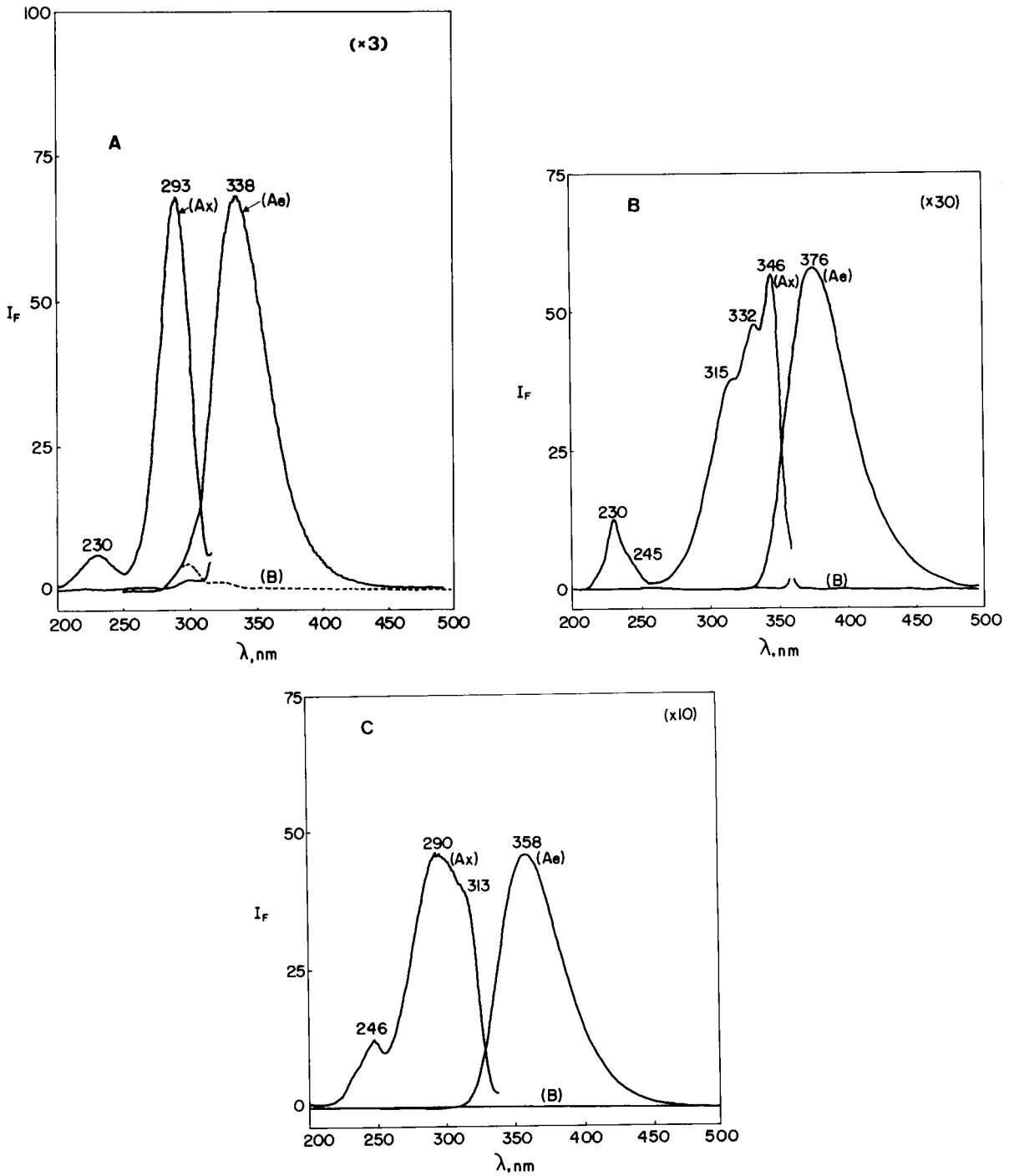

Fig. 9. (A) Fluorescence spectrum of the product of reaction of primin with sodium borohydride. Similar spectrum was obtained when sodium dithionite was used. (B) Fluorescence spectrum of the product of reaction of plumbagin with sodium dithionite. (C) Fluorescence spectrum of the prŏduct of reaction of tingenone with sodium dithionite. Similar spectrum was found after the reaction of pristimerin with sodium dithionite. Ax = Excitation spectra; Ae = emission spectra; B = blank. All spectra are uncorrected.

method shows a smaller variance at lower concentration. However, at high concentration (> 0.5 μg ml^{-1}) the second method is better. In the case of lapachol, no comparison was done due to the small linear portion of the curve observed when borohydride was used.

From the practical point of view, most of the borohydride methods are more viable, with the exception of the procedure suggested for lapachol, where the use of dithionite is superior.

In Table 1 the spectral characteristics of the compounds are also presented. Comparing the

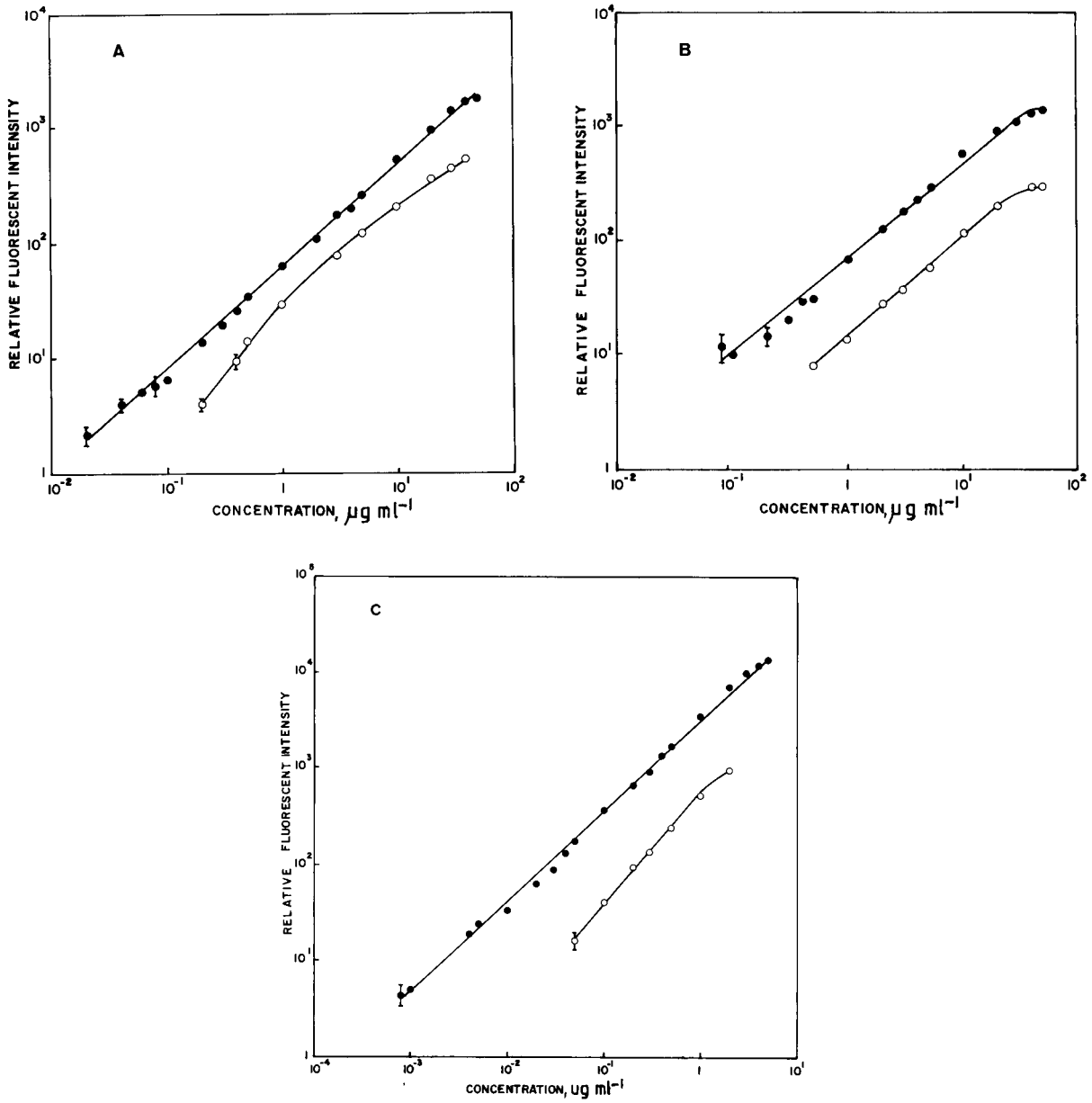

Fig. 10. Fluorescent calibration curves of some of the compounds studied with: (●) sodium dithionite and (○) sodium borohydride. (A) Lapachol; (B) tingenone and (C) plumbagin.

excitation spectra of one compound in the two different conditions of reduction (and in some cases modified by the presence of acid), we can see that in most cases the excitation maxima are similar, although small intensity bands and shoulders appear in some spectra. In contrast, the emission maxima behaved differently, with the exception of primin, which has an equal λ_{em} in both conditions. With plumbagin, a red shift occurred; with tingenone and pristimerin, a blue shift was present, when the positions of the λ_{em} are compared after reduction with dithionite versus the reduction with borohydride.

In the case of lapachol, the comparison cannot be done, as the fluorophore obtained after reduction with borohydride shows a continuous change in λ_{em}, with the increase of analyte concentration.

Despite the fact that the dithionite solution should be acidic (due to its decomposition) and the borohydride solution should be basic, the 'pH' effect cannot be conclusive, as the methods are carried out in ethanol–water mixtures or in pure ethanol. Also, in some cases, acid is added. According to Schulman [58] deprotonation of the hydroxyl substituent in a fluorophore should lead to a red shift in λ_{em} and as a result λ_{em} should suffer a red shift when at borohydride condition (in the absence of acid), in comparison with the situation where dithionite is used. This shift was only observed with plumbagin. However, in the case of tingenone and pristimerin, this rule was not obeyed.

Although the structural formula of the reduction products were not determined in the present work, we can expect, based on the literature examined [9,19,25,34,59], a substitution of the carbonyl group by a hydroxyl group, also resulting in the appearance or the increase in the aromatic character of the reaction product, resulting in the fluorescence. According to de Lima et al. [59], after reduction with dithionite, primin produced 2-methoxy-6-*n*-pentyl-1,4-dihydroxybenzene. In the case of plumbagin using dithionite, 2-methyl-1,4,5-trihydroxynaphtalene was found as a reduction product by Van Damme and De Nève [45]. Also, according to the literature [34] the reduction of tingenone with sodium borohydride yields tingenol, a trihydroxy product with an aromatic ring in the region where the hydroxydienone system was previously present.

It is also possible to suggest an alkenyl substituted 1,2,4-trihydroxynaphthalene structure for the lapachol reduced product based on a similar structure proposed by Abe et al. [9] and Lefevere et al. [11] for one of the reduction products of vitamin K_1, which, according to Lefevere et al. [11], is the major product responsible for the appearance of fluorescence.

Acknowledgements

Abstracted from the M.Sc. thesis submitted by S.K. de Barros Alcanfôr to the Departamento de Química, Universidade de Brasília, as partial requirement for the degree. The thesis was presented viva voce and approved on 30th April, 1991.

References

[1] R.H. Thomson, Naturally Occurring Quinones, Academic Press, London, 2nd edn., 1971.
[2] R.H. Thomson, Naturally Occurring Quinones, Chapman and Hall, London, 3rd edn., 1987.
[3] J.R. Poulsen and J.W. Birks, Anal. Chem., 61 (1989) 2267.
[4] M. Kofler, Helv. Chim. Acta, 28 (1945) 702.
[5] D.E. Duggan, R.L. Bowman, B.B. Brodie and S. Udenfriend, Arch. Biochem. Biophys., 68 (1957) 1.
[6] F.M. Veronese, A. Meani and E. Boccu, Acta Vitaminol. Enzymol., 22 (1968) 203.
[7] J.J. Aaron, J.E. Villafranca, V.R. White and J.M. Fitzgerald, Appl. Spectrosc., 30 (1976) 159.
[8] J.J. Aaron and J.D. Winefordner, Anal. Chem., 44 (1972) 2122.
[9] K. Abe, O. Hiroshima, K. Ishibashi, M. Ohmae, K. Kawabe and G. Katsui, Yakugaku Zasshi, 99 (1979) 192.
[10] O. Hiroshima, K. Abe, S. Ikenoya, M. Ohmae and K. Kawabe, Yakugaku Zasshi, 99 (1979) 1007.
[11] M.F. Lefevere, R.W. Frei, A.H.M.T. Scholten and U.A. Th. Brinkman, Chromatographia, 15 (1982) 459.
[12] W.E. Lambert, A.P. De Leenheer and M.F. Lefevere, J. Chromatogr. Sci., 24 (1986) 76.
[13] W.E. Lambert, A.P. De Leenheer and E.J. Baert, Anal. Biochem., 158 (1986) 257.
[14] W.E. Lambert and A.P. De Leenheer, Anal. Chim. Acta, 196 (1987) 247.

[15] T. Sakano, T. Nagaoka, A. Morimoto and K. Hirauchi, Chem. Pharm. Bull., 34 (1986) 4322.
[16] Y. Haroon, D.S. Bacon and J.A. Sadowski, Biomed. Chromatogr., 2 (1987) 4.
[17] Y. Haroon, D.S. Bacon and J.A. Sadowski, J. Chromatogr., 384 (1987) 383.
[18] M. Shimo, Analyst, 113 (1988) 393.
[19] Y. Usui, N. Nishimura, N. Kobayashi, T. Okanone, M. Kimoto and K. Ozawa, J. Chromatogr., 489 (1989) 291.
[20] J.P. Langenberg and U.R. Tjaden, J. Chromatogr., 305 (1984) 61.
[21] J.P. Langenberg, U.R. Tjaden, E.M. De Vogel and D. Is. Langerak, Acta Alimentaria, 15 (1986) 187.
[22] K. Hirauchi, T. Sakano and A. Morimoto, Chem. Pharm. Bull., 34 (1986) 845.
[23] K. Kusabe, K. Abe, O. Hiroshima, Y. Ishiguro, S. Ishikawa and H. Hoshida, Chem. Pharm. Bull., 32 (1984) 179.
[24] J.M. Morgan and B. Tan, Proc. Division of Environmental Chemistry, Denver, CO, 1987, p. 334.
[25] S.C. Kuo, S.C. Chen and C.L. Hong, Chim. Pharm. J., 41 (1989) 115.
[26] L. Saint-Rat, H.R. Olivier and J. Chateau, C.R. Acad. Sci., 224 (1943) 1587 (quoted in Antibioticos. Uma Revisão Crítica, W. Kurilowicz (Ed.), Universidade Federal de Pernambuco, Recife, Brazil, 1981).
[27] W.B. Wendel, Fed. Proc., 5 (1946) 406.
[28] S.S. Bhatnagar and P.V. Divekar, J. Sci. Ind. Res. (India), 10B (1951) 56; C.A., 45 (1951) 10511i.
[29] O.G. de Lima, I.L. D'Albuquerque, M.P. Machado, E. Silva and G.P. Pinto, An. Soc. Biol. Pernambuco, 14 (1956) 129.
[30] K.V. Rao, T.J. McBride and J.J. Oleson, Cancer Res., 28 (1968) 1952.
[31] C.F. de Santana, O.G. de Lima, I.L. D'Albuquerque, A.L. Lacerda and D.G. Martins, Rev. Inst. Antibiot. Recife, 8 (1968) 89.
[32] O.G. de Lima, G.B. Marini-Bettòlo, F. Delle Monache, J.S. de Barros Coelho, I.L. D'Albuquerque, G.M. Maciel, A. Lacerda and D.G. Martins. Rev. Inst. Antibiot. Recife, 10 (1970) 29.
[33] F. Delle Monache, G.B. Marini-Bettòlo, O.G. de Lima, I.L. D'Albuquerque and J.S. de Barros Coêlho, Gazz. Chim. Ital., 102 (1972) 317.
[34] F. Delle Monache, G.B. Marini-Bettòlo, O.G. de Lima, I.L. D'Albuquerque and J.S. de Barros Coêlho, J. Chem. Soc. Perkin I, (1973) 2725.
[35] A.M. Melo, M.L. Jardim, C.F. de Santana, Y. Lacet, J. Lobo-Filho, O.G. de Lima and I.L. D'Albuquerque, Rev. Inst. Antibiot. Recife, 14 (1974) 9.
[36] A.V. Pinto, M. do C.R. Pinto and B. Gilbert, Trans. R. Soc. Trop. Med. Hyg., 71 (1977) 133.
[37] J.N. Lopes, F.S. Cruz, R. Docampo, M.E. Vasconcellos M.C.R. Sampaio, A.V. Pinto and B. Gilbert, Ann. Trop. Med. Parasit., 72 (1978) 524.
[38] S.G. Goijman, J.F. Turrens, G.B. Marini-Bettòlo and A.O.M. Stoppani, Experientia, 41 (1985) 646.
[39] R.K. Goel, N.K.R. Pathak, M. Biswas, V.B. Pandey and A.K. Sanyol, J. Pharm. Pharmacol., 39 (1987) 138.
[40] O. Gottlieb and W. Mors, J. Agric. Food Chem., 28 (1980) 196.
[41] A.B. de Oliveira, D.S. Raslan, M. do C.M. Miraglia, A.A.L. Mesquita, C.L. Zani, D.T. Ferreira and J.G.S. Maia, Quimica Nova, 13 (1990) 302.
[42] H. Wagner, in K. Hostettman and P.J. Lea (Eds.), Biologically Active Natural Products, Clarendon Press, Oxford, 1987.
[43] R.H. Fetterer and M.W. Fleming, Comp. Biochem. Physiol., C: Comp. Pharmacol. Toxic., 100c (1991) 539; C.A., 116 (1992) 53625c
[44] J.M. Finkel and S.D. Harrison Jr., Anal. Chem., 41 (1969) 1854.
[45] J.G. Van Damme and R.E. De Nève, J. Pharm. Sci., 68 (1979) 16.
[46] J.B. Block, A.A. Serpick, P.H. Wiernik, P.K. Nayak and D. Molins, Fed. Proc., 29 (1970) 682.
[47] J.B. Block, A.A. Serpick, W. Miller and P.H. Wiernik, Cancer Chemother. Rep., 4 (1974) 27.
[48] G.G. Guilbault and D.N. Kramer, Anal. Chem., 37 (1965) 1395.
[49] D.V.C. Awang, D. Kindack and B.A. Dawson, J. Chromatogr. 368 (1986) 439.
[50] A. Marston and K. Hostettman, J. Chromatogr., 295 (1984) 526.
[51] A.D. Campiglia and C.G. de Lima, Anal. Chem., 59 (1987) 2822.
[52] J.C. Miller and J.N. Miller, Statistics for Analytical Chemistry, Ellis Horwood, Chichester, 1984.
[53] P.R.C. Holvorcem, A.V.C. Carvalho and C.G. de Lima, IVth National Analytical Chemistry Meeting, São Paulo, 1987.
[54] G.L. Long and J.D. Winefordner, Anal. Chem., 55 (1983) 712.
[55] P.M. Brown, M. Moir, R.H. Thomson, T.J. King, V. Krishnamoorthy and T.R. Seshadri, J. Chem. Soc., Perkin Trans. I, (1973) 2721.
[56] O.G. de Lima, J.S. de Barros Coelho, G.M. Maciel, E.P. Heringer and C.G. de Lima, Rev. Inst. Antibiot. Recife, 12 (1972) 19.
[57] D.A. Lyttle, E.H. Jensen and W.A. Struck, Anal. Chem., 24 (1952) 1843.
[58] S.G. Schulman, in S.G. Schulman (Ed.), Molecular Luminescence Spectroscopy: Methods and Applications, Part 1, Wiley, New York, 1985.
[59] O.G. de Lima, G.B. Marini-Bettólo, J.S. de Barros Coelho, I.L. D'Albuquerque, M.S.B. Cavalcanti, D.G. Martins and L.L. Oliveira, Rev. Inst. Antibiot. Recife, 10 (1970) 35.

ELSEVIER

Analytica Chimica Acta 289 (1994) 291–298

ANALYTICA CHIMICA ACTA

Determination of arsenic in sea water by cathodic stripping voltammetry in the presence of pyrrolidine dithiocarbamate

Jiri Zima [1], Constant M.G. van den Berg *

Oceanography Laboratories, Department of Earth Sciences, University of Liverpool, Liverpool L69 3BX, UK

(Received 25th October 1993; revised manuscript received 2nd December 1993)

Abstract

A procedure is presented for the determination of arsenite and total arsenic in sea water using differential pulse cathodic stripping voltammetry at a hanging mercury drop electrode in the presence of pyrrolidine dithiocarbamate (PDC). The deposition potential was −0.3 V, whereas the scan was initiated from 0 V. Optimised conditions include a PDC concentration of 0.5 μM and a pH ≈ 0.8. The detection limit of the method is 3 nM As. The method was tested by analysis of CASS-2 certified sea water and applied to determination of arsenic in Atlantic ocean water.

Key words: Voltammetry; Arsenic; Sea water; Waters

1. Introduction

Trace metals in aqueous solution can be determined by voltammetry, atomic absorption spectrometry, inductively coupled plasma spectrometric techniques or neutron activation analysis. Advantages of voltammetry are the possibility to investigate metal speciation and the low cost of the instrumentation.

Electrochemically arsenic can be determined by several techniques [1]. Arsenate is not electroactive, so usually arsenite is used for electrochemical studies. Arsenite can be determined by differential pulse polarography [2–4], cathodic stripping voltammetry (CSV) at a hanging mercury drop electrode (HMDE) [5–7] or anodic stripping voltammetry (ASV) using a gold electrode [8,9]. The ASV method suffers from problems related to poor reproducibility of and ready damage to the gold electrode surface. The sensitivity of the CSV methods is improved by addition of a high concentration of copper to preconcentrate a Cu–As compound on the surface of the HMDE prior to the scan [6]. However, preliminary experiments using the existing CSV method in our laboratory indicated that the response is non-linear (S-shaped) at low arsenic concentrations (10–20 nM) necessitating the use of a calibration curve instead of internal standard additions.

Various reducing agents have been investigated to reduce arsenate to arsenite prior to its determination by voltammetry including sulfite

* Corresponding author.

[1] On leave from Department of Analytical Chemistry, Charles University, Prague, Czech Republic.

SSDI 0003-2670(93)E0696-5

[8], hydrogensulfite [3], sulfur dioxide [9], hydrazine sulfate [5], hydrazinium hydrochloride [6] and hydroxylammonium chloride [7]. Although arsenate is considered to be electrochemically inactive, it can be determined directly by potentiometric and constant-current stripping analysis [10] without prior chemical reduction to arsenite, by the application of a negative overpotential in strongly acidic solution (4 M HCl) using a gold electrode. However, that method suffers from problems related to the generation of large amounts of hydrogen at the working electrode, and of chlorine at the counter electrode, during the deposition step, and the high acid concentration is corrosive to the electrode stand. For this reason we attempted to use chemically less aggressive conditions in our proposed method.

This paper deals with the determination of arsenite in sea water by cathodic stripping voltammetry preceded by a combination of electrolytic deposition as As(Hg) and reoxidation with adsorptive deposition of a complex of arsenite with pyrrolidine dithiocarbamate (PDC) on the HMDE in weakly acidic conditions. Total arsenic is determined after chemical reduction of the more abundant arsenate by sulfur dioxide.

2. Experimental

2.1. Apparatus and reagents

Voltammetric equipment was a PAR 174A polarographic analyser connected to a PAR Model 303 static mercury drop electrode. The drop size was "large" (ca 1.9 mm^2). The reference electrode was Ag/AgCl, saturated AgCl in 3 M KCl (SSCE), with Pt wire as an auxiliary electrode. The polarograph had been altered to increase the pulse rate to 10 s^{-1} and was used in the differential-pulse mode, with a modulation amplitude of 25 mV and a scan rate of 20 mV s^{-1}. The scans were recorded on an X–Y Kipp and Zonen recorder. The solution (10 ml) in the voltammetric cell was stirred with a polytetrafluoroethylene (PTFE)-coated star-shaped magnetic stirring bar and purged with water-saturated nitrogen (8 min) prior to the voltammetric analysis and during accumulation. The pH was measured using a Metrohm Model 605 pH meter, calibrated with NBS pH buffers.

High-density polyethylene (HDPE) bottles (Nalgene) were used to store water samples collected from the Atlantic Ocean. Prior to use these bottles were soaked in hot tap water with detergent for 1 day, rinsed with distilled water, soaked for 1 week in 6 M HCl (AnalaR, BDH), then for 1 week in 2 M HNO_3 (AnalaR, BDH), subsequently filled with 0.01 M HCl and stored in sealed plastic bags. Dissolved organic material in sea water samples was decomposed by 4 hours UV-digestion of the sample in capped 30 ml silica tubes with addition of 10 μl of 30% H_2O_2/10 ml sample using either a 100-W low-pressure or 1-kW medium pressure mercury vapour lamp (Hanovia), housed in an aluminium container fitted with a cooling fan.

Reagents used were of AnalaR grade from BDH unless indicated otherwise. Deionized water was produced by reverse-osmosis treatment of tap water followed by passage through a Milli-Q deionizer system (Millipore). Standard solutions of arsenite were prepared freshly weekly by diluting a stock solution of 13.3 mM $AsCl_3$ (BDH) by weighing into polystyrene tubes (Sterilin). Standard solutions of 0.01 M arsenate were prepared by dissolving an appropriate amount of $Na_2HAsO_4 \cdot 7H_2O$ (Merck) in water and by further dilution. An aqueous stock solution of 0.1 M PDC was prepared by dissolution of the ammonium salt in water. This solution was diluted with water to a working stock solution 0.2 mM in PDC.

2.2. Analytical procedure to determine arsenic in sea water

An aliquot of 10 ml of UV irradiated sea water was pipetted into a 30-ml silica tube and 20 μl of concentrated HCl were added. The solution was heated in a water bath to about 80°C. Sulfur dioxide was passed through the solution for 5 min and the solution was left capped for 5 min. SO_2 was purged through the solution for another 2–3 min to ensure complete saturation with SO_2 [9]. Then 80 μl of concentrated HCl were added and

the solution was heated to about 90°C for 2 min. The sample was cooled to room temperature, and evaporation losses were made up with deionized water. Solid ascorbic acid (2 mg/ml) was added and 25 μl of 0.2 mM PDC. The solution was transferred to the voltammetric cell and water-saturated nitrogen was passed through the solution for 16 min. A voltammogram was then carried out without prior deposition to check for traces of SO_2 which would cause a broad peak at -0.2 V in which case nitrogen was bubbled for another 4 min. The initial 16 min nitrogen bubbling can be carried out in the silica tube to save analysis time.

Deposition of arsenite on the HMDE was carried out for 1 min (or 3 min for As concentrations below 100 nM) at -0.3 V. Stirring and purging of the solution was switched off 5 s before the accumulation time elapsed and then the potential was set to 0 V followed by a further quiescence period of 5 s. The voltammetric scan was carried out from 0 V towards more negative potentials. The sensitivity (nA/nM arsenite) was calibrated by standard additions of arsenite to the sample.

3. Results and discussion

3.1. Voltammetry of arsenite

Arsenite is known to form a stable complex with PDC in acidic media. Formation of this complex has been used for the quantitative extraction of arsenite over a wide range of pH values between 0.6 and 6 into chloroform [11]. Previous voltammetric methods for the determination of arsenite involve an acidic medium, of typically 0.1 M or more concentrated HCl. Only ill-defined voltammetric waves of arsenite are reported in less acidic media. A concentration of 0.1 M HCl in water or sea water was chosen for this work.

3.2. Cyclic voltammetry

Cyclic voltammetry was used to investigate the electrochemistry of arsenite in the presence and absence of PDC. Cyclic voltammetry of arsenite

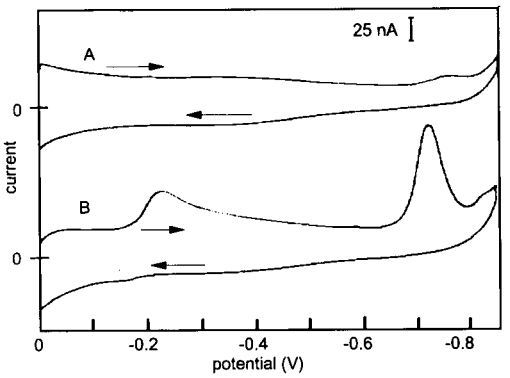

Fig. 1. Cyclic voltammetry of 0.1 M HCl (A) and 5×10^{-7} M arsenite in 0.1 M HCl (B). Each scan was preceded by stirred accumulation for 60 s at -0.3 V followed by adjustment of the potential to 0 V from where the scans were initiated. The scan rate was 20 mV s^{-1}.

(preceded by stirred collection for 60 s at -0.3 V whereafter the potential was adjusted to 0 V prior to the potential scans) yields two irreversible peaks in 0.1 M HCl (Fig. 1) in accordance with the reduction of arsenite to As(0) at -0.22 V and As(0) to As($-$III) at -0.72 V. Addition of PDC caused the formation of a third cathodic peak due to the reduction of PDC situated at -0.47 V, between the two reduction peaks of arsenite, and causing the second arsenite peak (As(0) → As($-$III)) to diminish (Fig. 2A). Interestingly the PDC addition also caused the appearance of an anodic peak at -0.14 V corresponding to the oxidation of As(0) back to arsenite. The reduction of arsenite therefore was quasi-reversible in this condition, forming the basis of a method to determine arsenite at nM levels using differential-pulse CSV with accumulation. Further experiments showed that the height of the arsenite/As(0) reduction peak at -0.2 V was linearly related to the concentration of arsenite so the voltammetry of this peak was optimised and is discussed below. The differential-pulse mode was used for analytical purposes as comparative scans showed that this gave better sensitivity and peak shape.

The presence of the anodic peak at -0.14 V indicates that anodic stripping voltammetry in the presence of PDC with accumulation at -0.3 V followed by a voltammetric scan towards more

positive potentials (Fig. 2B) could also be used to determine arsenic with good sensitivity. At a higher concentration (10 μM) of PDC the ASV sensitivity for arsenite is actually greater then by CSV. However, the calibration graph for low levels of As (20–100 nM) in sea water was curved necessitating the use of a calibration curve instead of internal standard additions to calibrate the arsenic determinations which is not precise when the concentration of interfering surface active matter varies between samples. Furthermore the anodic peak potential of arsenite was near the oxidation potential of mercury in sea water which interfered with the determination of low concentrations of arsenite.

3.3. Effects of varying the deposition potential, deposition time and concentration of PDC

Variation of the deposition potential (Fig. 3A) revealed that the CSV peak height for the arsenite/As(0) peak (at −0.16 V) for 200 nM arsenite in the presence of 1 μM PDC and 0.1 M HCl in sea water (with a deposition time of 1 min) was greatest after deposition at potentials between −0.3 and −0.5 V. No reduction peak of arsenite was present when deposition was carried out at potentials more positive than −0.1 V where arsenite is not reduced during deposition, or at potentials more negative than −0.8 V where PDC as well as arsenite are reduced. The optimal deposition potential therefore was in a narrow range between −0.3 and −0.5 V. A deposition potential at the positive end of this range (near −0.3 V) was preferred at PDC concentrations higher than 1 μM (to be used at high arsenite concentrations) as this minimised the deposition of free PDC and thus its interference with the reduction peak for arsenite.

Variation of the deposition time showed that the peak height for 200 nM arsenite in the presence of 1 μM PDC and 0.1 M HCl in sea water increased linearly between 0.5 and 3 min (Fig. 3B). Hence the analytical sensitivity can be increased considerably by extending the deposition time to 3 min (or longer) which is still a convenient accumulation time. A deposition time of 1 min with stirring was used for arsenite concentrations > 100 nM, whereas a deposition time of

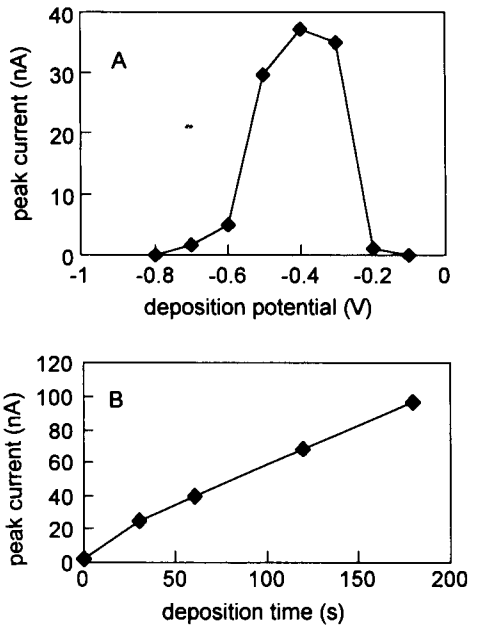

Fig. 3. Effect of varying the deposition potential (A) and the deposition time (B) on the CSV peak current for 200 nM arsenite in the presence of 1 μM PDC in 0.1 M HCl in sea water. The stirred deposition time was 60 s in A, and the deposition potential was −0.3 V in B.

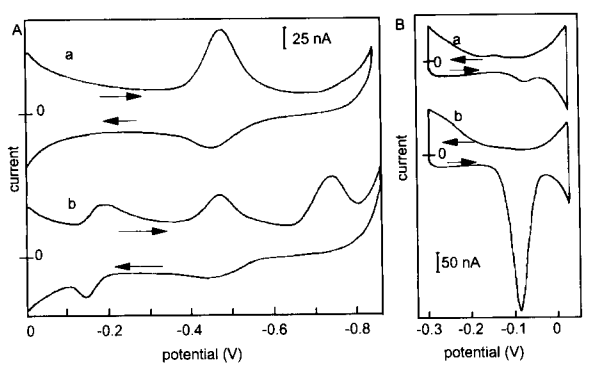

Fig. 2. Comparison of cyclic voltammetry (A) and reverse cyclic voltammetry (B) of arsenite in the presence of PDC in acidified (0.1 M HCl) sea water. Scans were preceded by 60 s stirred deposition at −0.3 V at a scan rate of 20 mV s^{-1}. A: 1 μM PDC before (a) and after (b) addition of 0.5 μM arsenite. The potential was set to 0 V prior to the CV scan. B: Reverse cyclic voltammetry of 10 μM PDC before (a) and after (b) addition of 0.5 μM arsenite. These CV scans were initiated from −0.3 V in a positive direction.

Table 1
Effect of varying the concentration of PDC on the CSV sensitivity (slope of a linear calibration graph) for arsenite in 0.1 M HCl in sea water preceded by stirred accumulation at −0.3 V. The limit of detection of 3 nM was calculated from 3 times the standard deviation at the lowest concentration determined

Arsenite (nM)	PDC (μM)	Deposition time (s)	Slope A l mol^{-1}	Correlation coefficient [a]
200–1000	1	60	0.123	0.998
200–1000	2	60	0.129	0.999
200–1000	5	60	0.127	0.994
10–100	0.2	300	0.093	0.998

[a] $n = 5$ repeated analyses.

3–5 min was used at lower levels of 10–100 nM arsenite.

The PDC is essential for the formation of the adsorptive arsenite complex, but unfortunately the free PDC also causes a reduction peak near to that of the arsenite–PDC complex. For this reason the concentration of PDC has to be kept low. The effect of varying the concentration of PDC on the CSV sensitivity for 200 nM arsenite in sea water is shown in Table 1. The sensitivity was found to increase with the PDC concentration until ca. 2 μM PDC, but showed little change at higher PDC concentrations. Similar behaviours were recorded in 0.1 M HCl in deionized water and in 0.6 M NaCl (of similar chloride concentration as in sea water) + 0.1 M HCl. However, the absolute sensitivity for arsenite in the presence of high chloride concentration in 0.6 M NaCl or sea water was always higher than in deionized water.

3.4. Interferences

Possible interferences in CSV include electroactive trace elements with a reduction potential similar to that of arsenite and competitive adsorption of surface-active organic compounds present in natural sea water. The possible interference by surfactants was studied with non-ionic Triton X-100, anionic sodium dodecyl sulfate (SDS) and cationic cetylpyridinium bromide (CPB, Sigma). The addition of Triton X-100 and CPB diminished the peak of arsenite considerably and with concentrations higher than 0.5 ppm (μg ml^{-1}) of surfactant the arsenic peak almost disappeared. The addition of SDS to a concentration above 0.5 ppm resulted in a deformation of the arsenic peak. UV-digestion was therefore necessary to get rid of the interference of surface-active organic matter in sea water.

The possible interferences of Cu(II), Cd(II) and Pb(II) were investigated by addition of these elements to sea water and determining their effect on the CSV determination of arsenite. Concentrations of 150 nM Pb(II) or higher resulted in widening of the arsenite peak probably as a result of a diffusion reduction peak for Pb adjacent to the arsenite peak. The influence of Cu(II) was more pronounced, possibly because of formation of a complex with PDC causing a peak near to that for arsenite. It was possible to determine low levels of arsenite in the presence of up to 50 nM Cu(II), the difference between both peaks being only about 30 mV. However, the concentration of copper in sea water is usually lower (about 6 nM) [12], so this element does not normally interfere with the voltammetric determination of arsenic except in waters severely contaminated with copper. Comparative measurements indicated that the difference in the peak potential increased with increasing concentration of HCl (lower pH); arsenic can then be determined also in the presence of higher concentrations of copper. Alternatively it would be necessary to remove interfering levels of copper by extraction [5] prior to the determination of arsenic or to use a different voltammetric method which utilises high copper levels [6].

3.5. Dynamic range and limit of detection

Measurement of the CSV peak height (preceded by stirred accumulation at −0.3 V) of increasing concentrations of arsenite in sea water containing 0.1 M HCl indicated that the peak height increased linearly with the arsenic concentration in a concentration range between 10 nM to 1 μM (Fig. 4); a stirred accumulation period of 60 s was used at arsenic concentrations > 100 nM, whereas the accumulation time was 180 or 300 s at lower concentrations. The sensitivities (calculated from the slope of the calibration

graphs) and the limit of detection are given in Table 1.

3.6. Conversion of arsenate to arsenite and stabilisation of arsenite

In sea water the most abundant arsenic species is arsenate [13]. Organoarsenic compounds constitute a minor fraction in sea water originating from open oceanic waters [13] whilst significant levels of organoarsenic compounds occur in estuarine water [14].

Preliminary experiments using arsenate indicated that no response is obtained for this oxidation state at deposition potentials between −0.3 V and −1.2 V. For this reason it is necessary to convert all arsenate to arsenite to determine the total arsenic concentration in sea water. Such experiments indicated that losses of arsenite, if this was added to sea water prior to the addition of PDC, probably occurred as a result of ready oxidation of low concentrations of arsenite in acidic solution [9]. It was found that the arsenite was stabilised by the addition of PDC suggesting that it was complexed in solution (in addition to the PDC complexation on the electrode surface); the stabilisation of arsenite is convenient if it is

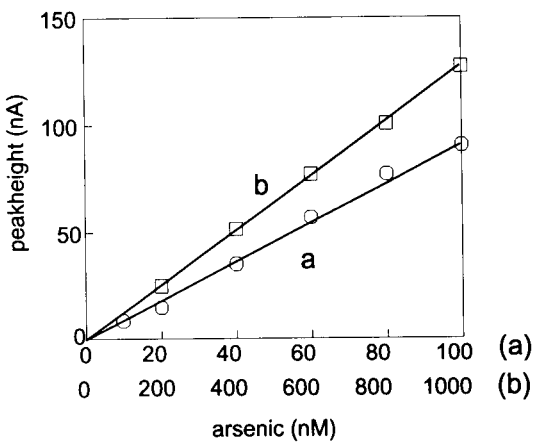

Fig. 4. Calibration curves for CSV of arsenite in the concentration range from 10 nM to 1 μM in 0.1 M HCl in Atlantic ocean water. (a) 60 s stirred accumulation at −0.3 V in the presence of 0.2 μM PDC; (b) 300 s stirred accumulation at −0.3 V in the presence of 2 μM PDC.

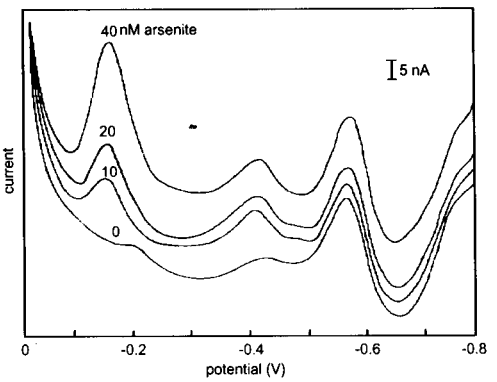

Fig. 5. Differential-pulse CSV of arsenite in Atlantic ocea water containing 0.1 M HCl and 0.2 μM PDC, preceded by 300 s stirred accumulation at −0.3 V. The concentrations of arsenite are indicated next to the scans.

required to determine arsenic in this oxidation state.

Several reduction methods were tested to evaluate whether they could be used to reduce the arsenate to arsenite without interference with the subsequent voltammetric analysis: the reduction was not successful using hydrazine or hydroxylammonium chloride, and interferences were recorded in CSV of arsenite in the presence of sulfite and hydrogensulfite. However, a reduction method based on the reaction with SO_2, which is bubbled in the solution heated to 80–90°C [9], was found to be satisfactory giving full recovery of added arsenate as arsenite whilst interference by residual SO_2 (causing a broad peak-shaped diffusion current overlapping with the reduction peak for the arsenite–PDC complex) was removed by purging with nitrogen.

The efficiency of the conversion of the non-electroactive arsenate to arsenite was tested by determining the recovery of arsenate added to sea water. The recovery of the added arsenate was complete (98–101%) after reduction with SO_2 as shown in Table 2. Ascorbic acid was added to the solution as an antioxidant after the treatment with SO_2 [9], but it was noticed that no losses of arsenite occurred when PDC was added immediately after cooling of the solution.

It is convenient to UV-irradiate the sample prior to the SO_2 reduction treatment to decompose any interfering surface active organic mate-

Table 2
(A) Recovery of arsenate added to Atlantic ocean water. The results are the average of 3 determinations each and are corrected for the initial arsenic concentration

Total As added	Total As found
500 nM	(492 ±8) nM
50 nM	(50.7±1.1) nM

(B) Determination of total arsenic in Atlantic ocean water and CASS-2 certified sea water. The results shown are an average of 3 determinations each

	Total As found	Certified As concentration
Atlantic ocean water	(10.4±2) nM	–
CASS-2	(12.6±1.5) nM	(13.5±0.9) nM

rial; this treatment converts any arsenite to arsenate and all organoarsenic compounds to free arsenate thus rendering all arsenic available as inorganic arsenate.

The concentration of total arsenic was determined by the CSV method in certified sea water with a known concentration of arsenic (CASS-2) to evaluate the accuracy of the proposed method; the sea water was UV-digested prior to the measurement and the arsenate was subsequently converted to arsenite as described above. Good agreement was obtained between the concentration found and the certified value (Table 2). The concentration of arsenic was also determined in sea water originating from the North Atlantic (a bulk sample of various depths collected at 20°W 40°N) giving a concentration of 10 nM total dissolved arsenic.

4. Discussion and conclusions

The narrow range of usable accumulation potentials (-0.3 V $< E_{acc} < -0.5$ V) situated between the reduction potential for arsenite and that for PDC followed by reoxidation of the accumulation As(0) to arsenite indicates that the deposition mechanism is a combination of electroplating of arsenite as As(0) with subsequent reoxidation to arsenite and adsorption as a complex with PDC. The reoxidation was irreversible in the absence of the PDC. The lack of deposition of arsenite at more positive deposition potentials indicates that the adsorptive arsenite–PDC complex does not occur in the dissolved phase (as opposed to the adsorbed phase) or is repulsed from the electrode surface by Coulombic effects. The adsorbed complex is apparently formed from arsenite being produced from As(0) diffusing out of the HMDE when the electrode potential is switched to 0 V after simultaneous deposition of PDC by adsorption on the electrode surface and As(0) by plating deposition of arsenite at -0.3 V. However, the stabilisation of arsenite in acidified sea water in the presence of added PDC suggests that some complexation of arsenite by PDC occurs although possibly as a complex different from that which adsorbs: for instance it is possible that a 2:1 PDC–arsenite complex is adsorbed on the electrode surface whereas a 1:1 complex was formed in the solution at the low dissolved concentrations of PDC employed.

The proposed CSV method is more sensitive than previous voltammetric methods using a HMDE in view of the low limit of detection. The recovery tests, and the measurements of arsenic in certified sea water confirmed the satisfactory accuracy of the method.

Acknowledgement

The visit of JZ to the laboratory in Liverpool was sponsored by TEMPUS project 1379–92/3 of the EC.

References

[1] J.P. Arnold and R.M. Johnson, Talanta, 16 (1969) 1191.
[2] D.J. Myers and J. Osteryoung, Anal. Chem., 45 (1973) 267.
[3] F.T. Henry, T.O. Kirch and T.M. Thorpe, Anal. Chem., 51 (1979) 215.
[4] F.T. Henry and T.M. Thorpe, Anal. Chem., 52 (1980) 80.
[5] W. Holak, Anal. Chem., 52 (1980) 2189.
[6] R.S. Sadana, Anal. Chem., 55 (1983) 304.
[7] M.R.B. Othman, J.O. Hill and R.J. Magee, J. Electroanal. Chem., 168 (1984) 219.
[8] T.W. Hamilton, J. Ellis and T.M. Florence, Anal. Chim. Acta, 119 (1980) 225.

[9] F.G. Bodewig, P. Valenta and H.W. Nürnberg, Fresenius' Z. Anal. Chem., 311 (1982) 187.
[10] H. Huiliang, D. Jagner and L. Renman, Anal. Chim. Acta, 207 (1988) 37.
[11] W.M. Mok, N.K. Shah and C.M. Wai, Anal. Chem., 58 (1986) 110.
[12] K.W. Bruland, in J.P. Riley (Ed.), Chemical Oceanography, Vol. 8, Academic Press, London, 1983, pp. 157–220.
[13] M.O. Andreae, Limnol. Oceanogr., 24 (1979) 440.
[14] A.G. Howard, M.H. Arbab-Zavar and S. Apte, Mar. Chem., 11 (1982) 493.

ELSEVIER

Analytica Chimica Acta 289 (1994) 299–306

ANALYTICA CHIMICA ACTA

Influence of perchlorates and halides on the electrochemical properties of indium(III)

Marina Zelić *, Marina Mlakar, Marko Branica

Center for Marine Research Zagreb, Rudjer Boskovic Institute, POB 1016, 41001 Zagreb, Croatia

(Received 29th July 1993)

Abstract

The influence of the composition and concentration of individual basic electrolytes on the electrode processes of the indium(III)/indium(0) (Hg) redox pair was studied. The results were mainly obtained using square-wave voltammetry because cyclic voltammetry does not seem to be a proper method of choice for this system. In non-complexing media the electrode reaction is controlled by the preceding reaction, which is probably the dissociation of the indium(III) aqua complex. In concentrated sodium perchlorate solutions an inverse proportionality between the peak height and water activity is observed. The peak current generally increases with increasing electrolyte concentration, indicating the acceleration of the overall electrode reaction. It can reach a constant value only in concentrated chloride and bromide media. Under such conditions tetracoordinated species seem to be the highest possible complexes.

Key words: Voltammetry; Electrolytes; Indium

1. Introduction

Indium(III) [1], together with bismuth(III) [2,3] and gallium(III) [4], belongs to a group of triply charged metal ions whose electrochemical properties are strongly influenced by the composition and concentration of the electrolyte solution. Dehydrating agents [3] and surface-active ligands, such as halides [2,5] and pseudohalides [6], can significantly accelerate the electrode process, which is generally of the type

$$M(III) + 3e^- \rightleftharpoons M(0)(Hg)$$

In complexing solutions of high ionic strength, relatively stable indium(I) species can also be formed as a result of the corresponding redox reaction [7], whereas indium(II) is treated as a short-lived intermediate [8], if considered at all.

Based on the comparison with other d^{10} cations, anion-induced adsorption [9] of the halide complexes on mercury electrodes was also expected [10]. Although found during experiments with bismuth(III) in chloride media [2,11], the phenomenon could not be firmly established in indium(III) solutions, irrespective of the halide applied [12]. One explanation given [13] is that adsorption and reduction take place in the same potential range and this should be the reason for

* Corresponding author.

SSDI 0003-2670(93)E0677-Y

the negative chronocoulometric results which are based on accumulation in the prefaradaic region.

Problems with the characterization of the reduction signal in non-complexing media and the reversibility of the electrode process that follows ligand concentration (with constant ionic strength) prevent the application of the usual polarographic procedures [14] for the determination of indium(III) complexation constants. Results obtained after the introduction of some modifications [10,15–17], however, are not generally accepted [18]. Unfortunately, other (independent) experimental methods do not seem to have been any more successful [18]. This is the reason why complex equilibria of indium(III), even in solutions of the usual ligands such as halides, remain unclear.

This paper is an introductory part of an extensive study of the interaction of indium(III) with organic surface-active ligands. Taking into account that perchlorates and halides are usually used as basic electrolytes, it is of prime importance to investigate their influence on the electrochemical processes of interest, using the same techniques as in the "main" experiments.

2. Experimental

Solutions of $NaClO_4$, $LiClO_4$, $Mg(ClO_4)_2$, NaCl, LiCl, $MgCl_2$, NaBr and NaI were prepared by dissolution of the analytical-reagent grade salts in doubly distilled water. The indium(III) chloride stock solution (0.01 mol l^{-1}) also contained $HClO_4$ (1 mol l^{-1}) in order to prevent hydrolysis.

Measurements were performed in an EA 875-20 conventional electroanalytical cell (50 ml) with a corresponding universal cap (Metrohm, Herisau, Switzerland). A hanging mercury drop electrode (Metrohm) was used as the working electrode. Another configuration included a Princeton Applied Research (PAR) Model 303A static mercury drop electrode (SMDE) and a small polarographic cell (10 ml). In both instances the potentials were referred to a saturated Ag/AgCl (NaCl) reference electrode with (or without) a salt bridge using a platinum wire as the counter electrode. Prior to the measurements, the solutions were deaerated with extra-pure nitrogen for 20 min.

Square-wave (SW) and cyclic voltammetric (CV) measurements were performed using a PAR Model 384B polarographic analyser connected to a Hewlett-Packard Model 9816S technical computer, as described elsewhere [19]. For recording of SW forward and reverse currents a BAS 100A electrochemical analyser (Bioanalytical Systems, West Lafayette, IN, USA) and a corresponding plotter were used instead.

All experiments were performed at room temperature (about 25°C).

3. Results and discussion

3.1. Measurements in perchlorate solutions

Although the indium(III) peak position and the character of the corresponding electrode process are strongly influenced by chloride ions, the present results were obtained using $InCl_3 \cdot 4H_2O$ as a starting material. Taking into account that in reality chloride-free solutions are more an exception than the rule, the intention was to keep this anion at a constant level instead of avoiding it completely.

If the concentration of sodium perchlorate is gradually increased (from 0 to 9.25 mol l^{-1}) at a constant level of In(III) ($1.4 \cdot 10^{-4}$ mol l^{-1}) and a constant acidity (0.01 mol l^{-1} $HClO_4$), the SW peak height changes as shown in Fig. 1. At first there is a current decrease with increasing electrolyte concentration up to 0.5 mol l^{-1} $NaClO_4$. This is followed by a relatively wide range in which the peak height is nearly constant. Finally, a very pronounced current enhancement is observed for perchlorate concentrations higher than about 4 mol l^{-1}.

The increase in the perchlorate concentration followed by the increased viscosity of the solution makes the diffusion coefficients lower. At the same time, the water activity (a_w) also decreases [3].

SW peak-height enhancement, observed under such conditions, can be a consequence of either the increased reaction rate or the reactant accu-

mulation at the electrode surface. As adsorption is not important in non-complexing media, it follows that the results in Fig. 1 should be interpreted mainly in terms of changed reaction rate, especially because lowering of the diffusion coefficients seems to be of minor importance.

A decrease in reaction rate with an increase in electrolyte concentration is a well known phenomenon [20,21], termed the Frumkin double-layer effect. This may be the reason for the observed decrease in peak height at lower perchlorate levels (Fig. 1).

In more concentrated electrolyte solutions, the decrease in the diffusion coefficients is completely masked by a much more pronounced effect of the decreased water activity. These results indicate that water molecules play an important role in the overall electrode reaction, dissociation of an aqua complex being most probable rate-determining step. In Fig. 1 the solid line gives $1/a_w$ as a function of log[$NaClO_4$], based on recently published data [3], whereas the points correspond to the experimentally obtained SW peak currents. Except at low perchlorate concentrations, the peak height is inversely proportional to a_w, indicating that water molecules from $In(H_2O)_6^{3+}$ [18,22] are released in the rate-determining step.

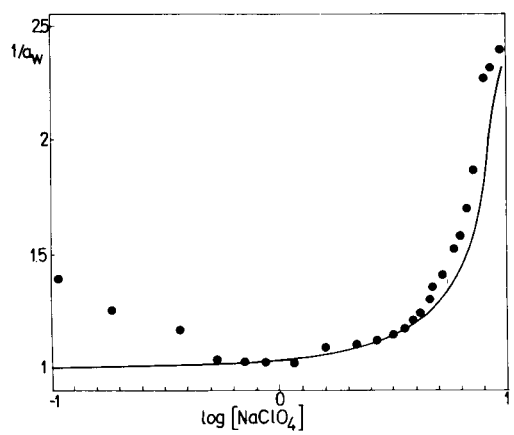

Fig. 1. SWV peak heights (●) in arbitrary units as a function of the electrolyte concentration, compared with the reciprocal values of water activity (full line). [In(III)] = 1.4×10^{-4} mol l^{-1}; [$HClO_4$] = 0.01 mol l^{-1}; initial potential, −0.8 V; frequency, 100 s^{-1}; amplitude, 16 mV; scan increment, 2 mV.

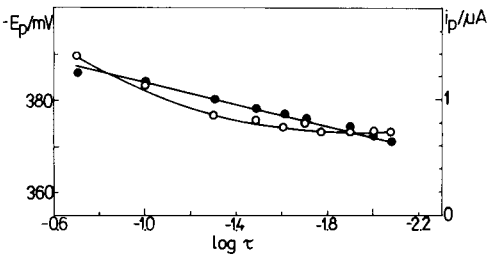

Fig. 2. Dependence of indium(III) SW peak height (○) and potential (●) on the characteristic time of measurement in 1 mol l^{-1} $NaClO_4$. Other conditions as in Fig. 1.

Unfortunately, their number cannot be calculated from the present results.

Additional evidence that the electrode process is controlled by the rate of the preceding reaction arises from the current–frequency (and potential–frequency) dependence. In 1 mol l^{-1} $NaClO_4$ the peak height decreases whereas the peak potential shifts positively with increasing SW frequency (f). If these results are presented as a function of log τ, where $\tau = 1/f$, the curves given in Fig. 2 are obtained. They are, together with virtually constant half-peak widths, in good agreement with theoretical predictions [23] for this type of process. For a sufficiently large $k\tau$ and sufficiently small K (where k denotes the sum of the forward and reverse first-order homogeneous rate constants and K is their ratio) a limiting slope $\delta nE_p/\delta \log(k\tau)$ of 29.6 mV is expected. In the present experiments with indium(III), the peak potential is shifted over 10 mV with a tenfold decrease in τ (i.e. a tenfold increase in frequency), which is in accordance with the theory [23], taking into account that three electrons are involved in the electrode process.

With an increase in perchlorate concentration, the peak potential shifts in the positive direction. The shape of the corresponding curve (Fig. 3) is similar to the dependence of a_w on log[$NaClO_4$], but the shift cannot be described by the simple equation $E_p = A + b \log a_w$.

In this type of measurement water is usually treated as a ligand [3,24] and, assuming the reversible (or unchanged) character of the electrode process, an anodic peak potential shift is described as a consequence of the "decomplexa-

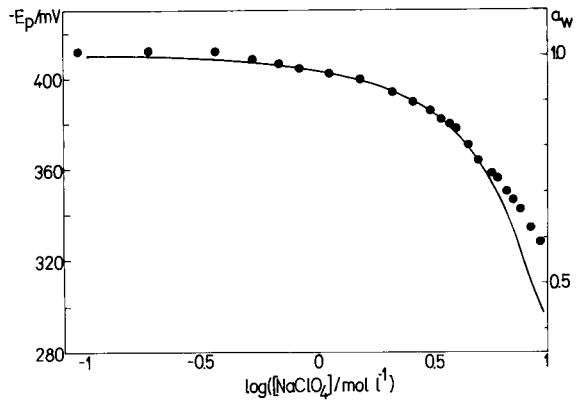

Fig. 3. Indium(III) SW peak potential (●) as a function of electrolyte concentration in comparison with the corresponding changes in water activity (full line). Conditions as in Fig. 1.

tion" process on lowering of the ligand concentration. From the linear part of such a curve, with or without further corrections for liquid junction potentials and other effects, the number of released water molecules can be calculated, assuming that Lingane's relationship [14] is valid. In the present situation a corresponding treatment of the experimental data is not appropriate because the degree of reversibility of the electrode process depends on the ligand concentration.

According to the literature data [5], the electrode process is pH dependent. Therefore, the experiments described above and performed in the presence of 0.01 mol l^{-1} $HClO_4$ were repeated at 10 and 100 times higher acidities. The general shape of the i_p vs. log[$NaClO_4$] curve,

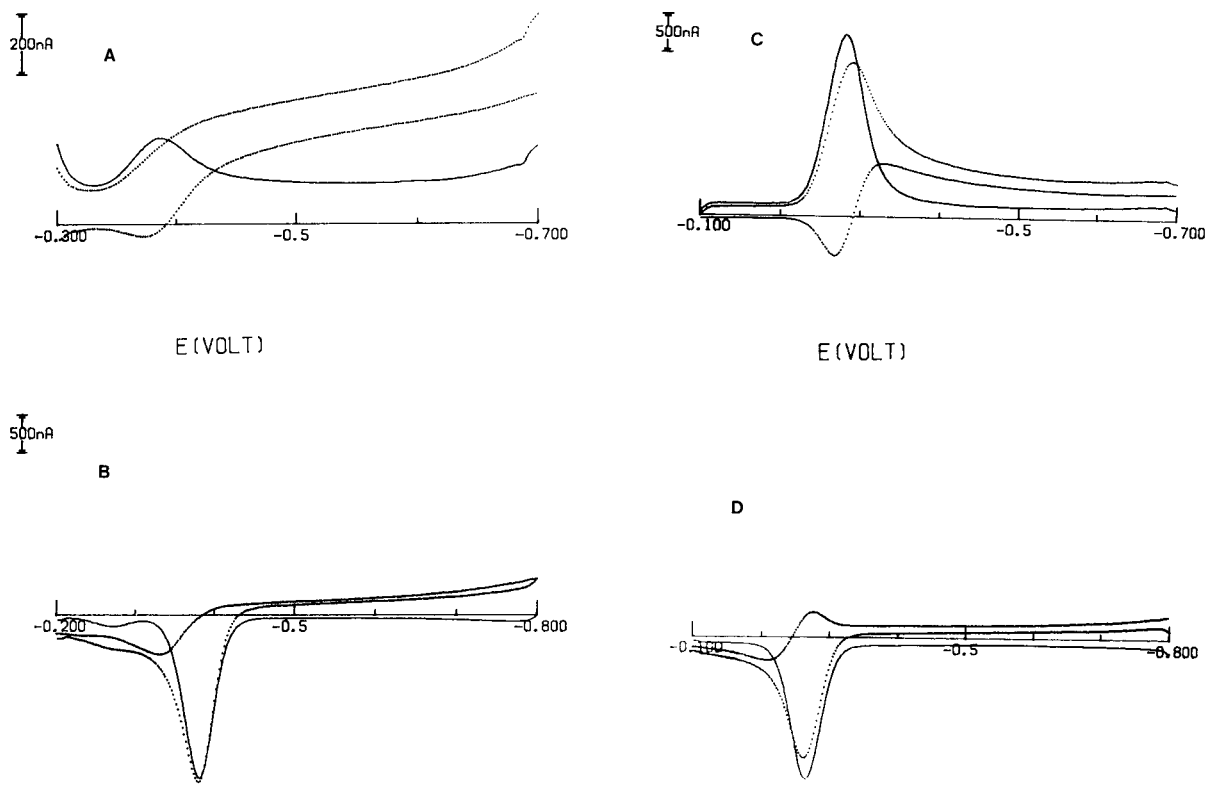

Fig. 4. Indium(III) SW peaks obtained from (A, B) 1 and (C, D) 9.25 mol l^{-1} $NaClO_4$ after scanning in the (A, C) cathodic and (B, D) anodic directions. Each full line gives the net signal whereas the dotted lines indicate forward and reverse currents.

however, was not significantly changed except for very low salt concentrations where the decrease of the curve was smaller or completely eliminated. Additionally, the peak currents within the "gap" were lower at higher acidities in accordance with some older literature data [5], indicating an extremely strong catalytic influence of OH^- ions even at trace levels.

All the results described above were obtained after scanning in the anodic direction. If a cathodic scan is applied instead, the peak height vs. electrolyte concentration and peak potential vs. electrolyte concentration relationships are of the same type as already mentioned. Some differences can only be observed in the shape of the signal and the absolute value of its current. After scanning in the anodic direction, the peaks are higher and better defined. Some of them (obtained under different conditions) together with their components are given in Fig. 4. By comparison of the forward and reverse currents, recorded at 1 and 9.25 mol l^{-1} $NaClO_4$, increased reversibility at higher electrolyte concentrations can be observed.

The electrode reactions of indium(III) at increasing sodium perchlorate concentration were also followed by cyclic voltammetry. For a process controlled by the rate of the preceding reaction (CE mechanism), theory [25] predicts that the ratio between the cathodic and the corresponding anodic current should be < 1. In the present system, the reduction peak was extremely low and elongated (Fig. 5), irrespective of the perchlorate level. Its height and potential could not be measured accurately (and in some instances peaks were not recognized by the instrument), preventing the usual treatment of experimental CV data. Only a well developed anodic signal could be followed without difficulty. In the applied perchlorate concentration range, its height gradually decreases to 46% of the initial value.

As a_w should tend to zero at sufficiently high electrolyte concentrations (i.e., $1/a_w \rightarrow \infty$), the SW peak current is expected to become nearly constant. Under such conditions dissociation of the aqua complex would not be the rate-determining step and the whole electrode process would become reversible. With sodium perchlo-

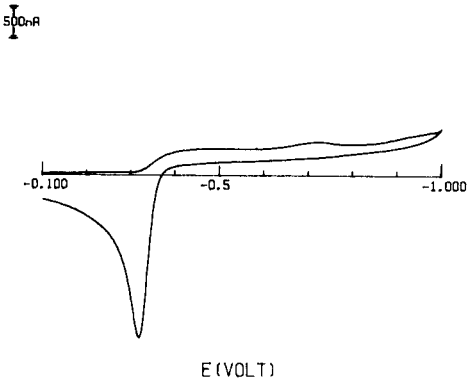

Fig. 5. Cyclic voltammogram of 1.4×10^{-4} mol l^{-1} $InCl_3$ in 4.6 mol l^{-1} $NaClO_4$ and 0.01 mol l^{-1} $HClO_4$. Scan rate, 50 mV s^{-1}.

rate this could not be reached because unreallistically high salt concentrations would be necessary.

If magnesium perchlorate (up to 3 mol l^{-1}) is used instead, the results are not better, although in this system lower water activities are expected [26]. Two reasons can be found for this: the water activity is not sufficiently low and the influence of Mg^{2+} is different to that of Na^+. As demonstrated in a study of the electrochemical reduction of zinc(II) [21], the rate parameter depends on the radius and charge of the inert cation.

3.2. Measurements in chloride solutions

In addition to decreased water activity, halide ions can also accelerate the rate of the indium(III) reduction process. It is generally accepted that partial replacement of coordinated water molecules with a ligand makes dissociation of the remaining water molecules easier [5]. In Fig. 6 the results for the system $[NaClO_4] + [NaCl] = 1$ mol l^{-1} (at a constant level of the total dissolved indium and a constant acidity) are given. This ionic strength corresponds to the "gap" in Fig. 1, i.e., perchlorate concentrations that give very low peak currents. By increasing the chloride concentration at a constant ionic strength the indium peak increases but does not reach a constant value. However, the character of the electrode process is obviously changed. This can be seen from the peak current and potential dependences

on the SW frequency, i.e., on the characteristic time of the experiment. In 1 mol l^{-1} NaCl, E_p becomes constant whereas i_p increases proportionally to $f^{1/2}$, indicating that the electrode process is diffusion controlled. In comparison with results obtained in 1 mol l^{-1} $NaClO_4$, the peaks recorded from 1 mol l^{-1} NaCl indicate obviously increased reversibility (Fig. 6B and C).

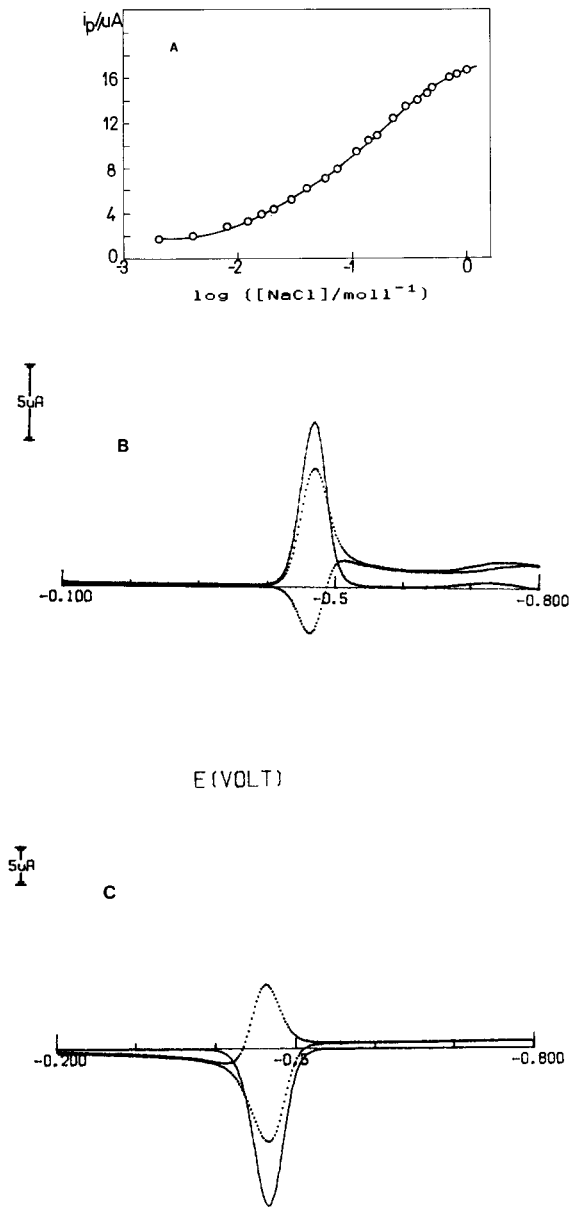

Fig. 6. (A) In(III) SW peak current as a function of chloride concentration measured at a constant ionic strength $I = 1$ mol l^{-1}. (B, C) Forward, reverse and net currents recorded from 1 mol l^{-1} NaCl by scaning in the (B) cathodic and (C) anodic directions. Other conditions as in Fig. 1.

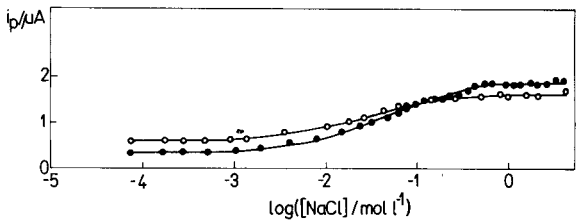

Fig. 7. In(III) SW peak current as a function of sodium chloride concentration. $I = (\bullet)$ 4 and $(\circ)$ 5 mol l^{-1}; $[HClO_4] = 0.01$ mol l^{-1}; $[In(III)] = 2.5 \times 10^{-5}$ mol l^{-1}; initial potential, -0.8 V; SW frequency, 100 s^{-1}; amplitude, 10 mV; scan increment, 2 mV.

Further experiments were performed at higher ionic strengths ($I = 4$ and 5 mol l^{-1}), i.e., corresponding to the ascending part of the curve in Fig. 1. Under such conditions a complete S-shaped curve is obtained. In the series with a lower total salt concentration (4 mol l^{-1}), the initial peak height, i.e., that before the addition of NaCl, is lower, whereas the final peak height is higher than that in more concentrated electrolyte solution (Fig. 7). At the higher ionic strength (5 mol l^{-1}), however, a constant peak height is reached at a lower chloride concentration.

Similar results were obtained with $[LiClO_4] + [LiCl] = 4$ mol l^{-1} (Fig. 8A) as with the corresponding sodium salts.

In the $Mg(ClO_4)_2 + MgCl_2$ system (Fig. 8B) at total electrolyte concentrations of 2 and 3 mol l^{-1}, respectively (i.e., $I = 6$ and 9 mol l^{-1}), the curves are shifted towards higher chloride concentrations, although their relative positions are similar to those in the $NaClO_4$–NaCl system. This can be partly explained by the formation of ion pairs in solutions of the doubly charged cation [27], which decreases the concentration of free chloride ions.

The total indium(III) concentration does not affect the type of experimental results in chloride–perchlorate solutions and virtualy identical conclusions arise from the measurements performed at 10^{-4}, 10^{-5} and 10^{-6} mol l^{-1} $InCl_3$.

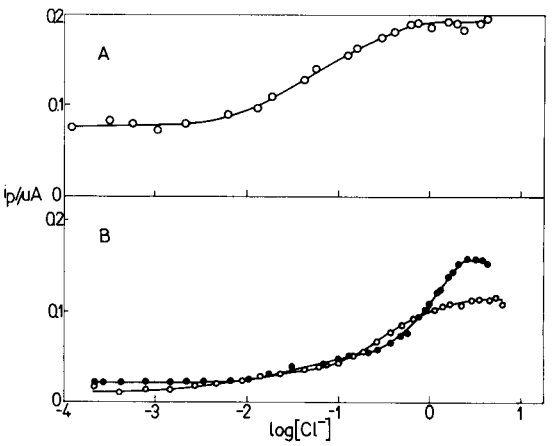

Fig. 8. Indium(III) SW peak height as a function of chloride concentration at a constant ionic strength. (A) $[LiClO_4]+[LiCl] = 4$ mol l^{-1}; (B) $[Mg(ClO_4)_2]+[MgCl_2] =$ (○) 2 and (●) 3 mol l^{-1}. $[In(III)] = 2.8\times10^{-6}$ mol l^{-1}. Other conditions as in Fig. 7.

The reproducibility of the results is good. The different peak currents obtained at the same metal and electrolyte concentrations, which can be observed by comparison of the different figures in this paper, arise from the application of different electrode systems.

As already mentioned, the number of possible chloride complexes and their formation constants at different ionic strengths had not been firmly established, so the present experimental results cannot be correlated with the fraction of the total dissolved indium bound in some or all coordination species. Only information about the maximum coordination number can be obtained from the highest slope of the curve that gives peak potential as a function of $\log[Cl^-]$.

At high chloride concentrations, which are characterized by a constant value of the indium(III) peak current, the electrode reaction rate can be taken as constant. Under such conditions it is possible to ascribe the observed peak potential shift to the complexation process. Irrespective of the applied ionic strength ($I = 4$–9 mol l^{-1}) or the cation of the basic electrolyte, a peak potential shift higher than 70 mV per decade was obtained. This result indicates that the most probable maximum coordination number is four, but the formation constant of $InCl_3$ is higher than that of $InCl_4^-$. This is in accordance with the statement, given in a critical review on indium(III) complexation constants [18], that partly hydrated InX_n species up to $n = 4$ must be considered for all halides and pseudohalides.

3.3. Measurements in bromide and iodide solutions

The peak current of indium(III) as a function of bromide concentration was followed at three different ionic strengths (4, 5 and 6 mol l^{-1}) maintained with $NaClO_4$. The results, i.e., the shapes of the corresponding curves and their relative positions (Fig. 9A), are very similar to those already described for the chloride–perchlo-

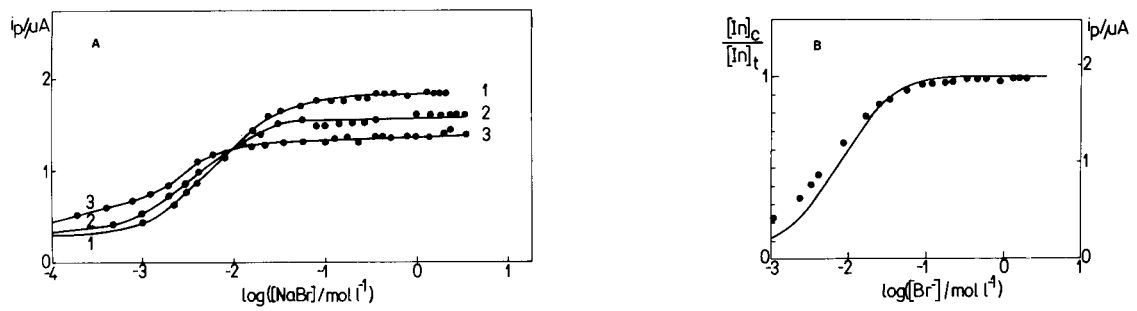

Fig. 9. In(III) SW peak current (A) as a function of bromide concentration at a constant ionic strength of (1) 4, (2) 5 (3) 6 mol l^{-1} and (B) in comparison with the fraction (In_c) of the total metal ($[In]_t = 2.5\times10^{-5}$ mol l^{-1}) bound in bromide complexes (full line) at $I = 4$ mol l^{-1}. Formation constants ($\log\beta_1 = 2.08$, $\log\beta_2 = 3.4$, $\log\beta_3 = 4.0$, $\log\beta_4 = 4.8$) taken from [28].

rate system. This applies also to the conclusion that $InBr_4^-$ is the highest complex under the applied conditions. Unfortunately, the number of water molecules included in this species cannot be evaluated from the voltammetric data, but $InBr_4(H_2O)_2^-$ is the expected composition.

The S-shaped curve that gives the SW peak current dependence on $\log[Br^-]$ at a constant metal concentration is very similar to the curve that gives the fraction of the total dissolved metal bound in bromide complexes (Fig. 9B), although the experimental results were not corrected for the small current that could be measured in the absence of bromide. This similarity cannot be just a coincidence because replacement of water molecules with halide ions really accelerates the dissociation of the "mixed" aqua–halide species in comparison with the simple aqua complex.

It would be interesting to investigate whether, in the absence of other complications, such a correlation is generally valid. In the chloride–perchlorate system, however, this could not be tested because the corresponding formation constants for high ionic strengths are not available.

When iodide is used instead of bromide, a completely different influence on the electrochemical behaviour of indium(III) is observed. Although adsorption processes cannot be proved at either cathodic or anodic potentials, the peak height dependence on $\log[I^-]$ is bell shaped. Additionally, from the change in the half-peak width, it seems that the number of exchanged electrons is not constant. For all these reasons the processes of indium(III) in iodide solutions should be studied in more detail.

Acknowledgements

This work was supported by the Ministry of Science, Technology and Informatics of the Republic of Croatia. Part of the experimental work was performed at the Institute for Applied Physical Chemistry, Research Centre (KFA), Jülich (Germany), within the framework of the joint project.

References

[1] V.V. Losev and A.I. Molodov, in A.J. Bard (Ed.), Encyclopedia of Electrochemistry of the Elements, Vol. 6, Dekker, New York, 1976, p. 1.
[2] Š. Komorsky-Lovrić, M. Lovrić and M. Branica, J. Electroanal. Chem., 241 (1988) 329.
[3] M. Lovrić, Š. Komorsky-Lovrić and M. Branica, Indian J. Chem., 29A (1990) 435; J. Electrochem. Soc., 140 (1993) 1850.
[4] E.D. Moorhead and T.S. Robinson, Anal. Chem., 64 (1992) 833, and references cited therein.
[5] A.J. Engel, J. Lawson and D.A. Aikens, Anal. Chem., 37 (1965) 203.
[6] L. Pospišil and R. de Levie, J. Electroanal. Chem., 25 (1970) 245.
[7] E. Malyszko and J. Malyszko, Monatsh. Chem., 124 (1993) 15.
[8] L. Kiss and J. Szalma, Acta Chim. Hung., 128 (1991) 781.
[9] F. Anson, Acc. Chem. Res., 8 (1975) 400, and references cited therein.
[10] A.M. Bond, Electrochim. Acta, 119 (1972) 1503.
[11] Š. Komorsky-Lovrić and M. Branica, J. Electroanal. Chem., 358 (1993) 273.
[12] G.W. O'Dom and R.W. Murray, J. Electroanal. Chem., 16 (1968) 327.
[13] M.C. Montemayor and E. Fatas, Electrochim. Acta, 33 (1988) 655 and 1779.
[14] D.R. Crow, Polarography of Metal Complexes, Academic, London, 1969.
[15] K. Momoki and H. Ogawa, Anal. Chem., 43 (1971) 1664.
[16] P. Kondziela and J. Biernat, J. Electroanal. Chem., 61 (1975) 281.
[17] J.N. Gaur, D.S. Jain and M.M. Palrecha, J. Chem. Soc. A, 1968, 2201.
[18] D.G. Tuck, Pure Appl. Chem., 55 (1983) 1477.
[19] I. Pižeta and M. Branica, J. Electroanal. Chem., 250 (1988) 293.
[20] N.S. Hush and J. Blackledge, J. Electroanal. Chem., 5 (1963) 420.
[21] H.L. Jindal, K. Matsuda and R. Tamamushi, J. Electroanal. Chem., 90 (1978) 185.
[22] H. Ohtaki and T. Radnai, Chem. Rev., 93 (1993) 1157, and references cited therein.
[23] J. O'Dea, J. Osteryoung and R.A. Osteryoung, Anal. Chem., 53 (1981) 695.
[24] M. Djogic and M. Branica, Anal. Chim. Acta, 281 (1993) 291.
[25] Southampton Electrochemistry Group, Instrumental Methods in Electrochemistry, Horwood, Chichester, 1990, p. 190.
[26] B. Behr and J. Malyszko, Roczn. Chem., 41 (1967) 1589.
[27] K.S. Johnson and R.M. Pytkowicz, Am. J. Sci., 278 (1978) 1428.
[28] E.A. Burns and D.N. Hume, J. Am. Chem. Soc., 79 (1957) 2704

ELSEVIER

Analytica Chimica Acta 289 (1994) 307–311

ANALYTICA CHIMICA ACTA

Detection of actomyosin depolymerization with a piezoelectric quartz crystal

Shigeru Kurosawa [a,1], Eiji Nemoto [b], Makoto Muratsugu [c], Minoru Yoshimoto [a], Yoshihito Mori [a], Naoki Kamo [a,*]

[a] *Faculty of Pharmaceutical Sciences, Laboratory of Biophysical Chemistry, Hokkaido University, Sapporo 060, Japan*
[b] *Department of Mechanical Engineering, Ibaraki National College of Technology, Katsuta 312, Japan*
[c] *Department of Laboratory Medicine, Asahikawa Medical College, Asahikawa 078, Japan*

(Received 20th April 1993; revised manuscript received 25th June 1993)

Abstract

A resonance method was previously proposed to measure the frequency change of piezoelectric quartz crystals [S. Kurosawa et al., *Anal. Chim. Acta,* 274 (1993) 209]. The ordinary method which incorporates the crystal into an oscillator circuit is here referred to as the oscillation method. Viscosity changes during the depolymerization of actomyosin can be detected by a piezoelectric quartz crystal because its frequency change is sensitive to the viscosity in a solution. This change is not detectable by the oscillation method (using TTL circuit), but may be detected by the resonance method using a 'spectrum analyzer', which shortens the analysis time, compared with the technique described earlier.

Key words: Piezoelectric methods; Actomyosin depolymerization; Quartz crystals

1. Introduction

The oscillating frequency of a piezoelectric quartz crystal changes in response to the adsorption of substances on the crystal surfaces [1,2]. When the crystal is dipped into a solution, it oscillates with a frequency depending on the solvent used [3,4]. A number of applications of such a crystal placed in contact with solutions have been published [5–8]. Previous authors measured oscillating frequencies in various solutions and developed experimental [3,4] and theoretical equations [9,10]. Bruckenstein and Shay [9] and Kanazawa and Gordon [10] derived the following equation:

$$\Delta F = -2.26 \times 10^{-6} \times n \times F_b^{3/2} \times \sqrt{\rho\eta} \qquad (1)$$

where η is the viscosity of the solution, ρ the density of the solution, n the number of surfaces of the crystal contacting the solution ($n = 1$ or 2), and F_b the fundamental oscillating frequency of the crystal. Hager pointed out a similar relation using an experimental system with an automatic gain control circuit [11].

* Corresponding author.
[1] Present address: National Institute of Materials and Chemical Research, Tsukuba 305, Japan.

SSDI 0003-2670(93)E0673-U

In the conventional method the piezoelectric crystal is used as an active element in an oscillating circuit. We showed that values of resistance or of capacitance in a circuit (using transistor logic: TTL) affect the frequency change when crystals are in solutions [12]. In this report, we refer to this method as the oscillation method. We have proposed a resonance method in which the crystal was used as a passive element; the transmission of the quartz resonator in a two-port set-up was measured at various frequencies [13]. The series resonant point F_s and parallel resonant point F_p can be readily determined by direct readout from the transmission curve. The differences of these values from the reference state (unloaded in the air) were denoted as ΔF_s and ΔF_p. We observed that ΔF_s is proportional to $\sqrt{\rho\eta}$, as is seen in Eq. 1. A similar passive method using an admittance locus [14,15] and a network analyzer [16] has been reported. Martin et al. [17] were recently able to combine an equivalent circuit model for the electrical behaviour of the quartz with liquid-phase properties.

Independent of the method of measurement, a viscosity change in a solution would cause a frequency change in the crystal, as shown in Eq. 1. Actomyosin is a fibrous muscle protein present in humans, beasts, fishes, birds, insects and reptiles [18]. The viscosity of an actomyosin solution under the condition of high ionic strength is greatly decreased by the addition of adenosine 5′-triphosphate (ATP); this decrease in viscosity is sometimes used as an index of the freshness of fish meat. We report here that decrease in the viscosity due to the depolymerization of actomyosin cannot be detected by the oscillation method, but is detectable by the resonance method. A long time was required by our previous resonance method [13], but the use of a spectrum analyzer shortens the assay time.

2. Experimental

AT-cut crystals of 9 MHz (Yakumo Tsushin, Tokyo) were used. One side of a quartz crystal was coated with a silicon sealant since the coating assured stable oscillation when the crystal was dipped in solutions over a wide range of $\sqrt{\rho\eta}$ [12,13].

The transmission of the crystal was measured using a Hewlett-Packard 3588A spectrum analyzer and the transmission curve was recorded with a Hewlett-Packard 7225A plotter. The signal source level was 0 dBm (1 mW). Frequencies scanned were between 8950000 and 9050000 Hz, and 1000 data points were stored during the single scanning. The measurement was repeated 10 times and averaged data were obtained. Less than 1 min was required for a ten-sweep accumulation, whereas a single manual sweep took about 15 min using our previous method [13].

The oscillating electronic circuit of the oscillation method was made of TTL gates (SN7400), and the resistance and capacitance of the circuit were the same as those in Circuit II in a previous paper [12].

Actomyosin was prepared from the dorsal muscle of a fresh carp (*Cyprinus carpio Linné*) by a slight modification of the method described previously [19,20]. The sample obtained had ATPase activity of 0.10 μmol min^{-1} mg^{-1}. The viscosity of actomyosin solution was determined by an Ostwald viscometer at 20 ± 0.1°C.

3. Results and discussion

With the spectrum analyzer, ΔF_s and ΔF_p were measured when the crystal was dipped in aqueous solutions of varying concentrations of sucrose whose $\sqrt{\rho\eta}$ values were covered up to 47 $g^{1/2}$ $cm^{-3/2}$ $cP^{1/2}$ [21]. The proportional relationship between ΔF_s and $\sqrt{\rho\eta}$ held up to about 25.45 $g^{1/2}$ $cm^{-3/2}$ $cP^{1/2}$ of $\sqrt{\rho\eta}$ (mean value of three crystal is: $\Delta F_s = 1.7975 + 3.1868\ \sqrt{\rho\eta}$ in unit of kHz, $r = 0.998$). The numerical value of $2.26 \times 10^{-6} \times Fb^{3/2}$ is 6.1 kHz $g^{-1/2}$ $cm^{3/2}$ $cP^{-1/2}$ since $n = 1$ and $F_b = 9$ MHz. Above 25.45 $g^{1/2}$ $cm^{-3/2}$ $cP^{1/2}$ of $\sqrt{\rho\eta}$ negative deviations were observed in the plots of ΔF_s against $\sqrt{\rho\eta}$. We did not observe a proportional relationship between ΔF_p and $\sqrt{\rho\eta}$. The similar results were already reported: for example, Zhou et al. [15]

showed the linear relation between ΔF_s and $\sqrt{\rho\eta}$ below ca. 25 $g^{1/2}$ $cm^{-3/2}$ $cP^{1/2}$ and the negative deviations above this value. In addition, they observed the discrepancy from the theoretical values for the slope in the ΔF_s vs. $\sqrt{\rho\eta}$ plot. These facts show that the present method and apparatus can follow the $\rho\eta$ change.

Weber and Protzehl [22] introduced the term ATP sensitivity (S_{ATP}) and defined it as

$$S_{ATP} = \frac{\log(\eta_r) - \log(\eta_{r\cdot ATP})}{\log(\eta_{r\cdot ATP})} \times 100 \qquad (2)$$

where η_r and $\eta_{r\cdot ATP}$ are the relative viscosity of actomyosin solution before and after addition of ATP · Mg (1 or 2 mM). The protein was dissolved in 0.6 M KCl–malate (pH 7.0, $I = 0.6$) and its concentration was adjusted to 3.0 mg/ml. Addition of ATP decreases the viscosity of the solution, because the fibrous actomyosin dissociates into globular proteins (actin and myosin). For fresh actomyosin, S_{ATP} is approximately 99.7 because the viscosity becomes very small with the addition of ATP: η_r and $\eta_{r\cdot ATP}$ of our sample were 2.62 and 1.62. If actomyosin becomes old or is extracted from old meat, S_{ATP} is small. Heat denaturation or lengthy storage (for about one year at 0°C) decreased S_{ATP} to almost zero.

When substances such as ADP (adenosine 5′-diphosphate), AMP (adenosine 5′-monophosphate) and NADH (β-nicotinamide adenine dinucleotide, reduced form) were added to induce the viscosity changes, the definition of sensitivity, S_i (i = ADP, AMP and NADH) was the same as S_{ATP}.

Since ρ is kept almost constant during the ATP-induced depolymerization of actomyosin, the viscosity change is proportional to the change of $\rho\eta$, to whose change the frequency of the piezoelectric crystal is sensitive. Detection of this change was attempted by two methods: the oscillation method and the resonance method with a spectrum analyzer.

Results are shown in Table 1, Fig. 1 and Fig. 2, where ΔF_{osc} stands for the frequency change obtained by the oscillation method. Transmission curves become sharp with the decrease in viscosity due to the depolymerization (see Fig. 3 in Ref. 12) and Po_{max}, the output voltage at F_s, should increase after to depolymerization. Both ΔF_s and Po_{max} met the expectations. In contrast, however, we did not observe ΔF_{osc}. When denatured sample (heat-treated or long stored) was used, no frequency change was observed, suggesting that

Table 1
Resonance and oscillating frequency change of quartz crystal associated with the actomyosin depolymerization

Chemical added [a]	S_i [b]	ΔF_{osc} (Hz)	ΔF_s (Hz)	ΔPo_{max} [c] (dBm)
ATP (1 mM)	99.7	2±5	200±57	0.15±0.02
ATP (2 mM)	99.7	3±7	300±93	0.20±0.05
ADP (1 mM)	53.0	2±3	50± 5	0.04±0.01
AMP (1 mM)	3.4	0	0± 3	0.01±0.01
NADH (1 mM)	2.8	0	0± 2	0.01±0.01
ATP (1 mM) [d]	0	0	0± 5	0.01±0.01
ATP (2 mM) [d]	0	0	0± 7	0.01±0.01
ATP (1 mM) [e]	0	0	0± 5	0.01±0.01
ATP (2 mM) [e]	0	0	0± 9	0.01±0.01

Actomyosin (3 mg/ml) was dissolved in 0.6 M KCl–malate (pH 7.5). Experiments were done three times and averages (±S.D.) are shown.

[a] Mg salt was added.

[b] The definition is given in the text.

[c] ΔPo_{max} stands for the change in the output of the spectrum analyzer at F_s. The input power to the crystal was 0 dBm (1 mW).

[d] Heat treatment (62°C for 2 min) was done for actomyosin denaturing.

[e] Long-time storage (about 1 year at 0°C) was done for actomyosin denaturing. All experiments were done at 20± 0.1°C.

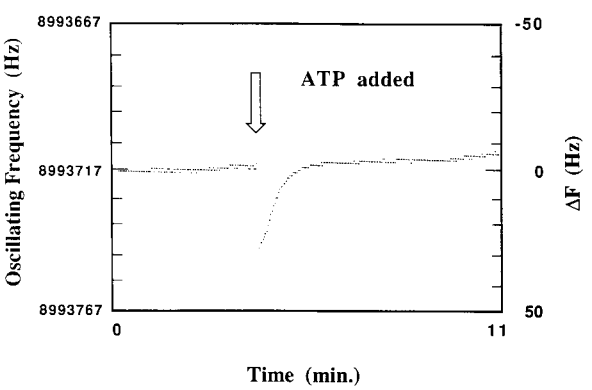

Fig. 1. No frequency change with the addition of 0.1 M ATP·Mg to actomyosin solution by the oscillation method. The transient change is an artefact due to ATP addition.

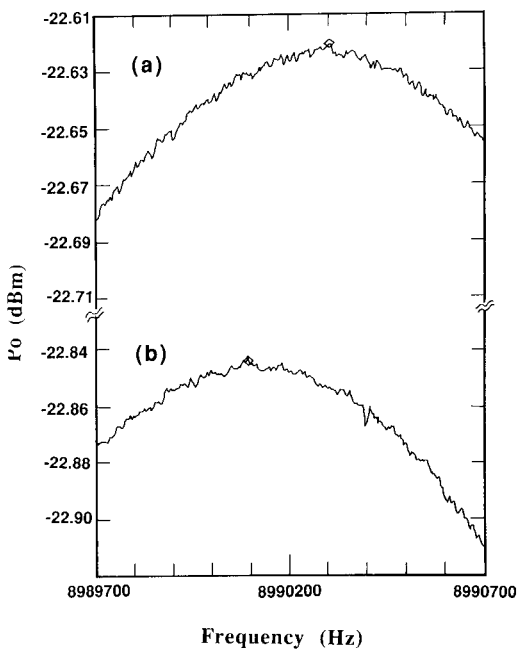

Fig. 2. Typical frequency change with the addition of ATP·Mg to actomyosin solution by the resonance method. Diamond symbol indicates the series resonant point F_s and the maximum output Po_{max} of transmission for a crystal. (a) Addition of 0.1 M ATP·Mg, F_s; 8 990 305 Hz, Po_{max}; −22.62 dBm. (b) Before addition of ATP·Mg, F_s; 8 990 092 Hz, Po_{max}; −22.84 dBm.

the change found by the resonance method may be caused by the depolymerization. On addition of 1 mM ADP a smaller change in ΔF_s was recognized; this is reasonable because there was minimal depolymerization of actomyosin with ADP (S_{ADP}, 53.0). When AMP and NADH were added, neither S_i nor ΔF_s changed.

In this paper, we have shown the possibility for producing a sensor for monitoring the freshness of meat, although separation of actomyosin is needed. Why is it that only the resonance method is able to detect the viscosity change of the depolymerization? We cannot answer this at present, and can only offer the following facts. With the oscillation method, we previously observed a parabolic curve in the plots of ΔF versus $\sqrt{\rho\eta}$ when various non-electrolyte polymer solutions were examined [12].

From the calibration line between ΔF and $\sqrt{\rho\eta}$, the change in the frequency is expected to be 1.1 kHz when η_r is changed from 2.62 to 1.62 at the depolymerization. The change actually observed is smaller than this value. Charlesworth [23] described that the molecular shape may affect the oscillation frequency of the quartz crystal. Reed et al. [24] also suggest that the polymers of high molecular weight exhibit viscoelasticity at MHz range. Muratsugu et al. [25] noted that ΔF_{osc} values in sucrose–phosphate buffer solutions were smaller than those of sucrose solutions though the viscosity and density were almost equal. In electrolyte solutions, the oscillating frequency is also influenced by the conductance of the solutions [3,4]. In addition, circuit parameters such as equivalent capacitors inside the transistors affect the oscillation frequency [12]. Therefore, we plan to measure the frequency change in various polymer solutions and in electrolyte solutions using both methods, and comparison of the values obtained by the two methods will hopefully give a clue.

Acknowledgement

The authors are grateful to Yokogawa-Hewlett-Packard for technical and instrumental support, to A. Yasuike and K. Hirama (Toyo Communication Equipment Co., Ltd.) for useful discussion of piezoelectric devices and to I. Endo (Ibaraki National College) for his generous instrumental support. This work was partially financially supported in part by the Suzuken Memorial Foundation.

References

[1] G. Sauerbrey, Z. Phys., 155 (1959) 206.
[2] G.G. Guilbault, in C.S. Lu and A.W. Czanderna (Eds.), Methods and Phenomena, Their Applications to Science and Technology, Vol. 7, Elsevier, New York, 1984, Chaps. 8 and 10.
[3] T. Nomura, M. Watanabe and T.S. West, Anal. Chim. Acta, 175 (1985) 107.
[4] S.Z. Yao and Z.H. Mo, Anal. Chim. Acta, 193 (1987) 97.

[5] J. Janata and A. Bezegh, Anal. Chem., 60 (1988) 62R.; J. Janata, Anal. Chem., 64 (1992) 196R.
[6] J.J. McCallum, Analyst, 114 (1989) 1173.
[7] M.D. Ward and D.A. Buttry, Science, 249 (1990) 1000; D.A. Buttry, in A.J. Bard (Ed.), in Electroanalytical Chemistry, Vol. 17, Marcel Dekker, New York, 1991, pp. 1–85.
[8] M. Thompson, A.L. Kipling, W.C. Duncan-Hewitt, L.V. Rajaković and B.A. Čavić-Vlasak, Analyst, 116 (1991) 881.
[9] S. Bruckenstein and M. Shay, Electrochim. Acta, 30 (1985) 1295.
[10] K.K. Kanazawa and J.G. Gordon II, Anal. Chim. Acta, 175 (1985) 99.
[11] H.E. Hager, Chem. Eng. Commun., 43 (1986) 25.
[12] S. Kurosawa, E. Tawara, N. Kamo and Y. Kobatake, Anal. Chim. Acta, 230 (1990) 41.
[13] S. Kurosawa, H. Kitajima, Y. Ogawa, M. Muratsugu, E. Nemoto and N. Kamo, Anal. Chim. Acta, 274 (1993) 209; S. Kurosawa, E. Tawara, N. Kamo and H. Kitajima, The Electrochemical Society Fall Meeting, Seattle, WA, Abstract No. 798, 1990, p. 1136.
[14] H. Muramatsu, E. Tamiya and I. Karube, Anal. Chem., 60 (1988) 2142.
[15] T. Zhou, L. Nie and S. Yao, J. Electroanal. Chem. Interfacial Electrochem., 293 (1990) 1.
[16] A.L. Kipling and M. Thompson, Anal. Chem., 62 (1990) 1514.
[17] S.J. Martin, V.E. Granstaff and G.C. Frye, Anal. Chem., 63 (1991) 2272.
[18] A.F. Huxley, Prog. Biophys. Molec. Biol., 7 (1957) 255; H.E. Huxley, Science, 164 (1969) 1356.
[19] R. Takashi, K. Arai and T. Saito, Bull. Jpn. Soc. Sci. Fisheries, 36 (1970) 169.
[20] S. Iwami and K. Arai, Bull. Jpn. Soc. Sci. Fisheries, 54 (1988) 2019.
[21] R.C. Weast, Handbook of Chemistry and Physics, 67th edn., CRC Press, Boca Raton, FL, 1986, D-262.
[22] H.H. Weber and H. Portzehl, in M.L. Anson, K. Bailey and T.T. Edsall (Eds.), Advances in Protein Chemistry, Vol. 7, Academic Press, New York, 1952, pp. 161–252.
[23] J.M. Charlesworth, Anal. Chem., 62 (1990) 76.
[24] C.E. Reed, K.K. Kanazawa and J.H. Kaufman, J. Appl. Phys., 68 (1990) 1993.
[25] M. Muratsugu, S. Kurosawa and N. Kamo, Anal. Chem., 64 (1992) 2483.

ELSEVIER

Analytica Chimica Acta 289 (1994) 313–319

ANALYTICA CHIMICA ACTA

Rapid detection of *Escherichia coli* using a separated electrode piezoelectric crystal sensor

Fengjiao He [a], Qing Geng [a], Wenghong Zhu [a], Lihua Nie [a], Shouzhuo Yao [a,*], Chang Meifeng [b]

[a] *New Material Research Institute, Hunan University, Changsha 410082, China*
[b] *Biology Department, Hunan Normal University, Changsha 410082, China*

(Received 11th May 1993; revised manuscript received 3rd August 1993)

Abstract

A separated electrode piezoelectric crystal sensor was used to determine *Escherichia coli* bacteria. This method is based on the fact that the resonant frequency shifts with the culture time in a culture medium where *E. coli* is inoculated, and the frequency detection time (FDT) is linearly related to the initial number of *E. coli* in the range $10–10^6$ cells ml^{-1}. Factors that affect the determination are discussed. *E. coli* determination in pure culture was tested by the FDT method and compared with the most probable number technique and standard plate counts method. A correlation coefficient of 0.96 was obtained between the FDT and the decadic logarithm of initial concentration of bacteria. The proposed piezoelectric method is much more rapid and sensitive for determining microorganisms than the traditional methods.

Key words: Biosensors; Piezoelectric sensors; *Escherichia coli*

1. Introduction

Coliform bacteria are one of the most important types of normal bacteria in human and animal intestines, and some types of coliform exhibit pathogenicity toward the human body. Hence the determination of coliform bacteria is very important in clinical medicine, food hygiene and environment monitoring. Standard methods employed for enumerating coliform bacteria involve the most probable number (MPN) technique and the pour plate counts technique with Violet Red Bile Agar (VRBA) [1]. Both techniques are relatively cumbersome and time consuming. Up to 72 h are required to obtain confirmable results. Recently, the use of a piezoelectric crystal sensor as an *Escherichia coli* detector was reported [2]. Anti-*E. coli* antibody was immobilized on the surface of the crystal and the piezoelectric resonant frequency shift due to the mass change caused by specific binding of the microorganisms to the surface was measured. The sensitivity of this method was relatively low, and the concentration range of microorganisms that can be de-

* Corresponding author.

SSDI 0003-2670(93)E0674-V

tected by using this method was narrow (10^6–10^8 cells ml^{-1}).

In this work, a separated electrode piezoelectric crystal sensor was used to determine *E. coli*. The proposed method relies on the facts that metabolizing bacteria change the chemical composition of the growth medium and that these chemical changes cause an alteration in the impedance of the medium. The total impedance alteration represents the changes in the conductance and permittivity components of the growth medium. The resonant frequency of the piezoelectric quartz crystal alters when the conductance and permittivity of the liquid medium change [3–5]. Frequency shifts are detectable when the concentration of the bacteria exceeds a threshold value of 1×10^6–1.5×10^6 cells ml^{-1}. The time required for the initial inoculum to reach the threshold value is defined as the frequency detection time (FDT) and is linearly related to the initial concentration of the bacteria. By using this method, *E. coli* at concentrations ranging from 10 to 10^6 cells ml^{-1} can be detected. The proposed method is much more sensitive than that suggested by Muramatsu et al. [2] and the application concentration range is much wider.

2. Experimental

2.1. Culture medium

An *E. coli* medium (CM) was derived from a medium originally described by Firstenberg-Eden and Klein [6]. The composition of CM is as follows: proteose peptone, 2.5 g; yeast extract, 6 g; lactose, 20 g; sodium desoxycholate, 0.1 g; sodium lauryl sulphate, 1.0 g; bile salts, 1.0 g; and distilled water, 1000 ml. The medium was dispensed into bottles and sterilized by autoclaving at 121°C for 15 min.

2.2. Stock culture

A 20-ml volume of sterilized culture medium was placed in a 50-ml sterilized conical vial and two loops of coliform in pure culture were inoculated on agar with an inoculating loop. After incubation for 16 h at 37°C, the conical vial was removed from the incubator and preserved in a refrigerator. The culture gave an approximate concentration of 3.9×10^9 cells ml^{-1}.

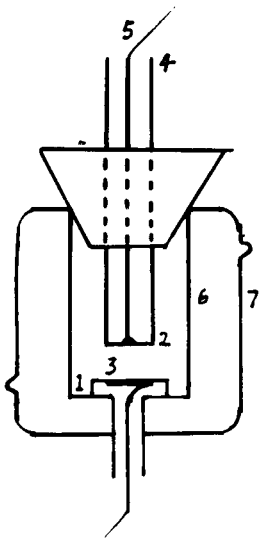

Fig. 1. Schematic diagram of separated electrode piezoelectric sensor: 1 = quartz crystal; 2 = platinum disc; 3 = electrode plated on the crystal; 4 = ground-glass tube; 5 = lead wire; 6 = detector cell; 7 = water jacket.

2.3. Separated electrode piezoelectric crystal

The separated electrode piezoelectric crystal is shown schematically in Fig. 1. The piezoelectric crystal used was an AT cut quartz crystal (diameter 12.5 mm) with a basic resonant frequency of 9 MHz and silver electrodes (diameter 5.5 mm) on both sides of the crystal surface. One side of the electrode was dissolved and a metal disc was placed opposite the quartz disc. The quartz and metal disc were fixed to the top and end of two tubes of the same central axis, respectively. The working electrode (i.e., a metal disc) is separated from the piezoelectric crystal by the liquid layer in the cell by a distance of 16 mm. This system is termed a piezoelectric crystal with one separated electrode.

A Model 4192A impedance analyser from Hewlett-Packard was used. A thermostat was used to control the culture temperature.

2.4. Frequency curve measurement

In an inoculating hood, a 3-ml aliquot of the sterilized medium was placed in each of two sterilized cells with inserted piezoelectric detectors, then coliform was inoculated in one of them. The two cells were removed from the hood and piezoelectric detectors were connected to the impedance analyser through a double-pole, double-throw switch. With the cell temperature controlled at 37°C, the resonant frequency was recorded as described by Wang and Miao [7] every 15 min or a shorter time interval near the FDT. If the frequency in the sample cell containing coliform is F_1 and that in the reference cell is F_2, then the frequency shift (ΔF) is calculated as $\Delta F = F_2 - F_1$. ΔF is plotted against time and the threshold time point (FDT) at which the change of ΔF can be detected was found.

2.5. Correlation of FDT with standard methods

Coliforms were inoculated in pure culture of various concentrations and the FDT was detected with the piezoelectric crystal sensor. At the same time, the same amount of coliform was also measured using the standard plate counts and MPN techniques.

3. Results and discussion

3.1. Frequency curve

A typical frequency curve is shown in Fig. 2. The frequency shift increases with increasing culture time. In Fig. 2, the region from 1 to 2 is called the baseline. Drift is defined as the average slope of the baseline expressed as the change in frequency shift per hour. It is calculated as the difference between the frequency shift at a time of 0.5 h after the beginning of data acquisition and the frequency shift at a time of 0.5 h before the FDT. It has been found that such drift is very insignificant. In most instances, no significant drift was found. The FDT (marked as point 3) is the onset of acceleration in the frequency shift curve. The frequency slope in the region from 3 to 4 is

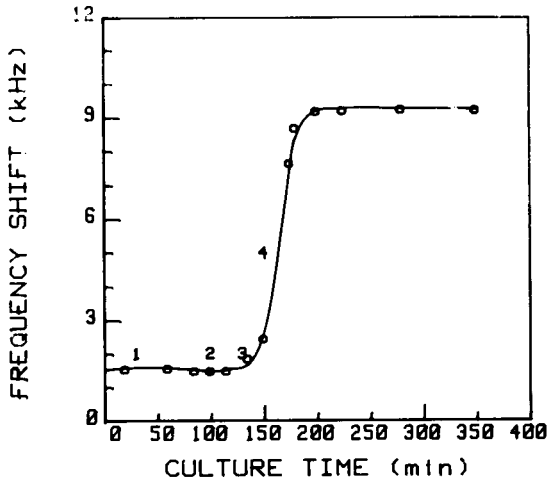

Fig. 2. Typical frequency curve for *E. coli* (concentration 3.6×10^5 cells ml^{-1}.

defined as the slope after the FDT and is expressed as the change in the frequency shift per minute. A frequency curve with low drift values and high frequency slopes is best.

It is worth noting that the drift with this method is much lower than that reported for the impedance method [6], and the frequency slope is much sharper in comparison with the latter. Hence the proposed piezoelectric method with a separated electrode crystal gives a response curve of better quality.

As is well known, low-molecular-weight organic acids, such as acetic and lactic acid, and gases are produced during the lacteose fermentation period by microorganisms [8], so different amounts of acetic and lactic acid were added to the same culture medium as in Fig. 2, in which no microorganisms were inoculated, to test the effects of such small organic acids on the frequency shift and to the FDT. The results are shown in Fig. 3. It can be seen that the curves of frequency shift vs. the concentration of acetic and lactic acid in Fig. 3 are similar to the curve of frequency shift vs. time for coliform growth in Fig. 2. Although the exact components of the medium during the growth of the microorganisms are difficult to detect quantitatively, it is believed that the frequency change in culture medium is probably caused by such small organic acids in the

metabolic process of microorganisms according to the experimental results here.

3.2. Calculation of generation time

The generation time affects the FDT. Generally, a longer generation time results in a greater FDT. In piezoelectric detection, the generation time (T_{gen}) can be calculated as follows:

$$T_{gen} = \frac{FDT \times \log 2}{\log N_2 - \log N_1} \quad (1)$$

where, N_1 = coliform number in the 10^{-5} dilution, N_2 = coliform number in the 10^{-3} dilution and FDT = frequency detection time of N_2 minus that of N_1. In the present experiment, $N_1 = 3 \times 10^3$ cells ml^{-1}, $N_2 = 3 \times 10^5$ cells ml^{-1} and FDT = 170 min, giving T_{gen} = 25.6 min.

3.3. Effect of initial conductance on E. coli detection

The conductance of the medium was adjusted to 0.652, 0.69 and 0.718 mS with sodium chloride; the natural conductance of this medium was 0.531 mS. These different media were sterilized by autoclaving and the same amount of *E. coli* was inoculated in each. Frequency curves were then recorded with the piezoelectric sensor and the results are shown in Fig. 4. It is seen that conductance of the medium affects the drift and slope of the curves significantly. The curve obtained at natural conductance shows an insignificant drift and a very sharp slope and those obtained with media with conductances higher than natural conductance exhibit much smaller slopes. The natural conductance of 0.531 mS was used throughout subsequent work.

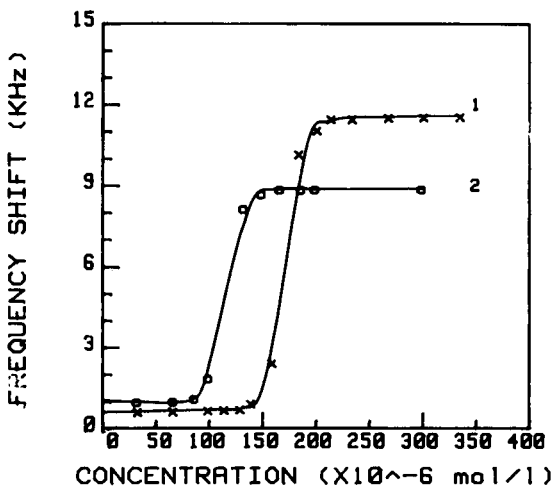

Fig. 3. Frequency curves for (1) acetic acid and (2) lactic acid.

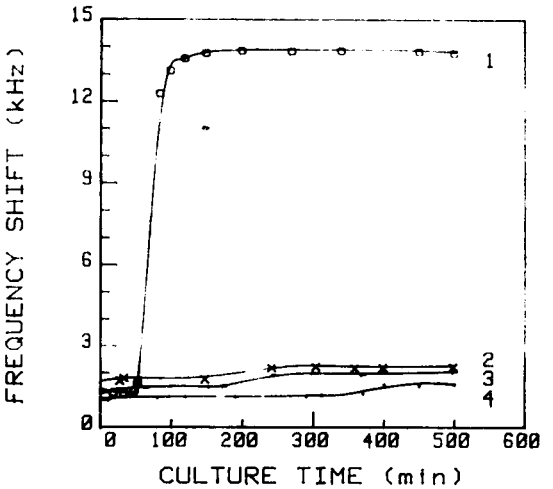

Fig. 4. Effect of conductance of the medium: (1) 0.531; (2) 0.652; (3) 0.690; (4) 0.718 mS.

3.4. Effect of amount of yeast extract on E. coli detection

Fig. 5 shows frequency shift versus culture time for different amounts of yeast extract (12, 6, 3 and 0.1 g). The results demonstrate that when amount of yeast extract is greater than 3 g, the drifts and the FDT are very close, but the FDT becomes longer for a medium containing less than 3 g of yeast extract. Perhaps this is caused by the decrease of nutrition and the *E. coli* generation time becomes longer.

3.5. Effect of amount of proteose peptone on E. coli detection

The effect of the amount of proteose peptone is shown in Fig. 6. Changes in the amount of proteose peptone in the range 2.5–10 g have

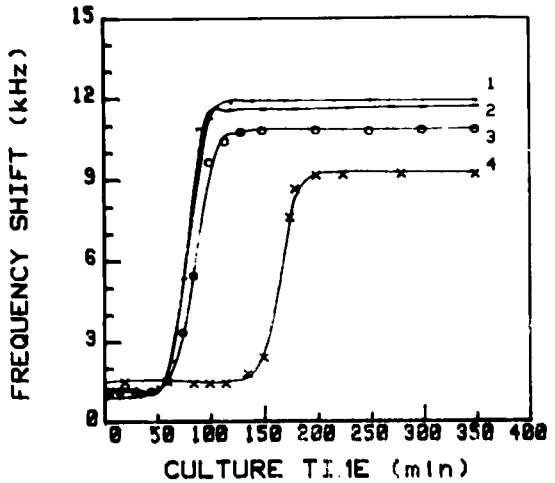

Fig. 5. Effect of amount of yeast extract on the frequency curve and the FDT: (1) 12; (2) 6; (3) 3; (4) 0.1 g.

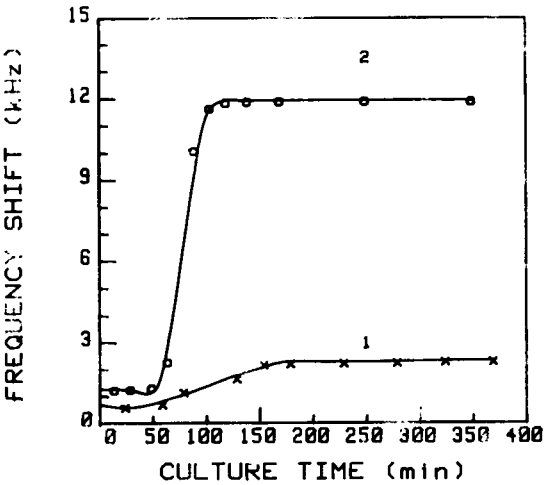

Fig. 7. Effect of cell constant on *E. coli* detection: (1) 0.92; (2) 0.66 cm.

virtually no effect on *E. coli* detection, but when 0.1 g of proteose peptone is used, the FDT becomes longer. The reason is the same as in Fig. 5. When more than 15 g of proteose peptone are used, the frequency shift changes only slightly with time. Of all the substances used in the preparation of the culture medium, proteose peptone has the highest conductance. Therefore, when its concentration is too high, the conductance of the culture medium may in turn be excessively high, and the piezoelectric sensor becomes insensitive to changes in conductance. In subsequent experiments, 5 g of proteose peptone were selected.

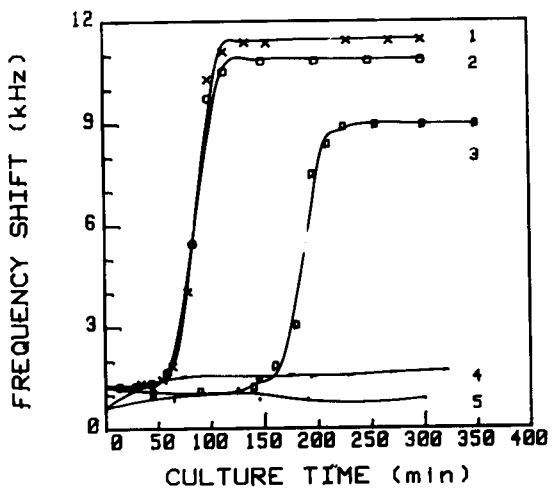

Fig. 6. Effect of amount of proteose peptone on *E. coli* detection: (1) 2.5; (2) 10; (3) 0.1; (4) 20; (5) 15 g.

3.6. Effect of the cell constant on E. coli detection

The cell constant is defined as the electrode area divided by the distance between the quartz crystal and the separated metallic electrode. Hence the cell constant varies with the electrode area or distance between the two electrodes. In these experiments, two cells with different cell constants resulting from the change in distance between the two electrodes were used to detect *E. coli*. The results are shown in Fig. 7. For the curve obtained by using a smaller cell constant, the slope is higher and the FDT is shorter, but for that obtained by using a higher cell constant, the slope is lower and the FDT is longer. This effect may be explained as follows. In a detection cell with a smaller cell constant, the frequency response of the piezoelectric sensor is more sensitive than that in a cell with a higher cell constant and the threshold value in the former is lower than that in the latter.

3.7. Effect of electrode materials on E. coli detection

A silver-plated electrode was used in this work, and it is necessary to consider whether silver could affect the growth of microorganisms. It has been reported that gold has no effect on the growth of microorganisms [9]. In order to check the effect of silver, gold and silver were used as the electrode material and detection cells with the same cell constant (0.92 cm) were used. Similar frequency curves were obtained (Fig. 8), hence silver has no significant effect on the determination when it is used as the electrode material. As silver is much cheaper than gold, a silver electrode was used throughout the work.

3.8. Effect of freezing on frequency curve

Frozen *E. coli* and fresh *E. coli* were tested under the same conditions. The results show that frequency curves obtained with frozen *E. coli* have a drift and a slope similar those obtained with fresh *E. coli*, but the FDT obtained with the frozen *E. coli* is ca. 1 h longer than that obtained with the fresh *E. coli.*, because the frozen *E. coli* are stressed and therefore require time to repair before reproduction begins. Hence in practical application, if the regression equation is obtained with frozen *E. coli*, the FDT of fresh *E. coli* is equals to the FDT detected plus 60 min. In these experiments, for convenience, frozen coliforms were used.

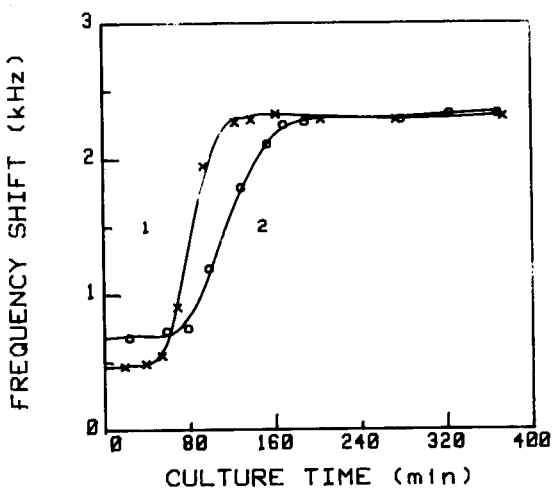

Fig. 8. Effect of electrode material on *E. coli* detection: (1) gold; (2) silver.

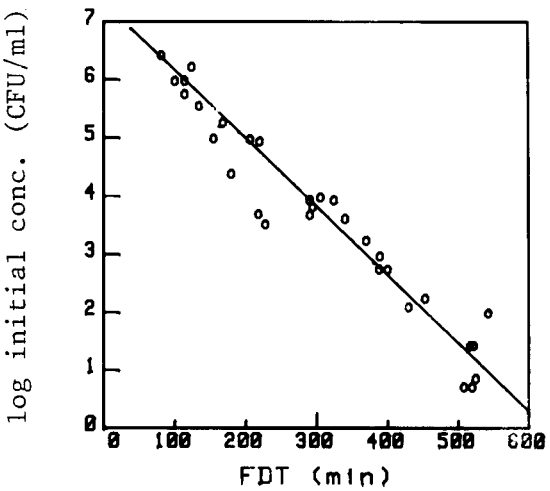

Fig. 9. FDT vs. *E. coli* concentration calibration graph. Frozen coliforms were used.

3.9. Determination of E. coli by the FDT method

Various concentrations of frozen coliform were inoculated in the detection cell and frequency shifts were recorded at different time intervals. Frequency curves were constructed and the FDTs were measured, then a calibration graph of FDT vs. *E. coli* concentration was constructed. The results (Fig. 9) show that FDT is linearly related to the initial concentration (c) of *E. coli* with a range of $10–10^6$ cells ml^{-1}. The regression equation is

$$\log C = -0.01173(\mathrm{FDT}) + 7.329 \qquad (2)$$

where C is the initial concentration of microorganisms in cells ml^{-1} and FDT is the frequency detection time in min; the correlation coefficient is $r = 0.96$ ($n = 31$). Hence if the FDT is determined, the number of *E. coli* can be calculated according to Eq. 2. As indicated above, if fresh coliforms are detected, 60 min must be added to the detected FDT before the substitution in Eq. 2.

Table 1
Comparison of the FDT method with pour plate count and MPN methods

No.	FDT (cells ml^{-1}) (calculated by Eq. 1)	Pour plate (CFU/ml)	MPN (MPN/ml)
1	9	12	26
2	23	35	15
3	18	39	26
4	1.9×10^2	39	1.2×10^2
5	3.0×10^2	39	1.5×10^2
6	17	39	15
7	15	39	76
8	16	43	34
9	1.0×10^2	2.7×10^2	1.7×10^2
10	5.8×10^2	3.5×10^2	9.2×10^2
11	4.3×10^2	6.2×10^2	2.1×10^2
12	7.6×10^3	2.0×10^3	6.4×10^3
13	8.4×10^3	3.9×10^3	4.6×10^3
14	2.2×10^3	3.9×10^3	1.7×10^3
15	3.4×10^3	3.9×10^3	1.2×10^4
16	5.6×10^3	3.9×10^3	9.4×10^3
17	9.7×10^2	3.9×10^3	1.7×10^3
18	8.4×10^3	1.3×10^4	5.8×10^3
19	5.9×10^4	2.0×10^4	4.8×10^4
20	4.5×10^4	5.0×10^4	1.4×10^4
21	8.2×10^4	8.1×10^4	4.3×10^4
22	2.3×10^5	1.1×10^5	9.0×10^4
23	5.7×10^5	3.9×10^5	2.0×10^5
24	1.4×10^6	3.9×10^5	9.2×10^5
25	7.6×10^5	3.9×10^5	9.4×10^5
26	3.2×10^5	3.9×10^5	1.7×10^5
27	2.0×10^5	3.9×10^5	6.4×10^5
28	9.8×10^5	6.3×10^5	1.2×10^6
29	7.5×10^5	6.4×10^5	3.2×10^5
30	9.8×10^5	1.8×10^6	3.2×10^6
31	2.4×10^6	1.7×10^6	4.1×10^6

3.10. Correlation of the FDT and standard methods

The proposed method was compared with the conventional pour plate counts and the most probable number techniques for determining *E. coli* amounts in pure culture. The results are given in Table 1. It can be seen that all the FDT estimates fall inside the 95% confidence limits of the pour plate counts value. The regression coefficient for the relationship between the FDT and colony-forming units (CFU) on the plate for 31 different concentrations of *E. coli* is 0.96 and that between the FDT and the most probable number (MPN) technique is 0.96. When the pour plate count technique is compared with the MPN method, the regression coefficient is 0.95. Therefore, it can be concluded that the proposed piezoelectric technique can yield results comparable to those given by the two widely used conventional techniques.

As described above, the piezoelectric sensor offers a new means for the efficient measurement of coliforms. In comparison with other methods, the piezoelectric technique is simple to execute, a good frequency curve is easily obtained and the determination of the FDT requires only one dilution of the sample. The detection time (ca. 1–10 h) is much less than that in conventional techniques (48–72 h).

Acknowledgements

This work was supported by the National Science Foundation and the Education Commission Fund of China.

References

[1] M.L. Speak, Compendium of Methods for the Microbiological Examination of Foods, American Public Health Association, Washington, DC, 1976.
[2] H. Muramatsu, Y. Watanabe, M. Hikuma, T. Ataka, I. Kubo, E. Tamiya and I. Karube, Anal. Lett., 22 (1989) 2155.
[3] S.Z. Yao and L.H. Nie, Anal. Proc., 24 (1987) 336.
[4] S.Z. Yao and T.A. Zhou, Anal. Chim. Acta, 212 (1988) 61.
[5] Z.H. Mo, L.H. Nie and S.Z. Yao, J. Electroanal. Chem., 316 (1991) 79.
[6] R. Firstenberg-Eden and C. Klein, J. Food Sci., 48 (1983) 1307
[7] J.F. Wang and Q.H. Miao, Acta Acoustica, 13 (1988) 401 (in Chinese).
[8] G.Z. Liu, Microbiology and Inspection of Microbiology, Peoples Hygiene Publishing House, Beijing, 1987, p. 148 (in Chinese).
[9] W.K. Hadley and G. Senyk, in D. Schlessinger (Ed.), Microbiology, American Society for Microbiology, Washington, DC, 1975, p. 12.

ELSEVIER

Analytica Chimica Acta 289 (1994) 321–327

ANALYTICA CHIMICA ACTA

Electrochemical deposition of avidin on the surface of a platinum electrode for enzyme sensor applications

Tomonori Hoshi, Jun-ichi Anzai, Tetsuo Osa *

Pharmaceutical Institute, Tohoku University, Aobayama, Sendai 980, Japan

(Received 14th May 1993)

Abstract

Avidin was electrochemically deposited on a platinum electrode without loss of binding activity to biotin, and biotin-labeled glucose oxidase was immobilized on the electrode through avidin–biotin binding. The electrodes thus prepared displayed excellent properties as a glucose sensor. The oxidation current is proportional to glucose concentration from 10^{-4} to 10^{-2} M, and the sensor could be used for more than 3 months.

Key words: Enzymatic methods; Sensors; Avidin; Biotin; Electrodeposition; Glucose oxidase; Immobilization

1. Introduction

In order to fabricate enzyme sensors, considerable effort has been devoted to the development of various techniques for immobilizing enzymes, including physical adsorption, covalent bonding, and physical entrapment within a polymeric matrix or a dialysis membrane. However, there are several problems to be overcome in each method, such as decrease of the specific enzyme activity, longer response time, or release of the enzyme. These problems are closely related to conformation changes of the enzyme, geometry of the enzyme layer and electrode, and adhesion between the enzyme and its support.

In order to solve these problems, we have explored a novel technique to immobilize enzymes using an avidin–biotin system. The affinity of biotin to avidin is extremely strong ($K_a = 1 \times 10^{15}$ M^{-1}), which is practically irreversible and similar in its stability to a covalent bond [1–3]. Owing to this specific and strong affinity, the avidin–biotin system has been used as a practical tool in affinity chromatography [4–6], binding assay [7], immunohistochemical stains [8,9], immunocytochemical stains [10,11], screening of cDNA expression libraries [12,13], etc. In very recent years, the avidin–biotin system has been applied to immobilizing enzymes on an electrode surface for the purpose of fabricating enzyme sensors. If it is possible to immobilize avidin or biotin molecules on the electrode surface, various molecular structures would be introduced on the electrode via the avidin–biotin complex. Kuhr and co-workers [14,15] have reported that enzyme sensors can be produced by the attachment of enzymes to a carbon surface through a biotin–

* Corresponding author.

SSDI 0003-2670(93)E0666-U

avidin–biotin molecular sandwich. They have covalently immobilized biotinylated glutamate dehydrogenase or horseradish peroxidase on a carbon-fiber microelectrode modified with biotin using avidin as binder. On the other hand, we have reported the application of the avidin–biotin system in a glucose sensor based on Langmuir–Blodgett membrane [16]. Snejdárková et al. [17] have employed another approach to prepare glucose sensors based on the streptavidin–glucose oxidase complex coupled with a self-assembled biotinylated phospholipid membrane. As indicated in these investigations, the avidin–biotin system has great applicability to the fabrication of biosensors.

An advantage of the avidin–biotin method is that the immobilization of the enzyme can be separated into two stages; surface derivatization and enzyme modification. This allows both processes to be optimized independently, which is one of the most convenient points in this architecture of the electrode surface.

In this report, we have attempted to immobilize avidin directly on a platinum electrode surface by electrolysis, and then introduced biotinylated glucose oxidase (GOx) to the avidin active layer. We have also verified optimum conditions of electrolysis of avidin to obtain higher performance probes.

2. Experimental

2.1. Chemicals

Dextrose (glucose) (anhydrous) was obtained from Wako (Japan). Glucose standard solutions of 1×10^{-2}, 3×10^{-2}, 0.1, 0.3 and 1.0 M were prepared to dissolve glucose in distilled water. Glucose oxidase (GOx) (EC 1.1.3.4) from *Aspergillus niger* and biotinylated glucose oxidase were obtained from Sigma (USA). Avidin was obtained from Calzyme (USA). The solutions containing enzyme and avidin were prepared by dissolving both materials in Dulbecco's phosphate buffered saline (PBS) solution. All other reagents were of highest grade available and used without further purification. The PBS was prepared by dissolving 8.0 g of NaCl, 0.2 g of KCl, 0.2 g of KH_2PO_4 and 1.15 g of Na_2HPO_4 in 1000 ml of distilled water. The pH of this solution was ca. 7.4 without further adjustment.

2.2. Instrument and materials

A potentiostat equipped with a function generator (Nikko Keisoku NPGF-2501A, Japan) was used to supply an alternating potential of triangular waveform or a fixed potential to the electrode. The working electrode was a platinum wire of 0.5 mm or 3.0 mm diameter. The reference electrode was an AgCl-coated silver wire with a liquid junction of 3.3 M KCl saturated with AgCl, and the auxiliary electrode was a platinum wire. The electrode materials (> 99.99%) were purchased from Tanaka (Japan).

2.3. Fabrication of glucose sensors

Avidin was deposited on the electrode surface by applying 200 V s^{-1} of an alternating potential of triangular waveform to a polished platinum working electrode immersed in the avidin solution at room temperature, according to the modified procedure reported for the preparation of an albumin film [18]. After electrolysis, the working electrode was immersed in PBS for 10 min and then immersed in biotinylated GOx solution (50 μg ml^{-1}) for 30 min to immobilize the GOx on the electrode through the avidin–biotin complexation. The working electrodes were preserved in PBS at 4°C when not in use. The procedure for constructing the glucose electrode is schematically shown in Fig. 1.

2.4. Determination of glucose concentration

The electrochemical response of the GOx-modified electrode was measured with a conventional three-electrode system at 0.6 V vs. the reference electrode. The GOx catalyzes the oxidation reaction of glucose to produce H_2O_2, and the H_2O_2 can be oxidized at the Pt surface at this potential.

A series of 0.1 ml of glucose standard solution was injected into 10 ml of the measuring buffer

solution (0.1 M phosphate of pH 6.8) with stirring. All measurements were carried out at room temperature.

3. Results and discussion

In order to verify a possibility of electrochemical deposition of avidin on the electrode surface, an alternating potential (200 V s^{-1}) of triangular waveform from −0.5 to +2.1 V vs. Ag/AgCl was applied for 10 min to two identically sized Pt electrodes immersed in a 10 mg ml^{-1} avidin solution. After electrolysis, one electrode was treated with biotinylated GOx and the other with native (non-labeled) GOx. Fig. 2 shows typical response curves of the electrodes to glucose. The output current increased immediately after the injection of glucose into the sample solution for the electrode treated with the biotinylated GOx (Fig. 2a). This result suggests that avidin was deposited on the electrode by electrolysis without loss of binding activity to biotin and that the biotin-labeled GOx was immobilized on the electrode through avidin–biotin complexation. This suggestion is further supported by the fact that little response was observed for the electrode treated with native GOx in place of the biotin-labeled GOx (Fig. 2b). It should be noted that the specific activity of the native GOx used is ca. 80 times higher than that of the biotin-labeled GOx. Thus the effectiveness of the electrochemical treatment of avidin has been demonstrated for the preparation of an active avidin layer on the electrode surface. In fact, we can see the formation of a slightly yellow avidin layer.

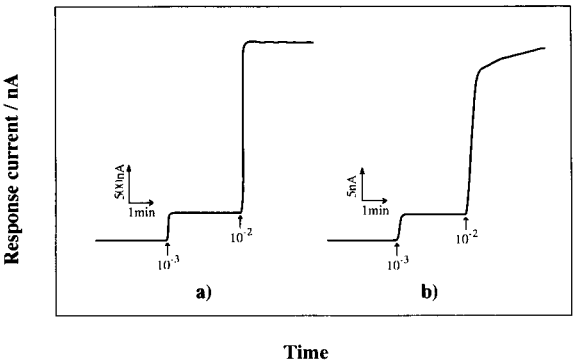

Fig. 2. Typical response curves of glucose sensors based on the electrodeposited avidin film coupled with (a) biotin-labeled GOx and (b) native GOx. Area of electrode: 0.08 cm^2.

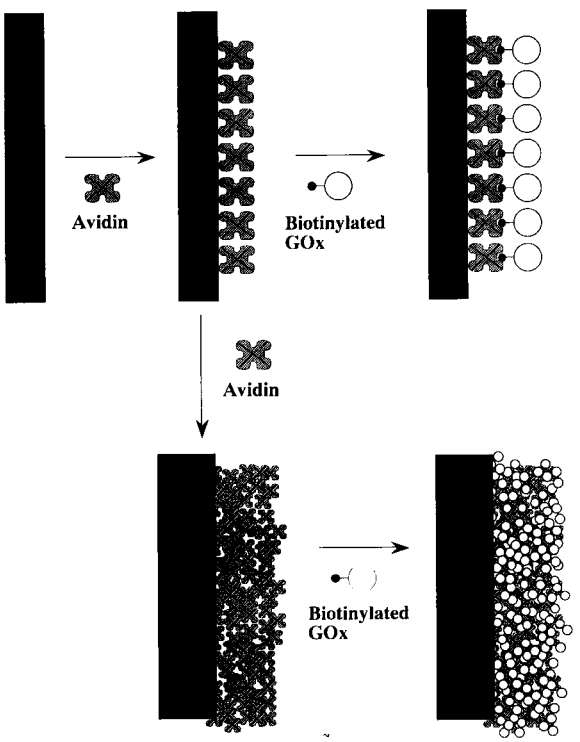

Fig. 1. Schematic representation of the construction of glucose sensors based on the electrodeposited avidin film.

We also tried to deposit directly the complex of avidin and biotin-labeled GOx on the electrode, by applying the alternating potential of triangular waveform to the Pt electrode immersed in the avidin–biotin-labeled GOx complex solution in a similar manner as in the case for the deposition of avidin. Unfortunately, the response of the electrode to glucose was very small (Fig. 3) as compared with that of the electrode based on the electrodeposition of avidin (Fig. 2). Thus, the direct deposition of the avidin–biotin-labeled GOx complex was confirmed not to be successful in the present conditions.

3.1. Optimum conditions for the electrodeposition of avidin

In order to optimize the deposition of avidin, such variables in electrolysis as the highest and lowest potentials of the triangular waveform, the concentration of avidin solution, and electrolysis time were systematically altered.

Fig. 4 represents the electrochemical responses of the glucose sensors prepared by using the avidin-deposited Pt electrodes, in which the highest and lowest potentials of the triangular waveform were varied in the range of 1.60 to 2.60 V and −1.00 to 0.00 V vs. Ag/AgCl, respectively. The results of the three independent preparations are shown in Fig. 4. It is clear that, to obtain a sensor with the highest response, avidin should be deposited by electrolysis with the alternating potential of triangular waveform from −0.50 to +2.10 V.

Fig. 5 depicts the effects of the concentration of avidin solution on the deposition. The results show that avidin is deposited more efficiently from higher concentration solutions. When avidin was deposited from lower (< 1 mM) concentration solutions, the sensors exhibited no appreciable response to glucose.

Fig. 6 shows that the electrolysis time is another crucial factor in determining the response

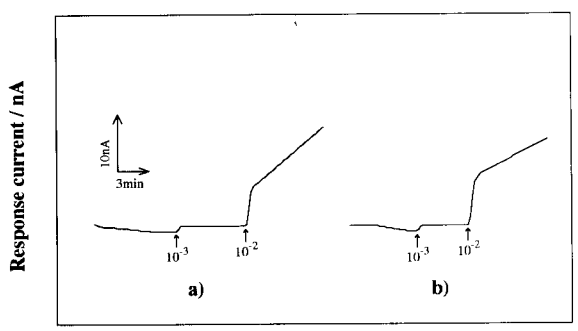

Fig. 3. Response of glucose sensors based on the direct electrodeposition of the complex of the avidin and biotin-labeled GOx. To deposit the avidin–biotin-labeled GOx complex, the electrolysis was continued for (a) 60 and (b) 300 s in the complex solution (100 μg ml^{-1} of avidin and 50 μg ml^{-1} of biotinylated GOx). Area of electrode: 0.16 cm^2.

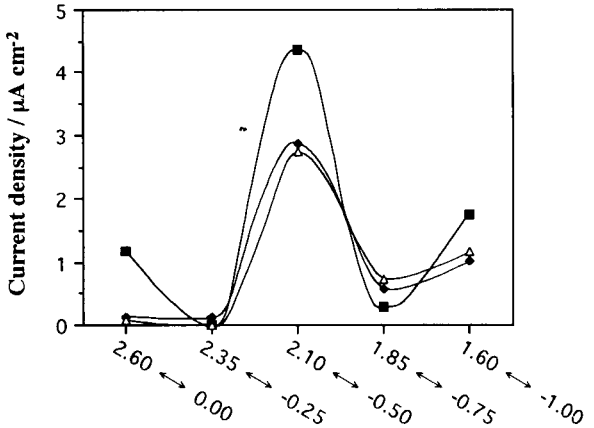

Fig. 4. Effect of electrode potential (V) on the deposition of avidin. The electrolysis was continued for 600 s in 10 mg ml^{-1} of avidin solution. The output current of sensors to 1 mM glucose was shown for three independent, apparently identical preparations (■, △, ◆).

of the glucose sensor. The output current of the sensor was very small when the sensor was prepared using the Pt electrode with 20–60 s deposition of avidin. On the contrary, for electrodes with 300 and 600 s deposition of avidin, the glucose sensors showed satisfactory responses.

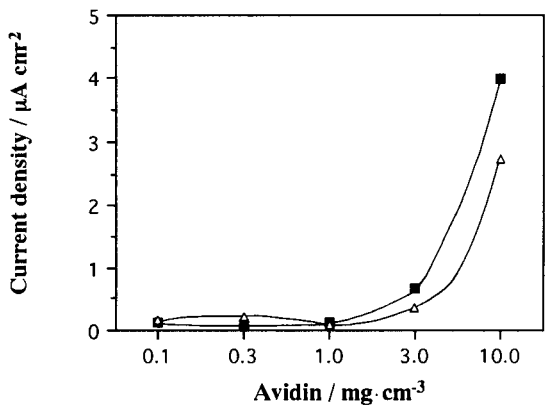

Fig. 5. Effect of the concentration of avidin solution on the deposition of avidin. Avidin was deposited on the electrode surface by applying an alternative potential of triangular waveform from −0.5 to +2.1 V vs. Ag/AgCl for 600 s to working electrodes immersed in the avidin solutions. The output current of the sensors to 1 mM glucose was shown for two independent preparations (△, ■).

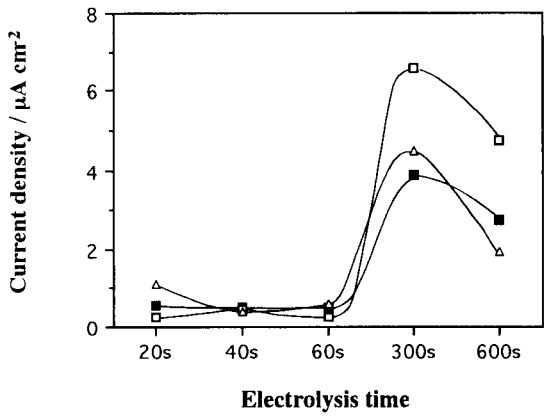

Fig. 6. Effect of the electrolysis time on the deposition of avidin. Avidin was deposited on the electrode surface by applying an alternative potential of triangular waveform from −0.5 to +2.1 V vs. Ag/AgCl for 20–600 s to working electrodes immersed in 10 mg ml^{-1} of avidin solution. The output current of the sensors to 1 mM glucose was shown for three independent preparations (□, ■, △).

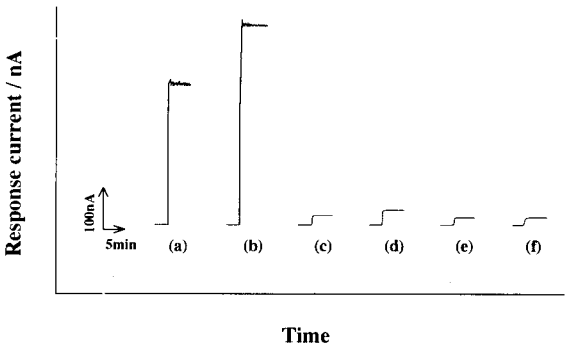

Fig. 7. The response time of the sensors with different loadings of avidin. Avidin was deposited by the electrolysis for (a) 600, (b) 300, (c) 60, (d) 40 and (e) 20 s, and by simple adsorption for (f) 600 s in 10 mg ml^{-1} avidin. Area of electrode: 0.08 cm^2. Sample: 1 mM glucose.

The time dependence of response may come from the different loading of avidin as is schematically illustrated in Fig. 1. In other words, the magnitude of the response may be determined by the thickness of the avidin layer, or by the loading of GOx. However, prolonged electrolysis lowered the response, which might originate from some morphological changes of the avidin layer. In fact, we saw a rather rugged surface of the avidin layer after a 10-min electrolysis, as compared with the relatively smooth surface prepared in a shorter time.

3.2. Performance of the glucose sensor

The response time, calibration and stability of the glucose sensor were elucidated for the probes prepared under nearly optimum conditions (the electrode potential for the deposition of avidin −0.5 to +2.1 V, concentration of avidin 10 mg ml^{-1}, and electrolysis time 600 s). Fig. 7 illustrates the dependence of the response curves on the deposition time of avidin. All probes showed satisfactorily fast response to glucose, the response being within 10 s. These results suggest smooth transport of glucose and the reaction products within the avidin layer irrespective of the thickness.

The changes in sensor output were plotted versus glucose concentration to give calibration graphs (Fig. 8). The frequency of the alternating potential for the deposition of avidin was 200 V s^{-1} (open circle) and 364 V s^{-1} (filled circle). For both cases, the calibration graphs were linear over the concentration range of 10^{-4} to 10^{-2} M glucose. The probe treated at 200 V s^{-1} showed a slightly higher response than those treated at 364 V s^{-1}. The long-term stability of the sensors was tested for the probes in which avidin was deposited with (a) 200 and (b) 364 V s^{-1} alternating

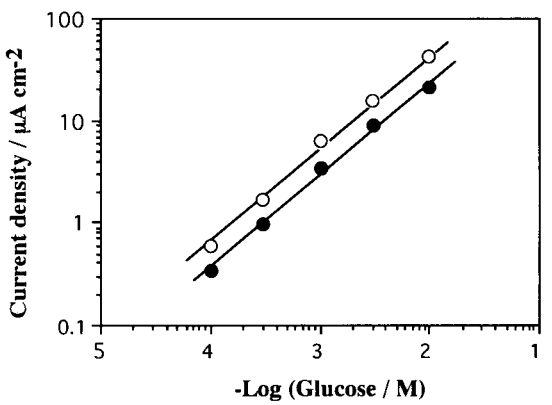

Fig. 8. Typical calibration graphs for the sensors. The frequency of the alternating potential for the deposition of avidin was (○) 200 and (●) 364 V s^{-1}.

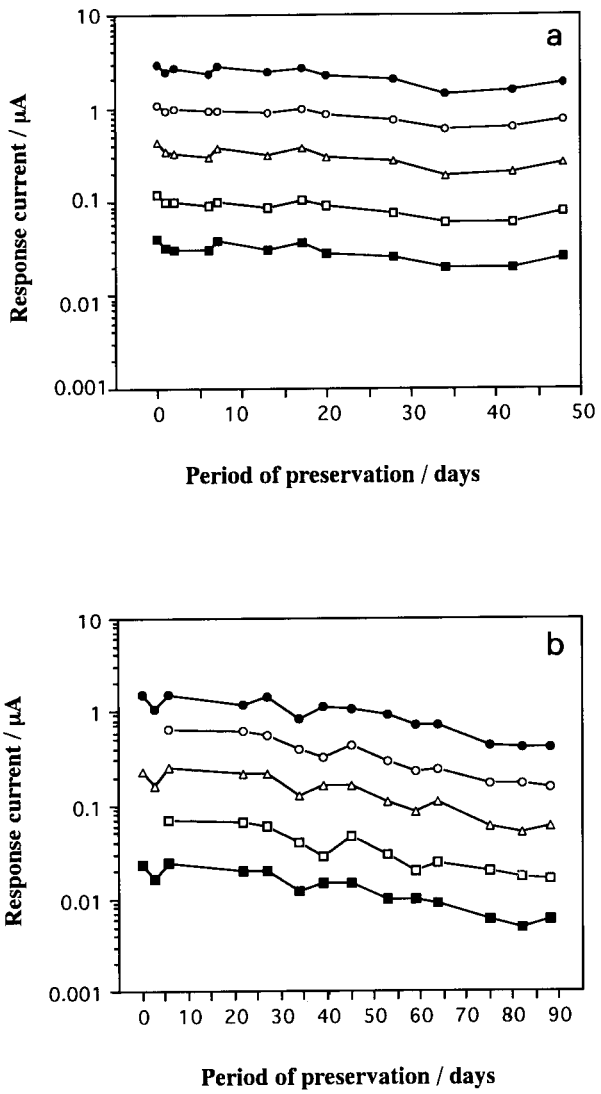

Fig. 9. Long-term sensitivity of the sensors. The frequency of the alternative potential for the deposition of avidin was (a) 200 and (b) 364 V s^{-1}. The concentration of glucose was: (■) 10^{-4}, (□) 3×10^{-4}, (△) 10^{-3}, (○) 3×10^{-3}, and (●) 10^{-2} M.

potentials (Fig. 9). The probes were stored in PBS at 4°C when not in use. The sensors were quite stable under these conditions, although a slight decrease in output current was observed for both probes.

The stability of the sensor stored in air was checked. The response of the sensor decreased to ca. 10% of the original value after one-day storage in air at room temperature in contrast to the 80% response of the probe stored in PBS. The biotin-binding activity of the electrodeposited avidin was also checked. After electrolysis of avidin, the avidin-deposited electrodes were stored in PBS at 4°C or in the air at room temperature. After one-day storage, the electrodes were treated with biotinylated GOx solution, and the response of the electrodes to glucose was measured. The results for five preparations agreed with each other within ca. 5% standard error. It is clear that the electrodeposited avidin loses its binding activity to biotin in the air, because the resulting sensor gave a response of ca. 3% of that with PBS storage. These results show that enzyme sensors prepared by the avidin–biotin complexation should be stored in buffered solution.

Avidin retains its binding affinity to biotin even in the electrodeposited film. Using this film, GOx can be immobilized on the surface of the Pt electrode through the avidin–biotin complexation, and the sensor probe thus prepared showed excellent properties as a glucose sensor. The facile and short-time preparation of the sensor is a great merit of this procedure. In the same manner, any biotin-labeled molecules would be deposited on the electrode. For this reason, we emphasize the usefulness of the deposited avidin film as a universal paste for immobilizing any biomolecules on the electrode. If the electrolysis conditions of avidin are further improved, more sensitive and durable probes would be fabricated. The quantitative estimation of the loading and structure of the immobilized avidin and GOx is now in progress. A further investigation is required to elucidate the mechanism of the electrodeposition of avidin.

References

[1] E.A. Bayer and M. Wilchek, Methods Biochem. Anal., 26 (1980) 1.
[2] M. Wilchek and E.A. Bayer, Anal. Biochem., 171 (1988) 1.
[3] D. Vaknin, J. Als-Nielsen, M. Piepenstock and M. Lösche, Biophys. J., 60 (1991) 1545.

[4] F.M. Finn, G. Titus, D. Horstman and K. Hofmann, Proc. Natl. Acad. Sci. USA, 81 (1984) 7328.
[5] F. Desarnaud, J. Marie, R. Larguier, C. Lombard, S. Jard and J.-C. Honnafous, J. Chromatogr., 603 (1992) 95.
[6] H. Hagiwara, T. Nagasawa, K.M. Lodhi, M. Kozuka, T. Ito and S. Hirose, J. Chromatogr., 597 (1992) 331.
[7] L. Chen, G.B. Martin and G. Rechnitz, Anal. Chem., 64 (1992) 3018.
[8] S.M. Hsu, L. Raine and H. Fanger, Am. J. Clin. Pathol., 75 (1981) 734.
[9] S.M. Hsu, L. Raine and H. Fanger, J. Histochem. Cytochem., 29 (1981) 577.
[10] G.V. Childs, G. Unabia and R. Tibolt, Am. J. Anat., 174 (1985) 409.
[11] F.M. Hofman, R.J. Billing, J.W. Parker and C.R. Taylor, Clin. Exp. Immunol., 49 (1982) 355.
[12] B.T. French, H.M. Maul and G.G. Maul, Anal. Biochem., 156 (1986) 417.
[13] P.-L. Hsu, S.-M. Hsu and E. Appella, Gen. Anal. Technol., 2 (1985) 30.
[14] P. Pantaro, T.H. Morton and W.G. Kuhr, J. Am. Chem. Soc., 113 (1991) 1832.
[15] P. Pantano and W.G. Kuer, Anal. Chem., 65 (1993) 623.
[16] S. Lee, J. Anzai and T. Osa, Sensors Actuators B, 12 (1993) 153.
[17] M. Snejdárková, M. Rehák and M. Otto, Anal. Chem., 65 (1993) 665.
[18] M.F. Suand-Chagny and F.G. Gonon, Anal. Chem., 58 (1986) 412.

ELSEVIER

Analytica Chimica Acta 289 (1994) 329–337

ANALYTICA CHIMICA ACTA

Adsorption and association of 6-thiopurine and 6-thiopurine riboside at charged interfaces

Z.A. Ahmed, M.E. Ahmed, M.S. Ibrahim, M.M. Kamal, Y.M. Temerk *

Chemistry Department, Faculty of Science, Assiut University, Assiut, Egypt

(Received 31st August 1993)

Abstract

A systematic study on the adsorption and association of 6-thiopurine (6-TP) and 6-thiopurine riboside (6-TPR) has been carried out at various pH values and the adsorption parameters were determined quantitatively. The adsorption was followed by out-of-phase alternating current voltammetry and cyclic voltammetry at a hanging mercury drop electrode. A comparative study was undertaken on the adsorption and association of the investigated thiopurines and the similar type of nucleic acid components containing purine bases. The base-containing thio group enhances stacking interaction and facilitates formation of the perpendicularly stacked layer on the electrode surface.

Key words: A.c. polarography; Cyclic voltammetry; Adsorption; Association; Nucleic acids; 6-Thiopurine; 6-Thiopurine riboside

1. Introduction

Purine and thiopurine compounds are substances of paramount biological and physiological significance. The purine bases are minor constituents of nucleic acid while thiopurine compounds interact with genetic material in the cell and have mutagenic or carcinogenic properties [1]. Interactions of purine base and thiopurine with a charged biological interface involve several specific processes, adsorption being the initial step [2–7]. Electrochemical methods have been used to assess the surface activity and interfacial phenomena of purine base at charged interfaces [8–12]. It was shown that purine bases can be adsorbed and undergo an association at the charged mercury–solution interface [5–12].

Continuing our quantitative studies on the adsorption stages and the association of nucleic acid components [7,11–16], the present paper is concerned with the comparison of the interfacial behaviour of 6-thiopurine and 6-thiopurine riboside and similar type of nucleic acid components containing the purine base. Due to the biological significance of both purine base and thiopurine it is of great interest to investigate how the "thio" group will affect the mode of base-pairing and the strength of stacking interactions at charged interfaces.

* Corresponding author.

SSDI 0003-2670(93)E0676-X

2. Experimental

2.1. Chemicals and solutions

6-Thiopurine monohydrate (6-TP) and 6-thiopurine riboside (6-TPR) were obtained from Sigma (USA) and were used without further purification. Solutions containing different concentrations of the investigated thiopurines were prepared by dissolving a known amount of the chemically pure product into a definite volume of Britton–Robinson buffer. The Britton–Robinson buffer was brought to a constant ionic strength of 0.5 M by addition of NaCl and adjusted to the desired pH. It served also as supporting electrolyte. All chemicals were reagent grade, KCl was "Suprapur" (Merck, Darmstadt). Triply quartz-distilled water served as solvent. The

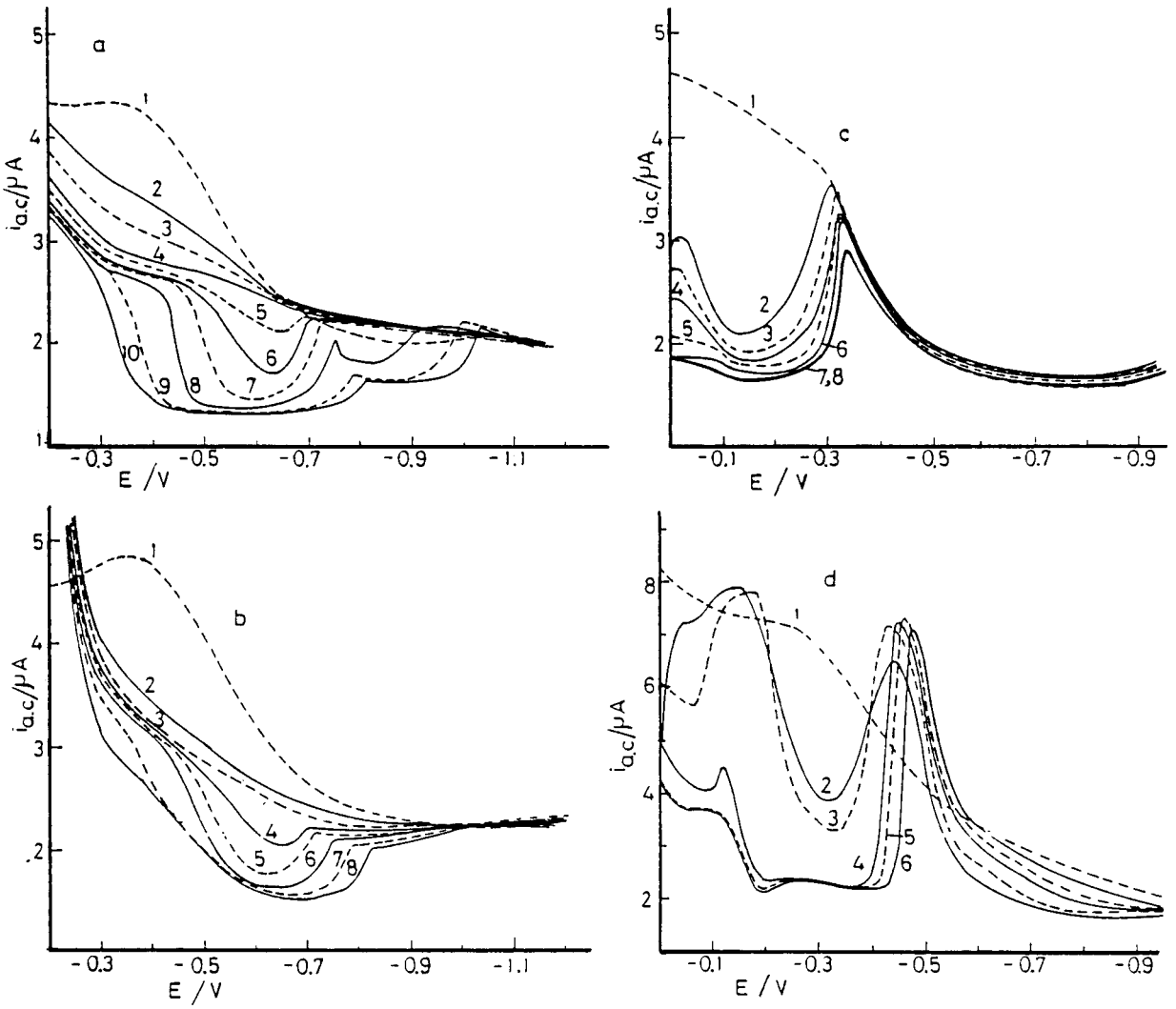

Fig. 1. A.c. voltammetric curves of 6-TP at pH (a) 3.2, (b) 5.2, (c) 7.2 and (d) 9.2. 0.5 M Universal buffer, 5°C, area of HMDE 1.2×10^{-2} cm^2, scan rate 2 mV s^{-1}, amplitude 10 mVpp, phase angle 90°, frequency 330 Hz and $t_s = 180$ s. (a): (1) 0.0, (2) 5.9, (3) 12, (4) 17, (5) 60, (6) 71, (7) 86, (8) 120, (9) 260 and (10) 340 μM 6-TP; (b): (1) 0.0, (2) 7.9, (3) 17, (4) 36, (5) 49, (6) 58, (7) 76 and (8) 120 μM 6-TP; (c): (1) 0.0, (2) 19, (3) 38, (4) 56, (5) 74, (6) 110, (7) 210 and (8) 260 μM 6-TP; (d): (1) 0.0, (2) 4.9, (3) 9.9, (4) 19, (5) 38, and (6) 99 μM 6-TP.

thiopurine content of the sample solutions was determined with a Unicam SP 800 spectrophotometer. The pH was measured with a digital Radiometer pH meter, Model pH M64.

2.2. Apparatus and methods

A Princeton Applied Research (PAR) Model 174 polarographic analyzer coupled with a PAR Model 174/50 alternating current (a.c.) polarographic analyzer interface and a PAR Model 510 (lock-in-amplifier) phase detector were employed for a.c. voltammetric measurements. Phase-sensitive a.c. voltammograms were recorded with the phase angle adjusted to 90°, corresponding to the out-of-phase component of the a.c. current (capacitive current component). The amplitude of the a.c. voltage was 10 mV peak-to-peak, the scan rate of the a.c. ramp of the mean electrode potential E was 2 mV s^{-1} and the a.c. frequency

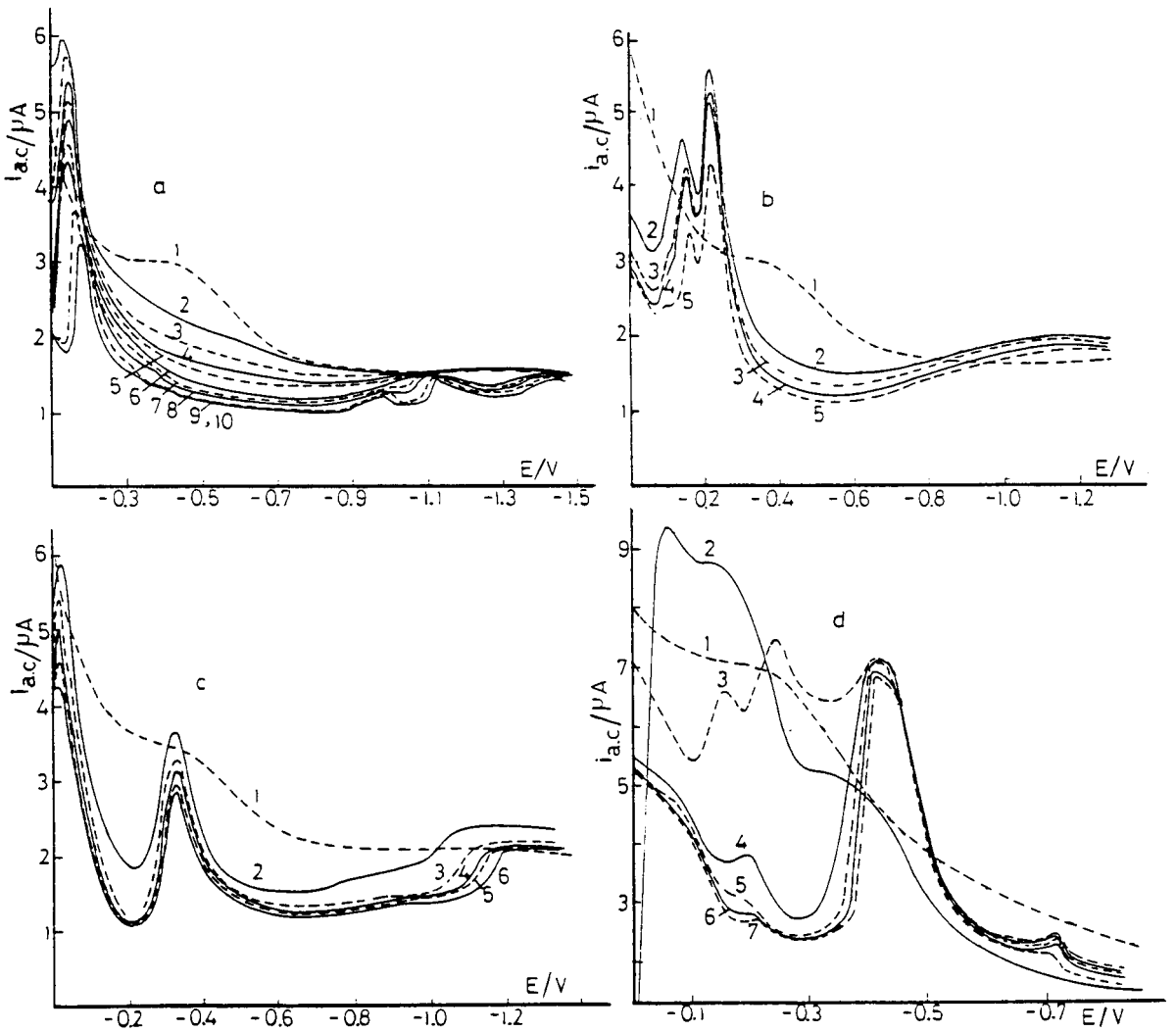

Fig. 2. A.c. voltammetric curves of 6-TPR at pH (a) 3.2, (b) 5.2, (c) 7.2 and (d) 9.2. (a): (1) 0.0, (2) 9.9, (3) 19, (4) 57, (5) 91, (6) 140, (7) 170, (8) 190, (9) 250 and (10) 330 μM 6-TPR; (b): (1) 0.0, (2) 38, (3) 57, (4) 110 and (5) 150 μM 6-TPR; (c): (1) 0.0, (2) 9.9, (3) 19, (4) 38, (5) 65 and (6) 82 μM 6-TPR; (d): (1) 0.0, (2) 4.9, (3) 19, (4) 38, (5) 57, (6) 74 and (7) 91 μM 6-TPR. Other conditions as in Fig. 1.

had a value of 330 Hz, unless otherwise stated. The time dependence of the a.c. component of the capacitive current at an adjusted constant mean electrode potential E_m was obtained as described earlier [11,12].

In the cyclic voltammetry mode a potentiostat/galvanostat Model 173, a PAR Model 175 universal programmer and a PAR Model 303A hanging mercury drop electrode were used. The cyclic voltammograms were recorded on an advanced X–Y recorder Model RE0089 after automatic deaeration of the electrolysed solutions.

Potentiometric titration experiments were done to determine the pK_a values of 6-TP and 6-TPR. The pK_a values of 6-TP and 6-TPR were found to be 6.9 and 8.9, respectively; these values are in agreement with those obtained previously [17] for the investigated compounds.

The cell used was a thermostatted Metrohm cell equipped with a three-electrode system as described earlier [15]. All potentials refer to the Ag/AgCl/KCl electrode.

3. Results and discussion

Phase-sensitive a.c. voltammograms corresponding to the out-of-phase component of the total a.c. response provide an overall pattern of the adsorption and interfacial behaviour of 6-TP and 6-TPR. The out-of-phase a.c. current of the investigated compounds recorded as function of the mean electrode potential in solutions of varying pH is represented in Figs. 1 and 2.

The interfacial behaviour of 6-TP in acidic buffer solutions (pH $\leq$ 5.2) and at relatively low bulk concentrations exhibits a sharp decrease in capacitive current giving a very sharply defined pit around the point of zero charge, or electrocapillary maximum (E_{ecm}). The pit reflects the association of the perpendicularly oriented adsorbed molecules at the electrode surface by intermolecular attraction forces and the formation of a compact layer. The association of the adsorbed species depends predominantly on the stacking of the neutral 6-TP molecules according to its pK_a value (pK_a 6.9).

At pH $\geq$ 7.2 the potential range of adsorption shifts to a less negative value and a new depression appears at -0.1 V (pH 7.2) and -0.3 V (pH 9.2). This new depression is located at a positively charged electrode and its occurrence at pH's > pK_a of 6-TP indicates that it corresponds to the adsorption of anionic species. At a potential around -0.5 V the a.c. voltammograms exhibit a desorption of adsorbed species existing in the film. The destabilization of the film at pH $\geq$ 7.2 may be due to the repulsion of the partly negatively charged species of the adsorbed molecules by the negatively charged electrode.

The in-phase component of a.c. of 6-TP in solutions of varying pH indicates two Faradaic peaks in the potential range between -0.1 V and -0.35 V (depending on pH). The more positive peak reflects the reduction of Hg(II) ion bound to 6-TP through the heterocyclic nitrogen atoms [5]. The second Faradaic peak is attributed to the reduction of the adsorbed Hg(II) thiolate compound. In this context thiopurine like other sulphur containing compounds [4] interacts with mercury forming $Hg(RS)_2$. The interactions of 6-TP with the mercury electrode are studied also by cyclic voltammetry as presented in this paper.

The aforementioned result indicates that the a.c. voltammograms of 6-TP in acidic buffer solutions (pH $\leq$ 5.2) is a purely capacitive current and the potential range of pit formation is observed around the point of zero charge whereas the perpendicularly oriented adsorbed neutral molecules interact with the charged electrode surface via the permanent dipole moment. At pH $\geq$ 7.2 the adsorption of anionic form of 6-TP is located at a positively charged electrode and the a.c. current is influenced by the Faradaic current as a result of reduction of the formed Hg(II) thiolate compound on the electrode surface.

The interfacial behaviour of 6-TPR in acidic buffer solutions (pH $\leq$ 7.2) shows around the E_{ecm} a progressive suppression of the capacitive a.c. signal upon increasing the concentration of 6-TPR. At more elevated bulk concentrations above a threshold value for 6-TPR, a pit is observed around E_{ecm}. The capacitive response in the potential range -0.3 V to -1.0 V is proportional to the differential double layer capacity as long as

no pseudocapacity due to a Faradaic current interferes. It should be noticed that the decrease of a.c. in the potential range 0.0 V to −0.30 V (depending on pH) reflects the adsorption of the formed Hg thiolate on the electrode surface and it has no influence on the adsorption of neutral 6-TPR molecules around E_{ecm}. The result indicates that the adsorption of 6-TPR in the potential range −0.3 V to −1.0 V depends predominantly on the stacking of the neutral molecules (pK_a 8.9) providing that even under these conditions the pit is formed due to the association of perpendicularly oriented molecules.

At pH ≥ 9.2 the potential range of adsorption of 6-TPR shifts to a less negative value and a new depression appears at about −0.2 V. This depression of a.c. current is located at a positively charged electrode and its occurrence at a pH above the pK_a of 6-TPR indicates that it corresponds to the adsorption of anionic species. The in-phase component of a.c. current of 6-TPR at pH 9.2 indicates that the interfacial capacitive curves of the adsorbed anionic species in the potential range −0.10 V to −0.40 V is influenced by the cathodic reduction of the adsorbed $Hg(RS)_2$ on the electrode surface.

Comparison of the adsorption and association of the investigated 6-TP and 6-TPR with similar type of nucleic acid components not containing sulphur which were recorded under the same conditions showed that the surface activity of the adenine and adenosine are significantly smaller in comparison to the corresponding thiopurine derivatives. The results indicate that a systematic and large decrease in the bulk solution activity of 6-TP and 6-TPR is required to cause formation of the compact adsorption layer. This reflects the fact that the introduction of the thio group (SH) to the purine molecule enhances the stacking interactions of the adsorbed molecules and hence would be expected to facilitate formation of the perpendicularly stacked layer of thiopurine compounds on the electrode surface.

The time dependence of the adsorption of 6-TP and 6-TPR for different bulk concentrations at various pH values is shown in Fig. 3. In acidic buffer solutions and at a constant mean electrode potential (E_m) the capacitive a.c. current slowly

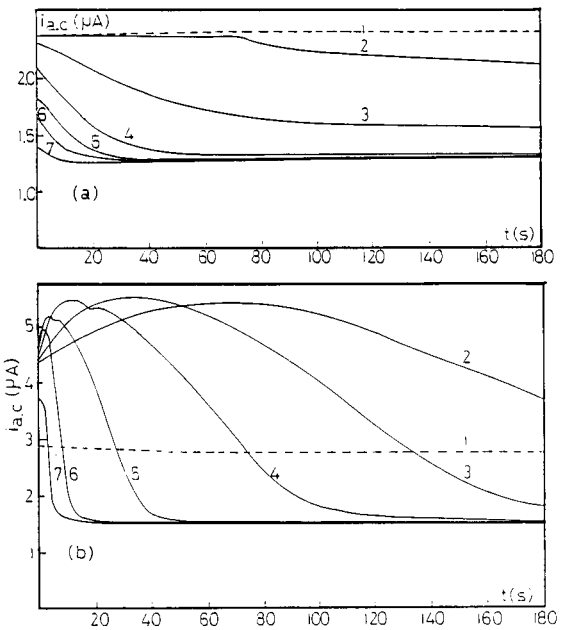

Fig. 3. Time dependence of the out-of-phase component of a.c. current of 6-TPR at (a) pH 5.2 and (b) pH 9.2. (a): (1) 0.0, (2) 9.9×10^{-5}, (3) 1.4×10^{-5}, (4) 3.8×10^{-5}, (5) 5.7×10^{-5}, (6) 8.7×10^{-5} and (7) 1.0×10^{-4} M 6-TPR (E_m = −0.55 V); (b): (1) 0.0, (2) 1.9×10^{-5}, (3) 2.9×10^{-5}, (4) 4.7×10^{-5}, (5) 8.2×10^{-5}, (6) 2.2×10^{-4} and (7) 3.2×10^{-4} M 6-TPR (E_m = −0.325 V). Other conditions as in Fig. 1.

decreases to an equilibrium value for low bulk concentrations of 6-TP (pH ≤ 5.2) and 6-TPR (pH ≤ 7.2). For concentrations larger than the threshold value, where the pit occurs on a.c. voltammograms, the current rapidly decreases to a equilibrium value corresponding to the compact layer formation for the adsorbed neutral molecules. At pH's above the pK_a values and at relative low bulk concentration of 6-TP or 6-TPR a condensed film is formed at the adjusted mean potential E_m (−0.325 V, pH 9.2) which corresponds to the adsorption of the anionic species and the formation of Hg thiolate compound on the electrode surface. In this case the rising of the a.c. current to a maximum at lower bulk concentrations which follows the initial part of curves reflects a substantial influence of the Faradaic current as a result of reduction of the adsorbed Hg(II) thiolate compound on the electrode surface.

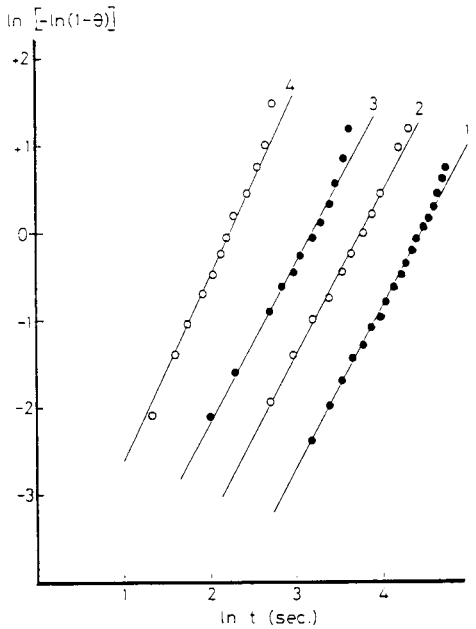

Fig. 4. Avrami plots for the short-time part of the capacitance vs. time transients for different bulk concentrations of 6-TP at pH 7.2. (1) 6.5×10^{-5}, (2) 9.1×10^{-5}, (3) 1.3×10^{-4} and (4) 2.2×10^{-4} M 6-TP ($E_m = -0.15$ V).

The time dependence of the surface coverage is described according to Avrami–Evans equation:

$$\theta = 1 - \exp(-bt^m) \quad (1)$$

where m is characteristic for a given type of nucleation mechanism, b is related to the rate of nucleation and growth and t is the adsorption time. The degree of coverage θ was evaluated using the relation:

$$\theta = (C_0 - C)/(C_0 - C_1) = (\Delta i_{a.c.})/(\Delta i_{a.c.})_{Max} \quad (2)$$

where C, C_0 and C_1 are the capacitance at t, $t = 0$ and t_1 at full coverage respectively, $\Delta i_{a.c.}$ the decrease of the capacitive a.c. current with respect to the $i_{a.c.}$ current value of the blank supporting electrolyte for a given bulk concentration and $(\Delta i_{a.c.})_{Max}$ the maximal decrease corresponding to full coverage.

Eq. (1) can be rearranged into the form:

$$\ln\{\ln[1/(1-\theta)]\} = m \ln t + \ln b \quad (3)$$

and is usually called the Avrami plot which was used for both the positive and negative pit potentials. Typical linear plots for different concentrations of the investigated thiopurine compounds are shown in Fig. 4. The parameter $m = 2,3,\cdots$ is characteristic for a given type of nucleation mechanism, where ln b is related to the rate of nucleation and growth. Statistical estimates of m and b as a function of applied potential were calculated by linear regression (Table 1). The fit of the experimental data with Eq. (3) is quite satisfying for all potentials provided that they are not too close to the pit edge. Significant deviations were observed near the pit edge, where the rate of nucleation and growth is very low. At pit potentials sufficiently far away from the pit edges, the rate of nucleation and growth (the parameter b) is so high that a limiting coverage of the electrode by a compact layer is rapidly reached.

The dependence of the capacitive a.c. response on the bulk concentration of the investigated compounds indicates that the adsorption of 6-TP and 6-TPR takes place at relatively low bulk concentration in the pit region leading to compact film formation in the adsorbed layer. The low bulk concentration of bases containing a thio group needed for the formation of a condensed film indicates that strong lateral interactions exist between the adsorbed species. The compact film

Table 1
Parameters of the least-squares fit of the Avrami plot of transients of 6-TP and 6-TPR at pH 7.2 and 5°C

C (mol l^{-1})	$-E$ (V)	ln b	m	r	δ
6-Thiopurine					
6.50×10^{-5}	0.10	12.28	3.07	0.984	0.082
6.50×10^{-5}	0.15	10.21	2.31	0.978	0.256
6.50×10^{-5}	0.20	13.70	3.76	0.988	0.096
9.10×10^{-5}	0.15	4.83	2.31	0.968	0.436
1.30×10^{-4}	0.15	5.50	2.31	0.981	0.438
2.18×10^{-4}	0.15	5.20	2.30	0.980	0.082
6-Thiopurine riboside					
6.50×10^{-5}	0.175	11.93	3.14	0.980	0.047
6.50×10^{-5}	0.200	11.67	3.20	0.973	0.093
6.50×10^{-5}	0.225	12.49	3.46	0.979	0.073
3.85×10^{-5}	0.200	13.93	3.13	0.993	0.096
1.38×10^{-4}	0.200	7.18	3.09	0.994	0.100

formation has been attributed to intermolecular association of the adsorbed species containing a thiol group at the electrode surface.

Further quantitative studies on the compact film formation of the compounds under investigation could be elucidated by computing the surface excess concentration Γ_m using Koryta's equation [18]. The Γ_m values (Table 2) indicate that the rather compact interfacial structure for the investigated compounds favours an orientation of the bases containing a thiol group perpendicular to the electrode surface. The interaction between the adjacent bases in the compact film is caused by stacking forces. Nevertheless, the rather low average surface area (S_m) for 6-TP and 6-TPR in the compact film indicates a densely packed structure of the base residue of the compound oriented perpendicularly toward the surface of the electrode. On the other hand, if one compares the magnitude of S_m for the investigated thiopurines and dinucleotides or polynucleotides under the same conditions, the same value of ca. 0.4 nm^2 emerges. This indicates that the structure of the condensed film is similar in all cases and corresponds to a stacked orientation of the base–base interactions.

Additional evidence and information on the adsorption and strong interaction of 6-TP and 6-TPR with the mercury electrode surface are gained from cyclic voltammetry (CV) at the HMDE. The CV of the investigated compounds as function of potential in solutions of varying pH

Table 2
Adsorption parameters of 6-TP and 6-TPR calculated from the results of a.c. voltammetry at different pH values

pH	$\Gamma_m \times 10^{-10}$ (mol cm^{-2})	$\Gamma_m \times 10^{14}$ (molecule cm^{-2})	S_m ($Å^2$)	$-E_m$ (V)
6-Thiopurine				
3.2	4.788	2.88	34.68	0.625
5.2	4.670	2.69	37.10	0.650
7.2	4.233	2.55	39.23	0.100
9.2	4.14	2.49	40.09	0.300
6-Thiopurine riboside				
3.2	4.75	2.86	34.90	0.500
5.2	4.15	2.49	40.01	0.550
7.2	3.87	2.33	42.89	0.175
9.2	3.85	2.32	43.11	0.325

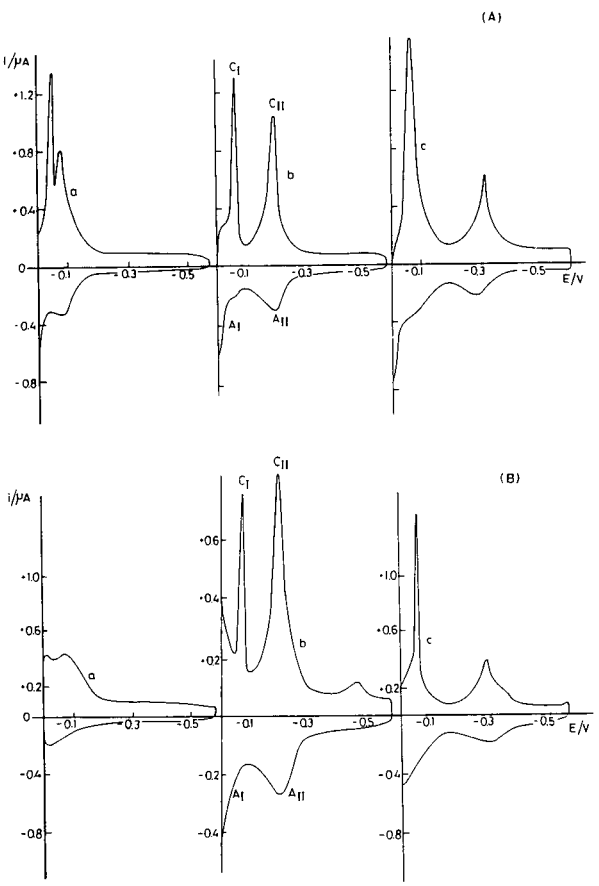

Fig. 5. Cyclic voltammograms of 5×10^{-6} M of (A) 6-TP and (B) 6-TPR at different pH values (a) 3.2, (b) 5.2 and (c) 7.2. $E_s = 0.0$ V, $t_s = 3$ min and scan rate 100 mV s^{-1}.

is represented in Fig. 5. Over the examined pH range very sharp and narrow cathodic peaks (C_I, C_{II}) were observed at completely separated reduction potentials. The cathodic peaks reflect the electrochemical reduction of adsorbed Hg thiolate compound on the electrode surface.

Upon comparison of the CV behaviour of 6-TP and 6-TPR and the corresponding nucleic acid components which do not contain a thio group such as 6-aminopurine and 6-aminopurine riboside, the following feature emerges. It is found that all compounds exhibit a cathodic peak at a potential close to 0.0 V during the electrode process involving nitrogen heterocycles whereas an additional binding occurs through the negatively charged sulphur ion with respect to thio-

purines. This indicates that the cathodic peak (C_I) corresponds to the reduction of Hg(II) ion bound to 6-TP or 6-TPR through heterocyclic nitrogen atoms, while the cathodic peak C_{II} is attributed to the reduction of Hg(II) ion bound to 6-TP or 6-TPR through the negatively charged sulphur ion. The result indicates also that the electroreduction of the adsorbed mercury thiolate $Hg(RS)_2$ is pH dependent ($dE_p/dpH = 60$ mV), whereas the reduction of $Hg(RSH)_2$ (C_I) is independent of $[H^+]$ over the studied pH range.

The CV behaviour 6-TP and 6-TPR exhibits two anodic oxidation peaks (A_I and A_{II}) during the reverse scan. The peak A_{II} is probably due to the reformation of adsorbed film of $Hg(RS)_2$ at more negative potentials. The oxidation peak A_I ("spike peak") at potential close to 0.0 V corresponds to oxidation of mercury in the presence of the investigated compounds and formation of adsorbed film of $Hg(RSH)_2$ on the electrode surface.

The results of CV indicate that the adsorbed amount of thiopurine under investigation is proportional to the total charge Q consumed during the reduction of adsorbed molecules, i.e. to the integral of the reduction current i_s over the potential range of reduction E_s and E_e according to equation

$$Q = \int_{E_s}^{E_e} i_s \, dE = nFA\Gamma \qquad (4)$$

Table 3
Adsorption parameters of 6-TP and 6-TPR calculated from the results of cyclic voltammetry at different pH values

pH	Q (μC cm^{-2})	$\Gamma_m \times 10^{-10}$ (mole cm^{-2})	$\Gamma_m \times 10^{14}$ (molecule cm^{-2})	S_m (nm^2)
6-Thiopurine				
3.20	0.539	2.790	1.68	0.59
5.20	0.609	3.157	1.90	0.52
7.20	0.625	3.238	1.95	0.51
9.20	0.820	4.250	2.56	0.39
6-Thiopurine riboside				
3.20	1.031	5.344	3.21	0.31
5.20	0.968	5.020	3.02	0.33
7.20	0.687	3.560	2.15	0.46
9.20	0.768	3.980	2.38	0.41

where n is the number of electrons in the electrode reaction, F the Faraday constant, A the surface area of the electrode and Γ the surface concentration of the adsorbed species. Therefore the value of surface concentration Γ_m was computed from the limiting value Q_m for the compact layer of the investigated compounds (Table 3). The calculated values of Γ_m and S_m are in agreement with those obtained from phase sensitive a.c. voltammetry. The Γ_m and S_m values show that the rather compact interfacial structure of adsorbed molecules favours an orientation of the base-containing thiol group perpendicular to the electrode surface due to the increase of the strength of stacking interactions between adjacent molecules.

Acknowledgements

The authors express their gratitude to the Alexander von Humboldt Foundation for financial support to purchase the PAR polarographic analyzer equipment.

References

[1] C.F. Beck and G.J. Howlett, J. Mol. Biol., 111 (1977) 1.
[2] E. Palecek, J. Osteryoung and R.A. Osteryoung, Anal. Chem., 54 (1982) 1389.
[3] G. Dryhurst, J. Electroanal. Chem., 28 (1970) 33.
[4] T.M. Florence, J. Electroanal. Chem., 99 (1979) 219.
[5] E. Palecek, F. Jelen, H. Mac. Anh and J. Lasovsky, Bioelectrochem. Bioenerg., 8 (1981) 621.
[6] E. Palecek, Anal. Chim. Acta, 174 (1985) 103.
[7] Y.M. Temerk, Z.A. Ahmed, M.E. Ahmed, M.S. Ibrahim and M.M. Kamal, Fresenius' J. Anal. Chem., 345 (1993) 733.
[8] P. Valenta, H.W. Nürnberg and D. Krznaric, Bioelectrochem. Bioenerg., 3 (1976) 418.
[9] D. Krznaric, P. Valenta, H.W. Nürnberg and M. Branica, J. Electroanal. Chem., 93 (1978) 41.
[10] B. Malfoy, J.M. Sequaris, P. Valenta and H.W. Nürnberg, Bioelectrochem. Bioenerg., 3 (1976) 440.
[11] Y.M. Temerk and M.M. Kamal, Bioelectrochem. Bioenerg., 8 (1981) 671.
[12] Y.M. Temerk and M.M. Kamal, Bioelectrochem. Bioenerg., 11 (1983) 457.
[13] Y.M. Temerk, Can. J. Chem., 57 (1979) 1136.

[14] Y.M. Temerk, M.M. Kamal, M.E. Ahmed and Z.A. Ahmed, Bioelectrochem. Bioenerg., 16 (1986) 497.
[15] Y.M. Temerk, M.M. Kamal, Z.A. Ahmed and M.S. Ibrahim, J. Electroanal. Chem., 260 (1989) 201.
[16] M.M. Kamal, Y.M. Temerk, Z.A. Ahmed and M.S. Ibrahim, Bioelectrochem. Bioenerg., 24 (1990) 165.
[17] G. Arena, E. Rizzarelli and S. Sammartano, Talanta, 26 (1979) 1.
[18] J. Koryta, Collect. Czech. Chem. Commun., 18 (1953) 206.

ELSEVIER

Analytica Chimica Acta 289 (1994) 339–346

ANALYTICA CHIMICA ACTA

Flow-injection biamperometry of phenothiazine derivatives

Jacek Michałowski [a], Anatol Kojło *,[a], Beata Magnuszewska [a], Marek Trojanowicz [b]

[a] *Institute of Chemistry, Warsaw University Branch, Białystok, Poland*
[b] *Department of Chemistry, University of Warsaw, Pasteura 1, 02-093 Warsaw, Poland*

(Received 31st August 1993; revised manuscript received 24th November 1993)

Abstract

A flow-injection method for indirect amperometric determination of promazine and thioridazine using two polarized platinum electrodes was developed. Among seven different indicating systems examined, the most suitable for the determination of phenothiazine derivatives was found to be the redox system Fe(III)/Fe(II). The method developed was applied to several commercial pharmaceutical preparations.

Key words: Amperometry; Flow injection; Phenothiazine derivatives; Promazine; Thioridazine

1. Introduction

The derivatives of phenothiazine (thiodiphenylamine) are widely used since the late 1950s as antipsychotic pharmaceuticals. For the control of pharmaceutical preparations and analysis of their content in body fluids spectrophotometric and chromatographic methods are most often used, although electroanalytical methods can also be employed [1]. Many of the developed methods of determination are based on the oxidation of phenothiazine derivatives in acidic medium to coloured products (free radicals or semiquinones) or to colourless sulphoxides.

Flow-injection analysis (FIA), which is used in an increasing number of applications in various fields of routine chemical analysis, was also already tested for the determination of phenothiazine derivatives. For this purpose optical detection methods were used in many cases [2–6], however, also a possibility for using amperometric [7] and voltammetric [8,9] detection was demonstrated.

In absorptive spectrophotometric determinations the oxidation of phenothiazine derivatives with iron(III) perchlorate in concentrated perchloric acid medium [2] or ammonium metavanadate [3] was applied. In both methods a large sampling rate was achieved. Chlorpromazine was also determined by spectrophotometric titration in a flow-system with perchloric acid as titrant [4]. The use of fluorimetric detection was based on the formation of fluorescent sulphoxides. In the stopped-flow system they were obtained during a reaction with oxygen in acidic medium [5] or as a result of UV irradiation of phenothiazine derivatives [6]. Both these methods have shown satisfac-

* Corresponding author.

0003-2670/94/$07.00
SSDI 0003-2670(93)E0678-Z

tory limits of detection, however, their sampling frequency is limited.

In electrochemical methods of detection the electrochemical activity of phenothiazine derivatives is utilized, as they can be easily oxidized in the anodic range of potentials. Amperometric detection of numerous derivatives was carried out using carbon fibre electrodes polarized with constant anodic potential [7], whereas for the voltammetric detection of chlorpromazine with a stationary carbon disk electrode differential pulse voltammetry at a scan rate of 2 V min^{-1} was used [8,9].

The aim of this study is to examine the possibility to use a simpler mode of electrochemical detection for the FIA determination of promazine and thioridazine than described in references mentioned above, namely amperometric detection with two polarized indicating electrodes (commonly named also as biamperometry). Such a detection method, especially in its indirect mode, has found already numerous applications for the determination of different analytes in various matrices (see [10] and references cited therein).

2. Experimental

2.1. Apparatus

Biamperometric detection was carried out using a PLP type polarograph 225C from Zalmed (Warsaw) as potentiostat with a TZ 4620 potentiometric recorder from Laboratorni Pristroje (Prague). The flow-through detector used with two Pt wire electrodes of 0.7 mm diameter and 13 mm long was described earlier [11]. The surface of the platinum electrodes was cleaned electrochemically by alternating polarization between +5 and −5 V in an alkaline phosphate bath (5 g Na_2HPO_4 and 2 g NaOH in 100 ml water) at 80°C. Such a treatment of working electrodes allowed to obtain a maximum sensitivity of detector response and was repeated every second day of the use of the measuring system.

The flow-injection set-up shown schematically in Fig. 1, consisted of a Gilson Minipuls 2 peristaltic pump and a Model 5021 rotary injection valve (Rheodyne, Cotati, CA). The flow system was made of PTFE tubing of 0.5 mm i.d.

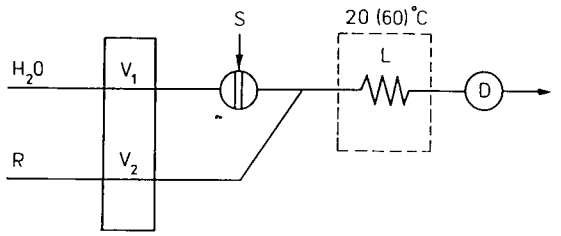

Fig. 1. Schematic diagram of the flow-injection system used for determination of promazine and thioridazine. R = Stream of oxidation reagent solution, S = sample injection valve, L = reaction coil in thermostat, D = biamperometric flow-through detector.

Reference spectrophotometric measurements were performed using a Hewlett-Packard Model 8452A diode array spectrophotometer.

2.2. Reagents

Hydrochlorides of promazine {10-[3-(dimethylamino)propyl]-phenothiazine} and thioridazine {10-[2-(1-methyl-2-piperydyl)ethyl]-2-(methylthio)-phenothiazine} were obtained from Polfa (Jelenia Gora, Poland). As the most effective oxidants $Fe(NO_3)_3 \cdot 9\ H_2O$ from Loba Feinchemie (Austria) and $K_3Fe(CN)_6$ from POCh (Gliwice, Poland) were used. All other reagents were of analytical grade from POCh.

3. Results and discussion

3.1. Comparison of different indicating redox systems

The application of indirect biamperometric detection to the determination of phenothiazine derivatives is based on the chemical oxidation of the analyte by the oxidant, of which the reduced form produced in a given reaction and the oxidant will form a reversible redox couple in the solution. The intensity of the current flowing in the detector with two identical electrodes polarized with a small potential difference in the pres-

ence of excess of the oxidant in the solution depends on the concentration of reduced species formed. In this study as oxidants $Fe(CN)_6^{3-}$, Fe(III) and iodine utilized earlier for indirect biamperometric detection were employed, as well as bromine, Ce(IV), Ti(IV) and VO_3^-, which were not used before for this purpose.

The comparison of different oxidizing species and different indicating systems was carried out in the two-line FIA set-up shown in Fig. 1. A 450-μl volume of 20 mg/l promazine hydrochloride solution was injected into the carrier stream of distilled water delivered at a flow-rate of 3.3 ml min^{-1}. This stream was merged with the stream of acidified solution of oxidizing species pumped with a flow-rate of 2.8 ml min^{-1}. Flow-injection measurements were carried out at 20°C with a 100-cm reaction coil in the system and polarization of the working electrodes with a potential difference of 150 mV. The comparison of numerical data obtained is presented in Table 1.

Using hexacyanoferrate(III) as the oxidant, it was found, that its optimum concentration in the reagent stream is 50 mM in the presence of 0.5 M HCl, which in this case was employed as carrier stream instead of water because of high instability of the oxidant in acidic solution. After one day storage of acidified solution of hexacyanoferrate(III) a blue precipitate was observed on the walls of the glass container, whereas neutral solution can be stored for several weeks without any change of concentration. For this oxidant, satisfactory precision and limit of detection were observed, however, flow-injection signals recorded were deformed by a negative pre-peak.

For iodine used as oxidant the best results were found for 0.3 mM I_2 concentration in reagent solution containing also 0.1 M sulphuric acid. Such a reagent solution is stable for one week. In this case a linear response was observed for lower promazine concentrations. The precision of measurements and detectability were poorer than for hexacyanoferrate(III).

Within this study also several other redox systems not applied earlier as indicating systems in flow-injection biamperometry were examined. Comparable results to those obtained for hexacyanoferrate(III) were observed for the use of bromine as oxidant with a linear response range, which was even slightly wider. The optimum concentration of bromine for the use in FIA systems was found to be 20 mM in the presence of 0.1 M sulphuric acid. The disadvantage of that system is the troublesome preparation of the reagent solution from liquid bromine.

The use of Ce(IV), Ti(IV) and vanadate has not yielded positive results. In case of cerium(IV) the most significant difficulty is substantial drift of the baseline. Even for the optimum 30 mM concentration of $(NH_4)_2Ce(NO_3)_6$ in 1.5 M sul-

Table 1
The comparison of the use of different indicating redox systems for the flow-injection determination of promazine with indirect biamperometric detection

Indicating system	Linear range of response (mg l^{-1})	Correlation coefficient of calibr. plot	R.S.D. (%) [a]	Detection limit (mg l^{-1})	Stability of baseline
Fe(III)/Fe(II)	40–160	0.9996	0.5	0.4 [b]	good
$Fe(CN)_6^{3-}/Fe(CN)_6^{4-}$	20–50	0.9969	0.9	0.8	good
$I_2/2I^-$	4–20	0.9976	1.3	1.3	good
$Br_2/2Br^-$	10–70	0.9970	0.7	0.6	good
Ce(IV)/Ce(III)	–	–	5.5	3.0	very bad
Ti(IV)/Ti(III)	–	–	–	2.0	good
VO_3^-/VO^{2+}	–	–	3.2	1.0	bad

[a] For 12 injections of 20 mg l^{-1} promazine hydrochloride solution.
[b] At 60°C; all other values were obtained at 20°C.

phuric acid, a stable baseline was not obtained. Also the precision of measurements for multiple injections was insufficient.

For the Ti(IV)/Ti(III) indicating system the largest signal magnitude was observed for 0.1 M Ti(IV) solution in 2 M HCl as reagent in a FIA system. The most essential drawback of this system is distinct gradual decrease of the signal magnitude for multiple injections of the same promazine solution. The cleaning of electrodes between measurements led to restoration of the initial magnitude of response. As a decrease of the sensitivity of detection is not observed during the exposure of electrodes for a long time to the flowing solution of Ti(IV), but only after promazine injections, it seems that deactivation of electrodes can be attributed to the adsorption of the product of the promazine reaction with Ti(IV) on the electrode surface.

When a 5 mM vanadate solution in 1.5 M sulphuric acid was used as reagent, similarly to cerium system, an unstable baseline could be obtained and an additional disadvantage of that system is the high instability of reagent solution in time.

As preliminary investigations indicated advantageous properties of the Fe(III)/Fe(II) system for the indirect biamperometric detection of phenothiazine derivatives, a more detailed study of this system was carried out.

3.2. Optimization of flow-injection determination with Fe(III) / Fe(II) indicating system

The variables affecting the obtained signal magnitude in the flow-injection set-up (Fig. 1) with Fe(III) as oxidant include chemical factors (concentration of Fe(III) and HCl), hydrodynamic parameters (flow-rates, diameter of tubings, geometry of the detector, sample volume), electrochemical factors (size of electrodes, polarizing voltage) and temperature. Some of them were not optimized in this study but based on earlier experiments [10–13]. They led to the optimal design of the flow-through biamperometric detector with platinum wire electrodes, size of the indicating electrodes and diameter of PTFE tubing used in the flow-injection system. For all other factors mentioned above a single parameter optimization was carried out separately for the detection of promazine and thioridazine using 20 mg l^{-1} solutions of both analytes. The optimized response of the measuring system was the flow-injection peak height.

In the two-line FIA set-up (Fig. 1) with an injection sample volume of 200 μl, $L = 100$ cm,

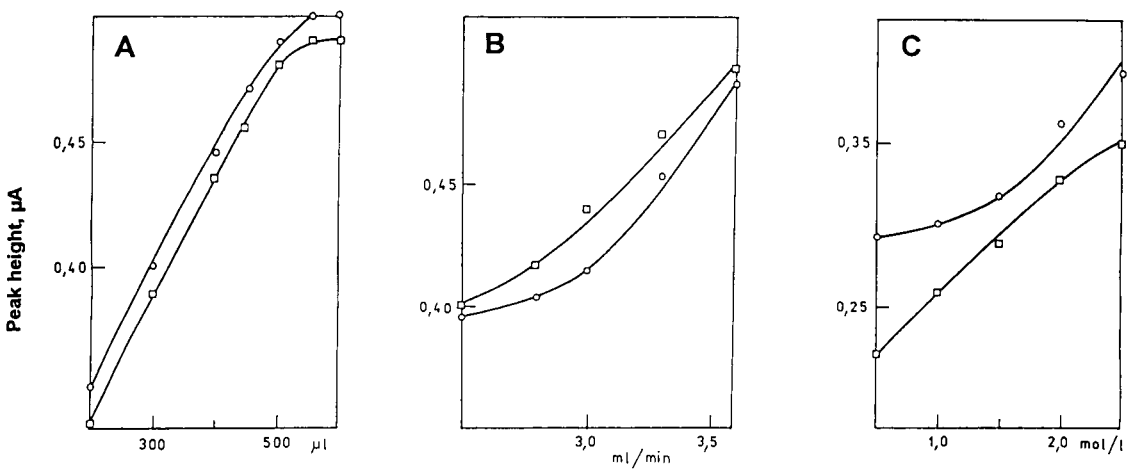

Fig. 2. Effect of the sample injection volume (A), flow-rate of carrier stream of distilled water (B) and concentration of hydrochloric acid in the reagent solution (C) for promazine (○) and thioridazine (□) on peak height in flow-injection measurements.

$V_1 = 3.0$ and $V_2 = 2.5$ ml min^{-1}, polarizing voltage 100 mV and 0.5 M HCl, the concentration of Fe(III) was optimized within the range 0.01–0.24 M. For both analytes no increase of the peak height was observed above 0.18 M Fe(III), hence this concentration was assumed as optimum. The effect of HCl concentration on the signal magnitude is shown in Fig. 2C. In further measurements 2 M HCl was used, although an increase of its concentration may result in some improvement of the detection sensitivity.

In the optimization of hydrodynamic factors the behaviour of the system for promazine and thioridazine was very similar. An increase of the sample volume results in an increase of the peak height (Fig. 2A), however, it is associated with the peak broadening. For further measurements a 450–500 μl sample volume was assumed as optimum. Also an increase of the flow-rate of the carrier solution results in an increase of the signal magnitude (Fig. 2B). For routine determinations flow-rates of 3.3 and 2.8 ml min^{-1} were used for carrier stream and reagent solution, respectively. The effect of the length of the reaction coil was studied in the range of 50–300 cm. An increase of its length above 100 cm resulted in a decrease of the peak height, hence a 100 cm coil was assumed to be the most appropriate.

To a significant extent the signal magnitude in measurements with biamperometric detection is affected by the potential difference used for the polarization of the indicating electrodes. This was also observed for both analytes considered in this study (Fig. 3A). A large increase of the peak height with the potential difference applied was observed for thioridazine up to 100 and for promazine up to 150 mV. Further increase of the applied potential difference results in a smaller increase of the flow-injection signal; therefore 150 mV was accepted as optimum potential difference. About 50% increase of the measurement sensitivity was found when the temperature was raised from 20 to 60°C (Fig. 3B), although it is accompanied with significant increase of the noise amplitude of the baseline. Above 60°C instability of the baseline makes the measurements impossible.

The list of the values of parameters of the flow-injection system used for the determination of promazine and thioridazine in real pharmaceutical samples is shown in Table 2, and an example of the obtained signal recording for promazine in

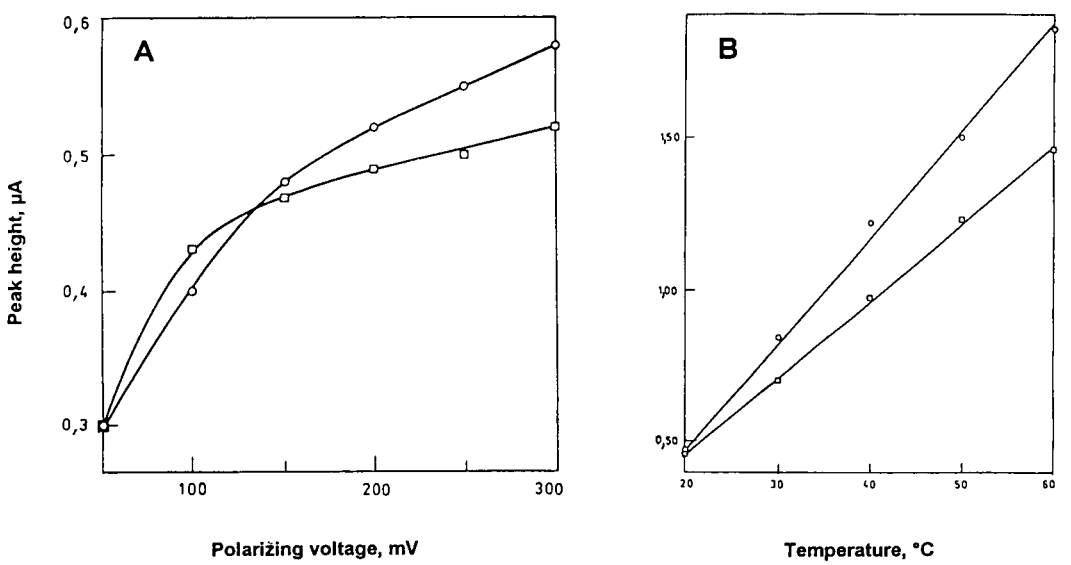

Fig. 3. Effect of the magnitude of polarizing voltage applied (A) and temperature in the reaction coil (B) on peak height in flow-injection measurements for promazine (○) and thioridazine (□).

Table 2
Optimized conditions for the flow-injection determination of promazine and thioridazine with biamperometric detection in the system shown in Fig. 1

Optimized parameter	Optimum value.
Fe(III) concentration (M)	0.18
HCl concentration (M)	2.0
Flow-rate V_1 (ml min^{-1})	3.3
Flow-rate V_2 (ml min^{-1})	2.8
Sample injection volume (μl)	450–500
Length of reaction coil L (cm)	100
Polarizing voltage (mV)	150

the optimized system is shown in Fig. 4. Under such a condition a linear response was observed for promazine from 40 to 160 mg l^{-1} and for thioridazine from 40 to 140 mg l^{-1} with correlation coefficients of 0.9996 and 0.9998 for promazine and thioridazine, respectively. Detection limit values estimated at 60°C for $S/N = 3$ were 0.4 and 0.5 mg l^{-1} for promazine and thioridazine, respectively and the maximum sampling rate for both analytes was 90 samples h^{-1}.

3.3. Effect of interferences

In order to evaluate the selectivity of the developed method for the analysis of pharmaceutical preparations, the effect of the presence of several species which can occur in real samples besides promazine and thioridazine [2] was investigated. Injected solutions containing 20 mg l^{-1} of promazine or thioridazine were spiked with different concentrations of the potentially interfering species listed in Table 3. As tolerated level of interferent was considered the concentration, which caused an error not larger than 5%.

Practically the same results were obtained for both analytes. Those for promazine are shown in Table 3 in the column corresponding to the indicating system Fe(III)/Fe(II). The most significant interferences are ascorbic acid and sulphite, however they do not occur at such high concentrations in commercial preparations. Weaker reducing species such as sugars or formaldehyde are tolerated until about 20-fold higher concentrations.

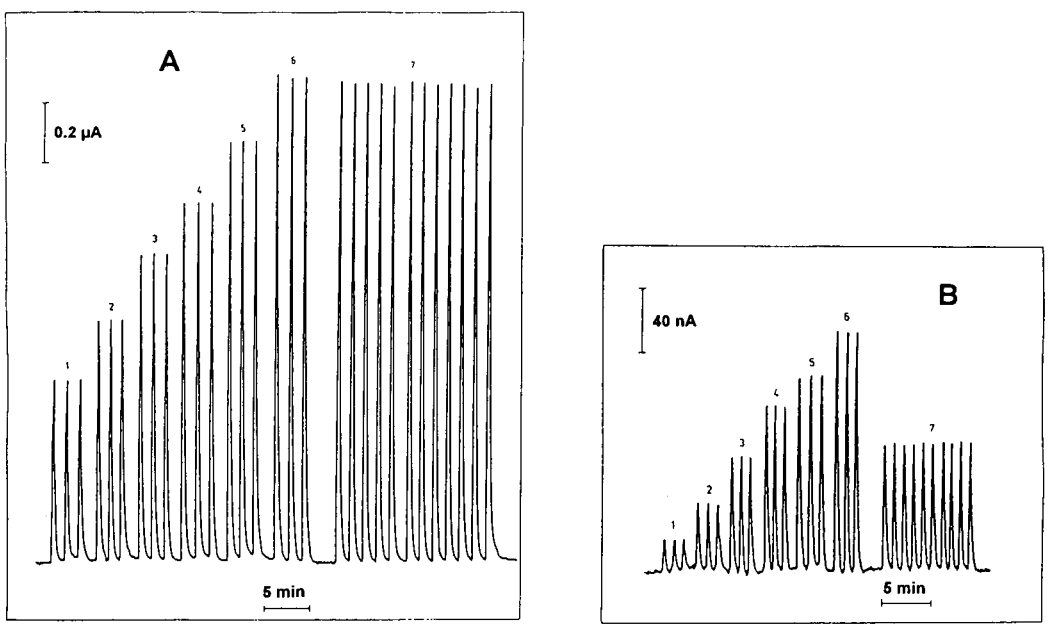

Fig. 4. Example of a recording of flow-injection signal under optimized conditions at 20°C (A) and 60°C (B) for injection: (A) 40 (1), 60 (2), 80 (3), 100 (4), 120 (5), 140 (6) mg l^{-1} promazine solution and solution of commercial preparation Promazin of concentration 140 mg l^{-1} promazine, and (B) 1 (1), 2 (2), 4 (3), 6 (4), 8 (5), 10 (6) mg l^{-1} promazine solution and solution of commercial preparation Promazin of concentration 4.4 mg l^{-1} promazine.

Table 3
Comparison of the tolerance level of interfering species in the flow-injection determination of promazine using biamperometric detection with various indicating systems

Interferent	Tolerated concentration (mg l^{-1}) causing an error of determination of $\leq 5\%$ for different indicating systems		
	$Fe(CN)_6^{3-}$ / $Fe(CN)_6^{4-}$	Fe(III)/ Fe(II)	$I_2/2I^-$
Ascorbic acid	1.0	10	0.05
EDTA	14900	200	1.0
Formaldehyde	7900	180	0.7
Glucose	49000	200	0.4
Lactose	70000	180	25
Phenol	1000	–	3.0
NaCl	94000	18000	–
Na_2SO_3	0.5	8.0	0.01
$CaCl_2$	89000	13500	0.1
Data obtained for promazine hydrochloride level (mg l^{-1})	60	20	10

In Table 3 also the effects of the same species on the biamperometric detection of promazine are compared for 3 different indicating systems. The most sensitive system for those interferences is iodine/iodide. For weaker reductants the largest excesses of interferents are tolerated, when the hexacyanoferrate(III) system is employed, but the least sensitive to the presence of strong reductants is the system with Fe(III) used as oxidant.

3.4. Flow-injection determinations in pharmaceutical preparations

The possibility to use the developed method in real samples was examined for four commercial preparations in tablets, injection solutions and droplets. The complete composition of all preparations was not known. Each tablet of Promazin contains 100 mg promazine hydrochloride and an unknown balancing substance up to 400 mg. Each tablet of Melleril contains 10 mg of thioridazine hydrochloride and a not described balance. Each ampule of injection solution Promazin contains 100 mg of promazine hydrochloride in 2 ml sodium chloride solution of physiological concentration. 100 ml of Melleril droplets solution contains 4 g thioridazine hydrochloride, 20 mg ascorbic acid, 100 mg sorbic acid, 33.3 mg propyl *p*-hydroxybenzoate, 66.7 mg methyl *p*-hydroxybenzoate, 50 mg disodium tetracemate and 3.0 g of 95% ethanol. The obtained results were compared with a spectrophotometric reference method based on absorption measurements at 254 nm in methanol solution of appropriate concentration [14]. The precision of the reference measurements expressed by the relative standard deviation (R.S.D.) for $n = 8$ was 0.4%.

For the determination in tablets, the powdered single tablet was dissolved in 100 ml of methanol, then the obtained solution was filtered and diluted 1 : 10 with distilled water prior to the injection in the flow-injection system. Similarly, one dose of the injection preparation with a certified amount of 100 mg promazine was diluted up to 100 ml with methanol and then 1 : 10 with water before injection. The same procedure was applied for droplets containing thioridazine. The precision of biamperometric determinations in given real samples was evaluated as 0.8% (R.S.D. for $n = 12$), and deviations from the results of photometric determinations have not exceeded 4% (Table 4).

Table 4
Results of determination of promazine and thioridazine in commercial pharmaceutical preparations

Analyzed preparation	Analyte	Results obtained (mg)	
		Flow-injection biamperometry	Reference photometric method [14]
Tablets Promazin	Promazine	102.9	98.8
Injection Promazin	Promazine	102.4	106.1
Tablets Melleril	Thioridazine	9.9	9.6
Droplets Melleril	Thioridazine	37.7	38.1

References

[1] H. Puzanowska-Tarasiewicz and J. Karpińska, Pharmazie, 47 (1992) H12.
[2] M.A. Koupparis and A. Barcuchova, Analyst, 111 (1986) 313.
[3] S.M. Sultan, Analyst, 116 (1991) 177.
[4] C.A. Georgiu and M.A. Koupparis, Analyst, 113 (1988) 755.
[5] M.C. Guttierrez, A. Gomez-Hens and D. Perez-Bendito, Anal. Lett., 20 (1987) 1847.
[6] D. Chen, A. Rios, M.D. Luque de Castro and M. Valcárcel, Analyst, 116 (1991) 171.
[7] F. Belal and J.L. Anderson, Analyst, 110 (1985) 1493.
[8] J. Wang and H.D. Dewald, Anal. Chim. Acta, 153 (1983) 325.
[9] J. Wang and D.H. Dewald, Talanta, 31 (1984) 387.
[10] J. Michałowski, A. Kojło, M. Trojanowicz, B. Szostek and E.A.G. Zagatto, Anal. Chim. Acta, 271 (1992) 239.
[11] A. Hulanicki, W. Matuszewski and M. Trojanowicz, Anal. Chim. Acta, 194 (1987) 119.
[12] M. Trojanowicz, W. Matuszewski, B. Szostek and J. Michałowski, Anal. Chim. Acta, 261 (1992) 391.
[13] J. Michałowski and M. Trojanowicz, Anal. Chim. Acta, 281 (1993) 299.
[14] J. Blazek and J. Krecmar, Česk. Farm., 16 (1967) 437.

ELSEVIER

Analytica Chimica Acta 289 (1994) 347–353

ANALYTICA CHIMICA ACTA

Dual-wavelength photometry with light emitting diodes. Compensation of refractive index and turbidity effects in flow-injection analysis

Hanghui Liu and Purnendu K. Dasgupta *

Department of Chemistry and Biochemistry, Texas Tech University, Lubbock, TX 79409-1061, USA

(Received 7th September 1993; revised manuscript received 14th November 1993)

Abstract

An approach to compensate for both refractive index and turbidity effects is described. A light emitting diode-based dual-wavelength, double-beam (fully referenced), dual-flow-cell photometric detection system is used. The only requirement is that the analyte yields a product (that can be detected by absorbance measurement) as a result of a reaction which does not affect the optical properties of the suspended matter. The principle is mathematically established and experimentally demonstrated by determining micromolar concentrations of bromthymol blue in samples containing up to 1.5% whole milk and 60% ethanol with an absolute error of $< 3.7\%$.

Key words: Flow injection; Sensors; Dual-wavelength photometry; Light emitting diodes; Refractive index effects; Turbidity effects

1. Introduction

Light emitting diodes (LEDs) cover much of the visible and some near infrared (NIR) wavelengths with acceptable monochromaticity for most analytical applications. The short term spatial and intensity stability values exhibited by an LED are much better than conventional light sources and they have far longer usable lifetimes. Additionally, LEDs are robust, compact, and inexpensive. Recently, the designs of LED-based optical absorption detector reported in the literature were reviewed and designs used by the investigators were described in detail with respect to construction, electronic design, performance and cost [1].

Flow-injection analysis (FIA) has proved to be a suitable tool for rapid and reproducible determinations with rather simple and inexpensive apparatus. Absorption photometry is the most widely used detection method in FIA. Naturally, LED-based photometric detectors, with the advantages discussed above, are well suited to the needs of many FIA applications [1–7].

In FIA applications, a difference of refractive index (RI) between the sample and the carrier is common. An uneven distribution of the sample in the radial dimension of the conduit is a conse-

* Corresponding author.

SSDI 0003-2670(93)E0690-9

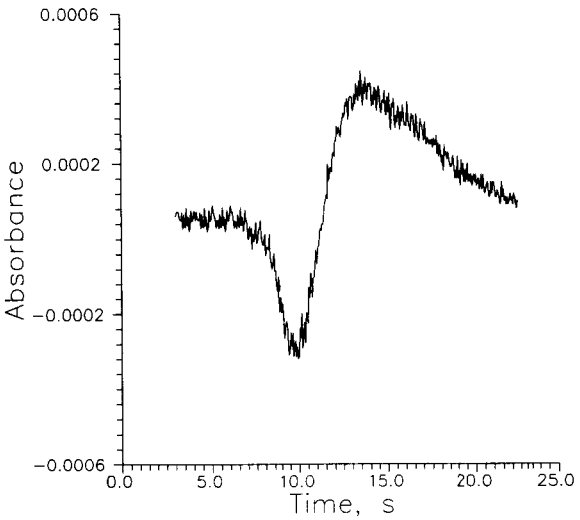

Fig. 1. Artifact absorbance response caused by the injection of 10 mM NaOH into a water carrier, LED-based detection at 605 nm.

quence of laminar flow and is unavoidable. This makes the sample zone in the flow cell act as a lens, either focusing the incident light better or dispersing it away from the photodetector that is placed on the other side of the flow cell. Consequently, an artifact absorbance signal, sometimes referred to as the Schlieren signal, is superimposed on the true absorption signal due to the RI difference. The magnitude of this effect is dependent on various factors, e.g., the RI difference between the sample and the carrier, extent of sample dispersion and the cell design. The pervasive extent to which such effects corrupt the absorbance measurement is rarely fully appreciated (see [8] and references cited therein). With a sufficiently sensitive and stable detector, RI signals can be discerned in seemingly innocuous cases, as illustrated in Fig. 1. Often, the effect is much larger and serious penalties are paid in attainable accuracy, precision and limit of detection (LOD).

A second problem with photometric detection in FIA arises with samples having any perceptible degree of turbidity, as with many real samples encountered in process monitoring. In many cases, on-line filtration to remove all of the suspended matter is not always practical or at least presents a major inconvenience.

Efforts have been made to compensate for error arising from either refractive index change or sample turbidity, taken individually. The optics of a photometric flow cell can be designed to greatly minimize Schlieren signals [9–11]. Nevertheless, in severe cases, the problem cannot be eliminated. Artifact absorbance signals arising from RI differences are not unique to FIA. Solvent "peaks" are commonly observed in photometric liquid chromatography (LC). In atomic absorption spectroscopy (AAS), Zeeman-split lines, that are at a different wavelength than the resonance line, can be used to correct for background absorption [12]. Zagatto et al. [13] report that while it has long been known that solvent peaks in LC can be eliminated in much the same way as Zeeman correction in AAS, namely by using a measurement at a second wavelength (where the analyte does not absorb but the Schlieren signal is still comparable), as a corrective tool, it had not been utilized in FIA. In FIA, the solvent is not separated from the analyte as in LC, and the problem is of much greater practical importance. Zagatto et al. [13] studied the efficacy of this technique for use in FIA applications and reported highly favourable results. Subsequently, Renn and Synovec [14] have also shown an ingenious way to correct for changes in RI (in their case, resulting from a thermal gradient deliberately introduced to perform a unique LC separation) using dual-wavelength spectrophotometry with a single fiber-optic interfaced flow cell and a position sensitive detector. Yamane and Saito [15] have correctly argued that if a very large volume of sample is used, in some part of the sample zone undispersed sample remains and this can be used to correct for the RI induced artifacts. This solution is not always practical and no correction is possible for RI-induced detector noise, etc.

Dual-wavelength photometry has been proposed as a solution to dealing with turbidity in samples as well. Huang et al. [6] described a photometric detector utilizing a dual-colour LED as light source. One wavelength responds both to the analyte and the suspended matter and the

second responds to the suspended matter alone. The difference between the signals from the two channels is used for quantitation. Such a simple subtraction method is acceptable only if the two wavelengths respond to the suspended matter to the same degree. This not only requires that the suspended particle size be relatively large but also imposes the rather conflicting necessity of having the two wavelengths proximate enough to respond to the suspended matter to the same degree, yet distant enough such that the analyte responds at only one of the two wavelengths. Few real samples will satisfy such criteria to perform adequate compensation. Worsfold et al. [3] utilized a dual-flow-cell arrangement to compensate for any intrinsic sample color or turbidity for unattended continuous analysis of phosphate in freshwater streams. The sample, used as the carrier, went first through one flow cell and then reagents were injected into it. The stream then went through the second flow cell, both having identical LED sources. The two detector outputs were fed into a differential amplifier. Since the wavelengths for the two cells are the same, the accuracy of compensation is not expected to be influenced by particle size variation from sample to sample.

Both an RI mismatch with the carrier and existence of sample turbidity can co-occur in real samples; an accurate measurement of the analyte obviously becomes much more difficult in such cases. This problem has never previously been addressed. In the present paper, we describe an approach to compensate for both RI and turbidity effects using an LED-based dual-wavelength, double-beam (fully referenced), dual-flow-cell photometric detection system. The only requirement is that the analyte yields a product (that can be detected by absorbance measurement) as a result of a reaction which does not affect the optical properties of the suspended matter.

2. Principles

Consider the simple manifold depicted in Fig. 2. A turbid sample, the RI of which does not match that of carrier C, is injected into the carrier stream by valve V. Following a short dispersion coil DC, the stream flows through a dual-wavelength detector D1. A merging stream of chromogenic reagent R is next added, this is followed by a reaction coil RC and then a second dual-wavelength detector D2.

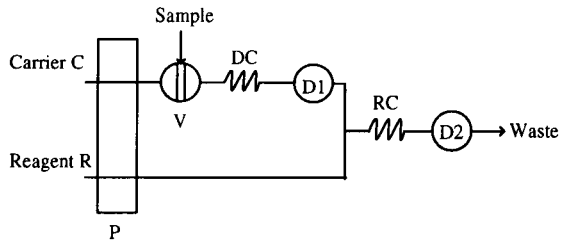

Fig. 2. Manifold design. V: six-port valve; DC: dispersion coil, D1: first dual wavelength detector, RC: reaction coil; D2: second dual-wavelength detector, P: pump, C: carrier, R: Chromogenic reagent.

The following notation is used: S1 and S2 are the signals from the first and second detector, respectively, with subscripts ($\lambda 1$ or $\lambda 2$) indicating the wavelength. Four raw signal outputs ($Si_{\lambda j}$, $i = 1–2$, $j = 1–2$) are measured. It is assumed that each of these raw signal outputs is the algebraic sum of the individual signals due to the analyte component (A), an RI component (R) and a turbidity component (T). These are indicated in subscripted parentheses, e.g., $S2_{\lambda 2(A)}$ is the signal from detector cell 2 at $\lambda 2$ due to the analyte. Only the total signals (indicated in bold font), can be directly measured, the components must be mathematically surmised. It is assumed for simplicity that the analyte reaction product absorbs solely at $\lambda 2$ and the analyte itself (prior to reaction) has no significant absorption at either $\lambda 1$ or $\lambda 2$.

Thus

$$S1_{\lambda 1} = S1_{\lambda 1(T)} + S1_{\lambda 1(R)} \quad (1)$$

$$S1_{\lambda 2} = S1_{\lambda 2(T)} + S1_{\lambda 2(R)} \quad (2)$$

$$S2_{\lambda 1} = S2_{\lambda 1(T)} + S2_{\lambda 1(R)} \quad (3)$$

$$S2_{\lambda 2} = S2_{\lambda 2(A)} + S2_{\lambda 2(T)} + S2_{\lambda 2(R)} \quad (4)$$

We now define two constants:

$$S2_{\lambda 1(T)}/S1_{\lambda 1(T)} = K_T = S2_{\lambda 2(T)}/S1_{\lambda 2(T)} \quad (5)$$

$$S2_{\lambda 2(R)}/S2_{\lambda 1(R)} = K_R = S1_{\lambda 2(R)}/S1_{\lambda 1(R)} \quad (6)$$

K_T is a wavelength independent ratio, it is a measure of the dispersion factor between the two detectors including volumetric dilution and any differences in detector sensitivities. It should preferably be measured with the agent responsible for turbidity although the particle size distribution need not reflect that in the real samples. The RI calibration factor K_R is the ratio of the artifact RI signal at the two wavelengths, it is cell-independent. It is also preferably measured with the type of sample matrix encountered. A sample can be centrifuged or ultrafiltered to remove turbidity and injected into the system with the chromogenic reagent C substituted by an inert carrier for the purposes of this calibration.

Now consider that the signal of interest is $S2_{\lambda 2(A)}$ and one wishes to compute exactly this. If this signal component is known, analyte concentrations can be computed from system calibration data that are obtained with standard analyte solutions that are prepared in the carrier matrix and contain no turbidity.

Transformation of Eq. 4 leads to:

$$S2_{\lambda 2(A)} = S2_{\lambda 2} - S2_{\lambda 2(T)} - S2_{\lambda 2(R)} \quad (7)$$

Substituting Eqs. 5 and 6 in Eq. 7,

$$S2_{\lambda 2(A)} = S2_{\lambda 2} - K_T S1_{\lambda 2(T)} - K_R S2_{\lambda 1(R)} \quad (8)$$

Substituting Eqs. 2 and 3 respectively to describe the second and third terms on the right hand side (r.h.s.) of Eq. 8:

$$S2_{\lambda 2(A)} = S2_{\lambda 2} - K_T[S1_{\lambda 2} - S1_{\lambda 2(R)}] - K_R[S2_{\lambda 1} - S2_{\lambda 1(T)}] \quad (9)$$

Eq. 9 can be written as:

$$S2_{\lambda 2(A)} = S2_{\lambda 2} - K_T S1_{\lambda 2} - K_R S2_{\lambda 1} + K_T S1_{\lambda 2(R)} + K_R S2_{\lambda 1(T)} \quad (10)$$

The last two terms in the r.h.s. of Eq. 10 can now be replaced with transformed equivalents of Eqs. 6 and 5, respectively, leading to:

$$S2_{\lambda 2(A)} = S2_{\lambda 2} - K_T S1_{\lambda 2} - K_R S2_{\lambda 1} + K_T K_R S1_{\lambda 1(R)} + K_R K_T S1_{\lambda 1(T)} \quad (11)$$

Substituting Eq. 1 in the last two terms of Eq. 11,

$$S2_{\lambda 2(A)} = S2_{\lambda 2} - K_T S1_{\lambda 2} - K_R S2_{\lambda 1} + K_T K_R S1_{\lambda 1} \quad (12)$$

All parameters on the r.h.s. of Eq. 12 are directly measurable.

3. Experimental

3.1. Reagents

All chemicals, except as specified, were of analytical-reagent grade, and distilled deionized water was used throughout. Bromthymol blue (BTB) (Kodak) was used without further purification.

3.2. Apparatus

The photometric detection system arrangement is schematically shown in Fig. 3. In this 80386/80387 personal computer (PC) based system, data acquisition and instrument control were executed through a 12-bit data acquisition board (DAS-16G1, Metrabyte Co., Taunton, MA). The LEDs were turned on and off alternately by the digital outputs, typically at 40 Hz, through individual 2N3565 transistors. The emitted light from each pair of LEDs were brought to the individual flow cells by a pair of bifurcated fiber optic bundles (common leg bundle diameter 1.5 mm, type E624, Dolan-Jenner, Lawrence, MA), connected at the common legs by a sleeve-type connector C. This arrangement allows half of the light to be incident on the detector flow cell (D1 or D2) and thence be read by a signal photodiode and the other half to be read by a reference photodiode (both type S2007, Electronic Goldmine, Phoenix, AZ). For this application $\lambda 1$ was chosen to be in the NIR, emitting at 950 nm (LED2,4; type AN 305) and $\lambda 2$ was chosen to be in the visible, emitting at 605 nm (LED1,3; type HAA5566×, Stanley Electric, Tokyo). Because the NIR LED is much more efficient, it was driven at approximately half as much current as

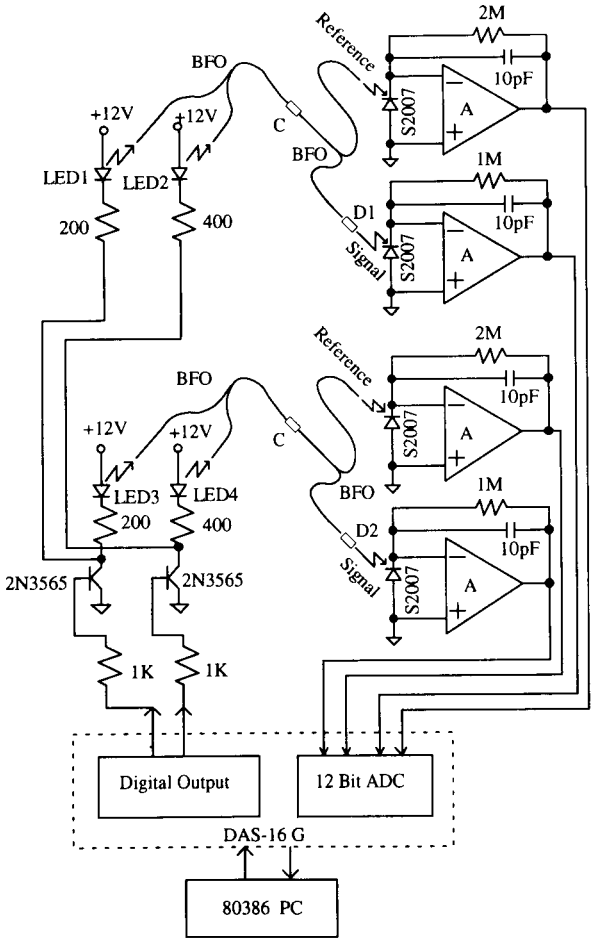

Fig. 3. Dual wavelength LED-based photometric detection system, shown schematically. See text for a detailed description.

the visible LED. Photocurrents corresponding to each LED were converted to voltage signals and then digitized. Any drift of the LED emission intensities was cancelled by computing the log ratio of the signal reading to the reference reading. After each LED is pulsed on, following a brief wait period for any jitter to subside (typ. 1–3 ms), the outputs of the current-to-voltage conversion amplifiers (1/2 OPA2107 AP, Burr-Brown, Tucson, AZ)) were repeatedly sampled and accumulated by the PC. Typically, the analog-to-digital (A/D) conversion rate was 33.3 kHz and 139 readings were accumulated in 16.7 mS for each of the four A/D channels. The software, coupled with an assembly language routine for data acquisition and LED on-off control, was written in C. For non-commercial use copies are available from the authors on request.

The manifold used is the same as that shown in Fig. 2. Samples (30 ml) were injected by an electropneumatically actuated six-port loop type rotary valve V (type 5020P, Rheodyne, Cotati, CA) into a carrier stream consisting of 0.025 M CH_3COOH and 1% Triton X-100 pumped at 0.8 ml/min. The surfactant is added to the carrier to prevent adherence of suspended solids (milk proteins) to the capillary wall. RC and DC are PTFE reaction conduits, 50 cm and 40 cm in length, respectively, with an i.d. of 0.5 mm. Reagent R is 0.4 mM NaOH, pumped at 0.13 ml/min. Pumping was provided by a multichannel peristaltic pump (FIA 8401, BiFok AB, Sweden). Demountable Z-path flow cells [1] with 1.5 mm bore and 6 mm path length were used for D1 and D2.

As illustrative samples, for the purposes of demonstration of this concept, we chose what we believe to be a challenging mix: homogenized whole milk, ethanol and BTB mixed in different proportions. BTB represents the analyte, milk contributes the turbidity component and ethanol produces artifact absorbance responses resulting from Schlieren signal. Injected into the mildly acidic carrier, BTB remains in the yellow form at D1 and is thus not detected at either 605 or 950 nm. The addition of base converts BTB to the blue form which is detected at 605 nm at D2.

4. Results and discussion

4.1. Performance of the detection system and the compensation method

The peak to peak noise levels of the photometric detection system under gravity flow conditions were ~ 10 and ~ 30 μAU, respectively, for the 950 nm and 605 nm wavelengths. With the peristaltic pump, pumping noise was by far the dominant factor, however. The maximum attainable switching rates of the LEDs was 200 Hz in this system, with concomitantly shorter data accumu-

lation periods. However, the noise increased at higher switching rates.

In so far as the compensation method is concerned, in principle the technique should be equally applicable whether peak heights or peak areas are used for the $Si_{\lambda j}$ values. Although Zagatto et al. [13] have reported strict additivity of RI and absorbance signals, we found that area additivity was much better than height additivity. Further, area integration helps to reduce much of the pumping noise present in our system. Fig. 4 shows an example of all the four detector outputs (a: $S1_{\lambda 1}$, b: $S1_{\lambda 2}$, c: $S2_{\lambda 1}$, and d: $S2_{\lambda 2}$) for a sample containing 48 μM BTB in the presence of 1.5% milk and 60% ethanol. Note that pumping noise is visible in all the outputs. We chose to use area counts therefore in all computations.

Table 1 shows one set of data for these types of samples in which the BTB content varies from 48 to 144 μM, milk content from 0 to 1.5% and ethanol content of 0–60%. The raw value of $S2_{\lambda 2}$ as well as the value of $S2_{\lambda 2(A)}$ computed according to Eq. 12 is shown. It is remarkable that in this range of samples where the value of the raw signal $S2_{\lambda 2}$ is up to 47% higher than the corrected analyte signal, the maximum absolute error encountered for any given sample is $< 3.7\%$. It should be noted that even for standard samples, the mean absolute error for computing the concentration of an assumed linear calibration plot is 1.2%. Reproducibility of the response from a given sample is better than the attainable accuracy of the compensation method; the relative standard deviation for the computed value of

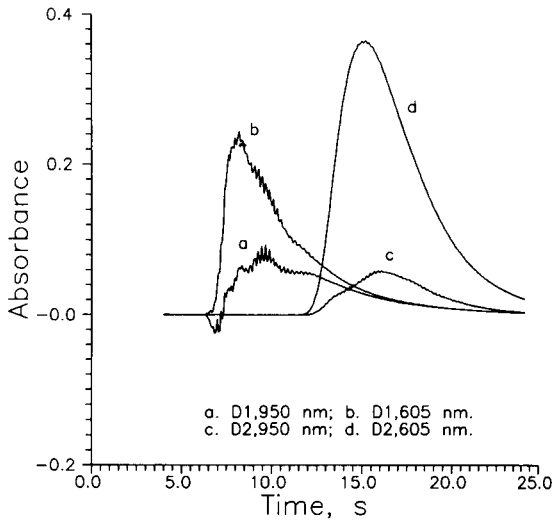

Fig. 4. Four different detector outputs recorded for a single injection of a sample containing 48 μM BTB in the presence of 60% ethanol and 1.5% milk. (a) $S1_{\lambda 1}$, (b) $S1_{\lambda 2}$, (c) $S2_{\lambda 1}$, (d) $S2_{\lambda 2}$.

Table 1
Compensation of turbidity and refractive index effects

BTB μM	Concentration		Peak area (arbitrary units)					
	Ethanol (%)	Milk (%)	$S2_{\lambda 2}$	$S2_{\lambda 2(A)}$ From Eq. 12	Computed BTB conc. (μM)	Percent error	Computed BTB conc. (μM) using alternate K_T and K_R^a	Percent error
8.0	0	0	16.18	16.19	48.7	1.4	48.7	1.4
48.0	20	0.5	20.23	16.23	48.8	1.7	49.1	2.2
48.0	40	1.5	25.23	15.80	47.5	−1.1	48.5	1.0
48.0	60	1.0	24.00	16.54	49.8	3.7	50.5	5.3
96.0	0	0	32.03	32.03	97.4	1.4	97.4	1.5
96.0	20	1.0	38.85	31.28	95.1	−1.0	95.9	−0.1
96.0	40	0.5	34.87	32.45	98.7	2.8	98.8	2.9
96.0	60	1.5	44.21	32.32	98.3	2.4	99.4	3.6
144.0	0	0	46.83	46.84	142.9	−0.8	142.9	−0.8
144.0	20	1.5	57.16	46.19	140.9	−2.2	142.3	−1.2
144.0	40	1.0	53.94	46.83	142.9	−0.8	143.5	−0.3
144.0	60	0.5	52.03	47.83	145.9	1.3	146.3	1.6

[a] K_T and K_R values were obtained by calibrations with $BaSO_4$ and glycerol, respectively.

$S2_{\lambda 2(A)}$ of a sample containing 96 μM BTB, 20% ethanol and 1% milk is 0.43% ($n = 10$).

When calibrated with three samples of milk in concentrations of 0.5, 1.0 and 1.5%, the values of K_T at $\lambda 1$ and $\lambda 2$ were $0.675 \pm .041$ and 0.622 ± 0.016, respectively. A mean value was used in our calculation. When calibrated with $BaSO_4$ or AgCl suspensions, the values were closer at the two wavelengths, $BaSO_4$: 0.615 ± 0.027, 0.580 ± 0.002 and AgCl: 0.805 ± 0.003, 0.800 ± 0.004 for $\lambda 1$ and $\lambda 2$, respectively. Similarly, mean values of K_R obtained with 20, 30 and 40% ethanol samples were 0.942 ± 0.017 and 0.890 ± 0.052 respectively for D1 and D2. A mean value for the two cells were used in our calculations. For 20% glycerol these values were 1.11 and 0.98 and for 25% $NaNO_3$ these values were 1.32 and 1.08, respectively, for D1 and D2. In so far as the principle itself is concerned, K_T or K_R values should be obtainable by any suitable turbid sample and a sample with a different RI from the carrier. In practice, the values of these parameters clearly depend on the standards chosen to measure them. In some cases, it may not be possible to calibrate with the relevant components of the sample matrix by themselves. However, It should be noted that an error in the K_T or K_R values does not result in a directly proportional error in the final analytical result. As an example, the BTB results have been recomputed for the same milk–ethanol–BTB samples using K_T and K_R values obtained with $BaSO_4$ and 20% glycerol, respectively. These results are also shown in Table 1. The correction is still a meaningful improvement compared to no correction.

In summary, the present technique provides a relatively simple and affordable approach to the photometric analysis of turbid samples that are injected in carrier streams with a considerably different RI. The present method does not require elaborate sample pretreatment steps and should be of particular value to process analysis.

Acknowledgements

We appreciate the generous gift of the pump used in this work by Bo Karlberg, BiFok AB. This research was supported partially by an unrestricted grant from the Shell Development Co., Houston, TX.

References

[1] P.K. Dasgupta, H.S. Bellamy, H. Liu, J.L. Lopez, E.L. Loree, K. Morris, K. Petersen and K.A. Mir, Talanta, 40 (1993) 53.
[2] D. Betteridge, Anal. Chem., 50 (1978) 832A.
[3] P.J. Worsfold, J.R. Clinch and H. Casey, Anal. Chim. Acta, 197 (1987) 43.
[4] M. Trojanowicz, P.J. Worsfold and J.R. Clinch, Trends Anal. Chem., 7 (1988) 301.
[5] M. Trojanowicz and J. Szpunar-Lobinska, Anal. Chim. Acta, 230 (1990) 125.
[6] J. Huang, H. Liu, A. Tan, J. Xu and X. Zhao, Talanta, 39 (1992) 589.
[7] P.C. Hauser and D.W.L. Chiang, Talanta, 40 (1993) 1193.
[8] A.G. Fogg, Analyst (London), 115 (1990) 593.
[9] J.E. Stewart, Appl. Opt. 20 (1981) 654.
[10] J.E. Stewart, Proc. SPIE, 492 (1984) 529.
[11] H.S. Bellamy, H. Liu and P.K. Dasgupta, Talanta, 40 (1993) 341.
[12] H.H. Willard, L.L. Merritt, Jr., J.A. Dean and F.A. Settle Jr., Instrumental Methods of Analysis, Wadsworth, Belmont, CA, 7th edn., 1988, p. 251.
[13] E.A.G. Zagatto, M.A.Z. Arruda, A.O. Jacintho and I.L. Mattos, Anal. Chim. Acta, 234 (1990) 153.
[14] C.N. Renn and R.E. Synovec, Anal. Chem., 63 (1991) 568.
[15] T. Yamane and M. Saito, Talanta, 39 (1992) 215.

ELSEVIER

Analytica Chimica Acta 289 (1994) 355–364

ANALYTICA CHIMICA ACTA

Zone circulating flow-injection analysis: theory

Yongsheng Li, Yoshio Narusawa *

Department of Chemistry, College of Science, Rikkyo (St. Paul's) University, 3-34-1, Nishi-Ikebukuro, Toshima-ku, Tokyo 171, Japan

(Received 2nd June 1993; revised manuscript received 9th August 1993)

Abstract

Zone circulating flow-injection analysis (ZCFIA) is a method for multi-detection of a sample zone injected into a closed-flow system formed by connecting the two ports of a single FIA manifold. Using an FIA instrument assembled with a multi-step pump, detection was carried out at various flow-rates. Subsequent analysis of the damped curves yielded a great deal of information concerning the theory of FIA. The data thus obtained were arranged to clarify correlations among general residence time, flow-rate, length and inner diameter of the reactor, sample volume injected and dispersion coefficient. As a result, several shortcomings and errors in FIA theory were discovered. Several qualitative formulations, containing variables suitable for the various conditions involved, were established and six qualitative conclusions were drawn.

Key words: Flow injection; Zone circulating flow injection

1. Introduction

Flow-injection analysis (FIA) has found wide applications in analytical chemistry since it was first proposed [1] and a number of books concerning the theory of FIA have been published [2–12]. Guidance for carrying out FIA experiments or studying FIA practices is based on the theory outlined by Ruzicka and Hansen [2,8]. However, in studying FIA applications, it has occasionally been found that some aspects are inconsistent with FIA theory. In particular, according to the general understanding of FIA, the dispersion coefficient of an injected sample zone decreases when the flow-rate of the carrier stream decreases in a tubular reactor. However, it has been reported that the result differs depending on how the conditions of the FIA system are set [6]. Therefore, work has been carried out in order to clarify some perceived and unidentified points of this type [13].

A multi-detection system has been reported by Rios et al. [14] as the manifold of a closed system in FIA, but the term "multi-detection" is not suitable for the present investigation. We propose the term "zone circulating flow-injection analysis" (ZCFIA). ZCFIA is a method for multi-detection of a sample zone injected into an enclosed-flow system formed by connecting the two ends of a single FIA manifold. With the ZCFIA method, except for the preparation of sample solutions, there is no chance of individual errors entering during the measurement. Once the instrument is

* Corresponding author.

SSDI 0003-2670(93)E0672-T

operating stably, detection is made on the sample as it is circulated mechanically in a closed-flow system. Consequently, this method yields very accurate and highly reliable data. For this reason, the ZCFIA method was adopted in this work to identify and clarify the quantitative comprehensive verification for the FIA theory.

In this study, a mini-pulse peristaltic pump with multi-step revolutions was used in the ZCFIA manifold. Sets of damped response curves were obtained at various flow-rates of the carrier stream. Subsequent analysis of the curves yielded a great deal of information concerning the theory of FIA. With the aid of the data obtained, the qualitative correlations among flow-rate, length and inner diameter of the reactor, sampling volume, residence time and dispersion coefficient of the injected sample zone were clarified. The data obtained coincided with the results of an earlier study [13]. It is thought that the conclusions presented here have universality as identical results have been obtained using different FIA instruments [15]. As a result, several shortcomings and errors in the current FIA theory were found. Several qualitative formulations, containing variables suitable for the various conditions involved, were established and six qualitative conclusions were derived. These conclusions have an important bearing on FIA theory and FIA experiments.

2. Experimental

2.1. Preparation of sample and carrier solutions

Preparation of carrier

A carrier solution was prepared with purified water. Because bubbles dissolved in water are easily released when the flow-rate of the carrier stream is increased and disturb the analysis of an injected sample, degassing was carried out in the following manner: by using a membrane filter (pore size 0.45 μm), the purified water was filtered under reduced pressure, then the vessel was placed in an ultrasonic cleaner for thorough degassing. The operation was continued until no further bubbles were evolved from the water.

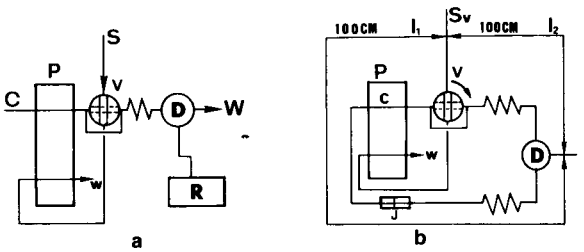

Fig. 1. Experimental manifold for ZCFIA. (a) Single-line manifold for ordinary FIA; (b) ZCFIA manifold. D = spectrophotometer; W = waste; S = sample ($K_2Cr_2O_7$, 800 μg ml^{-1}, S_v = 100 μl); P = multi-step peristaltic pump; C = carrier (purified water); R = recorder; J = joint; L = total reactor length ($l_1 + l_2$) (i.d. 1.0 mm).

Preparation of a sample solution [16]

Potassium dichromate solution was prepared by dissolving 0.4000 g of potassium dichromate (heated for 2 h at 110°C) in a 500-ml volumetric flask and diluting to volume with purified water. The orange solution thus obtained contains 800 μg ml^{-1} potassium dichromate with an absorption maximum at 440 nm.

Apparatus

A Soma Kougaku S-3250 single-beam spectrophotometer equipped with a flow cell (inner volume 8 μl, path length 10 mm) was used. A Denki Kagaku Keiki (DKK) minipulse-5 peristaltic pump with multi-step revolutions, a DKK one-channel injection valve and a System Instruments (SIC) Chromatocorder-12 were also used.

2.2. Spectrophotometer response time

An ordinary FIA single-line manifold was assembled as shown in Fig. 1a. When the instrument was operating stably and the baseline of the output signal of the spectrophotometer had reached a steady state, the spectrophotometer's response time corresponding to the flow-rate of the carrier stream was found by increasing the revolution speed scale of the pump step by step in the order 10, 20, 30, 40, 50, 60, 70, 80, 90 and 99. When the response time was set to 0.05 s, the signal height increased gradually until a pump scale (PS) of 40, but decreased thereafter in the form of a convex curve (Fig. 2a). It was thought

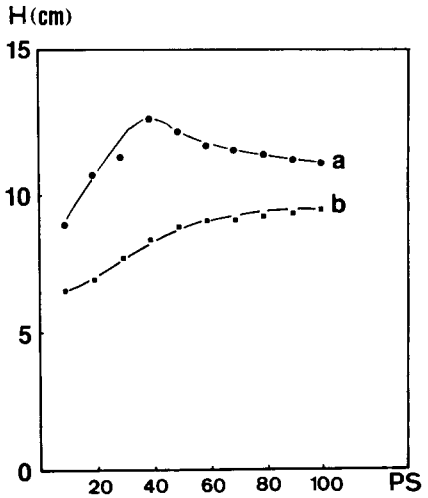

Fig. 2. Relationships between pump revolution speed scale (PS) and signal height. Response time: (a) 0.05 and (b) 0.01 s.

that this phenomenon was due to the detector's pick-up speed being slower than the flow-rate of the carrier stream at this response time. Therefore, detection was repeated in the same manner as mentioned above after setting the detector's response time to 0.01 s, by removing part of the resistance in the electrical circuit related to the damping. The curve of the signal height vs. pump speed then increased monotonically (Fig. 2b). A curve similar to this curve (Fig. 2b) was detected previously with an FIA-T1-721 spectrophotometer [15] (there is no signal attenuation circuit in this instrument). For this reason, if the response speed of the detector applied in studies on FIA theory is inadequate, erroneous results may be obtained. In Fig. 2, although the curve for a response time of 0.05 s is slightly higher than that for 0.01 s using the pump scales tested, it is caused by the difference in the signal attenuation set for the recorder.

2.3. Determination procedure using ZCFIA

First, when the instrument was operating stably, for testing its reproducibility a sample (S_v = 100 μl) of the potassium dichromate solution was injected into the flowing carrier stream and the potassium dichromate in the sample zone was detected with the spectrophotometer. The determination procedure was repeated eleven times and the relative standard deviation (R.S.D.) was found to be less than 0.5%.

Second, the purified water carrier was pumped into the tubular reactor, and simultaneously the sample solution was aspirated into a loop by a defined sample volume with the pump, and the pump was immediately stopped. After connecting the inlet of the carrier to the outlet of the waste on the single-line manifold so as to prevent bubbles from entering, the valve was switched from the load position to the inject position (Fig. 1b). Then the pump and the recorder were started at the same time, and the analysis of the injected sample was begun simultaneously. The time for one determination was 12 min. The procedures were repeated twenty times for each flow-rate, which was varied from 1.02 to 13.2 ml min^{-1} in ten steps, that is, the scale button of the pump's revolution speed was switched from 10 to 99.

Third, in order to find the dispersion coefficient [$D = H^0/H^{max}$ (see below)], H^0 was measured as the signal height of the sample solution flowing through the detector instead of the carrier stream. The H^0 value obtained in the experiment was 23.6 cm. The overall results obtained are sets of damped response curves as shown in Fig. 3. The initial peak that appears on a recorder chart is the result of the injected sample zone

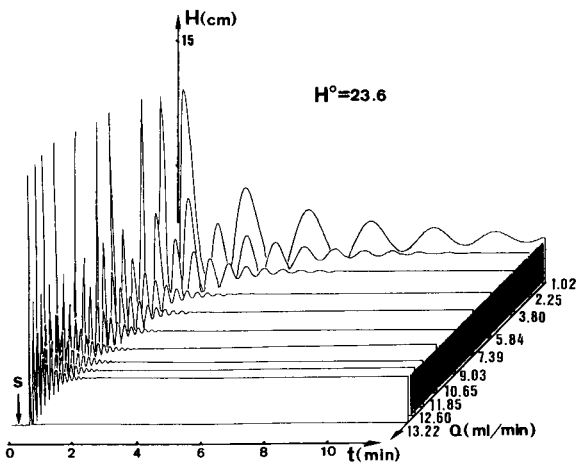

Fig. 3. Three-dimensional representation of the output signals obtained by ZCFIA at various flow-rates. t = Travel time; Q = flow-rate; H = signal height; S = injection point of the sample.

that has only travelled 100 cm. After this, the peaks of the damped curve will appear every 200 cm until the sample solution is completely homogenized, because the enclosed-flow system has a total length (L) of the tubular reactor of 200 cm. The number of FIA peaks obtained coincides with the number of times that the zone passes through the detector. As the sample zone diffuses when travelling forward through the tubular reactor, the peak height decreases with increasing residence time (T).

Fourth, as the zone is completely mixed with the carrier, the response signal (absorbance A or height H) changes to a plateau at the steady state. The curves detected at ten different flow-rates are depicted in a three-dimensional format as shown in Fig. 3. This figure contains a great deal of information concerning pure physical phenomena of FIA. By analysing these, it may be possible to clarify correlations among Q, L, t, r, S_v, D, σ (axial dispersion, which will be considered in another paper) and H (detector value) under various conditions in the FIA system.

3. Results and discussion

3.1. Analyses of the three-dimensional figure

Ideal flow model of the sample zone in a tubular reactor

First, the flow state of the sample zone in an FIA system not containing a chemical reaction is hypothesized as the ideal flow model shown in Fig. 4. By analysing the model, Eqs. 1–8 are derived. In these equations, L is the length (cm) of the tubular reactor, L_r is the distance travelled (cm) of the sample plug with physical dispersion and L_s is the plug width (mm) of the injected sample or, rather, the length of the sample plug injected at a split second; consequently, L_s obeys the following equation:

$$L_s = S_v/\pi r^2 \quad (1)$$

where S_v (μl) is the sample volume injected and r (mm) is the radius of the reactor. $L_{m,f}$ (cm) is the axial dispersion length caused by molecular motion or, rather, the dispersing distance of the

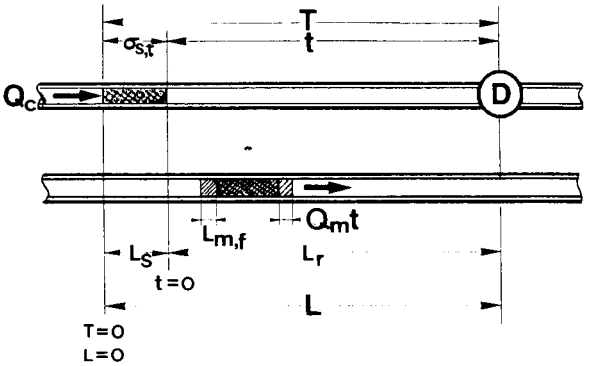

Fig. 4. Ideal flow model hypothesized for a sample zone through a narrow conduit. Definitions and explanations of the symbols are presented in the text.

injected sample plug forwards in the axial direction caused by Brownian molecular motion, and hence it can be described by the following equation (in fact, the injected sample zone disperses in two axial directions, but for the sake of simplicity it is considered that the sample zone disperses only in one axial direction):

$$L_{m,f} = Q_m t/\pi r^2 \quad (2)$$

where Q_m (cm^3 s^{-1}) is the volume of molecular dispersion per second, and is associated with the carrier viscosity, properties, diffusion coefficient and the dispersion process of the sample molecule, t (s) is the travel time or elapsed time, that is, the time of the sample zone dispersing after injection, and T is the residence time of the sample zone. Therefore, the following equation can be established:

$$T = t + \sigma_{s,t} \quad (3)$$

where $\sigma_{s,t}$ is the peak width expressed as the time elapsed of the sample zone having a length L_s, which passes through the detector. If the unit of $\sigma_{s,t}$ is seconds on the recorder chart, the peak width will be represented by the symbol $\sigma_{s,t}$(s); if the unit is millimetres, the peak width will be represented by the symbol $\sigma_{s,l}$(mm). The relationship between these two can be expressed as $\sigma_{s,l}$(mm) = $a\sigma_{s,t}$(s), where a is the chart speed of the recorder and is a constant. In the present experiment, a was set at 6 mm s^{-1}. When the speed of travel of the sample zone equals that of

the recorder chart, $\sigma_{s,l}$ will equal L_s under ordinary conditions, and the following equation is established:

$$\sigma_{s,t}(s) = \pi r^2 L_s/(Q_m + Q_c) \quad (4)$$

where Q_c ($cm^3\ s^{-1}$) is the flow-rate of carrier stream and relates to the process of the convection of the injected sample plug and the Q is the total flux of the sample zone during travel, i.e.,

$$Q = Q_m + Q_c \quad (5)$$

From the above definitions, the following equations can also be derived:

$$t = \pi r^2 L_r/(Q_m + Q_c) \quad (6)$$

$$T = \pi r^2 (L - L_s)/(Q_m + Q_c) + \sigma_{s,t} \quad (7)$$

$$L = (T - \sigma_{s,t})(Q_m + Q_c)/\pi r^2 + L_s \quad (8)$$

Second, the correctness of these equations was established from the following experimental data. According to the sets of damped response curves in Fig. 3, the relationships among Q_c, L_r and t were analysed and are depicted in Figs. 5 and 6. Subsequently, from linear regression, calculation, the group of plots in Fig. 7 was also obtained.

In Fig. 7, it is seen that even if Q_c is zero, L_r is not zero and the length of the intercept on the ordinate increases with increasing residence time (t). If analysing this phenomenon from the intercepts, when Q_c is zero it may be thought that the intercept length on the ordinate signifies that the total length (L) contains the injected sample plug length L_s and the diffusion distance caused by molecular dispersion of the sample plug, that is, $L_{m,f}$. According to Eq. 8, however, the following equation can be derived:

$$L = L_s + (T - \sigma_{s,t})(Q_m + Q_c)/\pi r^2$$
$$= L_s + Q_m t/\pi r^2 = L_s + L_{m,f}$$

that is, the theoretical prediction is the same as the experimental results, or rather, even if the travel of the carrier stream is stopped, the injected sample zone is still continuously dispersing, because the molecular motion never stops, and the travel distances due to molecular dispersion will increase monotonically with increase in the time during the carrier stream remains stationary when the pump is stopped.

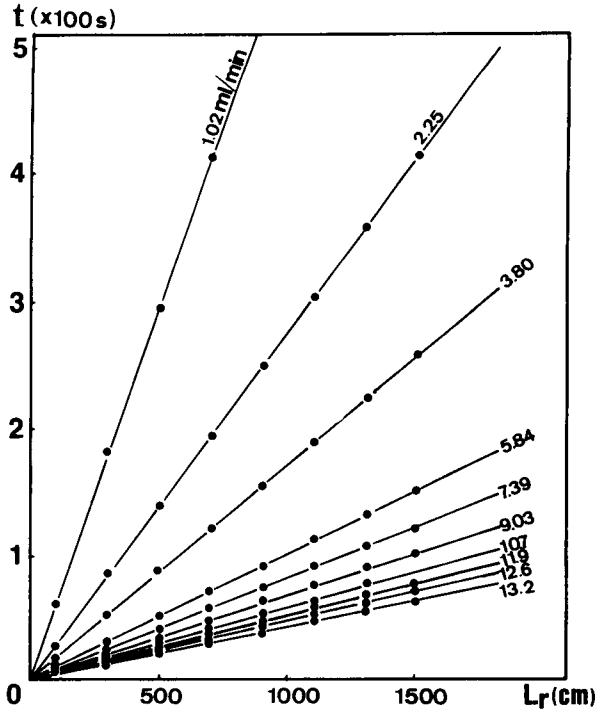

Fig. 5. Relationships between t and L_r at various flow-rates Q.

Conclusion 1

In FIA systems, the interrelationships among L, Q, T, r and S_v may obey Eqs. 6–8. When the flow-rate is fixed, the residence time of the sample zone would be proportional to the distance it has travelled; if the distance travelled is fixed, the residence time of the sample zone would be inversely proportional to the flow-rate of the carrier stream; if the residence time is fixed, the distance travelled by the sample zone would be proportional to the flow-rate of the carrier stream; if the flow of the stream is stopped, dispersion of injected sample zone continues and the dispersal distance of the sample zone increases monotonically with increase in the time the carrier has been stopped.

Interrelationships between Q, L, T, r, S_v and D.

The dispersion coefficient, D, is defined as the ratio of concentrations of sample material before and after the dispersion process has taken place in that element of fluid that yields the analytical

readout [8]. If the analytical readout is based on maximum peak height measurement, the concentration within that (imaginary) element of fluid which corresponds to the maximum of the recorded curve (C^{max}) has to be considered. Thus, be relating C^{max} to the original concentration of injected sample solution C^0, sample (and reagent) concentrations can be calculated:

$$D = C^0/C^{max} \quad (9)$$

Because a Chromatocorder 12 was used, that can handle output signals by electrical circuits with a logarithmic conversion, the height indicated as H (cm) of the peak of output signal is proportional to the concentration C^{max}, hence the above equation may be rewritten as

$$D = H^0/H^{max} \quad (10)$$

In the present experiment, the measured H^0 value obtained was 23.6 cm. Moreover, the above equation may be further rewritten as

$$D = 23.6/H^{max} \quad (11)$$

The numerical values of H^{max} of the peak heights in Fig. 3 are then substituted in Eq. 11 and used to calculate in turn, the dispersion coefficients of the sample zone were found under the various conditions. Analysis of the data thus obtained gave the results in Table 1 and the group of curves in Figs. 8 and 9. From the curves concerning Q, L and D in Figs. 8 and Fig. 9, the following expression was obtained:

$$D = K_1 L_r^{\mu_1} Q^{-\mu_2} + 1 \quad (0 < \mu_1 < 1,\ \mu_2 > 0)$$
$$= K_1 (L - L_s)^{\mu_1} Q^{-\mu_2} + 1 \quad (0 < \mu_1 < 1,\ \mu_2 > 0) \quad (12)$$

where K_1 is a constant and μ_1 and μ_2 are also constants but their values change in some definite ranges with variation in the experimental conditions.

Conclusion 2

In FIA systems, when the flow-rate of the carrier stream, the inner diameter of the tubular reactor, and the sample volume injected are fixed, dispersion increases with increase in the length of the reactor. However, if the length and inner diameter of the tubular reactor and the sample

Table 1
Relationships among Q_c, L_r, t and D

Q_c (ml min^{-1})	Parameter	L_r (cm)								
		100	300	500	700	900	1100	1300	1500	1700
1.02	t (s)	58.8	176.4	294.0	411.6	529.2	646.8			
	D	3.87	7.82	10.33	12.39	13.88	15.08			
2.25	t (s)	27.5	82.5	137.5	192.5	247.5	302.5	357.5	12.5	
	D	3.79	7.42	9.83	11.77	13.34	14.40	15.23	15.84	
3.80	t (s)	17.1	51.3	85.5	119.7	153.9	188.1	222.3	256.5	290.7
	D	3.51	7.26	9.60	11.46	12.94	14.22	15.08	15.73	16.05
5.84	t (s)	10.1	30.3	50.5	70.7	90.9	111.1	131.3	151.5	171.7
	D	3.38	6.95	9.27	11.13	12.52	13.76	14.71	15.28	15.79
7.39	t (s)	8.2	24.6	41.0	57.4	73.8	90.2	106.6	123.0	139.4
	D	3.35	6.69	8.88	10.73	12.20	13.33	14.48	15.23	15.73
9.03	t (s)	6.7	20.1	33.5	46.9	60.3	73.7	87.1	100.5	113.9
	D	3.24	6.61	8.81	10.66	12.14	13.45	14.44	15.23	15.90
10.7	t (s)	5.7	17.1	28.5	39.9	51.3	62.7	74.1	85.5	96.9
	D	3.02	6.32	8.45	10.13	11.52	12.76	13.80	14.57	15.13
11.9	t (s)	5:1	15.3	25.5	35.7	45.9	56.1	66.3	76.5	86.7
	D	3.03	6.30	8.43	10.22	11.57	2.73	13.72	14.48	15.13
12.6	t (s)	4.7	14.1	23.5	32.9	42.3	51.7	61.1	70.5	79.9
	D	3.06	6.25	8.40	10.07	11.49	12.52	13.60	14.35	15.03
13.2	t (s)	4.2	12.6	21.0	29.4	37.8	46.2	54.6	63.0	71.4
	D	3.05	6.21	8.33	9.96	11.46	12.59	13.64	14.44	15.03

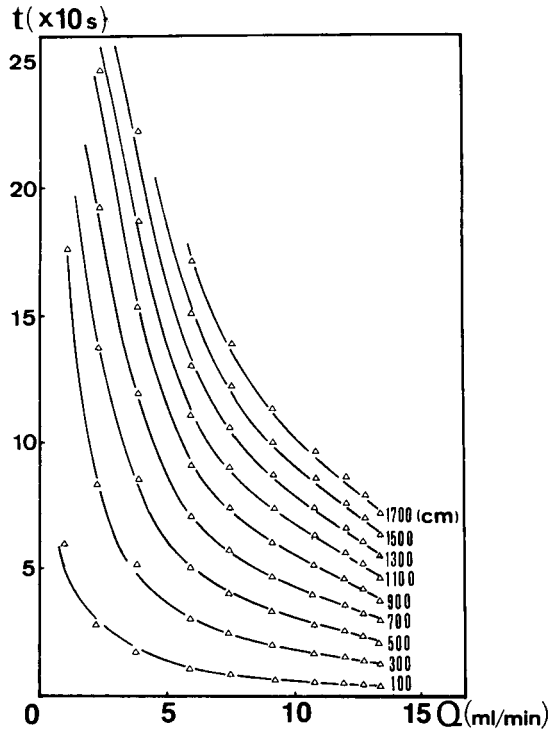

Fig. 6. Relationships between t and Q at various path lengths L_r.

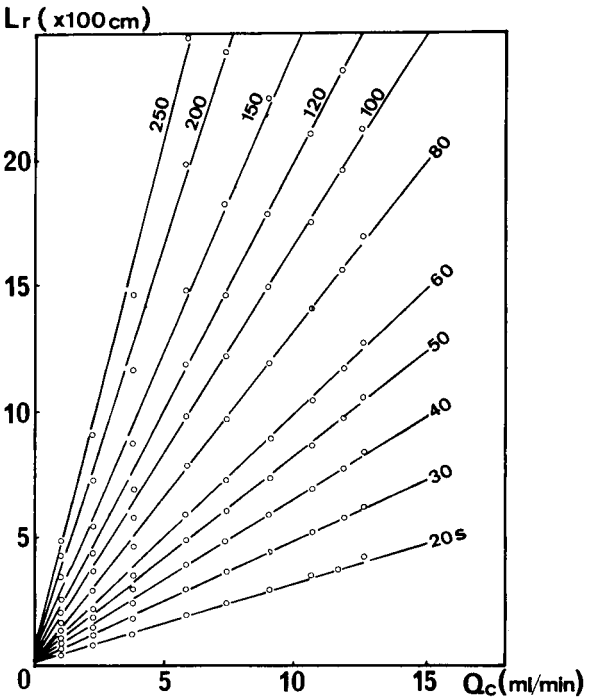

Fig. 7. Relationships between Q_c and L_r at various travel times t.

volume injected are fixed, the dispersion decreases with increasing flow-rate of the carrier stream.

If the peaks of the damped curves are connected with the curves in Fig. 3, H values at a certain time can be obtained. The H value are then substituted into Eq. 11 and the D values at a certain time can be found. These data are given in Table 2. From Table 2, the relationships between the dispersion of the sample zone and the flow-rate of the carrier stream can be further arranged into sets of curves as shown in Fig. 10. Consequently, the following expression, similar Eq. 12, is obtained by analysing the curves in Fig. 10:

$$D = K_2 t^{\mu_3} Q^{\mu_2} + 1 \qquad (0 < \mu_2, \mu_3 < 1)$$
$$= K_2 (T - \sigma_{s,t})^{\mu_3} Q^{\mu_2} + 1 \qquad (0 < \mu_2, \mu_3 < 1) \tag{13}$$

where K_2 is a constant and μ_3 is also a constant with some limited conditions.

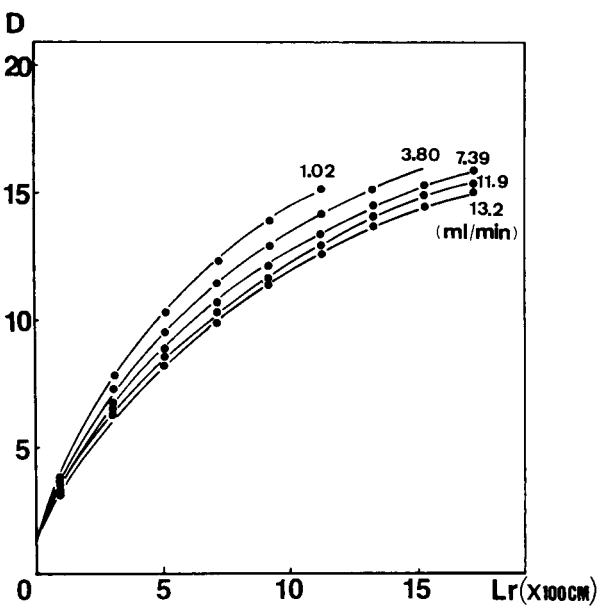

Fig. 8. Relationships between D and L_r at various flow-rates Q.

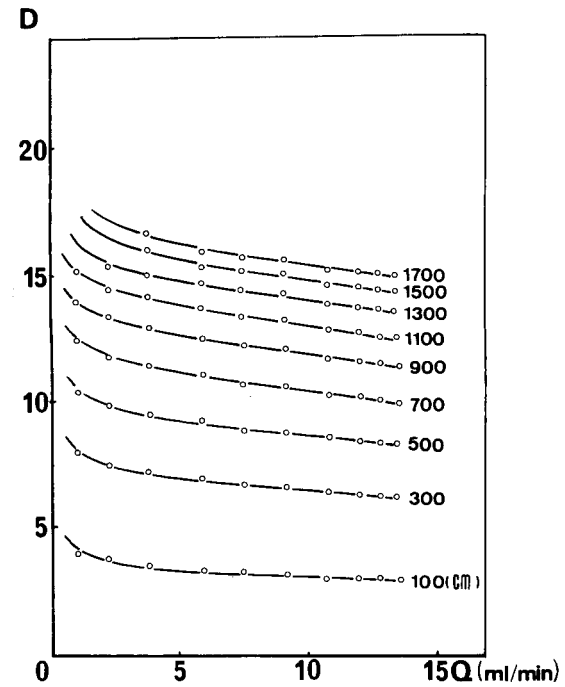

Fig. 9. Relationships between D and Q at various path lengths L_r.

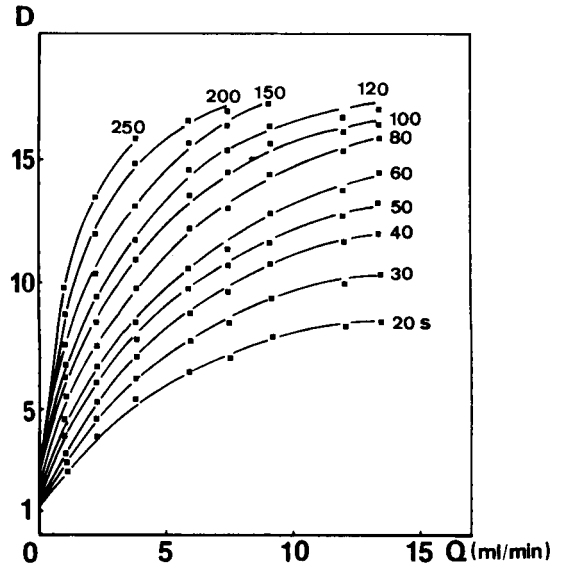

Fig. 10. Relationships between D and Q at various travel times t.

Conclusion 3

In FIA systems, if the residence time of the sample zone, the inner diameter of the reactor and the sample volume injected are fixed, the dispersion will increase with increasing flow-rate of the carrier stream within the narrow conduit system. If the the flow-rate of the carrier stream, the inner diameter of the reactor and the sample volume injected are fixed, the dispersion in-

Table 2
Correlations between Q_c and D at fixed t, r and S_v ($H^0 = 23.6$ cm)

Q_c (ml min^{-1})	Parameter	t (s)										
		20	30	40	50	60	80	100	120	150	200	250
1.02	H (cm)				6.00	5.12	4.36	3.85	3.52	3.13	2.70	2.41
	D				3.93	4.61	5.41	6.13	6.70	7.54	8.74	9.79
2.25	H (cm)		5.17	4.45	3.92	3.56	3.16	2.78	2.54	2.27	1.96	1.75
	D		4.56	5.30	6.02	6.63	7.47	8.49	9.29	10.4	12.0	13.5
3.80	H (cm)	4.39	3.82	3.36	3.07	2.79	2.41	2.16	1.98	1.79	1.59	1.50
	D	5.38	6.18	7.02	7.69	8.46	9.79	11.0	12.0	13.2	14.8	15.7
5.84	H (cm)	3.68	3.09	2.69	2.42	2.21	1.92	1.74	1.62	1.51	1.44	
	D	6.41	7.64	8.77	9.75	10.7	12.3	13.6	14.6	15.6	16.4	
7.39	H (cm)	3.39	2.88	2.50	2.23	2.09	1.82	1.65	1.55	1.46	1.41	
	D	6.96	8.19	9.44	10.6	11.3	13.0	14.3	15.2	16.2	16.7	
9.03	H (cm)	3.02	2.51	2.02	2.01	1.84	1.63	1.51	1.44	1.38		
	D	7.81	9.40	10.7	1.74	12.8	14.5	15.6	16.4	17.1		
11.9	H (cm)	2.85	2.38	2.15	1.89	1.76	1.58	1.49	1.43			
	D	8.28	9.92	11.5	12.6	13.4	14.9	15.8	16.5			
13.2	H (cm)	2.83	2.29	1.97	1.76	1.65	1.50	1.45	1.41			
	D	8.34	10.3	12.0	13.4	14.0	15.7	16.3	16.7			

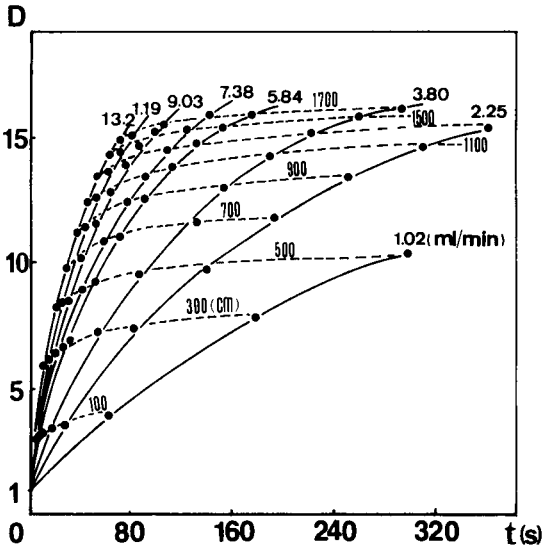

Fig. 11. Relationships among t, L_r, Q and D.

creases with increasing residence time of the sample zone [2,8].

This conclusion was contrasted with conclusion 2, and it was discovered that if there are no definite conditions restricting the definition of qualitative correlations among the parameters of Q, L, T and D in FIA systems, erroneous results will be obtained.

From Table 1, if the flow-rate of the carrier stream, the length and inner diameter of the reactor and the sample volume injected are not changed, data on the correlations between the residence time and dispersion coefficients of the sample can be found. These data are presented as the sets of curves in Fig. 11. In Fig. 11, the solid lines are sets of curves for t vs. D when the flow-rate is fixed and the dashed lines are sets of curves for t vs. D when the length of the reactor is fixed. From Fig. 11, the following expression was obtained:

$$D = K_3 L_r^{\mu_1} t^{\mu_3} + 1 \quad (0 < \mu_1, \mu_3 < 1)$$
$$= K_3 (L - L_s)^{\mu_1} (T - \sigma_{s,t})^{\mu_3} + 1 \quad (0 < \mu_1, \mu_3 < 1) \qquad (14)$$

where K_3 is a constant.

Conclusion 4

From the above expression, in FIA systems if the length and inner diameter of the reactor and the sample volume injected are fixed, the dispersion increases with increase in the residence time of the sample zone flowing through narrow conduit system; if the residence time of the sample zone and the sample volume injected are fixed, the dispersion increases with increasing length of the reactor and residence time of the sample zone flowing through the narrow conduit system.

In addition, if Eq. 1 is substituted in Eqs. 12 and 14, the following expressions are obtained:

$$D = K_1 (L - S_v/\pi r^2)^{\mu_1} Q^{-\mu_2} + 1 \quad (0 < \mu < 1, \mu_2 > 0) \qquad (15)$$

$$D = K_3 (L - S_v/\pi r^2)^{\mu_1} t^{\mu_3} + 1 \quad (0 < \mu_1, \mu_3 < 1) \qquad (16)$$

Conclusion 5

In FIA systems, if the length and inner diameter of the reactor and the flow-rate of the carrier stream (or the residence time of the sample zone) are fixed, the dispersion decreases with increase in the sample volume injected. If the sample volume injected is increased to the total volume of the reactor, the value of the dispersion coefficient will approach unity.

From Eqs. 6–8 and 14, the following expression is obtained:

$$D = K_3 L_r^{\mu_1+\mu_3} (\pi r^2/Q)^{\mu_3} + 1$$
$$= K_3 t^{\mu_1+\mu_3} (Q/\pi r^2)^{\mu_1} + 1 \quad (0 < \mu_1, \mu_3 < 1) \qquad (17)$$

Conclusion 6

From the above expression, in FIA systems, if sample volume injected, the length and inner diameter of the reactor (or the distance travelled by the sample zone) and the flow-rate of the carrier stream are fixed, the dispersion increases with increase in the inner diameter of the reactor. Further, if the sample volume injected, the residence time of the sample zone and the flow-rate of the carrier stream are fixed, the dispersion

decreases with increasing inner diameter of the reactor.

Acknowledgements

The authors gratefully thank Mr. S. Kitahama of Denki Kagaku Keiki for supplying the multi-step peristaltic pump and Mr. K. Takahashi for his help with some of the experimental work. Nomura Micro-Science Co. is acknowledged for the provision of ultra-pure water.

References

[1] J. Ruzicka and H. Hansen, Anal. Chim. Acta, 78 (1975) 145.
[2] J. Ruzicka and H. Hansen, Flow Injection Analysis, Wiley, New York, 1981.
[3] K. Ueno and K. Kina, Introduction to Flow-Injection Analysis—Experimental and Application, Kodansha Scientific, Tokyo, 1983 (in Japanese).
[4] M. Valcarcel and M.D. Luque de Castro, Flow-Injection Analysis—Principles and Applications, Horwood, Chichester, 1987.
[5] H. Hansen, Flow Injection Analysis, Polyteknisk Forlag, Trykteknik, 1986.
[6] Y.-S. Li and W.-C. Cheng, Flow Injection Analysis, Beijing University Press, Beijing, 1987, p. 19 (in Chinese).
[7] J. Möller, Flow Injection Analysis, Springer, Heidelberg, 1987.
[8] J. Ruzicka and H. Hansen, Flow Injection Analysis, Wiley, New York, 2nd edn., 1988.
[9] B.I. Karlberg and G.E. Pacey, Flow Injection Analysis—A Practical Guide, Elsevier, Amsterdam, 1989.
[10] J.L. Burguera, Flow Injection Atomic Spectroscopy, Dekker, New York, 1989.
[11] Y. Takashima and N. Yoza, Labo-Automation: Flow Injection Analysis (Fundamental and Experimental), Hirokawa, Tokyo, 1989 (in Japanese).
[12] R. Kuroda, K. Oguma and H. Nakamura, Flow Injection Analysis, Kyoritsu Shuppan, Tokyo, 1990 (in Japanese).
[13] Y.-S. Li, presented at the Second Chinese National Conference on Flow Injection Analysis, Sheng Yang, 19–21 October 1989.
[14] A. Rios, M.D. Luque de Castro and M. Valcarcel, Anal. Chem., 57 (1985) 1803.
[15] Y.-S. Li and W.-C. Cheng, Fengxi Yiqi, No. 3 (1986) 46.
[16] Y.-S. Li, Guowai Fengxi Yigi, 1 (1990) 46.

ELSEVIER

Analytica Chimica Acta 289 (1994) 365–370

ANALYTICA CHIMICA ACTA

Flow-injection method for the determination of tin in fruit juices using solid-phase spectrophotometry

L.F. Capitán-Vallvey *, M.C. Valencia, G. Mirón

Department of Analytical Chemistry, University of Granada, 18071 Granada, Spain

(Received 12th May 1993; revised manuscript received 24th November 1993)

Abstract

An integrated solid-phase spectrophotometric–flow-injection method is proposed for the determination of tin in fruit juices. The complex formed between Sn(IV) and Pyrocatechol Violet in the flow system is concentrated on Sephadex QAE A-25 gel packed in a flow cell. The analytes are monitored by UV–visible spectrophotometry at 576 nm. The method shows a detection limit of 0.3 ng ml^{-1} and a linear range of 2–40 ng ml^{-1}.

Key words: Flow injection; UV–Visible spectrophotometry; Fruit juices; Tin

1. Introduction

Flow analysis was originally devised as a method for continuous analysis to be carried out in a homogeneous phase. The integration of reaction, retention and detection steps offers an increase in the sensitivity of detection and a decrease in the dispersion, among other advantages.

This integration of the preconcentration, reaction and detection steps in flow analysis can be accomplished in several ways, e.g., using a solid support [1], usually an ion-exchange material placed in the flow cell to preconcentrate the analyte on the solid support, or by using a chromogenic reagent fixed on the material [2] or more usually [3–8] by retaining the product of a previous chemical reaction.

Three methods for the measurement of analytes or reaction products fixed on resins can be mentioned, among others: UV–visible absorption [1], fluorescence [9] and photoacoustic measurements [10].

One of the requirements when using automatic continuous methods relying on the use of these solid supports packed into a flow cell is the easy elimination of the analyte or reaction product fixed on the solid matrix. At least three approaches to this problem have been tried: (a) introduction of successive samples on to the solid support, which yields a graphical recording featuring successive plateaux as sample injections are performed, followed by adequate desorption at the end of the determinations [3,11]; a possible inconvenience of the method could be non-linearity of the retention isotherm; (b) elution after injection of each sample using a desorbing solution usually containing a complexing agent or an

* Corresponding author.

SSDI 0003-2670(93)E0681-V

acid that removes the chromogenic species from the support and allows its reuse; in this instance the recorded signal increases until a maximum value and then remains constant [4]; (c) a judicious choice of the acidity conditions or complexing agent providing a not too strong retention leading to self-elution by the carrier solution itself; some typical flow-injection analysis (FIA) recordings are presented in [5].

Integration of FIA and solid-phase spectrophotometry (SPS) [12] showed an increase in sensitivity and selectivity compared with conventional preconcentration methods, avoiding interferences because of the need for retention on to the solid.

The advantages of this approach have been utilized for the determination of traces of analytes, which grouped according to the kind of solid substrate are as follows: (a) copper [2,11], chromium [8], bismuth [3] and iron [5] using ion-exchange resins; (b) molybdenum on QAE-Sephadex A-25 [4]; (c) phosphate [6] and silicic acid [7] on a hydroxypropyl derivative of Sephadex dextran gel; (d) C_{18}-bonded silica [13] for the resolution of a mixture of 2,4-dinitrophenylhydrazine and 2- and 4-nitrophenylhydrazine.

Here, Sephadex QAE A-25 was used to develop a simple and sensitive method for measuring sub-$\mu g\ l^{-1}$ levels of tin by the flow technique. This was accomplished through retention of the Pyrocatechol Violet–tin(IV) system on Sephadex QAE A-25.

2. Experimental

2.1. Chemicals

All chemicals were of analytical-reagent grade. Reverse-osmosis quality water was used for the dilution of samples and reagents.

Tin(IV) stock standard solution was prepared by dissolving 50.0 mg of high-purity tin metal in 20 ml of hot, concentrated H_2SO_4 and, after cooling, addition of 100 ml of water and 30 ml of concentrated H_2SO_4, and dilution to 250 ml. A working standard solution was prepared by diluting the stock standard solution with water and H_2SO_4 to a 10% solution.

Pyrocatechol Violet (PCV) solution was prepared by dissolving 50.0 mg of PCV (Merck) in 1 l of water adjusted to pH 4.3 with monochloroacetic acid. This solution was stable for 2 days.

Carrier solution was prepared by dissolving 472.5 mg of monochloroacetic acid in water, adding NaOH until pH 3 and diluting to 500 ml. A desorbing solution was prepared by diluting 5 ml of concentrated HCl to 100 ml with water.

A dextran-type anion-exchange gel, Sephadex QAE A-25, in the chloride form was used.

2.2. Apparatus and flow diagram

Absorption measurements were made with a Bausch and Lomb Spectronic 2000 double-beam spectrophotometer equipped with a Hellma 138-OS flow cell with a 1.5-mm light path.

The flow analysis set-up consisted of a Gilson Minipuls-2 four-channel peristaltic pump working at a constant flow-rate, three variable-volume Rheodyne Model 5041 PTFE rotary valves controlled electromechanically by a method developed in this laboratory and a Bausch and Lomb Spectronic 2000 double-beam spectrophotometer equipped with a Hellma 138-OS flow cell with a 1.5-mm light path and connected to a conventional microprocessor that controls the pump, valves and spectrophotometer by sofware designed in-house, written in Basic and compiled. This set-up was interfaced using RS-232 C interfaces to a microprocessor. All the tubing was made of PTFE.

The ion-exchange gel was used without pretreatment to avoid contamination and packed into the flow-through cell using glass-wool in the outlet to retain the gel. The flow cell was packed with the gel up to 7 mm (total height of the optical window 11 mm) as a compromise to obtain the highest signal. The flow system is depicted in Fig. 1.

2.3. Procedure

Basic procedure

The sample solution (750 μl) at pH 2.2 and containing 2–40 ng ml^{-1} (1.5–30.0 ng) of tin(IV) was inserted into the carrier stream ($ClCH_2$-

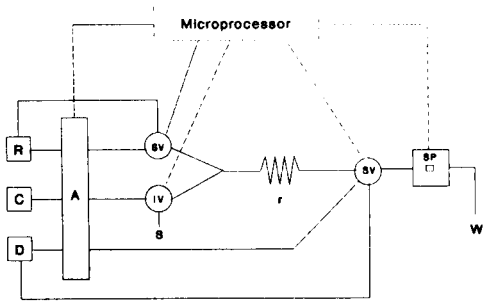

Fig. 1. Manifold. A = pump; S = sample; R = reagent solution; D = desorbing solution; C = carrier; SV = selection valve; IV = injection valve; r = reaction coil; SP = spectrophotometer; W = waste.

COOH–$ClCH_2COONa$, total concentration 1 M, pH 3.0) at a flow-rate of 0.6 ml min^{-1}. PCV solution (5×10^{-3}%) was introduced by means of a six-way rotary valve operating for a given time (100 s) at the same flow-rate. After simultaneous confluence with the sample by a Y-connection, the stream passed through the coil r (100 cm × 1 mm i.d.) and the PCV–Sn complex was formed. When the complex reached the flow cell, it was retained on Sephadex QAE anion exchanger and the absorbance increase at 576 nm was recorded.

After the maximum absorbance (attenuance) had been reached, the complex was quickly eluted by using a desorbing agent (5% HCl) introduced by a six-way rotary valve operating for 120 s and rendering the flow cell ready for a new sample. Before the introduction of a new sample, the loop tube was always washed with a small volume of 3% HCl and then with water.

The absorbance increment (ΔA) between 20 and 150 s after injection or the derivative signal was measured and the Sn(IV) concentration was determined by means of a calibration graph. A blank solution of water was used.

Procedure for fruit juices

About 10 g, exactly weighed, of the juice were heated to destroy the matrix in a sand-bath until nearly dry, digested with concentrated HNO_3 until the solution was clear, followed by treatement with concentrated HCl until evolution of NO_2 vapour ceased. The solution was then diluted to 50 ml and analysed as described under *Basic procedure*.

3. Results and discussion

The variables influencing the system can be classified into two main groups: chemical variables and manifold variables.

3.1. Optimization of chemical variables

In the presence of tin(IV) and PCV a 1:2 anionic violet-coloured species was fixed on Sephadex QAE gel showing maximum absorption at 576 nm. The optimum pH for fixation of the Sn–PCV complex in the gel was found to be 3 when changing the pH of the carrier, as previously found in the batch solid-phase method [14]. A 0.01 M monochloroacetic acid–monochloroacetate buffer of pH 3.0 was found to be the most convenient carrier.

The analytical signal and baseline absorbance were found to increase with increase in the PCV concentration (Fig. 2). A 6.5×10^{-5} M PCV solution and a time of 100 s for the opening time of the reagent selection valve were chosen, because larger amounts gave a higher baseline due to higher PCV retention.

As preservation purposes required the sample to be acidified (ca. 0.01 M H_2SO_4), the best results were obtained using a PCV solution of pH 4.

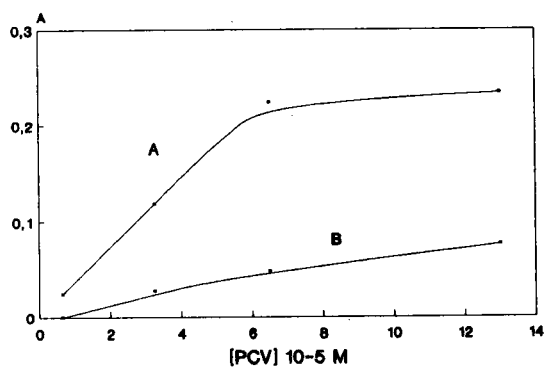

Fig. 2. Effect of concentration of reagent on colour development. (A) Sn–PCV complex; (B) blank. Sample volume, 0.4 ml; amount of Sn(IV), 8.7 ng; opening time of valve for PCV, 100 s; loop, 336 μl; cell length, 1.5 mm; solid support, Sephadex QAE A-25.

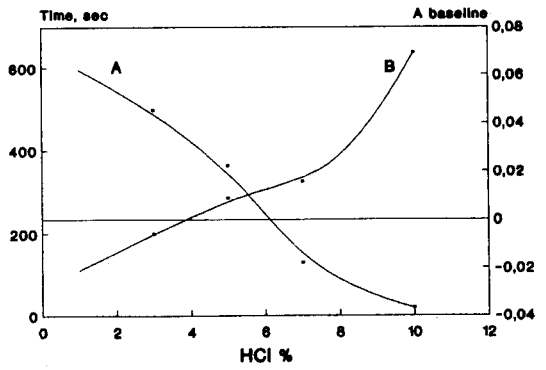

Fig. 3. Influence of concentration of desorbing agent (HCl) (A) on baseline and (B) on return time to baseline. [PCV] = 6.5×10^{-5} M; [Sn(IV)] = 10 μg l^{-1}; opening time of valve for PCV, 100 s; opening time for HCl valve, 120 s; loop, 781 μl; cell length, 1.5 mm; solid support, Sephadex QAE A-25.

Hydrochloric acid was selected as the eluent to desorb the Sn–PCV coloured species from the gel in the flow-through. Increasing concentrations of acid, although raising the time of return to the baseline owing to a swelling process, improved the efficiency of elution. We selected 5% HCl as the desorbing agent as a compromise between an increase in the baseline and a decrease in the return time (Fig. 3).

3.2. Variables in the flow-injection manifold

The length of the reaction coil has a small effect on the peak height due to the rapid formation of Sn–PCV species in solution. A reaction coil of 1 m gave the optimum results.

A decreased flow-rate resulted, as expected, in increased residence time and peak heights, which indicates that the fixation of Sn(IV) as a complex was not instantaneous. A total flow-rate of 0.6 ml min^{-1} was adopted as a compromise.

The analytical signal increased linearly with increasing size of the sample loop used and therefore the residence time and the baseline also increased. The use of loops of different lengths makes it possible to adapt them for a wide concentration range for analytical purposes as required. A loop with a volume of 780 μl was finally chosen in order to use it over a wide range of concentrations.

3.3. Analytical features

Two types of analytical signals can be used (see Fig. 4): the tangent, i.e., the absorbance increment (ΔA) at a fixed time after injection (between 20 and 150 s), with previous subtraction of the signal of the blank at the same wavelength; and the height (h) of the derivative signal of the flow-injection profiles.

The calibration graphs are linear for the concentration range 2–40 ng/ml of tin using the sample loop indicated above. The analytical parameters are summarized in Table 1.

The reproducibility was established for ten analyses of solutions containing 3.5 and 6.0 ng

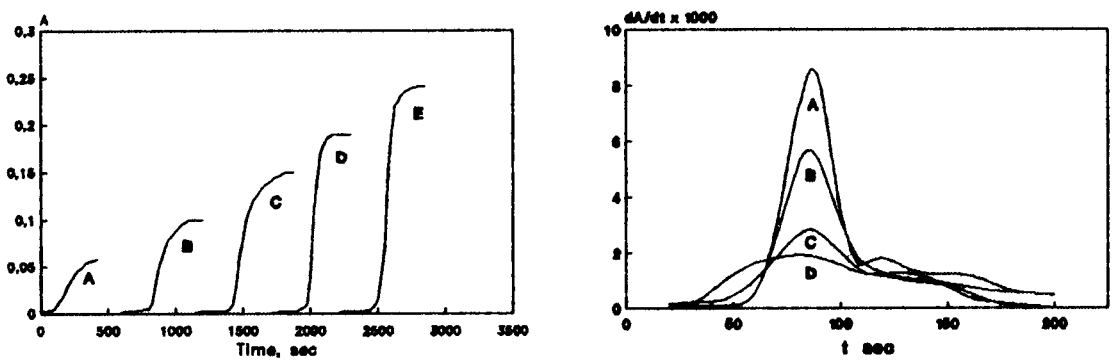

Fig. 4. Analytical recording. Left: Absorbance increment. (A) blank; (B) 1.6 ng Sn; (C) 4.7 ng Sn; (D) 9.2 ng Sn; (E) 13.8 ng Sn. Right: first-order derivative signal. (A) 25 ng Sn; (B) 12.5 ng Sn; (C) 6.25 ng Sn; (D) blank. Sample volume, 781 μl; cell length, 1.5 mm; solid support, Sephadex QAE A-25.

ml^{-1} of tin and the relative standard deviation (R.S.D.) was 2.5 and 6.5%, respectively using ΔA as the signal. One of the main contributions to the R.S.D. is the variability of the signal background, the R.S.D. for the blank signal being ca. 2.5% under the conditions stated under the *Basic procedure*.

The detection limit, using the IUPAC definition, was calculated from the R.S.D. of the background absorbance, and values of 0.4 and 0.3 ng ml^{-1} were obtained for the ΔA and h signals, respectively.

The use of tangent measurements as an analytical parameter provides a higher correlation coefficient whereas the R.S.D. values obtained are better using ΔA increase signals.

The sampling frequency is 7.2 h^{-1}, as is usual in methods that require a desorption step.

The effect of co-existing ions on the determination of 10 ng of tin was studied to define the tolerance (amount of foreign species that produced an error not exceeding ±5% in the determination of tin). The tolerance values obtained were as follows: Cl^-, NO_3^-, 1.4 mg; Ca(II), Sr(II), Mg(II), 140 μg; Fe(III), 14 μg in the presence of 1 μg of F^-; tartrate, 7.8 μg; oxalate, 6.9 μg; PO_4^{3-}, 1.4 μg; F^-, 1 μg; citrate, 160 ng; Zr, 30 ng; and Mo(VI) and W(VI), 5 ng.

3.4. Application to real samples

The proposed method was used as a test to determine tin(IV) in fruit juice samples presumed to present a variety of concentrations related to the remaining commercial storage life, i.e., to the recommended shelf time as indicated by the "best before ..." statement in order to check the applicability of the method.

Table 1
Analytical features of the flow-injection method

Parameter	ΔA method	Derivative signal method (h, absorbance s^{-1})
Intercept	0.022	−0.0033
Slope	0.0083	0.0026
Linear range (ng ml^{-1})	2–40	1–40
Correlation coefficient	0.998	0.999
Detection limit (ng ml^{-1})	0.4	0.3
R.S.D. (%)	2.5	4.1
Sampling frequency (h^{-1})	7.2	7.2

Table 2
Results found in the evaluation of tin in canned fruit juices

Fruit juice	Tin(IV) found (mg kg^{-1}) [a]		Difference (%)
	Proposed method	Reference method	
Juice 1	260.2	263.0	−1.14
Juice 2	724.4	724.0	0.05
Juice 3	908.6	941.0	−3.44

[a] Average value of four samples for each juice.

When the solid pulp usually present in fruit juices was filtered off and the tin contained in the remaining liquid was determined by the proposed method directly, the amounts found were very low with respect to the total tin contents found when the procedures described here (pulp destruction with acids) were used. Presumably this was because tin was fixed on the solid matter in the former instance. However, pretreatment of the samples as stated above yielded results comparable to those obtained using atomic absorption spectrometry (AAS) as a reference method (Table 2).

To check the accuracy of the proposed method, a recovery study was carried out on various commercial brands of steel-canned fruit juices. They were analysed after adequate additions of tin to establish the effects on tin total recovery in fruit juices canned at different times. Table 3 gives the average recoveries (means of three determinations) and the results are considered to be acceptable.

4. Conclusions

The proposed method shows the feasibility of an automatic continuous analysis based on integrated separation and spectrophotometric detection of tin. There are several advantages over the batch resin phase method [14]. The proposed method is faster and simpler because no isolation

Table 3
Study of tin(IV) recovery in fruit juices

Fruit juice	Added (ng ml^{-1})	Found (ng ml^{-1})	Recovery (%)
Juice 1	0	20.8	
	4	25.1	101.4
	8	29.4	103.1
	12	32.0	96.2
Juice 2	0	14.5	
	4	18.4	99.6
	8	22.3	101.5
	12	26.9	102.6
Juice 3	0	18.3	
	6	25.6	107.1
	10	28.4	100.5
	16	34.3	100.0

of the ion exchanger from samples is required, there are no equilibration steps, the resin or gel is always packed into the cell, a measurement at only one wavelength is needed and not at two wavelengths as is usual in solid-phase spectrophotometric methods and smaller amounts of sample and reagent are required (up to 70 times less). The sensitivity is much higher, as demonstrated by the fact that although the sensitivity levels for this method and for the batch method are alike (see Table 1 and [14]), the sample volume used here (0.750 ml) is much smaller than in the batch method (500–3000 ml), and the method is cheaper because there is no need for disposal of the resin after each determination as in the batch method and smaller amounts of reagents are required.

Regarding the more classical solution methods [15,16], for tin apparent molar absorptivities up to three orders of magnitude higher are found when ion-exchange gels are used in the batch method [14], as found again in the automatic continuous method in this work.

Acknowledgements

This study was funded by the Dirección General de Investigación Cientifica y Técnica (DGICYT) del Ministerio de Educación y Ciencia (Spain) (Project No. PS88-0101).

References

[1] M. Valcarcel and M.D. Luque de Castro, Analyst, 115 (1990) 699.
[2] F. Lazaro, M.D. Luque de Castro and M. Valcarcel, Anal. Chim. Acta, 214 (1989) 217.
[3] K. Yoshimura, Analyst, 113 (1988) 471.
[4] K. Yoshimura, S. Matsuoka and H. Waki, Anal. Chim. Acta, 225 (1989) 313.
[5] F. Lazaro, M.D. Luque de Castro and M. Valcarcel, Anal. Chim. Acta, 219 (1989) 231.
[6] K. Yoshimura, S. Nawata and G. Kura, Analyst, 115 (1990) 843.
[7] K. Yoshimura and U. Hase, Analyst, 116 (1991) 835.
[8] K. Yoshimura, Bunseki Kagaku, 36 (1987) 656.
[9] K. Yoshimura, S. Matsuoka, T. Tabuchi and H. Waki, Analyst, 117 (1992) 189.
[10] K. Yoshimura and S. Yamada, Talanta, 39 (1992) 1019.
[11] K. Yoshimura, Anal. Chem., 59 (1987) 2922.
[12] K. Yoshimura and H. Waki, Talanta, 32 (1985) 345.
[13] B. Fernandez-Band, F. Lazaro, M.D. Luque de Castro and M. Valcarcel, Anal. Chim. Acta, 229 (1990) 177.
[14] M.C. Valencia, D. Gimeno and L.F. Capitan-Vallvey, Anal. Lett., 26 (1993) 1211.
[15] W.J. Ross and J.C. White, Anal. Chem., 33 (1961) 421.
[16] R.M. Dagnall, T.S. West and P. Young, Analyst, 92 (1967) 27.

ELSEVIER

Analytica Chimica Acta 289 (1994) 371–380

ANALYTICA CHIMICA ACTA

Orthogonal array designs for the optimization of liquid chromatographic analysis of pesticides

Hai Bin Wan, Wei Guang Lan, Ming Keong Wong *, Chup Yew Mok

Department of Chemistry, National University of Singapore, Lower Kent Ridge Road, 0511 Singapore

(Received 31st August 1993; revised manuscript received 22nd November 1993)

Abstract

Orthogonal array designs were applied to the optimization of liquid chromatographic analysis of pesticides used in golf courses. Three variables related to the composition of the mobile phase were studied: the percentage of acetonitrile, percentage of methanol, and the buffer pH. In the first experiment, each variable was tested at three levels using an OA_9 (3^4) matrix, in which the interactions between the parameters were temporarily neglected. Based on the results of the first experiment, the second experiment was carried out following a two-level orthogonal array design with an OA_8 (2^7) matrix, in which more exact levels for each variable were chosen, and the interaction effects were considered separately. Finally, the optimum conditions for liquid chromatographic analysis of the pesticides were proposed. The advantages and the disadvantages of three-level and two-level orthogonal array designs were discussed.

Key words: Liquid chromatography; Orthogonal array design; Pesticides; Waters

1. Introduction

A liquid chromatographic (LC) method for determining more than 30 pesticides is required as part of a project aimed at developing an efficient method for analysing these pesticides in water samples. The pesticides, which are used in golf courses, include insecticides, fungicides and herbicides. The method will involve solid-phase extraction for sample preparation, liquid chromatographic screening and determination, and further confirmation by gas chromatography or liquid chromatography with different columns.

Optimization is an important step in developing liquid chromatographic methods. Two general systematic optimization procedures are the simultaneous and sequential methods [1]. In sequential methods (e.g. simplex optimization) the response surface is sequentially tracked until an optimum has been located, which is not, however, a priori a global optimum [2]. Other disadvantages of sequential methods are slow convergence on complex response surface and difficulty in dealing with response surface with high dimensionality. The methods may be suitable as a means for fine-tuning of a separation [3]. On the other hand, the simultaneous optimization methods, such as mixture designs [4] and factorial designs [5,6], do not suffer from these problems. The

* Corresponding author.

SSDI 0003-2670(93)E0658-T

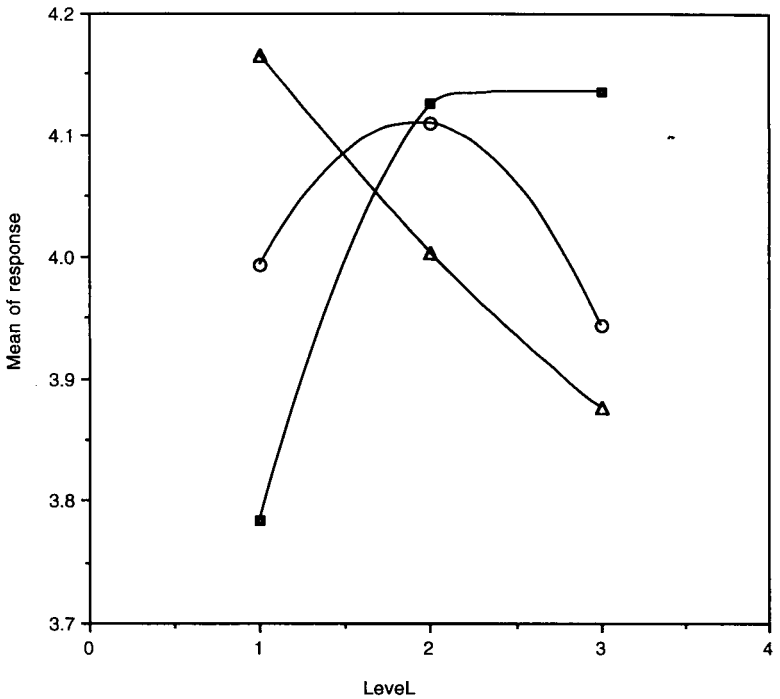

Fig. 1. Effects of the variables on the responses (IC). ■ = Acetonitrile (50, 40 and 30%); △ = methanol (5,10 and 15%); ○ = buffer pH (5.2, 3.0 and 2.0).

experiments to be carried out are previously planned. The experimental results are collected, and then the optimum can be located by constructing a response surface [7] or by retention mapping [8]. Mixture designs are useful for experiments where the response depends on the proportions of ingredients in a mixture rather than on their amounts, while factorial designs can also deal with other variables. One obvious disadvantage of the factorial designs is that the number of experimental trials required increases geometrically with increasing number of variables. Thus the number of experimental trials expands so rapidly that it is not feasible to implement these trials. Fortunately, this can be minimized by the use of fractional factorial experiments, such as Plackett-Burman schemes [9–11] or orthogonal array (OA) designs [6,12–16]. The latter methods have an advantage over the former in that three-level designs can be used, so as to extract more precise information than that obtained from the two-level designs [15].

In orthogonal array designs, orthogonal arrays are used to assign factors to a series of experiment combinations whose results can then be analyzed by using a common mathematical procedure. The main effects of the factors and preselected interactions are independently extracted. In an orthogonal array, different combinations of numerals of any two columns have equal appearance frequency. Here orthogonal means balanced. By arranging experiments orthogonally, different effects can be separated. For two-level design, the orthogonal array matrix is mathematically identical to the conventional factorial matrix with the same experimental trials except that the interceptions between the columns and the rows are rearranged, e.g. OA_8 (2^7) matrix corresponds to the 2^3 factorial matrix. As for three-level design, OA_9 (3^4) theoretically corresponds to the 3^2 factorials. Although three-level factorials have been described in detail, no three-level conventional factorial matrix has been constructed, whereas a three-level orthogonal array matrix is

available. Experiments can be arranged orthogonally also by using conventional factorial designs. However, in orthogonal array design, by using the associated triangular table, the variables and the interactions between the variables are easily assigned and quantitatively estimated [17]. This advantage is more significant when more complicated experiments are designed.

In the present study, orthogonal array designs were used to optimize the LC analysis conditions. The effects of the mobile phase composition and the buffer pH on the separation of over 30 pesticides was initially studied by a three-level orthogonal array design with an OA_9 (3^4) matrix without considering the interactions between the parameters. Based on the first experiment, more exact levels of the parameters were then chosen, and the second experiment was carried out following a two-level orthogonal array design with a OA_8 (2^7) matrix, in which the interaction effects were considered. Finally, the optimum conditions for LC analysis of the pesticides were proposed.

Most of the studies on the optimization of analytical procedures which used fractional factorial designs, such as Plackett-Burman schemes, adopted two-level designs only. An exception is the work by Jones [18] who used three-level designs. However, it has been proven that this design can lead to wrong conclusions about the influences of the different factors, due to the construction of the design [19]. For two-level designs, great care is required in setting the two levels for each factor. As for 3-level designs, however, selection of levels is much easier, the tendency of change of the responses is clearer, and it is less likely to obtain misleading results. Therefore a three-level design gives more detailed information on how the response function will be affected by the change of the variables. However, when the interactions between the variables are considered, an OA_9 (3^4) matrix can only accommodate two variables, the other two columns are occupied by the interaction between the two variables. Although this problem can be solved by using a larger orthogonal array design, for instance using an OA_{27} (3^{13}) matrix, much more experimental work is required (27 trials are needed). For this reason, it is advisable to find out the relation between the response function and the variables first by using a three-level orthogonal array design and temporarily neglecting the interactions between the variables. Based on the results of the three-level experiment, new levels of the variables can be chosen and the second experiment which follows two-level orthogonal array designs can then be carried out, in which the interaction effects are considered separately. In a two-level orthogonal array design, one interaction occupies only one column of the matrix. Hence, some two-level orthogonal array designs, such as OA_8 (2^7) and OA_{16} (2^{15}), can accommodate more factors with less trials than three-level orthogonal array designs.

2. Experimental

2.1. Reagents and apparatus

All pesticides used were analytical standards supplied by Supelco. They were dissolved in methanol at 1 mg ml^{-1} concentration as stock solutions. A mixed solution containing 20 μg of each pesticide per ml of methanol was prepared from the stock solutions and was used as working solution. HPLC-grade acetonitrile, HPLC-grade methanol, and buffer solution were used to prepare the mobile phase. Buffer solutions were prepared by dissolving 0.65 g diammonium hydro-

Table 1
Assignment of the factors and levels of the first experiment by using an OA_9 (3^4) matrix along with the results of the effects of selected variables on the responses

Trial No.	Column No. [a]				Response	
	1	2	3	4	n.d.p.	IC
1	50	5	5.2		24	4.014
2	50	10	3.0		20	3.757
3	50	15	2.0		19	3.582
4	40	5	3.0		30	4.377
5	40	10	2.0		30	4.144
6	40	15	5.2		21	3.854
7	30	5	2.0		29	4.106
8	30	10	5.2		24	4.111
9	30	15	3.0		27	4.192

[a] 1 = Percentage of acetonitrile; 2 = percentage of methanol; 3 = buffer pH; 4 = unassigned.

Table 2
The assignment of factors and levels of the second experiment using an OA_8 (2^7) matrix along with the results of the effects of selected variables on the responses

Trial No.	Column No. [a]							Response	
	1	2	3	4	5	6	7	n.d.p.	IC
	A	*B*	*A* × *B*	*C*	*A* × *C*	*B* × *C*	#		
1	42	5		2.6				29	4.126
2	42	5		5.4				28	4.140
3	42	0		2.6				33	4.528
4	42	0		5.4				30	4.526
5	48	5		2.6				26	4.104
6	48	5		5.4				27	4.018
7	48	0		2.6				31	4.218
8	48	0		5.4				30	4.203

[a] *A* = Percentage of acetonitrile; *B* = percentage of methanol; *C* = buffer pH; # = unassigned column; *A* × *B*, *A* × *C* and *B* × *C* = interaction between factor *A* and *B*, *A* and *C*, and between *B* and *C*.

genphosphate in 1 l deionized water, followed by adding phosphoric acid to adjust the pH. A Shimadzu LC-6A chromatograph equipped with a UV–visible spectrophotometric detector was used for the analysis. The wavelength of the detector was set at 215 nm. The flow rate of the mobile phase was set at 1.4 ml min^{-1}. A Supelco LC-ABZ column (25 cm × 4.6 mm i.d.) was used for the isolation. It is a silica-based reversed-phased column with amino groups, and is suitable for analysis of acidic, basic and neutral compounds. The column has a plate number of 9000 to 11 000.

2.2. Optimization strategy

As it is very difficult to analyze over 30 compounds simultaneously on one LC column, the study was designed to find an analytical condition which provides the best isolation of the pesticides. Then, half of the compounds which gave

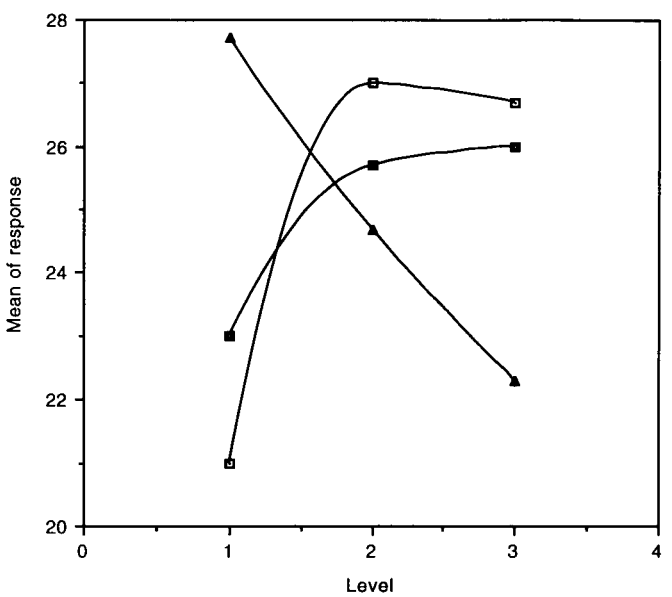

Fig. 2. Effects of the variables on the response (n.d.p.). □ = Acetonitrile; ▲ methanol; ■ = pH.

overlapping peaks were selected to form another group. In the later experiments for studying the efficiency of the solid phase extraction these two groups of pesticides will be studied separately. This approach will be more efficient than separating the compounds into two groups first and then optimizing the separation of each group. The latter approach will require twice as much experimental work as the former. Besides, when the retention behaviour of these compounds is not clear, the arrangement of the membership of the compounds in the two groups are mainly random. It is quite possible that compounds with very similar retention times are put in the same group, making the optimization of separation more difficult.

In the present study, a response function based on information theory was chosen to judge the quality of the chromatograms [14]. If a mixture of n components is chromatographed and the resulting chromatogram is composed of k_1 singlets, k_2 doublets and K_p p-multiplets with $\Sigma(pk_p) = n$, the contribution of the p-multiplets to the quantity of information is given by

$$I_p = (pk_p/n) \log_2(np)$$

where pk_p/n is the appearance frequency and $\log_2(n/p)$ is the quantity of specific information brought by the identification of a component in a p-multiplet. The total information from the chromatogram is the sum of the individual contributions (IC) of each peak groups:

$$\mathrm{IC} = \Sigma(pk_p/n) \log_2(n/p)$$

The value of IC varies between zero, all the peaks together ($p = n$, $k_p = 1$), and $\log_2(n)$, all the peaks separated ($p = 1$, $k_p = n$).

In addition to IC, the number of distinguishable peaks (n.d.p.) was also used as the response function. A distinguishable peak means that the top of the peak is not covered by other peaks. The advantage of using n.d.p. as the response function is that only one run is needed for each trial. The peak tracking work can be carried out after the optimum condition has been found. One unit increase of n.d.p. indicates that a totally overlapping doublet or triplet peak is at least partly separated because of the change of the variables. This is more important than the improvement in resolution of two already partly separated peaks as far as the purpose of the present study is concerned. Partly separated compounds can be analyzed by putting them in different groups. But, if more than two compounds have similar retention times, a third group is needed or one of the compounds has to be omitted. However, this response has never been used before by other chromatographers. It is certainly not suitable for sequential optimization, because it is not continuous. Besides, unlike IC which considers all the components to be separated, n.d.p. considers only completely overlapping peaks. Therefore when the number of completely overlapping peaks is small, the use of n.d.p. as a response can give very biased results. In the present case, as the number of completely overlapping peaks could be relatively large due to the large number of the components to be separated, n.d.p. may be able to reflect the quality of the chromatograms. Considering the convenience of using n.d.p. as a response and the uncertainty as a suitable response, a comparison between the two responses was made.

Three variables related to the mobile phase were tested: the percentage of acetonitrile, the percentage of methanol, and the pH of the buffer. The choice of the three variables was based on the knowledge that acetonitrile is the most suitable solvent for a LC-ABZ column, pH may affect the retention behaviour of some compounds on this column, and a small amount of methanol (ca. 10%) may improve the peak shape of some pesticides. In the first experiment, each variable was tested at three levels and the interaction effects between the variables were temporarily neglected. The selection of the experiment space was based on the previous information from liquid chromatography, so that the space is broad enough to include the possible optimum and not so broad as to cause inconvenience in experiment. For the variables of acetonitrile and methanol, the three levels were evenly distributed in the experiment space. In the case of buffer pH, the second level is set at 3 rather than 3.6. This is because some of the compounds are acidic. Our experience with other reversed-phased columns suggests that the buffer pH should be < 3 to

Table 3
ANOVA table for the second experiment by using OA_8 (2^7) matrix with IC as the response

Source of variance	Sum of square $\times 10^2$	Degree of freedom	Mean square $\times 10^2$	F value	Significance [a]
Acetonitrile (A)	7.53	1	7.53	77.6	$P < 0.01$
Methanol (B)	14.8	1	14.8	153	$P < 0.01$
$A \times B$	2.98	1	2.98	30.7	$P < 0.025$
Pooled error [b]	0.390	4	0.0975		
Total	25.7	7			

[a] The critical F value is 74.1 at 99% confidence and 12.2 at 97.5% confidence. [b] Pooled error results from pooling insignificant effects of $A \times C$, $B \times C$, C and the unassigned column effect.

prevent protolysis of the compounds and to obtain satisfactory separation and peak shapes. By setting the levels closer to the possible optimum, more accurate information may be obtained. The assignment of the factors and the levels in this design are shown in Table 1. Based on the results of the first experiment, the second experiment was then carried out by using a two-level orthogonal array design with an OA_8 (2^7) matrix, in which more exact levels of the variables were chosen (shown in Table 2) and the interaction effects between the variables were separately considered. The assignment of the variables and their interactions in the OA_8 (2^7) matrix followed the triangular table corresponding to this matrix (also shown in Table 2) [16]. The first experiment corresponds to a 3^{3-1} fractional factorial design and the second experiment is a 2^3 factorial design.

3. Results and discussion

The results of the first experiment are given in Table 1. Two graphs describing the relationship

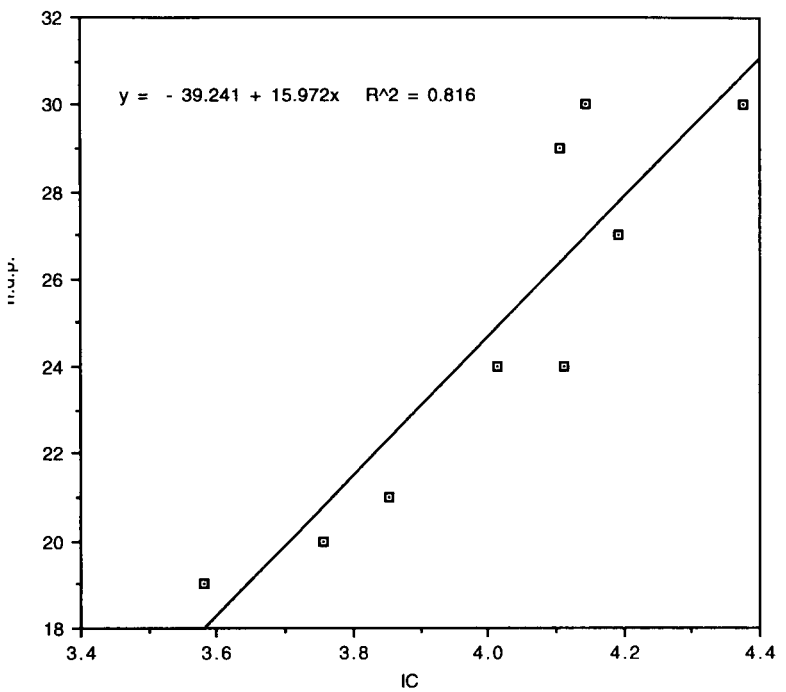

Fig. 3. Relationships between the two responses in the first experiment.

Table 4
ANOVA table for the second experiment by using OA_8 (2^7) matrix with n.d.p. as the response

Source of variance	Sum of square	Degree of freedom	Mean square	F value	Significance [a]
Acetonitrile (A)	4.5	1	4.5	18.0	$P < 0.1$
Methanol (B)	24.5	1	24.5	98.0	$P < 0.05$
pH (C)	2.0	1	2.0	8.0	$P > 0.1$
$A \times C$	2.0	1	2.0	8.0	$P > 0.1$
$B \times C$	2.0	1	2.0	8.0	$P > 0.1$
Pooled error [b]	0.5	2	0.25		
Total	35.5	7			

[a] The critical F value is 8.5 at 90% confidence, and 18.5 at 95% confidence. [b] Pooled error results from pooling insignificant effect ($A \times B$) and unassigned column effect.

between the two responses (IC and n.d.p.) and the tested variables are obtained by plotting the variable levels against the means of the responses at various levels (Figs. 1 and 2). The two graphs show very similar relationships between the responses and acetonitrile and between the responses and methanol. A difference in relationship between the responses and the buffer pH was observed with different responses. The use of the two different responses did produce similar conclusions: the separation will improve considerably when acetonitrile in the mobile phase is decreased from 50 to 40% and further decrease of acetonitrile has little effect on the responses; the separation will be improved with decreased methanol percentage; the buffer pH has much less effect on the response than other two variables and a pH of ca. 3 may be suitable. However, the analysis of variance (ANOVA) results of this experiment indicate that all the three variables

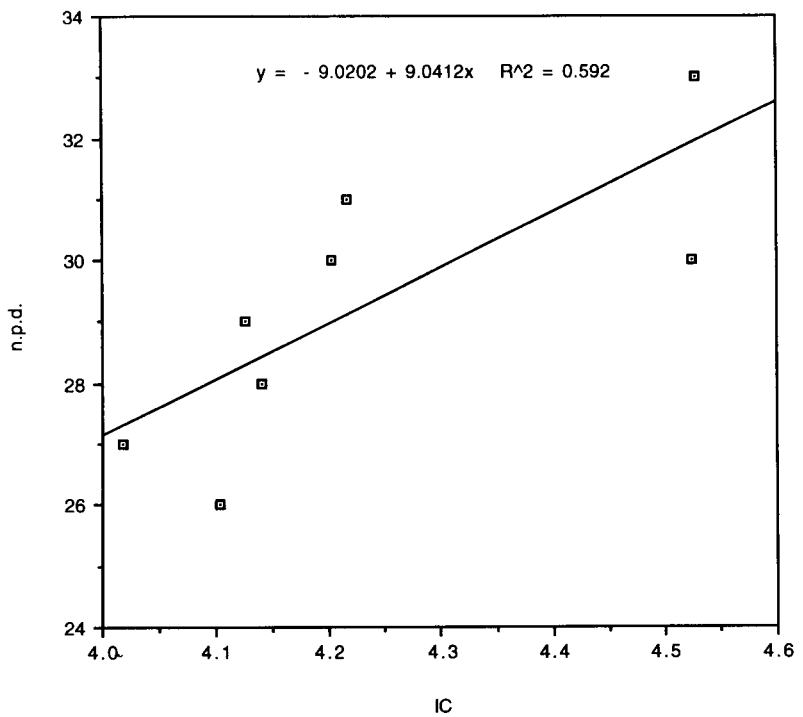

Fig. 4. Relationship between the two responses in the second experiment.

have no significant effects on both of the responses. In this experiment, the interactions between the variables were not considered. It is quite possible that the interaction effects were included in column 4 which was used to estimate the error, resulting in smaller F values for the effects of the variables. In other words, the significance of the effects of the variables were masked by their interaction effects.

The results of the second experiment are shown in Table 2. When IC is used as the response, the ANOVA results indicate that at 97.5% confidence level there is significant interaction between acetonitrile and methanol ($A \times B$) (Table 3). When the interaction effects are considered separately, the effects of acetonitrile and methanol become significant as well. These results support the explanation given to the first experiment. The ANOVA results also show that buffer pH has no significant effect on the response within the experiment space. When n.d.p. is used as the response, the ANOVA results also

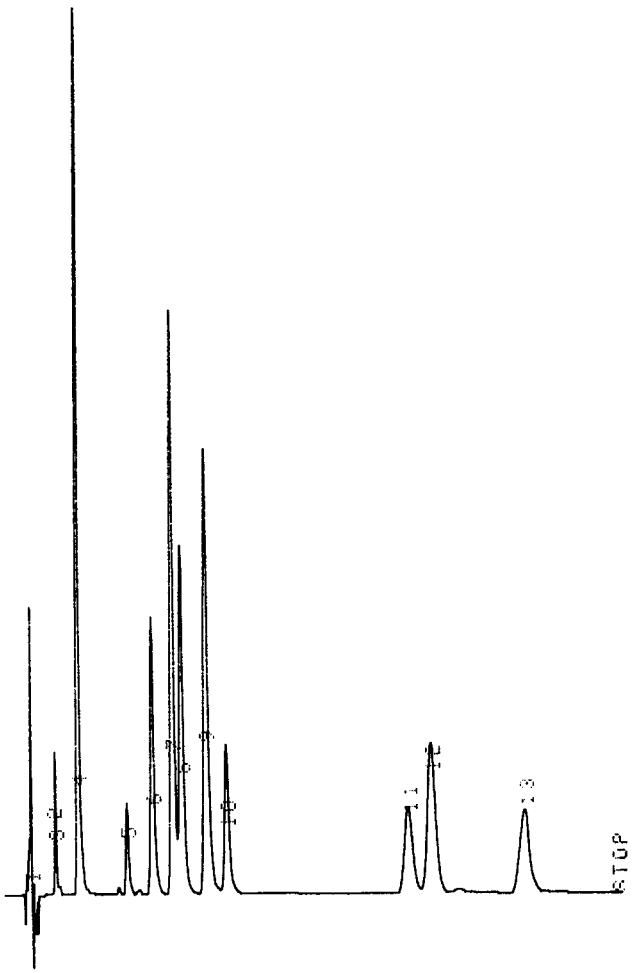

Fig. 5. Chromatogram of pesticides obtained under the optimum analytical conditions (acetonitrile + pH 2.6 buffer, 45:55; flow rate 1.4 ml min^{-1}). 2 = Dichlorvos (3.8 min), 4 = Thiram (5.5 min), 5 = Captan (9.2 min), 6 = Pyridalphenthion (11.1 min), 7 = Chloroneb (12.6 min), 8 = Pronamide (13.3 min), 9 = Chlorothalonil (15.2 min), 10 = Etridiazole (16.7 min), 11 = Bensulfite (30.3 min), 12 = Tolclofos (32.0 min), 13 = Isoxathion (39.2 min).

identify acetonitrile and methanol as significant factors, but fail to identify the interaction between acetonitrile and methanol (Table 4). It is also observed that the buffer pH has more effect although the it is not significant. However, the optimum conditions proposed according to the two responses are the same: acetonitrile at 42%, methanol at 0%, and the buffer pH at any value between 2.6 and 5.4. In the later experiments, the buffer pH was set at 2.6 because its effect was nearly significant when n.d.p. was used as the response.

Two graphs showing the correlation between two sets of the results obtained by using different responses indicate that the correlation is much more significant in the first experiment ($r = 0.903$, $n = 8$) than in the second ($r = 0.769$, $n = 7$) (Figs. 3 and 4). Fig. 3 also shows that the difference of the two sets of results becomes greater when the number of completely overlapping peaks becomes

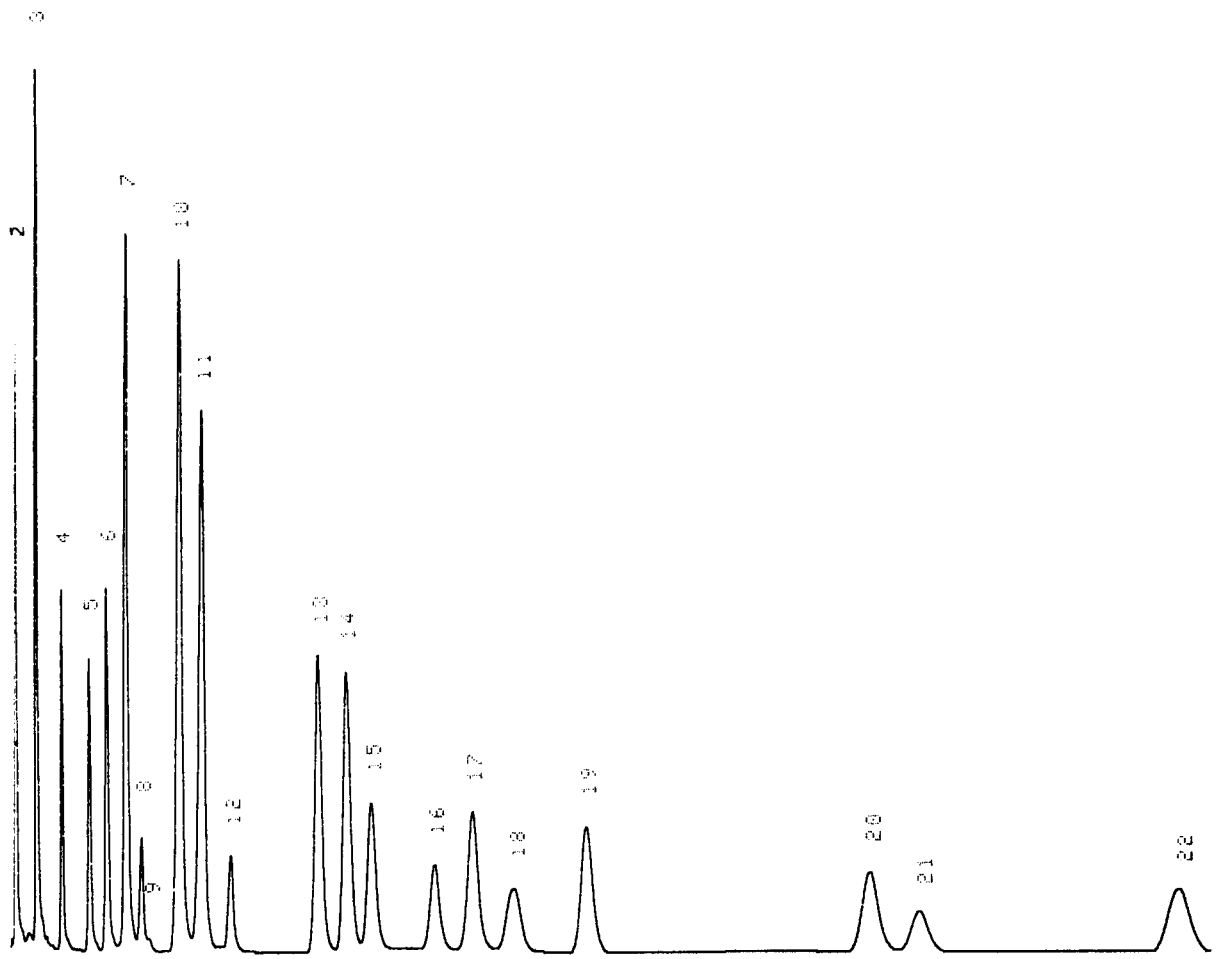

Fig. 6. Chromatogram of pesticides obtained under the optimum analytical conditions. 2 = Asulan (2.6 min), 3 = Simazine (4.2 min), 4 = Isoprocarb (6.2 min), 5 = Fenobucarb (8.5 min), 6 = Methyldymiron (9.9 min), 7 = Devrino (11.4 min), 8 = Isoprothiolane (12.6), 10 = Mepronil (15.4 min), 11 = Flutolanil (17.1 min), 12 = Diazinon (19.4 min), 13 = Thiobencarb (26.0 min), 14 = Aprodione (28.1 min), 15 = Terbutol (30.0 min), 16 = Isofenphos (34.7 min), 17 = Pencycuron (37.6 min), 18 = Butamifos (40.7 min), 19 = EPN (46.2 min), 20 = Prowl (67.5 min), 21 = Dursban (71.2 min), 22 = Balan (90.7 min).

smaller. The worse correlation in the second experiment is understandable, as this experiment is conducted within a region much closer to the optimum and thus the completely overlapping peaks are very few. It could be an efficient approach in separation optimization of relatively large number of components by factorial design to use n.d.p. as the response in the initial experiment for locating more exact experiment region. In the subsequent experiments which are within a region closer to the optimum, IC or other more suitable responses may be used. By this way, time spent in peaktracking could be considerably reduced.

Eleven pesticides which formed overlapping peaks under the optimum conditions were picked out to form another group. Two pesticides which could not be fitted in either of the two groups were omitted. The two groups of pesticides were chromatographed separately. Two chromatograms with all the compounds fully separated from each other were obtained. Later, when dealing with the two groups of pesticides, the ratio of acetonitrile was increased to 45% to reduce the analysis time. The chromatograms are shown in Figs. 5 and 6.

Acknowledgement

Hai Bin Wan and Wei Guang Lan wish to thank the National University of Singapore for the award of research scholarships.

References

[1] J. Wieling, H. Dijkstra, C.K. Mensink, J.H.G. Jonkman, P.M.J. Coenegracht, C.A.A. Duineveld and D.A. Doornbos, J. Chromatogr., 629 (1993) 181.
[2] J.C. Berridge, J. Chromatogr., 485 (1989) 3.
[3] S.N. Deming, J.M. Palasota, J. Lee and L. Sun, J. Chromatogr., 485 (1989) 15.
[4] P.M.J. Coenegracht, A.K. Smilde, H.J. Metting and D.A. Doornbos, J. Chromatogr., 485 (1989) 195.
[5] Y. Hu and D.L. Massart, J. Chromatogr., 485 (1989) 311.
[6] P.J. Oles, J. Assoc. Off. Anal. Chem., 76 (1993) 615.
[7] E. Morgan, K.W. Burton and P.A. Church, Chemom. Intell. Lab. Syst., 5 (1989) 283.
[8] J.L. Glajch and J.J. Kirkland, J. Chromatogr., 485 (1989) 51.
[9] J. Vindevogel and P. Sandra, Anal. Chem., 63 (1991) 1530.
[10] M. Mulholland and J. Waterhouse, Chromatographia, 25 (1988) 769.
[11] K. Jones, J. Chromatogr., 392 (1987) 1.
[12] P. Oles, G. Gates, S. Kensinger, J. Patchell, D. Schumacher, T. Showers and A. Silcox, J. Assoc. Off. Anal. Chem., 73 (1990) 724.
[13] P. Oles and A. Yankovich, LC–GC, 7 (1989) 579.
[14] P. Billot and B. Pitard, J. Chromatogr., 623 (1992) 305.
[15] W.G. Lan, M.K. Wong and Y.M. Sin, submitted for publication.
[16] G. Taguchi, System of Experimental Design, Vols. 1–2, Kraus, New York, 1987.
[17] Y. Wu, Taguchi Method: Selected Papers on Methodology and Applications, ASI Press, Dearborn, MI, 1988, pp. 191–201.
[18] K. Jones, J. Chromatogr., 392 (1987) 17.
[19] Y.V. Heyden, M.S. Khots and D.L. Massart, Anal. Chim. Acta, 27 (1993) 189.

ANALYTICA CHIMICA ACTA

An international journal devoted to all branches of Analytical Chemistry

Analytica Chimica Acta publishes original papers, rapid publication Letters and reviews dealing with every aspect of modern analytical chemistry.

Reviews are normally written by invitation of the editors, who welcome suggestions for subjects. Letters can be published within **four months** of submission. **For information on the Letters section, see p. 384.**

A special section of *Analytica Chimica Acta* is *Vibrational Spectroscopy*. Vibrational Spectroscopy publishes similar contributions dealing with infra-red, near infra-red and Raman spectroscopy.

A free reprint of detailed *Instructions to Authors* for *Vibrational Spectroscopy* can be obtained by application to the publisher.

Submission of papers

Authors should submit three copies of the manuscript in clear, double-spaced typing on one side of the paper only. Manuscripts should be sent to the appropriate editor at the address given below. Submission of a manuscript implies that the work described has not been, and will not be, published elsewhere (except as an abstract, or as part of a lecture, review or academic thesis). After acceptance of the manuscript, the author(s) will be asked to transfer the copyright of the article to the publisher, to ensure the widest possible dissemination of information.

The language of the journal is English.

Preparation of manuscripts

Authors are given every latitude, consistent with clarity and brevity, in the style and form of their papers.

Title and initial layout. All manuscripts should be headed by a concise but informative title followed by the names of the authors and the address of the laboratory where the work was carried out. The author to whom correspondence should be addressed must be indicated by an asterisk.

Abstract. All papers, reviews and Letter articles begin with an Abstract (50–250 words) which should comprise a factual account of the contents of the paper, with emphasis on new information.

Experimental. The experimental methods may be described after the introductory material, or after the discussion of results. Detailed experimental descriptions should be restricted to one section of the paper. Sufficient detail should be given to allow any experienced worker to implement the procedures described. Procedural steps should not be numbered.

Results and discussion. These may be treated together or separately.

Acknowledgements. These should be kept as short as possible.

References

The references should be collected at the end of the paper, numbered in the order of their appearance in the text (*not* alphabetically) and typed on a separate sheet. Titles of papers should not be given, but all authors should be named. References given in tables should be numbered according to the position of the table in the text. Every reference listed must be cited in the text. Reference numbers in the text are set in square brackets on the line.

In the list of references, the following forms should be adopted:

[1] R.D. Lowe and R.D. Snook, Anal. Chim. Acta, 250 (1991) 95.

[2] H. Grosjean and C. Houssier, in C.W. Gehrke and K.C.T. Kuo, Chromatography and Modification of Nucleosides, Part A (Journal of Chromatography Library, Vol. 45A), Elsevier, Amsterdam, 1990, p. A255.

Tables, computer programs and figures

Tables and figures should be essential for the clear and concise presentation of material. The same information should not be given in tables *and* figures.

Elsevier Science B.V., Desk Editorial Office Analytica Chimica Acta, P.O. Box 330, 1000 AH Amsterdam, Netherlands. Tel: +31 20 5862 791, Telefax: +31 20 5862 459, E-mail: chemistry@elsevier.nl. Office address: Sara Burgerhartstraat 25, 1055 KV, Amsterdam, Netherlands.

Tables. All tables should be numbered with Arabic numerals and have brief descriptive headings; they should be typed on separate pages. The layout should be given serious thought. Column headings should be brief, but should include the units in parentheses, where relevant.

Tables with only two or three headings are best printed horizontally, e.g.,

Hg^{2+} added (μg)	1.0	2.0	3.0	5.0
Extraction (%)	95.0	99.8	99.5	89.0

Footnotes to tables are denoted by superscript a, b, c... The following usage is recommended: e.g., if molar absorptivities are listed, the heading should be ϵ (10^4 l mol^{-1} cm^{-1}) so that a number 2.32 in the column signifies 23 200.

Alphanumeric computer output is usually unsuitable for reproduction and should therefore be retyped and presented as tables; capitals can be used to simulate computer output if such simulation is essential for illustration.

Computer programs. Algorithms should be described clearly and concisely by means of a suitable algorithmic notation, although a standard high-level programming language may also be used. Complete program listings are not normally admissible. Flow charts should be avoided in favour of a textual or tabulated description of the program or data flow. Statements on the portability of the software described to other computer systems, as well as on its availability to interested readers, should be given.

Figures. Figures should be suitable for direct reproduction and as rich in contrast as possible. One original (or sharp glossy print) and two photostat (or other) copies are required. Attention should be given to line thickness, lettering (which should be kept to a minimum) and spacing on axes of graphs, to ensure suitability for reduction in size on printing. Axes of a graph should be clearly labelled, along the axes, outside the graph itself.

The following standard symbols should be used in graphs:

▼ ▽ ■ □ + × ● ○ ▲ △

All figures should be numbered with Arabic numerals, and require descriptive legends which should be typed on a separate sheet of paper. Simple straight-line graphs are not acceptable, because they can readily be described in the text by means of an equation or a sentence. Claims of linearity should be supported by regression data that include slope, intercept, standard deviations of the slope and intercept, standard error and the number of data points; correlation coefficients are optional.

Photographs should be glossy prints and be as rich in contrast as possible; colour photographs cannot be accepted. Line diagrams are generally preferred to photographs of equipment.

Computer outputs for reproduction as figures must be good quality on blank paper, and should preferably be submitted as glossy prints.

Nomenclature, abbreviations and symbols

In general, the recommendations of the International Union of Pure and Applied Chemistry (IUPAC) should be followed, and attention should be given to the recommendations of the Analytical Chemistry Division in the journal *Pure and Applied Chemistry* (see also *IUPAC Compendium of Analytical Nomenclature, Definitive Rules*, 1987).

In accordance with IUPAC rules, ions should be expressed in the form PO_4^{3-} (*not* PO_4^{-3} or PO_4^{---}) and isotopes in the form ^{32}P (*not* P^{32} or P-32).

The Stock notation for the indication of stoichiometric oxidation stages (and indirectly the proportion of the constituents) should be used. Examples are iron(III) chloride rather than ferric chloride and potassium hexacyanoferrate(II) rather than potassium ferrocyanide.

Molarity (mol l^{-1} or M) and mg kg^{-1}, mg l^{-1}, μg kg^{-1}, μg l^{-1} etc. are the preferred concentration units, but ppm, ppb etc. will be accepted if defined on introduction.

Unusual abbreviations require definition when first used. Abbreviations for long chemical names (e.g., EDTA, HEDTA, en, Tris) are useful. Well known techniques must be abbreviated as capital letters without full stops, such as GC–MS, UV, AAS, ^{13}C NMR. Excessive use of abbreviations is not encouraged.

Greek letters and unusual symbols should be defined by name in the left-hand margin beside their first appearance in the paper. Wherever possible, mathematical expressions should be typed on one line, by using brackets, e.g., {[()]}, and the solidus, e.g., $A/b = x^{1/2}/(u + v)^{5/6}$.

Decimal points should be indicated by full stops in all papers. All decimal numbers smaller than unity should include a leading zero (e.g., 0.11).

Some basic SI units

metre	m	ampere	A
kilogram	kg	degree Kelvin	K
second	s	mole	mol

Some derived SI units

joule	J	$kg\ m^2\ s^{-2}$	farad	F	$A\ s\ V^{-1}$
newton	N	$J\ m^{-1}$	ohm	Ω	$V\ A^{-1}$
watt	W	$J\ s^{-1}$	henry	H	$V\ s\ A^{-1}$
coulomb	C	A s	hertz	Hz	s^{-1}
volt	V	$J\ A^{-1}\ s^{-1}$	degree Celsius	°C	K − 273.15

Some other units

litre	l	$10^{-3}\ m^3$	hour	h	3.6×10^3 s
gram	g	10^{-3} kg	dyne	dyn	10^{-5} N
poise	P	$kg\ m^{-1}\ s^{-1}$	atmosphere	atm	101.325 kN m^{-2}
electron volt	eV	1.6021×10^{-19} J	molar	M	mol l^{-1}
calorie	cal	4.184 J	molal	*m*	mol kg^{-1}
minute	min	60 s	curie	Ci	$3.7 \times 10^{10}\ s^{-1}$

Compuscripts: delivery of manuscripts on floppy disc

All accepted articles may now be submitted on computer disc. If you have questions while preparing a compuscript, please contact the *Analytica Chimica Acta* desk editorial office [P.O. Box 330, 1000 AH Amsterdam, The Netherlands, tel (+31-20)5862791, fax (+31-20)5862459] to obtain full instructions. The advantages of delivery of manuscripts on floppy disc are that no typographical errors will be introduced into the text during the typesetting phase and that production times will be reduced still further. The preferred storage medium is a $5\frac{1}{4}$ or $3\frac{1}{2}$ inch disc in MS-DOS or Macintosh format, although other systems are also welcome. Discs should be clearly labelled with your name, software & hardware used, and the name of the file.

Addresses for submission of papers

Americas

Prof. Harry L. Pardue
Department of Chemistry
1393 BRWN Bldg, Purdue University
West Lafayette, IN 47907-1393
USA

Tel:(+1-317) 494 5320
Fax:(+1-317) 496 1200

Computer Techniques

Prof. J.T. Clerc
Universität Bern
Pharmazeutisches Institut
Baltzerstrasse 5, CH-3012 Bern
Switzerland

Tel:(+41-31) 6314191
Fax:(+41-31) 6314198

Prof. Sarah C. Rutan
Department of Chemistry
Virginia Commonwealth University
P.O. Box 2006
Richmond, VA 23284-2006
USA
Tel:(+1-804) 367 1298
Fax:(+1-804) 367 7517

Other Papers

Prof. Alan Townshend
Department of Chemistry
The University
Hull HU6 7RX
Great Britain

Tel:(+44-482) 465027
Fax:(+44-482) 466410

Prof. Willem E. van der Linden
Laboratory for Chemical Analysis
Department of Chemical Technology
Twente University of Technology
P.O. Box 217, 7500 AE Enschede
The Netherlands
Tel:(+31-53) 892629
Fax:(+31-53) 356024

Prof. Paul Worsfold
Dept. of Environmental Sciences
University of Plymouth
Plymouth PL4 8AA
Great Britain

Tel:(+44-752) 233006
Fax:(+44-752) 233009

Rapid Publication Letters Section

Recently the introduction of a *Letters* section in *Analytica Chimica Acta* was announced. The *Letters* section will allow the analytical chemist to communicate rapidly short papers that describe innovative research. The section will be included in regular issues of the journal, which will appear approximately weekly. Submissions to the *Letters* section will be subjected to a strict quality control. The criteria for accepting letters are novelty, quality, significance, urgency and brevity. The editors invite analytical scientists to submit research results meeting the criteria mentioned above. The following publication procedure will apply for letters:

- A letter should occupy no more than *two printed pages*, i.e., an equivalent of 7200 characters including space for figures, tables, abstract and references.
- An abstract is *essential*, but should be short (e.g., 3 lines). Only the most significant experimental details, if any, should be given. Only key references should be added.
- To reduce publication time, proofs will not be sent to authors. Accordingly, it is critical for authors to check manuscripts carefully before submission.
- A letter should be submitted – preferably by FAX – to one of the editors (see addresses above). A disc with the text, and original figures should be sent to the same editor by separate mail. Submission on disc will facilitate the rapid publication process.
- The editor will have the letter reviewed: reviewers will be invited to recommend acceptance or rejection of the letter. No revision will be possible.
- After acceptance the letter will be published in the first available issue of the journal.
- If the guidelines are adhered to, the total publication time of a letter, from submission to publication, will not exceed 4 months.

ELSEVIER

Analytica Chimica Acta 289 (1994) 385–388

ANALYTICA CHIMICA ACTA

AUTHOR INDEX

Aebersold, B., see Eugster, R. 1
Ahmed, M.E., see Ahmed, Z.A. 329
Ahmed, Z.A.
—, Ahmed, M.E., Ibrahim, M.S., Kamal, M.M. and Temerk, Y.M.
Adsorption and association of 6-thiopurine and 6-thiopurine riboside at charged interfaces 329
Amez del Pozo, J.
—, Costa-García, A. and Tuñón-Blanco, P.
Novel mercury-coated carbon fibre voltammetric detector for use in adsorptive stripping flow analysis 169
Anzai, J.-i., see Hoshi, T. 321
Atkinson, G., see Inerowicz, H.D. 249

Bandow, H., see Zeng, Y. 195
Bell, S.E., see Davis, D.M. 263
Bianco, P., see Haladjian, J. 15
Bishop, P.L., see Ma, Y.L. 21
Branica, M., see Zelić, M. 299
Brinkman, U.A.Th., see De Boer, J. 261
Bruschi, M., see Haladjian, J. 15

Cabalín, L.M., see Laserna, J.J. 113
Calvo, N., see Laserna, J.J. 113
Cammann, K., see Wortberg, M. 177
Capitán-Vallvey, L.F.
—, Valencia, M.C. and Mirón, G.
Flow-injection method for the determination of tin in fruit juices using solid-phase spectrophotometry 365
Cardoso, S.V., see De Barros Alcanfôr, S.K. 273
Chandrasekhar, T.M., see Inerowicz, H.D. 249
Chen, J., see Zhao, X. 163
Chen, K., see Yao, S. 47
Cleven, R.
— and Fokkert, L.
Potentiometric stripping analysis of thallium in natural waters 215
Coche-Guérente, L.
—, Deronzier, A., Mailley, P. and Moutet, J.-C.
Electrochemical immobilization of glucose oxidase in poly(amphiphilic pyrrole) films and its application to the preparation of an amperometric glucose sensor 143
Costa-García, A., see Amez del Pozo, J. 169

Csapó, J.
—, Csapó-Kiss, Z., Folestad, S. and Tivesten, A.
Mercaptoethanesulphonic acid as a protecting and hydrolysing agent for the determination of the amino acid composition of proteins using an elevated temperature for protein hydrolysis 105
Csapó-Kiss, Z., see Csapó, J. 105

Dasgupta, P.K., see Liu, H. 347
Davis, D.M.
—, Harden, C.S., Shoff, D.B., Bell, S.E., Eiceman, G.A. and Ewing, R.G.
Analysis of ion mobility spectra for mixed vapors using Gaussian deconvolution 263
De Barros Alcanfôr, S.K.
—, Cardoso, S.V. and De Lima, C.G.
Fluorimetric studies of some quinones and quinonoid compounds after reduction reaction 273
De Boer, J.
— and Brinkman, U.A.Th.
TCDD equivalents of mono-*ortho* substituted chlorobiphenyls. Influence of analytical error and uncertainty of toxic equivalency factors 261
De Lima, C.G., see De Barros Alcanfôr, S.K. 273
Deronzier, A., see Coche-Guérente, L. 143

Eiceman, G.A., see Davis, D.M. 263
Engström, S., see Razumas, V. 155
Eugster, R.
—, Rosatzin, T., Rusterholz, B., Aebersold, B., Pedrazza, U., Rüegg, D., Schmid, A., Spichiger, U.E. and Simon, W.
Plasticizers for liquid polymeric membranes of ion-selective chemical sensors 1
Ewing, R.G., see Davis, D.M. 263

Fokkert, L., see Cleven, R. 215
Folestad, S., see Csapó, J. 105
Fukushima, M.
—, Taga, M. and Nakamura, H.
Interaction between humic acids and copper(II) oxinate 223

Galal, A., see Ma, Y.L. 21
Gao, Z., see Zhao, X. 163

Geng, Q., see He, F. 313
Georgiou, C.A., see Sideris, E.E. 87
Grasserbauer, M., see Lendl, B. 187
Gupta, A.R.L., see Murthy, A.S.N. 43

Hahn, M.
—, Liebau, A., Rüttinger, H.H. and Thamm, R.
Electrochemical investigation of chloramine T 35
Haladjian, J.
—, Bianco, P., Nunzi, F. and Bruschi, M.
A permselective-membrane electrode for the electrochemical study of redox proteins. Application to cytochrome c_{552} from *Thiobacillus ferrooxidans* 15
Haraguchi, H., see Hu, W. 231
Harden, C.S., see Davis, D.M. 263
Hart, R.J., see McDonald, I. 237
He, F.
—, Geng, Q., Zhu, W., Nie, L., Yao, S. and Meifeng, C.
Rapid detection of *Escherichia coli* using a separated electrode piezoelectric crystal sensor 313
Högfeldt, E.
Regular mixtures 259
Hoshi, T.
—, Anzai, J.-i. and Osa, T.
Electrochemical deposition of avidin on the surface of a platinum electrode for enzyme sensor applications 321
Hu, W.
— and Haraguchi, H.
Direct determination of sodium, potassium, magnesium, and calcium ions in human saliva by ion chromatography using a taurine-conjugated bile salt micelle-coated stationary phase 231
Huang, Z.F., see Ma, Y.L. 21
Hwang, C.-j.
— and Jiang, S.-J.
Determination of arsenic compounds in water samples by liquid chromatography–inductively coupled plasma mass spectrometry with an in situ nebulizer–hydride generator 205

Ibrahim, M.S., see Ahmed, Z.A. 329
Inerowicz, H.D.
—, Chandrasekhar, T.M., Atkinson, G. and White, R.L.
Comparison of structure-thermal property relationships for barium bis(1,1,1,5,5,5-hexafluoro-2,4-pentanedionate) polyether complexes 249

Jen, J.-F.
— and Yang, S.-M.
Simultaneous speciation determination of vanadium(IV) and vanadium(V) as EDTA complexes by liquid chromatography with UV detection 97
Jenkins, T.F.
—, Miyares, P.H., Myers, K.F., McCormick, E.F. and Strong, A.B.
Comparison of solid phase extraction with salting-out solvent extraction for preconcentration of nitroaromatic and nitramine explosives from water 69
Jiang, S.-J., see Hwang, C.-j. 205
Jin, W., see Zhao, X. 163

Kamal, M.M., see Ahmed, Z.A. 329
Kamo, N., see Kurosawa, S. 307
Kanapienienė, J., see Razumas, V. 155
Karube, I., see Mitsubayashi, K. 27
Katerkamp, A., see Wortberg, M. 177
Kojło, A., see Michałowski, J. 339
Koupparis, M.A., see Sideris, E.E. 87
Krause, J., see Wortberg, M. 177
Kurosawa, S.
—, Nemoto, E., Muratsugu, M., Yoshimoto, M., Mori, Y. and Kamo, N.
Detection of actomyosin depolymerization with a piezoelectric quartz crystal 307

Lan, W.G., see Wan, H.B. 371
Larsson, K., see Razumas, V. 155
Laserna, J.J.
—, Calvo, N. and Cabalín, L.M.
Imaging and space-resolved spectroscopy in the Xe–Cl laser ablation of noble metals with charge-coupled device detection 113
Lendl, B.
—, Ríos, A., Valcárcel, M. and Grasserbauer, M.
Automatic study of selectivity by the flow-rate gradient technique 187
Li, S.
— and Mottola, H.A.
Continuous-flow determination of relative diffusion coefficients of iron complexes with ligands of the 1,10-phenanthroline family and with 3-(2-pyridyl)-5,6-diphenyl-1,2,4-triazine in acetonitrile–water solutions 79
Li, Y.
— and Narusawa, Y.
Zone circulating flow-injection analysis: theory 355
Liebau, A., see Hahn, M. 35
Liu, H.
— and Dasgupta, P.K.
Dual-wavelength photometry with light emitting diodes. Compensation of refractive index and turbidity effects in flow-injection analysis 347
Lu, L., see Zhao, M. 121

Ma, Y.L.
—, Galal, A., Zimmer, H., Mark, Jr., H.B., Huang, Z.F. and Bishop, P.L.
Potentiometric selective determination of hydrogen sulfide by an electropolymerized membrane electrode based on binaphthyl-20-crown-6 21
Macheras, P.E., see Sideris, E.E. 87
Magnuszewska, B., see Michałowski, J. 339
Mailley, P., see Coche-Guérente, L. 143
Mark, Jr., H.B., see Ma, Y.L. 21
McCormick, E.F., see Jenkins, T.F. 69

McDonald, I.
—, Hart, R.J. and Tredoux, M.
Determination of the platinum-group elements in South African kimberlites by nickel sulphide fire-assay and neutron activation analysis 237
Meifeng, C., see He, F. 313
Michałowski, J.
—, Kojło, A., Magnuszewska, B. and Trojanowicz, M.
Flow-injection biamperometry of phenothiazine derivatives 339
Middendorf, C., see Wortberg, M. 177
Mirón, G., see Capitán-Vallvey, L.F. 365
Mitsubayashi, K.
—, Suzuki, M., Tamiya, E. and Karube, I.
Analysis of metabolites in sweat as a measure of physical condition 27
Miyares, P.H., see Jenkins, T.F. 69
Mlakar, M., see Zelić, M. 299
Mok, C.Y., see Wan, H.B. 371
Mori, Y., see Kurosawa, S. 307
Mottola, H.A., see Li, S. 79
Moutet, J.-C., see Coche-Guérente, L. 143
Mukai, H., see Zeng, Y. 195
Muratsugu, M., see Kurosawa, S. 307
Murthy, A.S.N.
— and Gupta, A.R.L.
NADH sensor with electrochemically modified TCNQ electrode 43
Myers, K.F., see Jenkins, T.F. 69

Nakamura, H., see Fukushima, M. 223
Narusawa, Y., see Li, Y. 355
Nemoto, E., see Kurosawa, S. 307
Nie, L., see He, F. 313
Nie, L., see Yao, S. 47
Nojiri, Y., see Zeng, Y. 195
Nunzi, F., see Haladjian, J. 15
Nylander, T., see Razumas, V. 155

Osa, T., see Hoshi, T. 321

Pedrazza, U., see Eugster, R. 1
Pratt, K.W.
Automated, high-precision coulometric titrimetry. Part I. Engineering and implementation 125
Pratt, K.W.
Automated, high-precision coulometric titrimetry. Part II. Strong and weak acids and bases 135

Razumas, V.
—, Kanapienienė, J., Nylander, T., Engström, S. and Larsson, K.
Electrochemical biosensors for glucose, lactate, urea, and creatinine based on enzymes entrapped in a cubic liquid crystalline phase 155
Ríos, A., see Lendl, B. 187
Rosatzin, T., see Eugster, R. 1

Rüegg, D., see Eugster, R. 1
Rump, T., see Wortberg, M. 177
Rusterholz, B., see Eugster, R. 1
Rüttinger, H.H., see Hahn, M. 35

Schmid, A., see Eugster, R. 1
Shoff, D.B., see Davis, D.M. 263
Sideris, E.E.
—, Georgiou, C.A., Koupparis, M.A. and Macheras, P.E.
Automated flow-injection serial dynamic dialysis technique in the study of drug binding with cyclodextrins 87
Simon, W., see Eugster, R. 1
Spichiger, U.E., see Eugster, R. 1
Strong, A.B., see Jenkins, T.F. 69
Suzuki, M., see Mitsubayashi, K. 27

Taga, M., see Fukushima, M. 223
Tamiya, E., see Mitsubayashi, K. 27
Temerk, Y.M., see Ahmed, Z.A. 329
Thamm, R., see Hahn, M. 35
Thomas, R.N.
Effects of contaminants and charge transfer on the molar absorptivities of fullerene solutions 57
Tivesten, A., see Csapó, J. 105
Tredoux, M., see McDonald, I. 237
Trojanowicz, M., see Michałowski, J. 339
Tuñón-Blanco, P., see Amez del Pozo, J. 169

Valcárcel, M., see Lendl, B. 187
Valencia, M.C., see Capitán-Vallvey, L.F. 365
Van den Berg, C.M.G., see Zima, J. 291

Wan, H.B.
—, Lan, W.G., Wong, M.K. and Mok, C.Y.
Orthogonal array designs for the optimization of liquid chromatographic analysis of pesticides 371
Wang, F., see Zhao, X. 163
White, R.L., see Inerowicz, H.D. 249
Wong, M.K., see Wan, H.B. 371
Wortberg, M.
—, Middendorf, C., Katerkamp, A., Rump, T., Krause, J. and Cammann, K.
Flow-injection immunosensor for triazine herbicides using Eu(III) chelate label fluorescence detection 177

Yang, S.-M., see Jen, J.-F. 97
Yao, S.
—, Chen, K. and Nie, L.
Application of a surface acoustic wave sensor system for the detection of non-aqueous solutions and phase transitions in lipid multibilayers 47
Yao, S., see He, F. 313
Yoshimoto, M., see Kurosawa, S. 307

Zelić, M.
—, Mlakar, M. and Branica, M.

Influence of perchlorates and halides on the electrochemical properties of indium(III) 299
Zeng, Y.
—, Mukai, H., Bandow, H. and Nojiri, Y.
Application of gas chromatography–combustion–isotope ratio mass spectrometry to carbon isotopic analysis of methane and carbon monoxide in environmental samples 195
Zhao, M.
— and Lu, L.
Abolition of the equivalent. Rule of equal amount of substance 121
Zhao, X.
—, Jin, W., Chen, J., Gao, Z. and Wang, F.
Investigations on bioanalytical chemistry. Part V. Adsorption voltammetry of adenine 163
Zhu, W., see He, F. 313
Zima, J.
— and Van den Berg, C.M.G.
Determination of arsenic in sea water by cathodic stripping voltammetry in the presence of pyrrolidine dithiocarbamate 291
Zimmer, H., see Ma, Y.L. 21

PREP '94

Preliminary Program

International Symposium on Preparative Chromatography

June 12-15, 1994

Washington, DC, USA

(Professor Georges Guiochon, chairman)

The 1994 PREP Symposium & Exhibit will be held June 12-15, 1994, at the Georgetown Conference Center by Marriott in Washington, DC, USA. ***For information, contact Mrs. Janet Cunningham, Symposium Manager, 10120 Kelly Road--BOX 279, Walkersville, Maryland 21793 USA (phone 301-898-3772; fax 301-898-5596).***

- ☑ Practical educational lectures presented by world-renown scientists
- ☑ Extensive sessions dedicated to the discussion of special topics
- ☑ Roundtable Discussions
- ☑ Problem-solving workshops
- ☑ Opportunities to interact with leading authorities in the field
- ☑ Exhibit of equipment & products for preparative chromatography
- ☑ Vendor seminars to present the scientific basis of new products and the illustration of new applications

SUNDAY, JUNE 12, 1994

- Laboratory-Scale Preparative Chromatography Workshop
- Review and Application of the Fundamentals of Preparative Chromatography Workshop
- Development of Preparative Separations by Displacement Chromatography Workshop

MONDAY, JUNE 13, 1994

- **Column Homogeneity, Bed Compressibility, and Column Performance** — *G. Guiochon, T. Sarkas, M. Sarker, T. Yun*
- **Application of Simulated Moving Bed Chromatography to Enantiomer Fractionation** — *R.-M. Nicoud, M. Perrut*
- **Preparative Stacked-Membrane Chromatography of Proteins and Optical Isomers** — *D. Keith Roper, E.N. Lightfoot*
- **Separation of Optical Isomers by Chromatography** — *A.E. Rodrigues, Z.P. Lu, J. Loureiro, L. Pais*
- **Preparative Chiral Separations by Gas Chromatography** — *D.U. Staerk, A. Shitangkoon, G. Vigh*
- **POSTER SESSION**
- **EXHIBIT**
- **ROUNDTABLE DISCUSSIONS**
- **Large Scale Displacement Chromatography of a Synthetic Peptide** — *F.D. Antia, H. Hellster*
- **Rapid Development and Implementation of High Performance Displacement Chromatography in a Bioprocess Setting** — *J.M. Jacobson*
- **Application of Synthetic Adsorbent to Simulated Moving Bed System** — *J. Fukuda, R. Sugimoto, S. Ando, A.D. Sharpe*
- **Experiments with Dynamic Compression Columns** — *M. Sarker, G. Guiochon*
- **Shock Layer Theory in Preparative Chromatography: Counter-Current Adsorption Separation** — *G.M. Zhong, G.A. Guiochon*

TUESDAY, JUNE 14, 1994

- **Ion-Exchange Preparative Chromatography of a Protein Mixture, Modelling and Experimental Approach** — *J.C. Bellot, M. Graber, J.S. Condoret*
- **Adsorption of Biologicals by Porous Polymeric Adsorbents: Equilibrium, Mass Transfer, and Regeneration** — *G. Carta, D.S. Grzergorczyk*
- **Novel Displacement Chromatographic Systems for Protein Purification** — *S.M. Cramer*
- **Molecular Basis for Ion-Exchange Retention of Proteins Under Linear and Overload Conditions** — *C.M. Roth, C.A. Johnson, A.M. Lenhoff*
- **A Model for Ion-Exchange Equilibria of Macromolecules in Preparative Chromatography** — *Y.-L. Li, N.G. Pinto*
- **Effects of Reactions on Retention and Isotherm Measurements in Hydrophobic Adsorption Systems** — *Z. Ma, J. Grosser, N.-H.L. Wang*
- **POSTER SESSION**
- **EXHIBITS**
- **ROUNDTABLE DISCUSSIONS**
- **Perfusion Chromatography: The Effects of Microsphere Size, Pore Diffusion and Dynamics of the Adsorption Step within the Microspheres on Column Performance** — *A.I. Liapis, O.K. Crosser, A. Tongta, Y. Xu*
- **Controlled-Pore Zirconia for HPLC of Proteins** — *A. McCormick, P. Carr, M. Flickinger*
- **A New, High Capacity, Porous Resin** — *T.L. Smith, D.K. Miller, R.P. Rohrbach*
- **Chromatographic Separation Medium in a Novel Shape: Porous Polymer Rods**—*F. Svec, Q. Wang, J.M.J. Frechet*

WEDNESDAY, JUNE 15, 1994

- **Preparative Reversed-Phase Chromatography of Proteins from a Multi-Protein Complex** — *T.J. Sereda, C.T. Mant, R.S. Hodges*
- **The Utilization of Theoretical Calculations Validated by Laboratory Scale Preparative Chromatography to Simulate Large Scale Column Performance** — *M.R. Schure, K.C. Deissler, J.J. Maikner, P.G. Cartier*
- **Separation of Biotin Labeled Proteins from Their Unlabeled Counterparts Using Immobilized Platinum Affinity Chromatography** — *D. Mile, A.A. Garcia*
- **Preparative Purification of Peptides** — *M. Knight, K. Takahashi, A. Geblaoui, B. Chandrasekar, Y. Ito, Y. Ma*
- **Optimization of Preparative Gradient Elution Separations: The Purification of Insulins** — *G.B. Cox, H. Colin*
- **Validation Studies in the Regeneration of Ion-Exchange Celluloses** — *P.R. Levison, S.E. Badger, D.W. Toome, M. Streater, J.A. Cox, S. Wheeler, N.D. Pathirana*
- **Cellulose-Based Continuous Stationary Phases in Protein Chromatography** — *M.R. Ladisch, J. Liu, K. Hamaker, R. Hendrickson, Y. Yang, A. Velayudhan, K. Kohlmann, P. Westgate, C. Ladisch*
- **Ligand Efficiency in Axial and Radial Flow Immunoaffinity Chromatography of Factor IX** — *J. Tharakan, M. Belizaire*
- **Separation of Lactose and Proteins from Dairy Whey by Large Scale Liquid Chromatographic Methods** — *S.J. Gerberding, C.H. Byers*

TrAC - Trends in Analytical Chemistry: Reference Edition

Volume 11: 1992

TrAC Compendium Series Volume 11

The Reference Edition of Trends in Analytical Chemistry (TrAC) is a compilation of the archival material reprinted from the regular issues of the journal. TrAC provides a topical digest of current developments and new ideas in the analytical sciences. It does so in the form of broadly-based, easy-to-read scientific reviews, backed up by news and other features of interest to the international analytical chemistry community. For subscribers to the library edition of TrAC, the reference editions form an integral part of the annual subscription, but for others these indispensable sources of information can be purchased individually. They provide informative and stimulating reading for all those who use analytical methods.

This latest volume contains all the archival material published in 1992. It covers a wide range of analytical techniques and applications of interest to academic and research workers in chemistry, biochemistry, clinical chemistry, pharmaceutical chemistry and toxicology.

A selection of the Contents.

Capillary Electrophoresis in Chemical/Pharmaceutical Quality Control *(A. Pluym, W. Van Ael, M. De Smet)*. Image Analysis in Chemistry. I. Properties of Images, Greylevel Operations, the Multivariate Image. II. Multivariate Image Analysis *(P. Geladi et al.)*. Silica Based, Solid Phase Reagents for Derivatizations in Chromatography *(F.-X. Zhou, J.M. Thorne, I.S. Krull)*. Mapping Post-Translational Modifications of Viral Proteins by Mass Spectrometry *(J.J. Gormann)*. Fluorescence Detection in Capillary Electrophoresis *(L.N. Amankwa, M. Albin, W.G. Kuhr)*. Biomolecular Tracing through Accelerator Mass Spectrometry *(J.S. Vogel, K.W. Turteltaub)*. Solid-Phase Reactors in Flow Injection Analysis *(M.D. Luque de Castro)*. Capillary Electrophoresis: A Powerful Tool for Biomedical Analysis and Research? *(D. Perrett, J. Ross)*. Bioanalytical Sample Preparation using Microdialysis and Ultrafiltration Capillaries *(M.C. Linhares, P.T. Kissinger)*. Models of Time-Series Analysis - a Helpful Tool for Evaluation of Noisy Data in Distribution Analysis *(K. Doerffel)*. Bio-Analytical Applications of Fourier Transform Infrared Spectroscopy *(M. Jackson, H.H. Mantsch)*. X-ray Absorption Spectroscopy in Chemistry. I. Extended X-ray Absorption Fine Structure. II. X-ray Absorption near Edge Structure *(P. Behrens)*. Mechanism of the Peroxyoxalate Chemiluminescence Reaction *(P.J.M. Kwakman, G.J. de Jong, U.A.Th. Brinkman)*. Plasma Spectrometric Detection for Supercritical Fluid Chromatography *(J.M. Carey, J.A. Caruso)*. Electrochemistry of Biopolymers *(J.A. Cox, A. Pryzjazny)*. High-Field NMR Spectroscopy as an Analytical Tool for Quantitative Determinations: Pitfalls, Limitations and Possible Solutions *(Cs. Szántay, Jr.)*. Abrasive Stripping Voltammetry - an Electrochemical Solid State Spectroscopy of Wide Applicability *(F. Scholz, B. Lange)*. Polymer Coatings as Stationary Phases in High-Performance Liquid Chromatography *(M. Hanson, K.K. Unger)*. Lasers in Mass Spectrometry *(J. Gorbally)*. Author Index. Subject Index.

1993 viii + 402 pages
Price: US $ 354.25 / Dfl. 620.00
ISBN 0-444-89926-X

ELSEVIER
SCIENCE

ORDER INFORMATION

For USA and Canada
ELSEVIER SCIENCE

Judy Weislogel
P.O. Box 945
Madison Square Station,
New York, NY 10160-0757
Tel: (212) 989 5800
Fax: (212) 633 3880

In all other countries
ELSEVIER SCIENCE

P.O. Box 211
1000 AE Amsterdam
The Netherlands
Tel: (+31-20) 5803 753
Fax: (+31-20) 5803 705

US$ prices are valid only for the USA & Canada and are subject to exchange rate fluctuations; in all other countries the Dutch guilder price (Dfl.) is definitive. Customers in the European Community should add the appropriate VAT rate applicable in their country to the price(s). Books are sent postfree if prepaid.

PUBLICATION SCHEDULE FOR 1994

	S'93	O'93	N'93	D'93	J	F	M	A	M	J	J	A
Analytica Chimica Acta	281/1 281/2 281/3	282/1 282/2 282/3	283/1 283/2	283/3 284/1 284/2	284/3 285/1–2 285/3	286/1 286/2 286/3	287/1–2 287/3 288/1–2	288/3 289/1 289/2	289/3 290/1–2 290/3	291/1–2 291/3 292/1	292/2 292/3 293/1–2	293/3 294/1–2 294/3
Vibrational Spectroscopy		6/1			6/2		6/3		7/1		7/2	

INFORMATION FOR AUTHORS

Detailed "Instructions to Authors" for *Analytica Chimica Acta* was published in Volume 289, No. 3, pp. 381–384. Free reprints of the "Instructions to Authors" of *Analytica Chimica Acta* and *Vibrational Spectroscopy* are available from the Editors or from: Elsevier Science B.V., P.O. Box 330, 1000 AH Amsterdam, The Netherlands. Telefax: (+31-20) 5862459.

Manuscripts. The language of the journal is English. English linguistic improvement is provided as part of the normal editorial processing. Authors should submit three copies of the manuscript in clear double-spaced typing on one side of the paper only. *Vibrational Spectroscopy* also accepts papers in English only.

Rapid publication letters. *Letters* are short papers that describe innovative research. Criteria for letters are novelty, quality, significance, urgency and brevity. Submission data: max. of 2 printed pages (incl. Figs., Tables, Abstr., Refs.); short abstract (e.g., 3 lines); *no* proofs will be sent to the authors; submission on floppy disc; *no* revision will be possible.

Abstract. All papers and reviews begin with an Abstract (50–250 words) which should comprise a factual account of the contents of the paper, with emphasis on new information.

Figures. Figures should be prepared in black waterproof drawing ink on drawing or tracing paper of the same size as that on which the manuscript is typed. One original (or sharp glossy print) and two photostat (or other) copies are required. Attention should be given to line thickness, lettering (which should be kept to a minimum) and spacing on axes of graphs, to ensure suitability for reduction in size on printing. Axes of a graph should be clearly labelled, along the axes, outside the graph itself. All figures should be numbered with Arabic numerals, and require descriptive legends which should be typed on a separate sheet of paper. Simple straight-line graphs are not acceptable, because they can readily be described in the text by means of an equation or a sentence. Claims of linearity should be supported by regression data that include slope, intercept, standard deviations of the slope and intercept, standard error and the number of data points; correlation coefficients are optional.

Photographs should be glossy prints and be as rich in contrast as possible; colour photographs cannot be accepted. Line diagrams are generally preferred to photographs of equipment. Computer outputs for reproduction as figures must be good quality on blank paper, and should preferably be submitted as glossy prints.

Nomenclature, abbreviations and symbols. In general, the recommendations of IUPAC should be followed, and attention should be given to the recommendations of the Analytical Chemistry Division in the journal *Pure and Applied Chemistry* (see also *IUPAC Compendium of Analytical Nomenclature, Definitive Rules*, 1987).

References. The references should be collected at the end of the paper, numbered in the order of their appearance in the text (*not* alphabetically) and typed on a separate sheet.

Reprints. Fifty reprints will be supplied free of charge. Additional reprints (minimum 100) can be ordered. An order form containing price quotations will be sent to the authors together with the proofs of their article.

Papers dealing with vibrational spectroscopy should be sent to: Dr J.G. Grasselli, 150 Greentree Road, Chagrin Falls, OH 44022, U.S.A. Telefax: (+1-216) 2473360 (Americas, Canada, Australia and New Zealand) or Dr J.H. van der Maas, Department of Analytical Molecular Spectrometry, Faculty of Chemistry, University of Utrecht, P.O. Box 80083, 3508 TB Utrecht, The Netherlands. Telefax: (+31-30) 518219 (all other countries).

0003-2670/94/$07.00

This issue is printed on acid-free paper.

PRINTED IN THE NETHERLANDS

Directory of Capillary Electrophoresis

(TrAC Supplement No. 1)

©1994 Paperback 156 pages Price:Dfl.137.00(US$ 70.00)

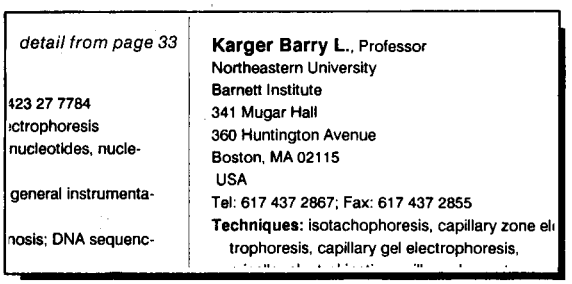

detail from page 33

423 27 7784
ctrophoresis
nucleotides, nucle-

general instrumenta-

nosis; DNA sequenc-

Karger Barry L., Professor
Northeastern University
Barnett Institute
341 Mugar Hall
360 Huntington Avenue
Boston, MA 02115
USA
Tel: 617 437 2867; Fax: 617 437 2855
Techniques: isotachophoresis, capillary zone el
trophoresis, capillary gel electrophoresis,

- **Containing over 450 V.I.P.s Worldwide**
- **Including Complete Addresses, Fax and Phone Numbers, and E-Mail Addresses (where available)**
- **Giving Techniques, Applications and Research Topics**
- **Providing an Extensive Subject Index**

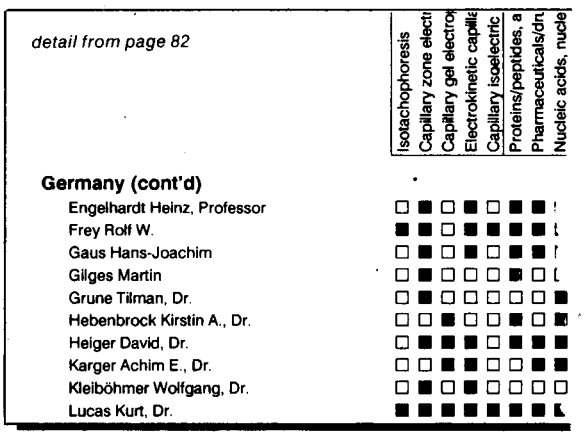

detail from page 82

	Isotachophoresis	Capillary zone electr	Capillary gel electro	Electrokinetic capill	Capillary isoelectric	Proteins/peptides, a	Pharmaceuticals/dn	Nucleic acids, nucle
Germany (cont'd)								
Engelhardt Heinz, Professor	□	■	□	■	□	■	■	!
Frey Rolf W.	■	■	□	■	■	■	■	t
Gaus Hans-Joachim	□	■	□	■	□	■	■	!
Gilges Martin	□	■	□	□	□	■	□	[
Grune Tilman, Dr.	□	■	□	□	□	□	□	■
Hebenbrock Kirstin A., Dr.	□	□	■	□	□	■	□	■
Heiger David, Dr.	□	■	■	■	□	■	■	■
Karger Achim E., Dr.	□	□	■	■	□	□	■	■
Kleiböhmer Wolfgang, Dr.	□	■	□	■	□	□	□	□
Lucas Kurt, Dr.	■	■	■	■	■	■	■	[

This directory of researchers in capillary electrophoresis not only contains the names and addresses of most leading scientists in this rapidly developing field. The papers in this area that each listed scientist considers as his or her most significant contribution are given. A geographical index with techniques and application areas shows who is doing what in each country. Instrument manufacturers and suppliers are also listed on a country by country basis, along with the products or services they offer.

The editors have endeavoured to collect together, in this one source, information on who's who and the major research trends in the field of capillary electrophoresis.

ORDER FORM

Please send this form to your regular supplier or to:

Elsevier Science B.V.
Attn. Eugene P.M. Wijnhoven
P.O. Box 330, 1000 AH Amsterdam The Netherlands
Fax: +31 (20) 586 2845

☐ **Yes,** Please send me a copy of **Directory of Capillary Electrophoresis**

☐ Please charge my credit card:
☐ Eurocard ☐ Mastercard ☐ American Express ☐ VISA ☐ Access

Card number: _____ Expiry Date: _____

Vat registration number: _____ Signature: _____

Name: _____

Address: _____

US$ prices are valid only for the USA & Canada and are subject to exchange rate fluctuations; in all other countries the Dutch guilder price (Dfl.) is definitive. Customers in the European Union should add the appropriate VAT rate applicable in their country to the price(s). Books are sent postfree if prepaid.

ACA

0003-2670(19940510)289:3;1-7